Dipl-Ing. Manuel Feurhuber, BSc

A novel approach for investigating important phenomena of steam sterilization processes using CFD

Dissertation

to achieve the university degree of
Doctor of Technical Sciences

submitted to
Graz University of Technology
Faculty of Mechanical Engineering and Economical Sciences

Supervisor
Univ.-Prof. Dipl-Ing. Dr.techn. Christoph Hochenauer

Second Supervisor
Univ.-Prof. Dr.-Ing. habil. Tim Zeiner

Graz, September 2019

Statutory Declaration

I declare that I have authored this thesis independently, that I have not used other than the declared sources/resources, and that I have explicitly marked all material which has been quoted either literally or by content from the used sources.

Graz, _____ _____

Date Signature

Eidesstattliche Erklärung[1]

Ich erkläre an Eides statt, dass ich die vorliegende Arbeit selbstständig verfasst, andere als die angegebenen Quellen/Hilfsmittel nicht benutzt, und die den benutzten Quellen wörtlich und inhaltlich entnommenen Stellen als solche kenntlich gemacht habe.

Graz, am _____ _____

Datum Unterschrift

[1] Beschluss der Curricula-Kommission für Bachelor-, Master- und Diplomstudien vom 10.11.2008; Genehmigung des Senates am 1.12.2008

Acknowledgements

Firstly, I wish to thank my supervisor, Professor Christoph Hochenauer, for mentoring me during my time at the Institute of Thermal Engineering (IWT) at the Graz University of Technology. He gave me the opportunity to work as a junior scientist and develop myself both in terms of my technical expertise, as well as on a personal level, at the IWT in Graz. His extensive knowledge in the fields of numerical simulations and analytical calculations of flow fields was always a big help for me. I also want to thank Professor Hochenauer for his patience during times when things were not going so well. Thank you in particular for your constant support.

This thesis is the result of a three-year research project "Optimization of Steam Sterilizers" in cooperation with W&H Sterilization S.r.l.. Therefore, I would also like to thank W&H Sterilization for funding this project and making this thesis possible. Special thanks are due to Marino Magno, Marco Miranda, Walter Crotti and Antonello Cattide for the ever-pleasant working relationship, their constant support during the experimental work, and the very constructive meetings we had over the course of this project. Furthermore, I want to thank the whole software department team at W&H Sterilization for creating the software we needed during our project. Furthermore, I would like to thank Rene Prieler for his work on a previous project and the help he gave me during my first month at the IWT.

I would also like to thank my co-supervisor, Professor Tim Zeiner, for agreeing to review and evaluate my PhD thesis.

During my five years at the IWT, I was lucky to have wonderful colleagues. Therefore, I want to thank all of them for the great working atmosphere. Special thanks are due to my colleagues, Paul Burian, Bernhard Stöckl, Michael Preininger, Raphael Neubauer, Markus Raiber and Christian Gaber for the working environment in the office, the nice lunch breaks, and for your help and support while I was working on my PhD thesis.

Friendship is something you can't buy in life. I am very happy to have wonderful and supportive friends. I would particularly like to thank Christoph Windhager, Josef

Edtmayer, Herwig Aistleitner and Georg Krimberger for all the great times we have spent together and their support during school, at university, and during my time working on this PhD thesis.

I am also deeply grateful to my lovely siblings, Sophie and Julian Feurhuber, for their support and encouragement during my whole life. I will never forget the great times the three of us have spent together in Vienna, Graz, and Mondsee. Life would be boring without you, my siblings.

It would be beyond the scope of this short text to thank my girlfriend Sarah for all the things she has done for me over the years. Nevertheless, I would like to say thank you, Sarah, for all the love you have given me and the belief you have had in me since the first day we met. You have always given me the support I needed, especially when things were tough. Without your support, it would not have been possible to achieve all my dreams. Thank you for everything, Sarah!

Last but not least, I would like to express my deepest appreciation to my parents, Anita and Josef Feurhuber, for making all my dreams come true. Without your love and support throughout my entire life, I would not be sitting here and writing these lines within my PhD thesis. Thank you both! Danke Mama, Danke Papa!

To my family and Sarah!

Abstract

Steam sterilization is the most common method of sterilizing both wrapped and unwrapped pieces of medical equipment prior to re-use. The steam sterilization process is based on high heat transfer rates from the steam to the load, which occur as a result of condensation effects. At the beginning of the steam sterilization process, the steam sterilizer is filled with Non-Condensable Gases (NCGs) (namely air). These NCGs have to be removed from both the sterilization chamber and hollow loads in order to enable high heat transfer rates due to steam condensation effects.

The goal of this thesis was to develop a Computational Fluid Dynamics (CFD) model, able to predict all of the relevant phenomena inside a steam sterilizer. To achieve this goal, four main research questions must be answered:
i) Is it possible to simulate the heating process of the load?
ii) Which approach can be used to simulate the influence of the wrapping of the load?
iii) Is it possible to simulate the inactivation of different bacteria types on the surface of the load?
iv) Which approach works best to simulate the air removal and the steam penetration inside the steam sterilizer as well as inside hollow loads (cavities)?

To answer these research questions, this thesis deals with four major subjects:

To investigate the first question, the sterilization phase of the steam sterilization cycle was considered in detail. To validate the CFD model, transient measurements of the pressure, the fluid temperature, and the load temperature were performed. In this part, a two phase Eulerian-Eulerian multiphase model was used to simulate both the condensation and evaporation effects inside the steam sterilizer. A numerically efficient heat transfer model was developed in order to simulate the heat transfer from the steam to the load. The measured and simulated pressures, fluid temperatures, and load temperatures were all in very good accordance. These results prove that i) the developed CFD model is able to accurately predict the heating process of the load.

To answer the second research question, the heat transfer to wrapped load was investigated. To model the permeability of the paper in which the load is usually wrapped, a time-efficient porous media model was developed. The permeability of the paper was measured on a novel test rig, which was developed in-house. The results indicate that the wrapping has a negligible influence on the load temperature; however, it has a massive influence on the quality of the steam inside the steam sterilizer. These results prove that ii) it is possible to simulate the influence of the wrapping on the sterilization process.

Thirdly, a first-order reaction kinetic approach, coupled with the Arrhenius equation, was added to the CFD code in order to simulate the inactivation of different types of bacteria inside the sterilization chamber as well as on the surface of the load. With this approach, iii) the inactivation of bacteria can be predicted on the surface of the load. In this thesis different types of bacteria were investigated, including the most heat-resistant bacteria type, *Geobacillus stearothermophilus*.

Finally, both air-removal and steam penetration were investigated in the steam sterilization chamber as well as inside hollow loads (cavities). For this purpose, a three-phase Eulerian model was used to simulate the steam, water, and NCGs (namely, air) mixture, which is present inside the steam sterilizer. Furthermore, the heat transfer model was enhanced so as to also be able to predict the heat transfer due to condensation effects in the presence of NCGs. With this CFD model, it was possible to iv) simulate the air-removal inside the steam sterilizer. To investigate research question iv) the removal of the NCGs was simulated and measured in both a vacuum and a non- vacuum steam sterilizer. The measured and simulated NCGs ratios were in very good accordance. Furthermore, the NCGs ratio was investigated in two different helix tests. These simulation results were validated by means of chemical indicator measurements. The simulated results matched the measured ones very well.

The CFD models developed in the course of this research project are able to predict numerous physical phenomena inside modern steam sterilizers. Thus, the results presented in this thesis should support both the developers of steam sterilizers and researchers of steam sterilization processes as they attempt to optimize the performance of such devices.

Kurzfassung

Die Dampfsterilisation ist eine weitverbreitete Methode, um nicht verpackte sowie verpackte medizinische Instrumente vor der Wiederverwendung zu sterilisieren. Der Dampfsterilisationsprozess basiert auf sehr hohen Wärmeübergangszahlen vom Dampf auf die Beladung. Diese sehr hohen Wärmeübergangszahlen entstehen durch Kondensation des Dampfes an der Oberfläche der Beladung. Zu Beginn des Dampfsterilisationsprozesses ist der Dampfsterilisator mit Nicht-Kondensierbaren Gasen (NKGs) (i.d.R. Luft) gefüllt. Die NKGs müssen aus der Sterilisationskammer sowie aus den Hohlräumen gebracht werden, um einen hohen Wärmeübergang aufgrund von Dampfkondensationseffekten zu ermöglichen.

Das Ziel dieser Arbeit war es, ein rechnergestütztes Computational Fluid Dynamics (CFD) Modell zu entwickeln, welches alle relevanten Phänomene innerhalb eines Dampfsterilisators berechnen kann. Um dieses Ziel zu erreichen, mussten vier zentrale Forschungsfragen beantwortet werden:
i) Kann der Aufheizvorgang der Beladung simuliert werden?
ii) Welcher Ansatz kann verwendet werden, um den Einfluss der Verpackung (der Beladung) zu simulieren?
iii) Ist es möglich, die Abtötung verschiedener Bakterienstämme auf der Oberfläche der Beladung zu simulieren?
iv) Wie kann die Entlüftung und das Eindringen von Dampf in der Sterilisationskammer als auch in Hohlkörper simuliert werden?

Um diese Forschungsfragen zu beantworten, befasst sich diese Arbeit mit vier Hauptthemen:

Zur Behandlung der ersten Forschungsfrage wurde die Sterilisationsphase des Dampfsterilisationszyklus untersucht. Es wurden Messungen des Drucks, der Dampftemperatur und der Temperatur der Beladung durchgeführt. Zusätzlich wurde ein zweiphasiges Euler-Euler-Mehrphasenmodell verwendet, um Kondensation und Verdampfung im Dampfsterilisator zu simulieren. Ein numerisch sehr effizientes Modell wurde entwickelt, um den Wärmeübergang zwischen Dampf und Beladung zu berechnen.

Gemessene und simulierte Drücke, Dampftemperaturen, und Temperaturen der Beladung stimmten sehr gut mit Messungen überein. Diese Ergebnisse haben gezeigt, dass i) das entwickelte CFD-Modell in der Lage ist, den Aufheizvorgang der Beladung sehr genau zu simulieren.

Für die Untersuchung der zweiten Forschungsfrage wurde der Wärmeübergang auf die verpackte Ladung untersucht. Um die Durchlässigkeit des Verpackungspapiers (in welches die Beladung normalerweise gewickelt ist) zu modellieren, wurde ein zeiteffizientes poröses Medium Modell entwickelt. Die Durchlässigkeit des Verpackungspapiers wurde an einem neuartigen Prüfstand gemessen, der am Institut für Wärmetechnik entwickelt wurde. Die Ergebnisse zeigten, dass der Einfluss der Verpackung auf die Temperatur der Beladung sehr gering ist. Der Einfluss der Verpackung auf die Dampfziffer im Dampfsterilisator ist jedoch sehr groß. Ohne das entwickelte Modell zur Simulation der Durchlässigkeit der Verpackung als poröses Medium, wäre es nicht möglich diese genauen Ergebnisse zu erzielen. Darüber hinaus zeigen die Ergebnisse, dass ii) der Einfluss der Verpackung auf den Sterilisationsprozess genau und numerisch effizient simuliert werden kann.

Drittens wurde ein Reaktionskinetik-Modell erster Ordnung in Verbindung mit der Arrhenius-Gleichung zum CFD Code hinzugefügt, um die Abtötung verschiedener Bakterienstämme innerhalb der Sterilisationskammer sowie auf der Oberfläche der Beladung zu simulieren. Mit diesem Modellansatz kann iii) die Abtötung von Bakterien auf der Oberfläche der Beladung örtlich und zeitlich aufgelöst vorhergesagt werden. In dieser Arbeit wurden verschiedene Bakterienstämme untersucht, darunter der am schwersten abzutötende Bakterienstamm, *Geobacillus stearothermophilus*.

Schließlich wurde die Entlüftung und das Eindringen von Dampf in die Sterilisationskammer sowie in Hohlräumen untersucht. Daher wurde ein Euler-Euler-Modell mit drei Phasen verwendet, um das Dampf-, Wasser- und NKGs- (i.d.R. Luft-) Gemisch zu simulieren, das sich im Dampfsterilisator befindet. Darüber hinaus wurde ein Wärmeübertragungsmodell weiterentwickelt, um die Wärmeübertragung aufgrund von Kondensationseffekten in der Gegenwart von NKGs vorherzusagen. Mit dem entwickelten CFD-Modell konnte iv) die Entlüftung im Dampfsterilisator simuliert werden. Zur Demonstration wurde das Entfernen der NKGs in einem Vakuum- und einem Nicht-Vakuum-Dampfsterilisator simuliert und gemessen. Gemessene und simulierte NKGs-Anteile stimmten sehr gut überein. Darüber hinaus wurden die NKGs-Anteile in zwei verschiedenen Helix-Tests untersucht. Diese Simulationsergebnisse wurden auch mit Messungen mit chemischen Indikatoren validiert. Die simulierten Ergebnisse stimmten mit den gemessenen Ergebnissen gut überein.

Die in dieser Arbeit entwickelten CFD-Modelle können viele physikalische Phänomene in modernen Dampfsterilisatoren vorhersagen. Die Ergebnisse sollen Entwicklern von Dampfsterilisatoren und Forschern von Dampfsterilisationsprozessen bei ihrer zukünftigen Arbeit unterstützen.

Contents

List of Figures

List of Tables

Acronyms

CAD	Computer-Aided Design
CAF	Convective Augmentation Factor
CFD	Computational Fluid Dynamics
FVM	Finite Volume Method
IWT	Institute of Thermal Engineering
NCGs	Non-Condensable Gases
PCD	Process Challenge Device
PPS	Polyphenylensulfid
PTFE	Polytetrafluorethylen
QUICK	Quadratic Upstream Interpolation for Convective Kinematics
RANS	Reynolds-Averaged-Navier-Stokes equations
SAL	Sterility Assurance Level
SIMPLE	Semi-Implicit Method for Pressure Linked Equations
UDF	User-Defined Function
UDS	User-Defined Scalar

Symbols

Symbol	Description	Unit
α	Permeability	m^2
C_2	Inertial resistance factor	$1/m$
D	D-value	min
Δn	Thickness	m
Δp	Pressure drop	Pa
Δp_{air}	Pressure drop of the air over the paper	Pa
Δp_{steam}	Pressure drop of the steam over the paper	Pa
E_d	Activation energy	J/mol
η	Dynamic viscosity	Pa s
F_0	F_0-value	min
f_{CFD}	Physical value simulated with CFD	dependent on the value
$f_{Measurement}$	Measured physical value	dependent on the value
g	Gravity	m/s^2
k	Total number of the fluid cells of the numerical grid	–
k_d	Inactivation rate	1/s
k_{d0}	Pre-exponential factor	1/s
L_c	Characteristic length	m

Symbol	Description	Unit
λ	Thermal conductivity	$\mathrm{W/(m\,K)}$
λ_{fluid}	Thermal conductivity of the fluid	$\mathrm{W/(m\,K)}$
λ_w	Thermal conductivity of the water	$\mathrm{W/(m\,K)}$
$m^{'}$	Mass of the boiling water	kg
$m^{''}$	Mass of the saturated steam	kg
m_{air}	Mass of the air	kg
m_b	Mass of the collected NCGs	kg
m_{NCGs}	Mass of the NCGs	kg
$m_{saturated\ steam}$	Mass of the saturated steam	kg
m_{steam}	Mass of the steam	kg
$\dot{m}_{sw}$	Rate of mass transfer due to condensation	$\mathrm{kg/(s\,m^3)}$
m_{total}	Total mass of the mixture	kg
m_{water}	Mass of the water (condensed steam)	kg
$m_{wet\ steam}$	Mass of the wet steam	kg
$\dot{m}_{ws}$	Rate of mass transfer due to evaporation	$\mathrm{kg/(s\,m^3)}$
μ_{steam}	Mass fraction of the steam	–
N_0	Initial number of the bacteria	–
N	Current number of the bacteria	–
Nu	Nusselt number	–
$Nu_{condensation}$	Nusselt number due to condensation	–
$Nu_{condensation\ NCGs}$	Nusselt number due to condensation in the presence of NCGs	–
Nu_{conv}	Nusselt number due to convection	–
$Nu_{ideal\ flow}$	Nusselt number of the ideal flow	–
Nu_p	Nusselt number of the p^{th} phase	–
ν	Kinematic viscosity	$\mathrm{m^2/s}$
ν_w	Kinematic viscosity of the water	$\mathrm{m^2/s}$
$p_{ambient}$	Ambient pressure	Pa
p_{CFD}	Simulated pressure with the CFD model	Pa
p_m	Pressure in the measurement system	Pa
$p_{Measurement}$	Measured pressure	Pa
p_{NCGs}	Partial pressure of the NCGs	Pa
Pr	Prandtl number	–

Symbol	Description	Unit
Pr_p	Prandtl number of the p^{th} phase	–
p_{SS}	Pressure at the measured point inside the steam sterilizer	Pa
$p_{sterilization}$	Sterilization pressure	Pa
ϕ_{CFD}	Volume fraction in the CFD model	–
ϕ_{NCGs}	Volume fraction of the NCGs	–
$\phi_{NCGs,i}$	Volume fraction of the NCGs in the i^{th} cell	–
ϕ_{Norm}	NCGs ratio according to the norm	–
ϕ_{real}	Real volume fraction of the NCGs	–
ϕ_s	Volume fraction of the steam phase	–
ϕ_{steam}	Volume fraction of the steam	–
ϕ_w	Volume fraction of the water phase	–
$\dot{q}_p$	Heat flux density at the point p	$\mathrm{W/m^2}$
R	Universal gas constant	$\mathrm{J/(kmol\,K)}$
r	Heat of evaporation	J/kg
Ra	Rayleigh number	–
Re	Reynolds number	–
Re_p	Reynolds number of the p^{th} phase	–
R_{NCGs}	Gas constant of the NCGs	$\mathrm{J/(kg\,K)}$
r_{sw}	Coefficient of the Lee Model for condensation	1/s
r_{ws}	Coefficient of the Lee Model for evaporation	1/s
ρ	Density	$\mathrm{kg/m^3}$
ρ_s	Density of the steam	$\mathrm{kg/m^3}$
ρ_w	Density of the water	$\mathrm{kg/m^3}$
S_i	Momentum source term	$\mathrm{N/m^3}$
T	Temperature	K
t	Time	s
t_0	Time when the sterilizaton process starts	s
T_b	Bulk temperature of the fluid	K
T_{CFD}	Simulated temperature with the CFD model	K
t_{Cycle}	Cycle duration	s
T_m	Temperature in the measurement system	K

Symbol	Description	Unit
$T_{Measurement}$	Measured temperature	K
t_n	Time when the sterilizaton process ends	s
T_s	Steam temperature	K
T_{sat}	Saturation temperature	K
$T_{Simulation}$	Simulated temperature	K
T_{SS}	Temperature at the measured point inside the steam sterilizer	K
T_w	Water temperature	K
T_{wall}	Wall temperature	K
v	Velocity	m/s
$V^{'}$	Volume of the boiling liquid	m^3
$V^{''}$	Volume of the saturated steam	m^3
V_{air}	Volume of the air	m^3
V_b	Volume of the collected NCGs	m^3
V_c	Volume of the collected condensed steam	m^3
$V_{Cell,i}$	Cell volume of the i^{th} cell	m^3
v_i	Velocity of the i^{th} component	m/s
$\vec{v}_i$	Velocity vector	m/s
V_{NCGs}	Volume of the NCGs	m^3
$V_{saturated\ steam}$	Volume of the saturated steam	m^3
$V_{Sterilizer}$	Volume of the sterilizer	m^3
V_{total}	Total volume	m^3
x	Steam quality	–
X_p	Location of the point p	m
y^+	Dimensionless wall distance	–
z	z-value	°C

1

Introduction

The sterilization of medical equipment is of major importance to ensure patients' safety. By making it possible to reuse medical equipment, sterilization allows societies to maintain cost-efficient and environmentally sustainable healthcare systems. To guarantee that medical equipment can be reused safely, all bacteria must be inactivated prior to contact with a new patient. To this end, sterilization processes refer to the procedures used to inactivate all bacteria on the surfaces of medical equipment. Many scientists have investigated different aspects of steam sterilization processes in the past. Nevertheless, to understand all of the phenomena that take place during the steam sterilization process, there is still more research to be done. To contribute to this field, the overarching goal of this thesis was to develop a numerical model able to simulate all of the relevant phenomena inside a steam sterilizer, resolved in time and space.

This chapter begins with an overview of the journal publications that provided the basis of this PhD thesis as well as an assessment of the author's own contribution to the total work. Subsequently, this chapter presents an overview of the motivation behind this project, the state of the art in this field, the methods that were employed in the course of these investigations, the impact this research may have on the scientific community, and future fields of application for this thesis.

This PhD thesis is based on three peer-reviewed journal publications, which are presented in the following list:

- M. FEURHUBER, A. CATTIDE, M. MAGNO, M. MIRANDA, R. PRIELER, C. HOCHENAUER, Prediction of the fluid flow, heat transfer and inactivation of microorganism at medical devices in modern steam sterilizers using computational fluid dynamics, Applied Thermal Engineering 127 (2017) 1391-1403. https://doi.org/10.1016/j.applthermaleng.2017.08.085

- M. FEURHUBER, M. MAGNO, M. MIRANDA, R. PRIELER, C. HOCHENAUER, CFD Investigation of Non-Condensable Gases in Vacuum and Non-Vacuum Steam Sterilizers, Chem. Ing. Tech. 91 (4) (2019) 502-513. https://doi.org/10.1002/cite.201800088

- M. FEURHUBER, M. MAGNO, M. MIRANDA, C. HOCHENAUER, CFD investigations of steam penetration, air-removal and condensation inside hollow loads and cavities, Applied Thermal Engineering 147 (2019) 1070-1082. https://doi.org/10.1016/j.applthermaleng.2018.10.135

Paper [1] presents a study in which a CFD model was developed to predict the heat transfer from the steam to the load and the inactivation of bacteria on the surface of wrapped cylindrical loads made out of different materials. The CFD model for this study was developed by the author, with the help of Professor Christoph Hochenauer and Rene Prieler. Antonello Cattide, Marco Miranda, and Marino Magno contributed their experimental work, which was needed to validate the CFD model.

In paper [2], the removal of NCGs inside both a vacuum and a non-vacuum steam sterilizer was investigated. The measured and simulated NCGs contents were compared and found to be in good accordance. The CFD simulations for this work were done by the author, with the help of Professor Christoph Hochenauer and Rene Prieler. Marco Miranda and Marino Magno assisted with the measurements performed for this study.

Paper [3] presents further developments of paper [2]. In this paper, the air-removal and the steam penetration processes were investigated inside the sterilisation chamber, as well as inside two different kinds of helix tests. The results of the simulation of steam penetration in the helix tests were validated with measurements of chemical indicators. The author carried out the CFD simulations for this work under the supervision of Professor Christoph Hochenauer. Marco Miranda worked on the experiments under the supervision of Marino Magno.

Furthermore, during work on this thesis, two more publications were written. The fourth publication was submitted to the journal *Physics in Medicine*. For this paper the revision has already been uploaded. The fifth publication is accepted for publication in the *International Journal of Heat and Mass Transfer*.

- M. FEURHUBER, P. BURIAN, M. MAGNO, M. MIRANDA, C. HOCHENAUER, Development of a spatially and timely resolved CFD model of a steam sterilizer to predict the load temperature and the inactivation of bacteria, under review.

- M. FEURHUBER, P. BURIAN, M. MAGNO, M. MIRANDA, C. HOCHENAUER, CFD simulation of the inactivation of *Geobacillus stearothermophilus* on dental handpieces, International Journal of Heat and Mass Transfer 144 (2019), Article 118649.

[4] investigates the time and spatially resolved CFD simulation of both load temperature and the inactivation of bacteria on the surface of an unwrapped cylindrical load. The author and Paul Burian worked on the development of the CFD model under the supervision of Professor Christoph Hochenauer. Marino Magno and Marco Miranda worked on the experimental part and helped with the validation of the CFD model.

[5] is a further development of paper [1] and paper [4]. In this paper, the inactivation of the bacteria type *Geobacillus stearothermophilus* was investigated on the surface of both wrapped and unwrapped dental handpieces. The author and Paul Burian worked on the development of the CFD model with the support Professor Christoph Hochenauer. Again, the experimental work was done by Marco Miranda and supported by Marino Magno.

The interpretation of the results of papers [1–5] was done by the author with the support of Professor Christoph Hochenauer. All of the papers were written by the author under the supervision of Professor Christoph Hochenauer. In total the author's own contribution to the total work of papers [1–5] is estimated to be more than 85 %.

1.1 Motivation and state of the art [1]

Steam sterilization is the most commonly used method to sterilize re-usable medical equipment. Nowadays, many different steam sterilizers and steam sterilization processes are available on the market. The correct use of steam sterilizers is important in order to avoid contaminated surgical instruments [6]. Criteria for effective sterilization processes can be found in the European standards [7, 8] and in international norms [9].

Many authors have investigated the steam sterilization process experimentally. Van Doornmalen, for example, showed that the quality of the sterilization process depends on factors such as the load, the pouches, the wrapping and, obviously, the sterilizer itself [10]. Another work by van Doornmalen et al. pointed out that the orientation of hand pieces has an influence on the sterilization process [11]. Furthermore, the presence

[1] Segments of this section have already been published in [1, 3].

of NCGs, such as air, has a big influence on the quality of the sterilization process due to the fact that increasing volume fractions of NCGs lead to decreasing rates of heat transfer due to condensation. Bowie et al. found that NCGs that were absorbed by textile or porous loads have a negative influence on sterility due to a lower heat transfer rate from the steam to the load [12]. Other authors have also investigated the sterility of the load. Van Doornmalen and Dankert validated 197 steam sterilizers. The results revealed that only 40 % of these steam sterilizers met the standards [13]. Esel et al. looked at the polymicrobial ventriculitis and the evaluation of an outbreak in a surgical intensive care unit due to inadequate sterilization. Their work demonstrated that strict infection control is necessary to prevent surgical infections [14]. Vadrot and Darbord investigated the evaluation of prion inactivation by comparing chemical sterilization and steam sterilization [15]. Lapanaitis et al. [16], investigated the relationship between the length of the steam sterilization cycle and the weight of the load. Many other authors have also investigated air removal from and steam penetration into hollow loads (helix tests) [17–20]. The work of Kaiser [21] shows the influence of NCGs on the steam sterilization cycle. Another study has shown that a non-vacuum sterilizer failed to sterilize dental handpieces [22]. Winter et al. investigated steam penetration into dental handpieces with narrow internal lumen during sterilization by means of both vacuum and non-vacuum processes. They found that a non-vacuum sterilizer was not able to reliably achieve sterilization conditions inside the handpieces [23]. This is due to the fact that it is more difficult for a non-vacuum steam sterilizer to remove the NCGs inside the handpieces. As a result, the heat transfer from the steam to the load decreases. In contrast, it is easier for a vacuum steam sterilizer to remove the NCGs inside hollow cavities (volumes) of dental handpieces; this means that they are able to achieve higher heat transfer rates and, therefore, to inactivate bacteria more effectively.

All of these studies underline the importance of a thorough understanding of the steam sterilization cycle. To further this understanding, numerical simulations are an extremely useful tool to clarify the relevant phenomena that take place inside a steam sterilizer. Despite their advantages, there are still few numerical simulations of steam sterilization processes published in scientific literature. One of these, Lau et al. [24], developed a numerical model of a steam sterilizer without load. In a further study, the same authors incorporated load effects on the steam sterilizer [25]. The major disadvantage of the models by Lau et al. [24, 25] is that they do not enable researches to investigate the relevant phenomena inside a steam sterilizer, resolved in time and space. Therefore, in this PhD thesis, a numerically inexpensive CFD model was developed to simulate the air-removal, steam penetration, fluid temperatures, load temperatures,

pressures, condensation and evaporation effects as well as the inactivation of different types of bacteria, allowing all of the above to be resolved in both time and space.

1.2 A short overview of this study

This thesis is based on both experimental and numerical investigations. As reflected in the title of this thesis, the main focus of this work is on CFD simulations of steam sterilization processes. The aim of this research project was to develop CFD models capable of simulating all of the relevant phenomena inside a steam sterilizer. As a result of this goal, different aspects were considered in the developed CFD models. With this goal in mind, the following research questions were defined:

i) Is it possible to simulate the heating process of the load?
ii) Which model can be used to simulate the wrapping of the load?
iii) How can the inactivation of bacteria on the surface of the medical equipment be predicted?
iv) Which approach works best to simulate the air removal and the steam penetration inside the steam sterilizer as well as inside hollow loads (cavities)?

This thesis consists of six chapters. Chapter 2 presents a theoretical background of the principles of steam sterilization processes, including a description of the different working principles, steam sterilization cycles, the inactivation of bacteria, the air-removal and steam penetration process, and the different kinds of loads (medical equipment).

Chapter 3 provides an overview of all the experiments that were performed in the course of this research project. It also presents the experimental set-ups that were used to measure the pressures, fluid temperatures, and load temperatures. Furthermore, the test rig that was used to measure the permeability of the paper in which loads can be wrapped is introduced. Finally, the measurement set-up that was used to measure the NCGs inside the steam sterilizer and the steam penetration inside hollow loads is presented.

Chapter 4 describes the numerical models, the heat transfer model that was developed by the author to answer with research question i), and the boundary conditions as well as the numerical grids that were used for all of the simulations carried out in the course of this thesis. In Chapter 5, all of the results of this study are presented, and research questions i), ii), iii) and iv) are answered.

Finally, Chapter 6 presents the conclusions that can be drawn from all the work presented in the context of this dissertation and make suggestions regarding future research in this area.

1.3 Impact of this study on the scientific community

Numerical simulations are a useful tool for the description and analysis of the spatial and temporal occurrence of phenomena related to a medical field of research. For example, past studies have investigated the flow and the heat transfer in the human eye [26, 27]. Other studies have simulated the behaviour of infant radiant warmers [28] and infant incubator [29]. Another study investigated the 3D blood flow [30]. However, when it comes to numerical simulations of steam sterilization processes, hardly any studies can be found in existent scientific literature.

This thesis presents a flexible and numerically inexpensive model for 3D simulations in order to predict all the relevant transient phenomena inside various types of steam sterilizers. Particular attention was paid to simulating the fluid temperatures as well as the load temperatures within the steam sterilizer. To predict the heat transfer to the load and to the walls of the steam sterilizer, a very numerically efficient heat transfer model was developed. The main advantage of this model is that the condensation wall film does not have to be modelled. The heat transfer model developed by the author was adapted so as to be able to predict the heat transfer from the fluid to the load in the presence of NCGs. A first-order reaction kinetic approach was added to the CFD code to simulate the inactivation of different kinds of bacteria. The CFD model was thereafter extended to simulate the removal of air and the penetration of steam inside hollow loads (cavities). With the CFD model that was developed in the course of this research project, it is possible to gain deep numerical insight into the steam sterilization process. As a result, very complex and time-consuming experiments can be reduced. Thus, valuable time and money can be saved.

The model and the findings that presented in this thesis are new to the scientific community. To the best knowledge of the author, no CFD simulations of steam sterilization processes were published in scientific literature prior to the simulations presented in this thesis. These models can help both researchers and the developers of steam sterilization processes gain a deep and thorough insight into different types of steam sterilization processes. Hopefully, the advantages of these models will prompt researchers to carry out further CFD simulations in the field of steam sterilization, and

will be of significant assistance to the development of future steam sterilizers and sterilization techniques.

1.4 Methods and future fields of application

The CFD models presented in this thesis are an exact geometrical reproduction of the steam sterilizers investigated. These CFD models are based on the commercially available software, ANSYS Fluent, with additional customized code to model the heat transfer due to condensation as well as the inactivation of different types of bacteria.

For the purpose of this investigation, both numerical and experimental investigations were performed to gain more insight into steam sterilization processes. In this thesis, the load temperatures and the inactivation of bacteria were evaluated for unwrapped and wrapped cylinders, as well as unwrapped and wrapped dental handpieces. Furthermore, the removal of air and the penetration of steam were investigated for different kinds of hollow loads (cavities). As mentioned above, the simulation model that was developed in this thesis is extremely versatile; it can be used for a variety of multiple applications in different kinds of steam sterilizers as well as for different kinds of loads.

The CFD model presented in this thesis is capable of simulating the inactivation of all bacteria types on the surface of all kinds of medical equipment. Furthermore, the air-removal and steam-penetration processes can be simulated inside any kind of medical equipment, as well as inside all kinds of commercially available helix tests. The deep numerical insight that this model provides into many relevant phenomena that occur during the steam sterilization process is of great interest to the developers of steam sterilizers.

2

Steam sterilization principles

This chapter provides a theoretical overview of certain aspects of the steam sterilization process. This overview includes the different types of steam sterilizer, the theoretical background that was used to calculate the inactivation of bacteria, the difficulty of the air-removal and steam penetration processes, and the different kinds of loads that can be sterilized. In this thesis, two different steam sterilizers were investigated: one benchtop vacuum steam sterilizer [31] and one benchtop non-vacuum (gravity displacement) steam sterilizer [32].

Generally in this PhD thesis, 'steam' refers to saturated steam, wet steam or slightly superheated steam, while 'water' refers to condensed steam or boiling water.

2.1 The steam sterilization cycle

Before a steam sterilization cycle begins, the steam sterilizer is loaded, e.g., with the medical instruments that need to be sterilized. After the door has been closed, the steam sterilization cycle itself can start. At the beginning of every steam sterilization cycle, the steam sterilizer contains both the load and ambient air at ambient conditions.

A steam sterilization cycle can generally be divided into three phases:

In the first phase of the steam sterilization cycle, referred to as the pre-sterilization phase, the ambient air inside the steam sterilization chamber must be removed and replaced with steam. There are different methods of steam sterilization that can be carried out according to norm [8]. This thesis considers a type B [31] vacuum steam sterilization cycle (see Section 2.1.1) and a type N [32] (gravity displacement) non-vacuum steam sterilization cycle (see Section 2.1.2). In both of these cycles, saturated

steam is fed into the sterilization chamber to remove the ambient air. This saturated steam partially condenses on the cold surfaces of the sterilization chamber as well as on the cold surface of the load. As a result, wet steam, condensed water, and air are present inside the sterilization chamber. In vacuum steam sterilization cycles, a vacuum pump is used to remove the air from the sterilization chamber. In non-vacuum steam sterilizers, the outlets are opened and saturated steam pushes the air out of the sterilization chamber. More information about the process of air removal inside vacuum and non-vacuum steam sterilizers is provided in Sections 2.1.1 and 2.1.2, respectively.

In the second phase, the actual sterilization takes place. First, the pressure and the temperature are increased to a pre-defined level in order to inactivate the bacteria. After this initial increase in pressure, the pressure and temperature are held constant for a set amount of time (holding time). To raise the pressure as well as to hold the pressure constant, saturated steam is permanently fed into the sterilization chamber. During this phase, only saturated steam, wet steam, condensate and the load are present within the steam sterilizer's chamber. A small amount of NCGs (air) may be present inside hollow loads (cavities). The saturated and wet steam condenses on all surfaces of the load (medical equipment) as well as on the surface of the sterilization chamber. As a result, very high heat transfer rates occur between the steam and the surface of the load. These high heat transfer rates mean that the load is homogeneously heated to nearly the same temperature as the saturated steam. The higher the load temperature, the faster the bacteria can be inactivated [33, 34]. As a result, the holding time depends on the sterilization temperature. An overview of different holding times as a function of the sterilization temperature is provided in Table 2.1 [8].

Table 2.1: Minimum holding time in the sterilization phase for different sterilization temperatures [8].

Sterilization temperature	Minimum holding time
121 °C	15 min
126 °C	10 min
134 °C	3 min
143 °C	1 min

During the third phase, referred to as the drying and cooling phase, the pressure within the steam sterilizer is reduced to very low levels; this is done using the vacuum pump for vacuum steam sterilizers or an externally cooled condenser for non-vacuum steam sterilizers. The purpose of this phase is to dry and cool the load. During this

phase, wet air, the load, and small amounts of unevaporated water are present inside the sterilization chamber. At the end of the third phase the steam sterilizer is filled with ambient air to guarantee a safe opening and un-loading of the steam sterilizer and a further cooling of the hot walls and the load.

2.1.1 Vacuum sterilization cycle

Vacuum steam sterilizers (type B) are frequently used to sterilize wrapped reusable medical instruments, such as forks, knives, scalpels, and dental handpieces. After the loading of the steam sterilizer, the steam sterilizer is filled with the load and air at ambient pressure and ambient temperature. In the course of the vacuum steam sterilization cycle, a vacuum pump removes the air from inside the steam sterilizer before the saturated steam enters. To ensure sterility at every point inside the sterilization chamber, high heat transfer rates are required. To achieve these high heat transfer rates, all of the air inside the steam sterilizer has to be removed. Hollow volumes and cavities are the most difficult shapes to penetrate with steam. Thanks to the vacuum pump, vacuum steam sterilizers are more effective when it comes to ensuring the steam penetration of hollow loads and cavities. The pressure reduction leads to a reduction of the total mass of the NCGs. As a result, it is easier to ensure the sterility of medical equipment using a vacuum steam sterilizer.

The working principle of a vacuum steam sterilizer is shown in Figure 2.1. The pressure trend during a typical vacuum steam sterilization cycle is shown in Figure 2.2.

At the beginning of the pre-sterilization phase, the vacuum pump reduces the pressure from ambient values (see ”ambient pressure” in Figure 2.2) to the minimum pressure (see ”minimum pressure” in Figure 2.2). Until this point, the steam sterilizer contains only air and the load. Once the minimum pressure has been reached for the first time, the steam generator feeds saturated steam into the sterilization chamber. The saturated steam that enters the sterilization chamber is partly needed to raise the pressure and the temperature, and partly to condense on the chamber’s walls, as well as the trays and the load. As a result, the inner walls of the steam sterilizer are heated up. Due to gravity, a large part of the condensed water is collected in the bottom region of the steam sterilizer. The steam generator stops feeding steam into the sterilization chamber when the pressure reaches the ”top pulse pressure” (see Figure 2.2). Afterwards the vacuum pump works at full power and the steam generator is switched off (see Figure 2.1(a)). The mixture (steam, condensed water and air) flows through a condenser as it exits of the sterilization chamber. Afterwards, the condensate

is collected in the used water tank. The vacuum pump stops when the pressure reaches the “minimum pressure” for the second time. In the sterilizer that was investigated in this work, such a vacuum pulse is repeated three times. In general, the pressure levels (minimum pressure and top pulse pressure) and the number of vacuum pulses can vary between different models of vacuum steam sterilizers.

The sterilization phase starts after the last (in this case, the third) vacuum pulse. All outlets are closed and the steam generator increases the pressure inside the steam sterilizer to the sterilization pressure (see ”pressure rise” in Figure 2.2). The saturated steam, which is fed into the sterilization chamber, is generated in a steam generator. In order to produce the steam, water is pumped from the fresh water tank to the steam generator (see Figure 2.1(b)). In the sterilization phase, hardly any air is present inside the steam sterilizer due to the fact that the air was removed in the pre-sterilization phase. Therefore, in this phase, the sterilization chamber contains only saturated steam, condensed water and the load. Due to condensation of the saturated and wet steam on the trays, load, and chamber walls, the time it takes to reach the sterilization pressure is mainly influenced by the mass of the load [16]. Once this point has been reached, the pressure and the temperature are held for the pre-defined holding time (see Table 2.1). To maintain a constant pressure within the sterilization chamber, the steam generator operates in a pulse mode. This is necessary because of ongoing condensation effects. The holding time is important in order to inactivate bacteria strains with a high thermal resistance. Therefore, in this phase of the steam sterilization cycle the main inactivation of the bacteria takes place.

The third phase starts after the defined holding time has elapsed. In this phase, the vacuum pump reduces the pressure to the minimum pressure (see Figure 2.2). The minimum pressure is held for a certain time. At pre-defined times, air at ambient temperatures is fed into the sterilization chamber to reduce the partial pressure of the water. During this low-pressure period, the evaporation of the condensed water takes place. As a result, the load is dehumidified. Due to the heat that is needed to evaporate the condensed water, the load is cooled by this process. At the very end of the steam sterilization cycle, the steam sterilizer is refilled with ambient air. Therefore, the pressure rises to ambient levels and the user can safely open the door.

Generally, at all times when the pressure decreases inside the steam sterilizer, the vacuum pump works at full power and the steam generator is switched off (see Figure 2.1(a)). Whenever the pressure is rising, the outlets are closed and the vacuum pump is switched off, the steam generator works at full power and feeds steam into the sterilization chamber (see Figure 2.1(b)). During the pre-sterilization phase and the

drying and cooling phases, a heater is used to heat up the walls of the steam sterilizer's chamber.

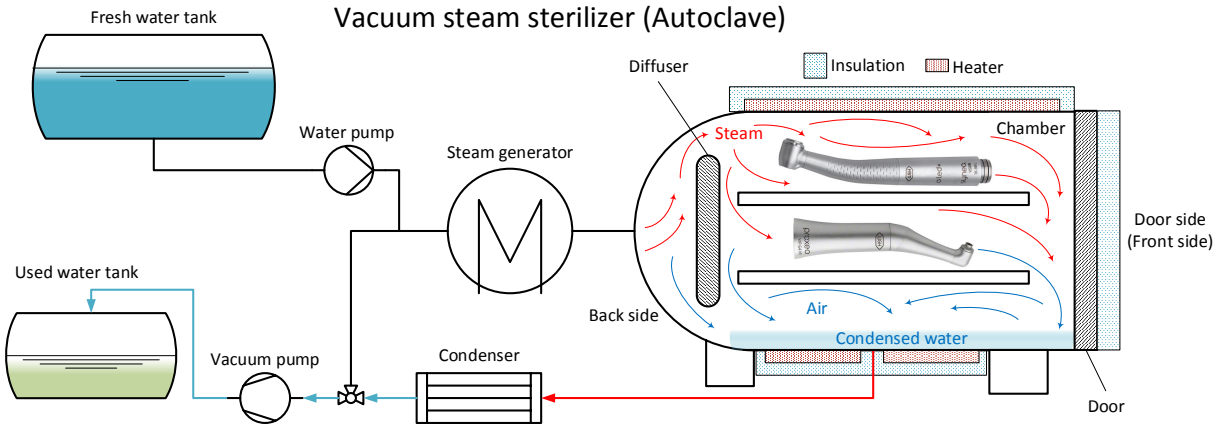

(a) Functional sketch of the working principle of a vacuum steam sterilizer in the pre-sterilization phase.

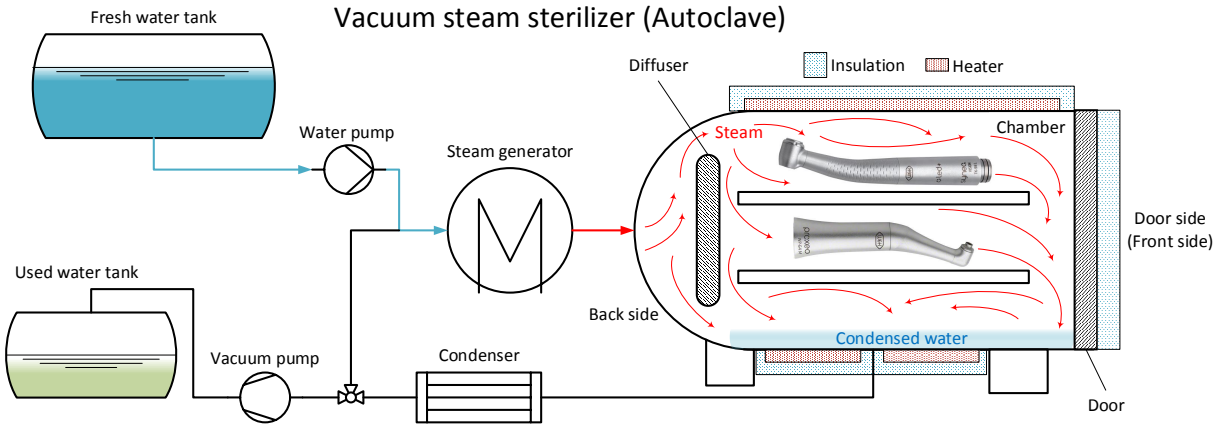

(b) Functional sketch of the working principle of a vacuum steam sterilizer in the sterilization phase.

Figure 2.1: Functional sketch of the working principle of a vacuum steam sterilizer in the (a) pre-sterilization phase and (b) sterilization phase.

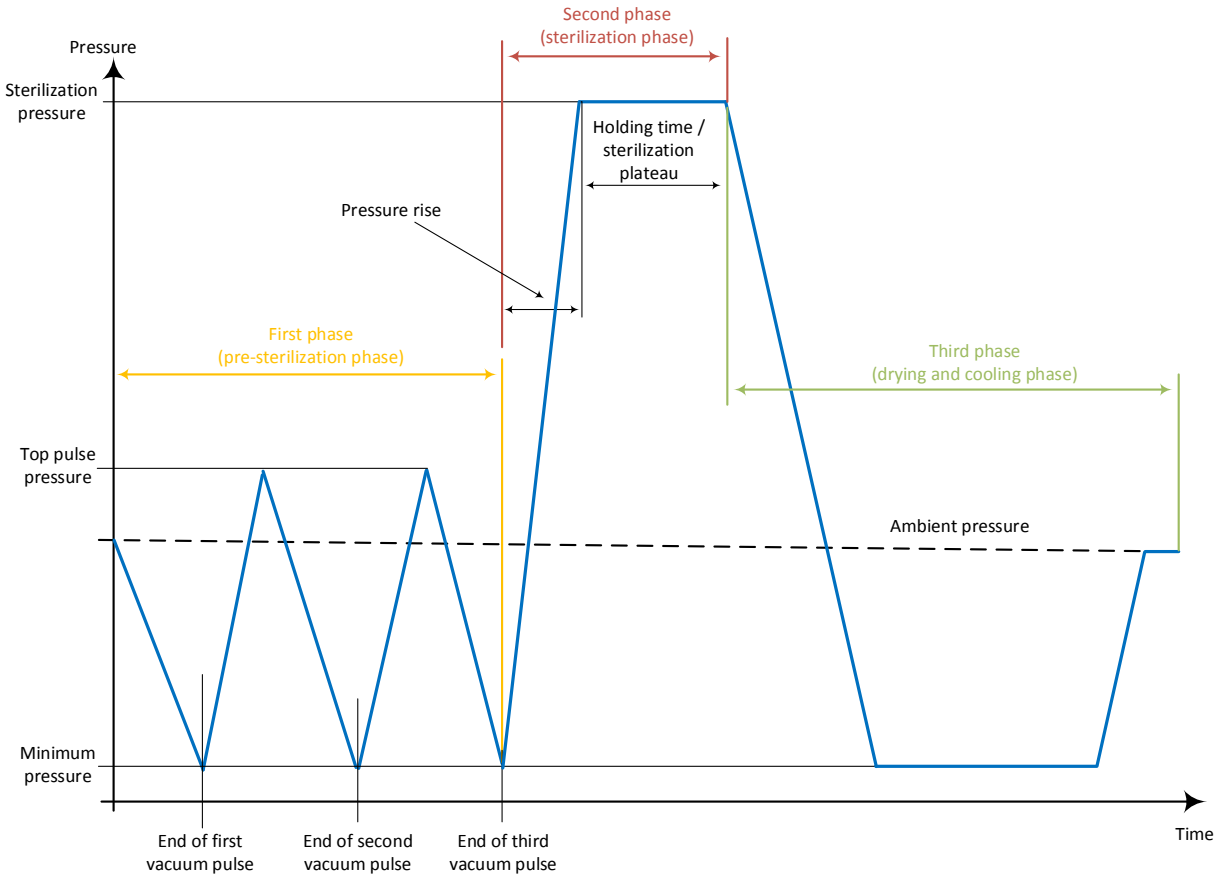

Figure 2.2: Pressure trend during a vacuum steam sterilization cycle.

2.1.2 Non-vacuum sterilization cycle

A non-vacuum steam sterilizer (gravity displacement, type N) is another frequently used instrument to sterilize medical equipment. Compared to the vacuum steam sterilization cycle described above, the main difference is, logically, that no vacuum is used during the pre-sterilization phase.

The working principle of the air-removal process in a non-vacuum steam sterilizer is shown in Figure 2.3. Figure 2.4 shows the pressure trend during a non-vacuum steam sterilization cycle.

At the beginning of the cycle, the steam sterilizer contains the load and air at an ambient pressure and temperature. In the pre-sterilization phase, the air is removed as it is displaced by the steam entering the steam sterilizer. Thus, in this case, the air-removal process occurs due to gravity. To release the air from the steam sterilizer's chamber, its outlet is opened. The steam generator works at full power and feeds saturated steam into the sterilization chamber. The water for the steam production flows through the water pump to the steam generator. Afterwards, the steam generator evaporates the water to saturated steam. The entering steam is partially mixed with

the air in the sterilization chamber, partially condenses on the cold walls, and partially exits out of the sterilization chamber through the outlet pipe (see Figure 2.3). In the pre-sterilization phase, saturated and wet steam, condensed water, and air are present in the sterilization chamber. The exiting mixture (steam, water and air) flows through the outlet pipe to a condenser. After the condenser, the condensed steam and the water flow to the used water tank. By opening and closing the outlet valve, the pressure during the pre-sterilization phase is varied between the ”maximum pulse pressure” and the ”minimum pulse pressure” (see Figure 2.4). In this regard, the main difference of the non-vacuum from the vacuum steam sterilization cycle is that the minimum pulse pressure is determined by the atmospheric pressure. During the pre-sterilization phase, the heater, which is mounted on the outside of the chamber, is used to heat up the steam sterilizer's chamber.

After the pre-sterilization phase, the outlet is closed and the sterilization phase begins. In the sterilization phase, hardly any air (NCGs) is present inside the steam sterilizer. The steam generator feeds steam into the steam sterilizer to increase the pressure to the sterilization pressure (see ”pressure rise” in Figure 2.4). Afterwards, the pressure and the temperature are held constant for a pre-defined length of time (see ”holding time / sterilization plateau” in Figure 2.4). To achieve constant temperatures and pressures during the holding time, steam is constantly being partially fed into the sterilization chamber in order to compensate for the ongoing condensation effects. The sterilization phase of the non-vacuum steam sterilization cycle is very similar to the sterilization phase of the vacuum steam sterilization cycle (see Section 2.1.1).

In the drying and cooling phase, the pressure is reduced to the ambient pressure (see blue line in Figure 2.4) or to lower pressures. The pressure reduction to lower pressures happens with an externally cooled condenser (see dashed blue line in Figure 2.4). In order to dry the load, a heater heats up the walls of the steam sterilizer's chamber and dries the load by means of radiation and convection. In the drying phase, ambient air is partially fed into the sterilization chamber to reduce the partial pressure of the steam. As a result, more water evaporates and, therefore, cools down the load. At the end of the non-vacuum sterilization cycle, the sterilization chamber is filled with ambient air to guarantee that the door of the non-vacuum steam sterilizer can safely be opened.

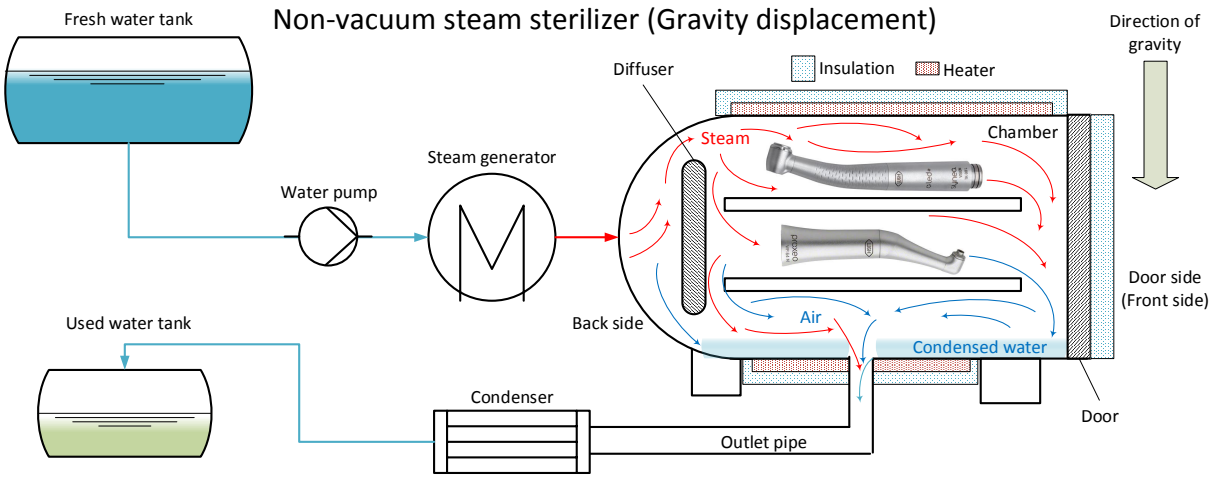

Figure 2.3: Working principle of a non-vacuum steam sterilizer during air-removal in the pre-sterilization phase.

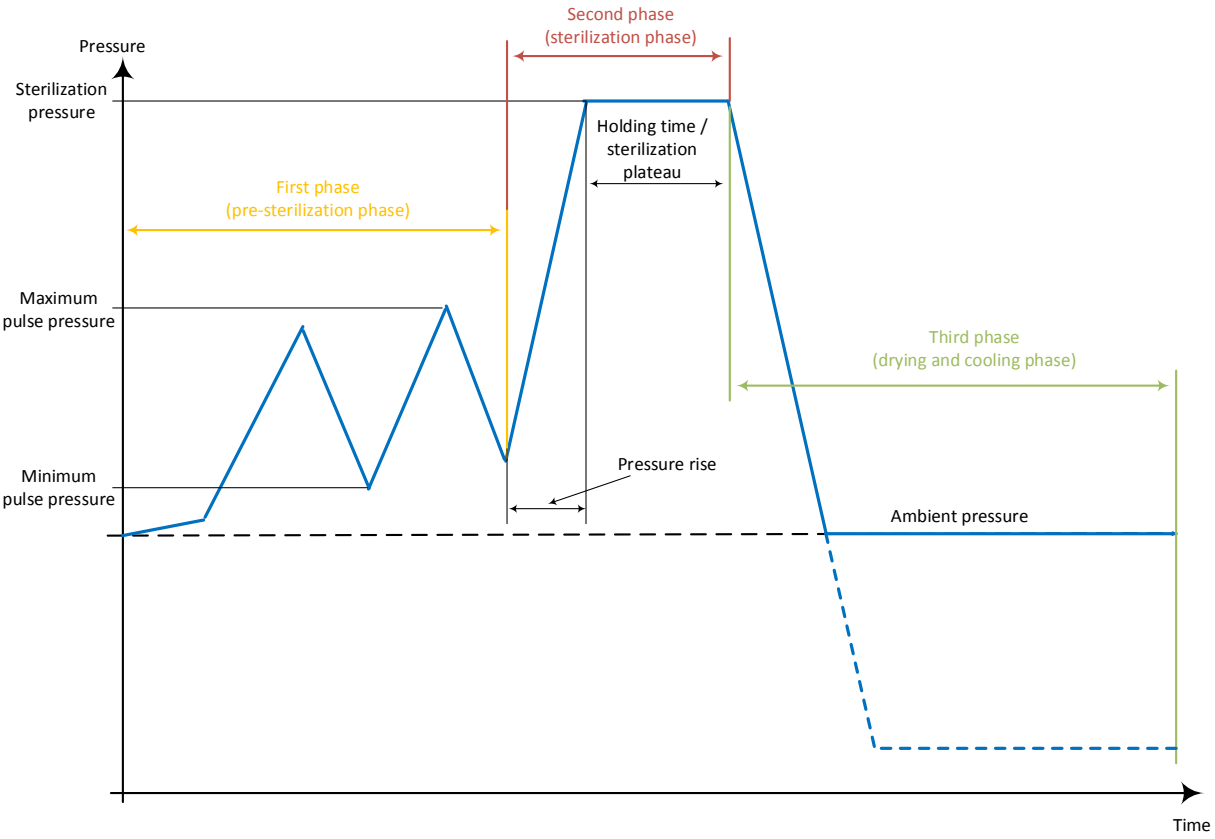

Figure 2.4: Pressure trend during a non-vacuum (gravity displacement) steam sterilization cycle.

2.2 Inactivation of bacteria

This section presents the theoretical background of how the inactivation of bacteria takes place within steam sterilizers. The variables which are used to describe the steam sterilization process and the resistance of the bacteria, such as the F_0-value, D-value, and z-value are described in this section as well.

2.2.1 First-order reaction kinetic approach

The inactivation of bacteria by means of steam autoclaving follows an exponential decrease curve. For steam sterilization processes, the inactivation of bacteria can be modelled with a first-order kinetic approach (see Eq. (2.1)) [33, 35].

$$\frac{dN}{dt} = -k_d(T) \cdot N \tag{2.1}$$

where N stands for the current number of bacteria, $k_d(T)$ is the inactivation rate of the bacteria for a given temperature (T), and t is the sterilization time. Eq. (2.1) was integrated to get the final equation to model the inactivation of different types of bacteria (Eq. (2.2)):

$$N = N_0 \cdot e^{-k_d(T) \cdot t} \tag{2.2}$$

where N_0 is the initial number of the bacteria at the time ($t = 0\ s$). In the past, many researchers have demonstrated that a first-order reaction kinetic approach is able to predict the inactivation of bacteria by steam sterilization [36, 37].

2.2.2 Arrhenius equation

The rate of bacteria inactivation is usually modelled with the Arrhenius equation (see Eq. (2.3)) [38].

$$k_d(T) = k_{d0} \cdot e^{\frac{-E_d}{R \cdot T_{(t)}}} \tag{2.3}$$

where k_{d0} is the pre-exponential factor, E_d is the activation energy, R is the universal gas constant ($R = 8.3144598 \frac{kJ}{kmol \cdot K}$) and $T_{(t)}$ is the temperature at a given time t.

2.2.3 D-value and z-value

The resistance of bacteria can also be described by the D-value and the z-value. The D-value represents the exposure time (in minutes), which is needed to reduce 90 % of the bacteria at a given temperature (T) [39]. The smaller the D-value, the faster the inactivation of the bacteria takes place. Generally, each bacteria type has its own specific D-value for steam sterilization. Figure 2.5(a) shows the definition of the D-values for the thermal-death curves of a specific bacteria type at 111 °C and 121 °C. The horizontal black dashed lines in Figure 2.5(a) represent 1 log-reduction of the active bacteria. The D-value for 111 °C is the time which is needed to reduce 1 log-value of the active bacteria at this temperature (see horizontal distance between the vertical blue dashed lines in Figure 2.5(a)). The distance between the vertical red dashed lines in Figure 2.5(a) shows the D-value for the same bacteria type for 121 °C. Usually, the higher the temperature, the lower the D-value. The D-value is only given for one specific temperature and one specific bacteria type.

To model the inactivation rate (k_d) the Arrhenius equation is usually used (see Eq. (2.3)). Eq. (2.4) presents a simple correlation between the D-value and the inactivation rate (k_d) [40]. Eq. (2.4) calculates the D-value in seconds. More information about Eq. (2.4) and the correlation between the D-value and the inactivation rate (k_d) can be found in literature [41, 42].

$$D = \frac{2,303}{k_d} \tag{2.4}$$

The temperature dependency of the D-value is determined and described with the z-value. The z-value describes how the inactivation of bacteria changes with changes in the temperature. Mathematically, the z-value is defined as the number of degrees (in Celsius) the temperature has to be increased to achieve a reduction of the D-value by a factor of 10 or 1 log-in step. The z-value describes the temperature dependency of the D-value for one specific type of bacteria. The definition of the z-value for a given thermal resistance curve is shown in Figure 2.5(b). The D-value is shown on the y-axis, while the x-axis shows the temperature in degrees Celsius. The vertical distance between the two black dashed horizontal lines represent a reduction of the D-value by

a factor of 10. The two vertical dashed blue lines start at the interception point between the black dashed horizontal lines and the thermal resistance curve. The horizontal distance between these lines represents the z-value.

To get a better understanding of the D-value and the z-value, Table 2.2 shows these values for the bacteria types *Geobacillus stearothermophilus*, *Bacillus subtilis*, *Bacillus megaterium* and *Colstridium sporogenes*.

Table 2.2: D-value and z-value for different types of bacteria [37].

Bacteria type	**D-value in min for 115 °C (D_{115} °C)**	**D-value in min for 121 °C (D_{121} °C)**	**z-value in °C**
Geobacillus stearothermophilus	15 - 24	1,5 - 4,0	6 - 7
Bacillus subtilis	2,2	0,4 - 0,7	8 - 13
Bacillus megaterium	0,025	0,04	7
Clostridium sporogenes	2,8 - 3,6	0,8 - 1,4	13

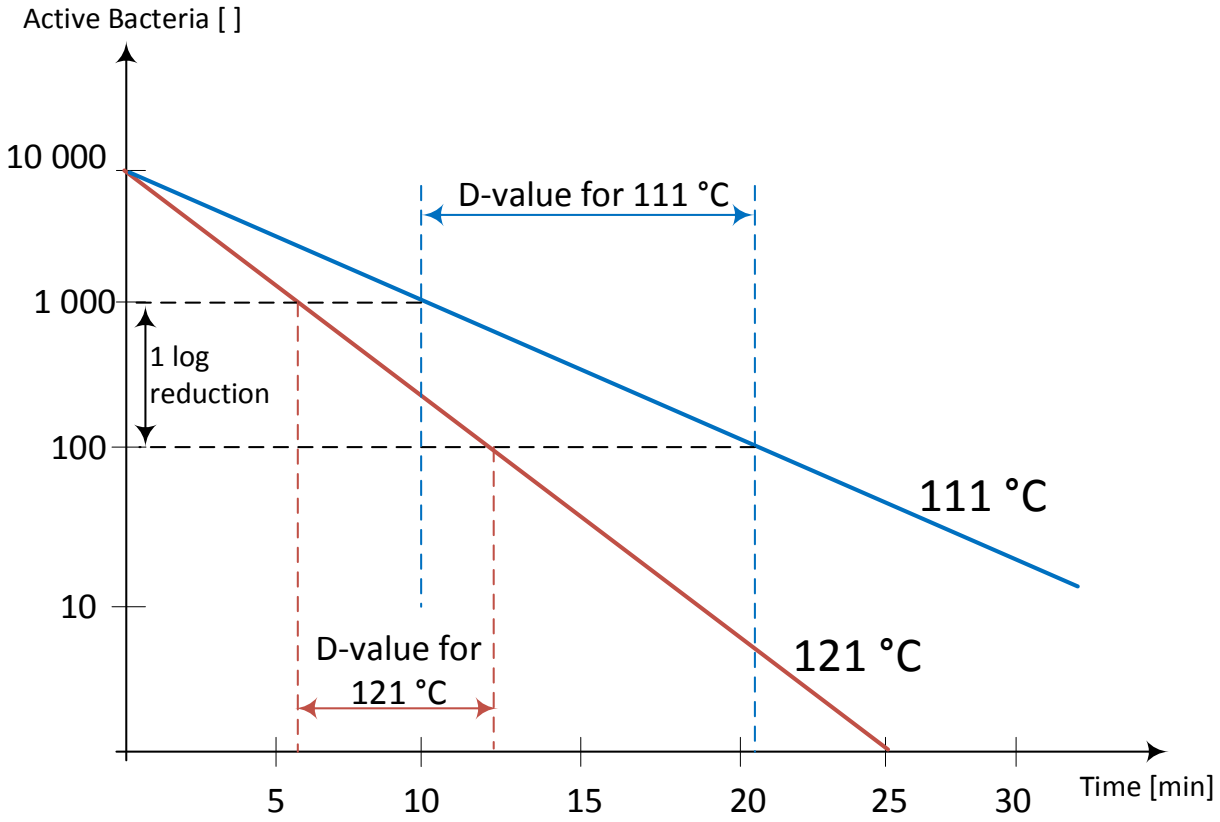

(a) Thermal-death curves for two temperatures with the definition of the D-value for 121 °C and 111 °C.

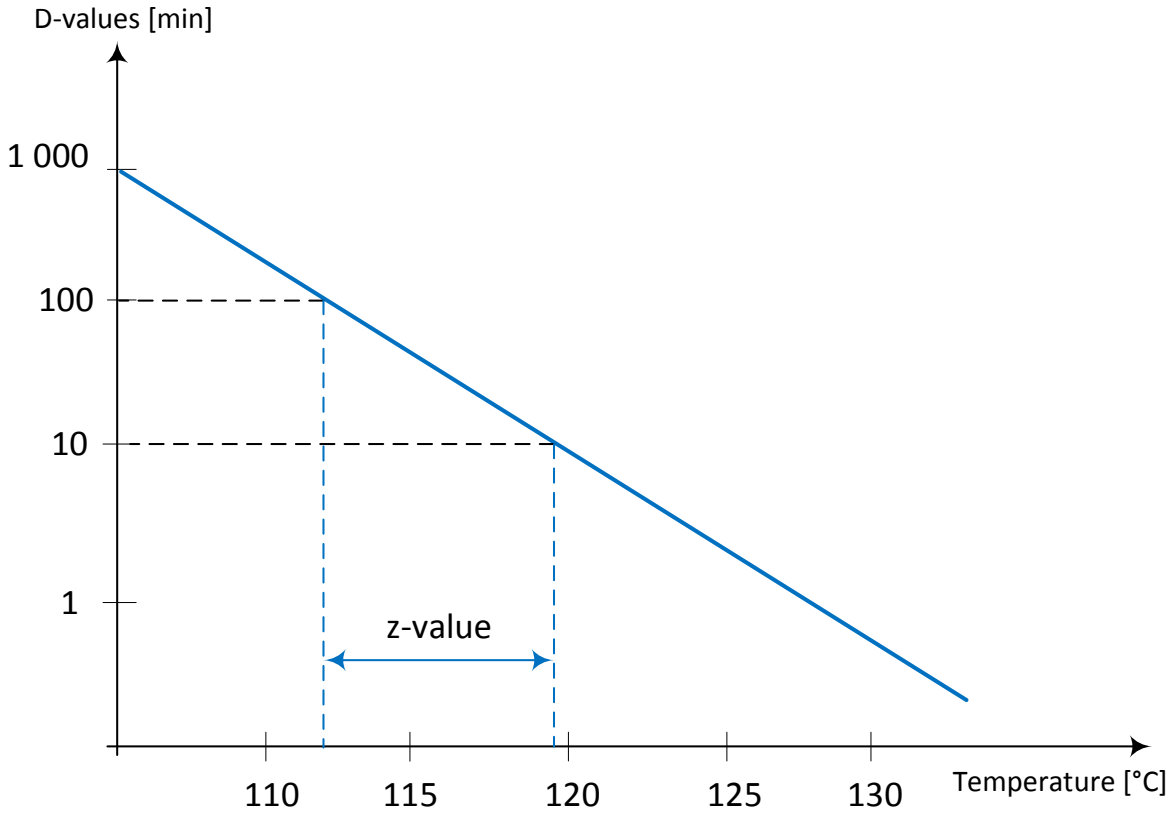

(b) Thermal resistance curve for bacteria with the definition of the z-value.

Figure 2.5: (a) Thermal-death curves with the definition of the D-value and (b) a thermal resistance curve with the definition of the z-value.

2.2.4 F_0-value

The F_0-value is defined as the number of equivalent minutes of a steam sterilization process delivered to a product, compared to a steam sterilization at a constant temperature of 121.1 °C. The higher the F_0-value the higher the theoretical inactivation of bacteria during the sterilization process. The F_0-value is often specified as a reference for many processes in the steam sterilization industry [43]. The equation to calculate the F_0-value on the surface of medical equipment is given by Eq. (2.5),

$$F_0 = \int_{t_0}^{t_n} 10^{\left(\frac{T_{wall}-121.1}{z}\right)} \tag{2.5}$$

where T_{wall} is the surface wall temperature (in degrees Celsius) of the medical equipment, t_0 and t_n are the times when the sterilization process starts and ends, respectively. In this thesis, the count for the F_0-value starts when the temperature is over 100 °C due to the fact that exposure to temperatures below 100 °C has hardly any influence on the inactivation of temperature-resistant bacteria. All F_0-values were calculated according to the norm for a reference z-value of 10 °C [8]. More information about F_0-values can be found in literature [44–46].

2.2.5 Log-reduction and SAL

The inactivation log ratio of the investigated bacteria type was calculated as the number of surviving bacteria for a given time after sterilization (N) to the number of the bacteria at the beginning of the steam sterilization process (N_0), as shown in Eq. (2.6).

$$inactivation\ log\ ratio = log\frac{N_0}{N} \tag{2.6}$$

Furthermore the log survival ratio can be used to calculate the inactivation of bacteria. The log survival ratio is defined by dividing the current number of bacteria (N) by the initial number of the bacteria before the sterilization process (N_0) (see Eq. (2.7)).

$$log\ survival\ ratio = log\frac{N}{N_0} \tag{2.7}$$

The difference between the inactivation log ratio and the log survival ratio is simply that the inactivation log ratio is a positive value whereas the log survival ratio is a

negative one. An inactivation log ratio of 14 represents a log survival ratio of -14 and vice versa.

The Sterility Assurance Level (SAL) describes the probability that an item is not sterile. Generally, a SAL of 10^{-6} is required; this represents the probability that one in a million items is not sterile. Due to the fact that no inactivation log ratio higher than six or a log survival ratio lower than minus six can be measured using spore stripes, an inactivation log ratio of 12 or higher, or a log survival ratio of -12 or lower, is required to achieve a SAL of 10^{-6}.

2.3 Steam specification

During a steam sterilization cycle, the steam conditions inside the steam sterilizer are constantly changing. Furthermore, the fluids inside the steam sterilizer can be removed or fed to the sterilization chamber. This section provides a theoretical overview of the different types of steam that can be present during a steam sterilization cycle.

2.3.1 Superheated steam

Superheated steam is steam that has a higher temperature than its saturation temperature at the current pressure. This means that superheated steam can lose some energy (e. g., due to convective heat transfer) without condensing [47]. Superheated steam has significantly lower heat transfer rates compared to saturated steam, which condenses on cold walls [48]. Therefore, superheated steam is not suitable for steam sterilization [49]. Dry heat (superheated steam) requires higher temperatures to inactivate the bacteria or to generate the same F_0-values [50].

2.3.2 Saturated steam and wet steam

Saturated steam and wet steam represent steam at the saturation temperature for the current pressure. Under these conditions, water and steam can co-exist. Saturated and wet steam condense as soon as they come into in contact with cold walls. The heat transfer rates that can be achieved depend on the steam quality inside the steam sterilizer, especially near the load. Generally, high steam qualities lead to high heat

transfer rates due to condensation [51–53]. The steam quality (x) is defined by dividing the mass of the saturated steam through the mass of the wet steam (see Eq. (2.8)).

$$x = \frac{m_{saturated\ steam}}{m_{wet\ steam}} = \frac{m''}{m' + m''} \tag{2.8}$$

where $m_{saturated\ steam}$ stands for the mass of the saturated steam, $m_{wet\ steam}$ stands for the mass of the wet steam, m' stands for the mass of the boiling liquid, and m'' represents the mass of the saturated steam that is in the thermodynamic equilibrium. Saturated steam is steam with a steam quality of one ($x = 1$), while wet steam is steam with a steam quality between 0.01 and 0.99 (> 0 and < 1). According to the norm, the steam at the inlet of the steam sterilizer should have a steam quality of 0.975 or higher [8].

It is very difficult to measure steam quality inside the steam sterilizer. Therefore, in this thesis, the steam quality was investigated using CFD. With the CFD model that was developed in this work, the steam quality was investigated in the steam sterilizer's chamber as well as near different kinds of loads. Per its definition, the steam quality can only be calculated when saturated steam and wet steam are both present inside the steam sterilizer. Therefore, in this thesis, the steam quality was calculated during the sterilization phase of the two investigated steam sterilization cycles (see Figure 2.2 and Figure 2.4).

2.3.3 Steam-air mixture

As described in Section 2.1, in the pre-sterilization phase, not only steam, but a mixture of steam, condensed water, and NCGs (air) is present within the sterilization chamber. In a mixture with three different fluids, it is not possible to calculate the steam quality (see Section 2.3.2).

Due to the fact that the heat transfer that occurs from the hot steam to the load due to condensation effects is mainly influenced by the presence of NCGs (air) [54–58], it is important to analyse the spatial distribution of NCGs inside the sterilization chamber. To this end, the mass fraction of the saturated steam (μ_{steam}) (shown in Eq. (2.9)) can be considered:

$$\mu_{steam} = \frac{m_{saturated\ steam}}{m_{wet\ steam} + m_{air}} = \frac{m''}{m' + m'' + m_{air}} \tag{2.9}$$

where $m_{saturated\ steam}$ stands for the mass of the saturated steam, $m_{wet\ steam}$ stands for the mass of the wet steam, and m_{air} stands for the mass of the air. If the NCGs (air) are completely removed from the sterilization chamber, the mass fraction of the steam (μ_{steam}) is equal to the steam quality (x).

Furthermore, the volume fraction of the saturated steam (ϕ_{steam}) can also be investigated (see Eq. (2.10)).

$$\phi_{steam} = \frac{V_{saturated\ steam}}{V_{total}} = \frac{V''}{V' + V'' + V_{air}} \tag{2.10}$$

where $V_{saturated\ steam}$ stands for the volume of the saturated steam inside the sterilization chamber, V_{total} stands for the total volume, $V^{'}$ stands for the volume of the boiling liquid, $V^{''}$ stands for the volume of the saturated steam which is in the thermodynamic equilibrium, and V_{air} stands for the volume of the air (NCGs).

2.3.4 Condensed water

Condensed water can have a negative impact on the heat transfer rates [59–61]. Condensed water is inherently present when steam enters the sterilization chamber due to condensation. At times when the pressure decreases, some condensed water evaporates again. This effect is utilized in both the drying and cooling phases of the sterilization cycle.

To explore the extent of this impact, in this thesis, both wrapped and unwrapped load were used so as to consider influence of condensed water near the surface of the load, on the surface temperature, and on the inactivation of bacteria.

2.4 Air-removal and steam penetration

High surface temperatures on the medical equipment are beneficial to inactivate all types of bacteria (see Eq. (2.2) and Eq. (2.5)). To reach these high surface temperatures, high heat transfer rates are needed, and these high heat transfer rates occur due to condensation effects. In the past, many studies have shown that the heat transfer rates that occur due to condensation decrease in the presence of NCGs (air) [27, 62–66]. As a result, all the NCGs present inside the steam sterilizer at the beginning of the steam sterilization cycle must be removed from the steam sterilizer's chamber as well

as from all hollow spaces (cavities) within the medical equipment. During the air-removal process (pre-sterilization phase), steam, water, and NCGs (see Section 2.3.3), are contained within the sterilization chamber.

2.4.1 Air-removal from the steam sterilizer's chamber

All of the ambient air (NCGs) present inside the sterilization chamber at the beginning of the sterilization cycle has to be removed and replaced with steam before the sterilization phase begins in order to guarantee that effective sterilization can take place [11, 12, 50, 67]. To remove the air from the steam sterilizer's chamber, different working principles can be used [8]. In this thesis, both a vacuum- and a non-vacuum steam sterilizer were investigated. The air-removal procedures of both the vacuum and non-vacuum steam sterilizers were described in Section 2.1.1 and Section 2.1.2.

During the sterilization plateau, international norms demand that the volume of NCGs is below 3.5 % of the total mixture of the fluids [8]. The mixture of fluids consists of steam, condensed water, and NCGs (air). The normalized measurements require a randomly chosen break in the sterilization cycle during the sterilization plateau. During this break, the measurement is taken by analysing the fluid mixture exiting the sterilizer's outlet. The exiting steam is condensed by an external condenser followed by a quantitative comparison between the volumes of condensed water and condensed steam (liquid) and the volume of the NCGs (gaseous). A detailed description of the procedure used to measure the ratio of the NCGs as well as the volumes for considered these measurement can be found in Section 3.5 of this thesis. According to the definition of the norm, a gas volume is compared with a liquid volume. Therefore, the real volume fraction of NCGs is significantly lower compared to the content of the NCGs as defined by the norm. In this thesis, a new approach was developed to calculate the real volume fraction of the NCGs out of the measurements, according to EN 13060 [8]. A detailed description of that approach can be found in Section 3.6.

2.4.2 Air-removal and steam penetration in hollow loads (cavities)

To guarantee high wall temperatures, and, therefore, high heat transfer rates in all hollow volumes during the steam sterilization cycle, the air must be removed and the steam must penetrate all hollow volumes (cavities). Helix tests are normally used to investigate air removal and the steam penetration. A helix test is a specific type of a

PCD used to investigate air-removal and steam penetration in thin tubes. For small steam sterilizers, this is a standardized test required by EN 13060. According to EN 13060, the helix must have a length-to-internal diameter ratio of $\geq 750 : 1$, with a maximum length of 1500 mm [8]. Many different types of PCDs are available on the market [68]. In this thesis, two different types of helix tests were investigated, both experimentally and numerically (see Section 3.7 and Section 5.6).

2.5 Different types of loads

This section provides an overview of the different kinds of loads that can be sterilized in a steam steriliser. Solid loads can be wrapped or unwrapped. Helix test are required to investigate the steam penetration and the air-removal in hollow loads (cavities). Finally, the load can be porous, for example, textile equipment.

2.5.1 Solid unwrapped loads

Unwrapped solid loads are one of the most common types of load to be sterilized in steam sterilizers. Examples of solid loads include knives, scalpels, glassware, surgical instruments, and machine parts. For all of these loads, the steam is in direct contact with the load. Therefore, the steam is responsible for heating the load as well as for sterilizing the load. Figure 2.6 shows dental handpieces, an example of an unwrapped solid load. According to the norm, screws can also be used to measure the influence of the load on the steam sterilization process [8]. In this thesis, unwrapped cylinders and unwrapped dental handpieces were investigated.

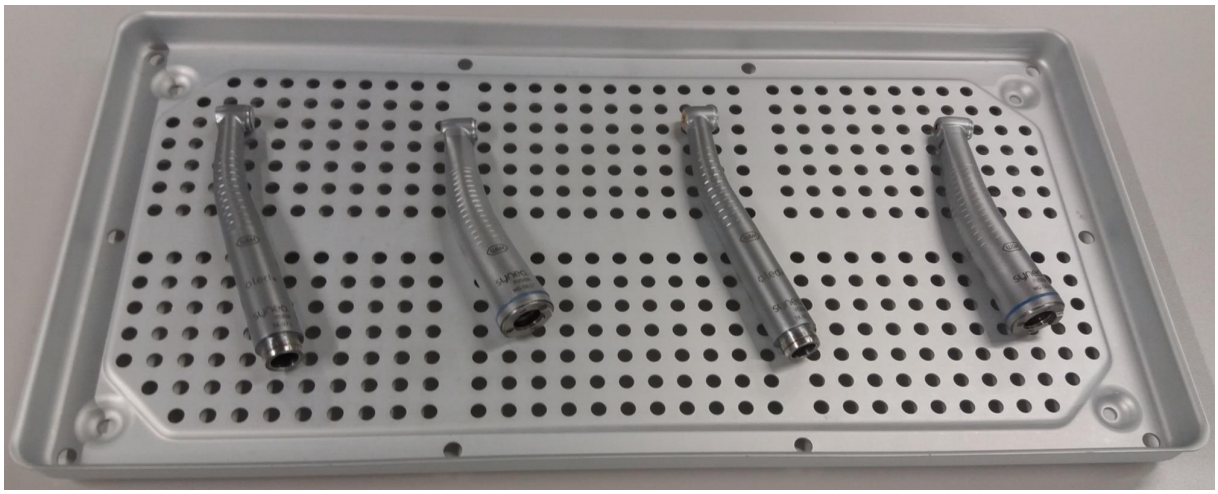

Figure 2.6: Picture of a typical unwrapped load of dental handpieces on an aluminium tray.

2.5.2 Solid wrapped loads

In order to store or transport solid loads, pieces of medical equipment are often placed in pouches to guarantee sterile conditions [69]. Such pouches may consist of different materials. In this thesis, the wrapping of the load made of a specific paper, on one side, and of a plastic foil, on the other side [70]. Wrapped dental handpieces are visible with the plastic foil in Figure 2.7(a), whereas wrapped dental handpieces with the paper visible are shown in Figure 2.7(b). In the steam sterilizer investigated [31], placing the wrapped load in the steam sterilizer with the paper visible is recommended for the sterilization process. This paper represents only a flow resistance as the wet and saturated steam reaches the load, whereas the plastic foil is impermeable to the steam. The paper is also a flow resistance for the air (NCGs) near the load. Furthermore, the paper is a huge flow resistance to the condensed water. This condensed water forms when saturated or steam flows through the paper and condenses on the surface the load. The condensed water has to be evaporated in order to remove it from the inside of the pouch (during the drying and cooling phase). To determine the permeability of the paper, a test rig was developed (see Section 3.4). The influence of the paper on the steam quality, the load temperature, and the inactivation of the bacteria was investigated as well (see Section 5.4).

(a) Wrapped dental handpieces on an aluminium tray with the plastic foil visible (on the top).

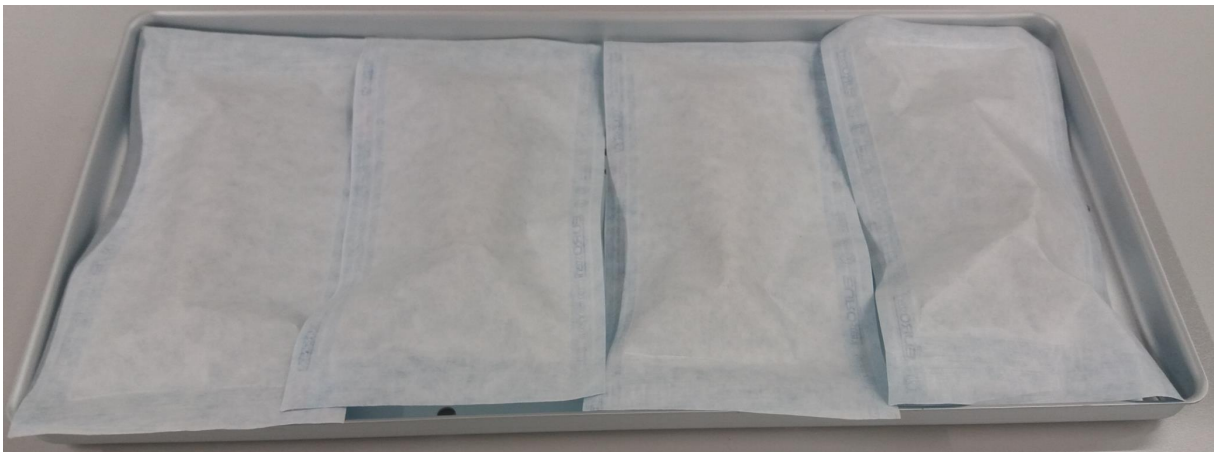

(b) Wrapped dental handpieces on an aluminium tray with the paper visible (on the top).

Figure 2.7: (a) Wrapped dental handpieces on an aluminium tray with the plastic foil visible (on the top) and (b) Wrapped dental handpieces on an aluminium tray with the paper visible (on the top). Position (b) is recommended to sterilize medical equipment inside the investigated steam sterilizer.

2.5.3 Liquid loads

Liquid loads also present a common sterilization issue. The main difference between liquid loads and solid loads is that the steam comes into direct contact with a solid load, whereas the steam only comes into indirect contact with a liquid load, due to the fact that a material is between the steam and the liquid in order to prevent leakage. Generally, the materials used for this purpose include glass and plastic foils. In the case of liquid loads, the steam is only used to heat the liquid load, rather than for sterilization itself. Figure 2.8 shows a dialysis bag as an example of a liquid load. Other examples include infusions and filled laboratory glassware. More information about liquid loads can be found in [43, 71, 72]. Liquid loads were not investigated in the course of this thesis.

Figure 2.8: Picture of dialysis bag as an example of a liquid load.

2.5.4 Porous loads

The sterilization of porous loads is achieved through direct contact with the steam. The heat transfer takes place when the steam condenses on the surface of the porous items. Before the porous load can be sterilized, all air (NCGs) has to be removed from its pores. To this end, a vacuum steam sterilizer uses vacuum pulses (as described in Section 2.1.1). After the removal of the NCGs, it is easier for the steam to diffuse into the pores inside the porous load. There, the steam condenses on the cold surfaces of the pores and heats up the porous load. This heating process is is beneficial for the

inactivation of all kinds of bacteria (see Eq. (2.3) and Eq. (2.5)). Due to the fact that it is very difficult for steam to penetrate all of the pores of porous loads, and because they are usually not very heat resistant, porous loads are typically sterilized at 121 °C with a holding time of 20 min [8]. Figure 2.9 shows towels as an example of a porous textile load. Other examples of porous loads include filters, cloths, and cleaning equipment. Additional information on the sterilization of porous loads can be found in [43, 73, 74]. Porous loads were not investigated in the course of this thesis.

Figure 2.9: Picture of towels as an example of a porous load.

2.5.5 Helix tests (PCDs)

A PCD is a process challenge devise that is used as a functional control of the air-removal and the steam penetration of the steam sterilizer. In large steam sterilizers, the Brownie and Dick test [12] is used in order to measure air-removal and steam penetration. Helix tests are predominantly used in the field of dentistry, due to the fact that medical instruments come in direct contact with the patients' blood; therefore, it is necessary to protect subsequent patients from contamination by ensuring that such tools are adequately sterilized. In order to guarantee that the effective sterilization of various instruments, including hollow loads, has taken place, helix tests are used to check if the steam sterilizer is able to penetrate steam through the length of a lumen or a small tube (cavities). Generally, helix tests can be divided into two types [8, 75]:

- Type A: This type of test considers small devices, including wands and turbines. The helix test can be done on a one-side open tube, with a length-diameter ratio between $1 \leq L/D \leq 750$ and a tube-length of no longer than 1500 mm. The tube can also be open on both sides. In this case, the length-diameter ratio must be between $2 \leq L/D \leq 1500$. The maximum length must be smaller that 3000 mm.
- Type B: This type of test considers tips and tubes. The helix test can be open on one side or on both sides. The length-diameter ratio for the one-side open helix must be between $1 \leq L/D \leq 5$. The length-diameter ratio when both sides are open must be between $2 \leq L/D \leq 10$. In both cases, the diameter of the tube must be equal to or greater than 5 mm.

Figure 2.10 shows two different examples of Type A helix tests. There are a wide variety of helix tests available on the market [68]. In this thesis, two different types of Type A helix tests were investigated experimentally, using two different types of chemical indicators (see Section 3.7). Furthermore, both the air-removal and the steam penetration were investigated using CFD (see Section 5.6).

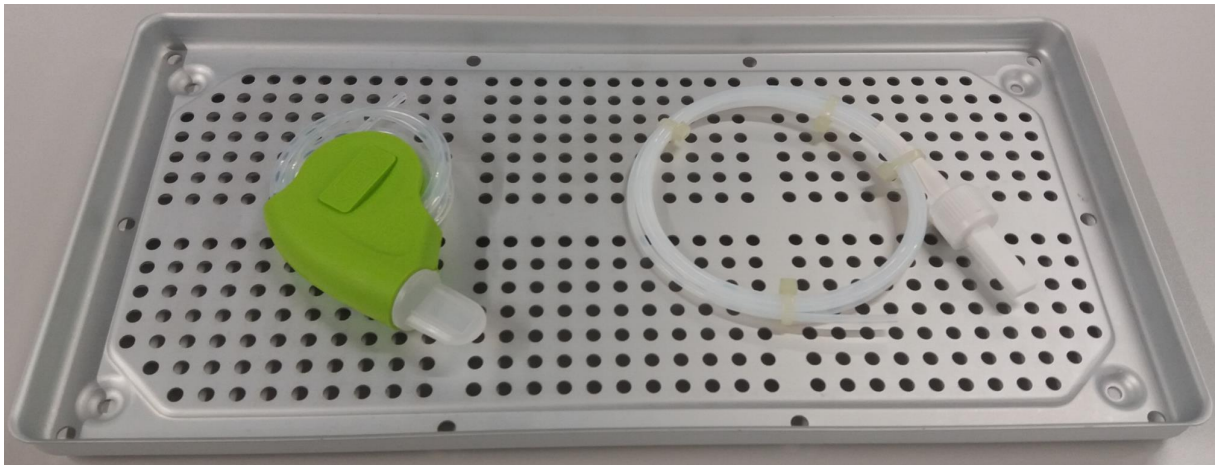

Figure 2.10: Picture of two helix tests: (left) a typical Type A helix test with a tube diameter of 2 mm and a 1500 mm long tube and (right) another type of a Type A helix test with the same dimensions. Both PCDs are in accordance with [75].

3
Experimental set-up

This chapter provides insight into all of the experimental work that was carried out for this thesis. It describes the procedures that were followed to measure the pressures, fluid temperatures, load temperatures, and the mass flow rate of the steam generator. A test rig was built to measure the permeability of the paper in which the load may be wrapped during the sterilization process. Furthermore, it describes the experimental set-up that was used to measure the NCGs inside the steam. Finally, this chapter presents the experimental set-up that was used to evaluate the air-removal inside hollow loads (cavities).

3.1 Experimental set-up to measure the pressure and the fluid temperature [1]

It is necessary to obtain transient measurement data of both the fluid temperature and the pressure during vacuum- and non-vacuum sterilization cycles in order to validate the CFD results. In this thesis, these measurements were performed using eight thermocouples and one pressure sensor. In this section, the positions of the eight thermocouples and the pressure sensor inside the steam sterilizer are described. Individual measurements of the fluid temperature and the pressure inside the steam sterilizers were performed for each type of investigated load. In all of these tests, the pressure sensor and the thermocouples remained in the same positions.

[1] Segments of this section have already been published in [1–5].

3.1.1 Measurement of the pressure and the fluid temperature inside a vacuum steam sterilizer

The measurement data were obtained using a commercially available benchtop vacuum steam sterilizer [31]. To measure the fluid temperature inside the vacuum steam sterilizer, eight type J thermocouples were placed at different positions within its chamber (see T1 - T8 in Figure 3.1). The pressure inside the steam sterilizer was measured with one pressure sensor (see p in Figure 3.1). The pressure sensor has an accuracy of $\pm$ 0.75 %. The complete measurement set-up, including the positions of all of the thermocouples (T1 - T8) and the pressure sensor (p) for the sterilization cycle with a helix test can be seen in Figure 3.1.

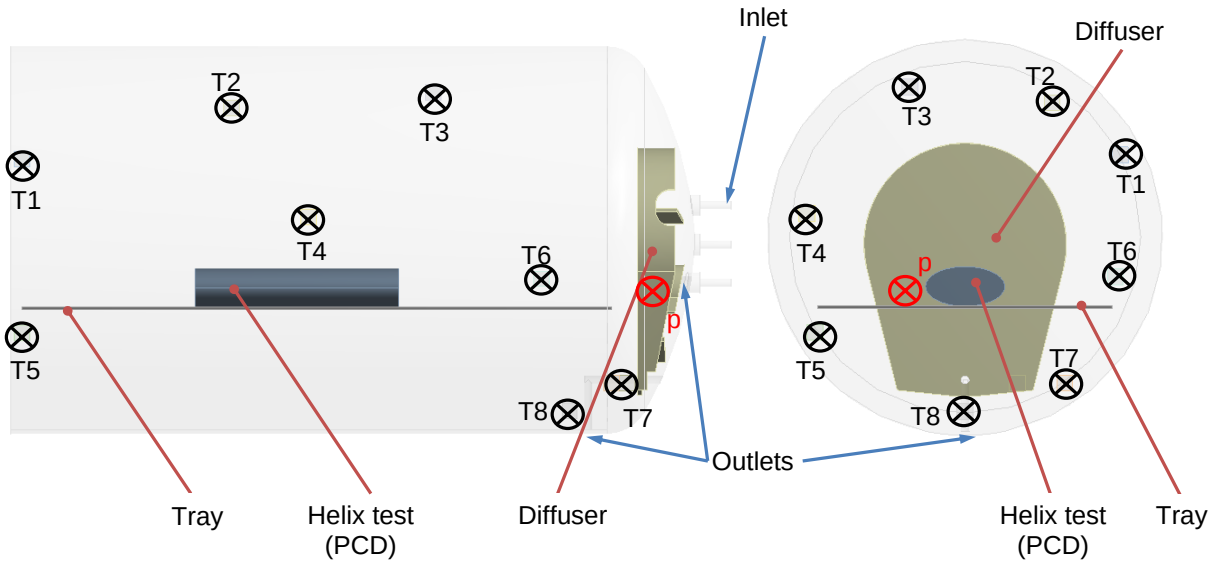

Figure 3.1: Geometry of the vacuum steam sterilizer with the positions of the eight thermocouples (T1 to T8) and the pressure sensor (p) [2].

The vacuum steam sterilizer considered in this investigation has a cylindrical shape and a volume of 22 litres. The chamber of the steam sterilizer has a diameter of approximately 250 mm and a length of approximately 430 mm. A diffuser is mounted on the back wall of the steam sterilizer to distribute the steam within the steam sterilizer. The inlet is located at the back of the chamber. One of the steam sterilizer's outlets is located behind the diffuser, while the other outlet is located at the bottom in front of the diffuser. The positions of the inlet and the outlets can be seen in Figure 3.1. A heater was mounted on the outside of the chamber's walls. All of the walls and the heater were insulated. The steam sterilizer's chamber is made of stainless steel, whereas the diffuser is made of Polyphenylensulfid (PPS). More information about the investigated vacuum steam sterilizer can be found in Section 2.1.1.

3.1.2 Measurement of the pressure and the fluid temperature inside a non-vacuum steam sterilizer

To validate the CFD simulations of the non-vacuum steam sterilizer, eight type J thermocouples were distributed inside the chamber of the non-vacuum steam sterilizer. Additionally, a pressure sensor was added to the experimental set-up. The experimental set-up of the non-vacuum steam sterilizer, with the positions of the eight thermocouples (T1 - T8) and the pressure sensor (p) can be seen in Figure 3.2. The present investigation considers a small, high-end benchtop non-vacuum steam sterilizer with a volume of 22 litres [32]. The diameter of the sterilization chamber is approximately 260 mm, while its length is approximately 410 mm. The inlet of the steam sterilizer is located at the back of the chamber. The diffuser (made of PPS) is mounted in front of the inlet in order to ensure the turbulence of the entering steam. Compared to the vacuum steam sterilizer (see Figure 3.1), the position of the inlet is higher and the diffuser has a different shape. The non-vacuum steam sterilizer has three outlets, which are all located at the bottom of the chamber. The sterilization chamber was made of stainless steel. On the outside of the sterilization chamber a heater was mounted to heat up the chamber's walls. All outer walls of the sterilization chamber as well as the heater were insulated.

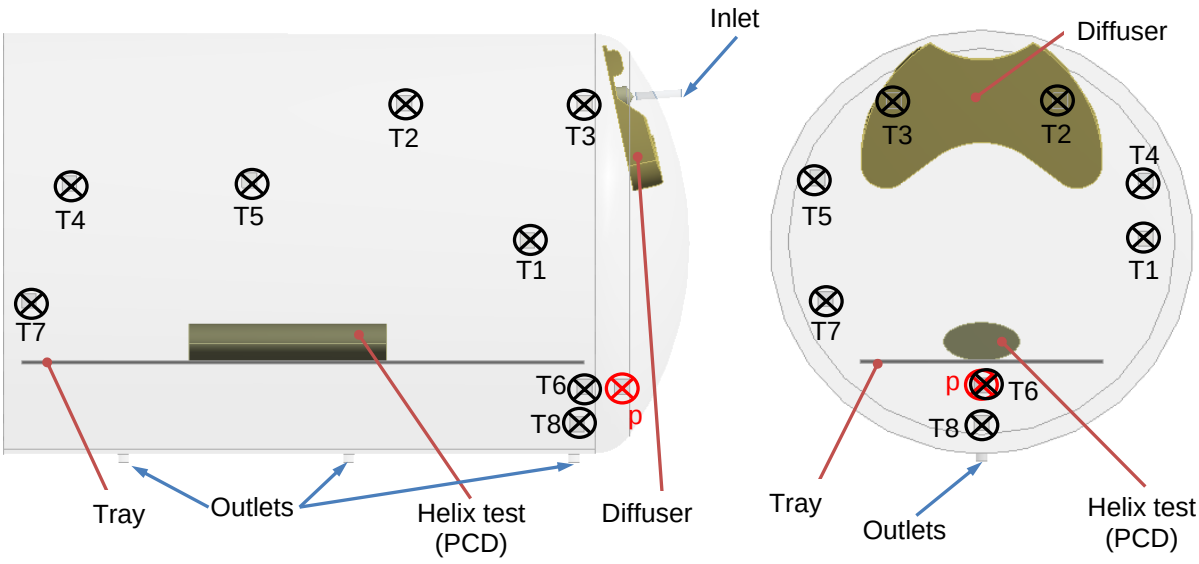

Figure 3.2: Geometry of the non-vacuum steam sterilizer with the positions of the eight thermocouples (T1 to T8) and the pressure sensor (p) [2].

More information about the investigated non-vacuum steam sterilizer and the non-vacuum steam sterilization cycle can be found in Section 2.1.2.

3.2 Experimental set-up to measure the load temperature [2]

To inactivate all bacteria, not only the steam temperature, but also the surface temperature of the load plays a crucial part. In this thesis, the load temperature was measured for different materials, as well as for wrapped and unwrapped loads. These measurements are the basis of an indirect validation of the simulated heat transfer to the load. This validation of the heat transfer is considered indirect because the (transient) increase in the load temperature was measured, rather than the heat transfer coefficients.

3.2.1 Measurement of the load temperature of an unwrapped load

In this thesis, unwrapped cylinders made of four different materials were investigated. The eight cylinders were distributed on two trays. The measurement set-up used to measure the unwrapped load temperatures can be seen in Figure 3.3. The materials considered were steel, aluminium, brass, and plastic (Polytetrafluorethylen (PTFE)), due to the fact that most pieces of medical equipment are made of one of these materials. The cylinders had a diameter of approximately 25 mm and a length of approximately 100 mm. With these dimensions, it was possible to investigate the heat transfer to heavy solids (steel cylinder) as well as light solids (plastic cylinder). The trays had dimensions of 380 mm $\times$ 186 mm $\times$ 2 mm and were made out of aluminium. The load temperature was measured at the centre of gravity. Therefore, four thermocouples were placed in the centre of gravity of the cylinders of the upper tray (see "T Steel", "T Aluminium", "T Brass" and "T Plastic" in Figure 3.3). All of the type J thermocouples used for these measurements have an accuracy of $\pm$ 1 K. These measurements were performed with the vacuum steam sterilizer [31].

3.2.2 Measurement of the load temperature for a wrapped load

In addition to the unwrapped cylinders, wrapped cylinders made of three different materials were investigated. As described in Section 2.5.2, loads may be wrapped for transport or storage reasons [69]. During the steam sterilization process, the wrapping represents a barrier between the steam and the load's surface. Thus, to investigate the

[2] Segments of this section have already been published in [1, 4].

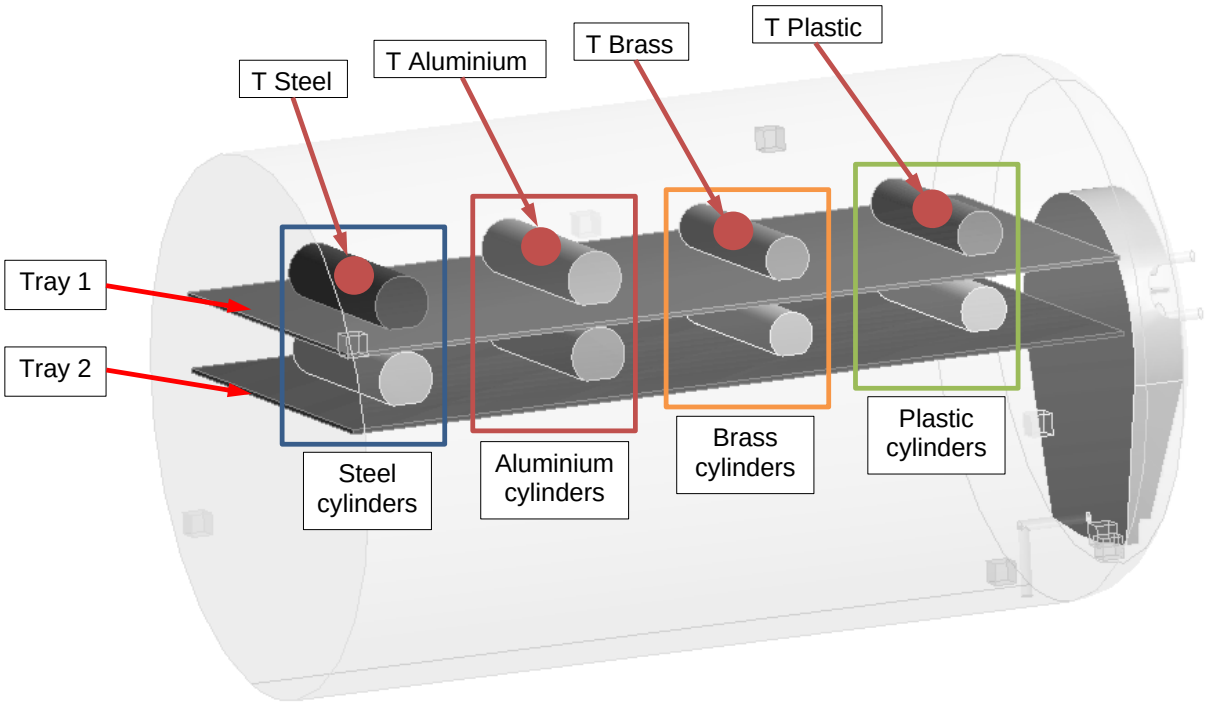

Figure 3.3: Geometry of the vacuum steam sterilizer with the unwrapped load and the locations of the thermocouples ("T Steel - T Plastic") to measure the load temperature in the centre of gravity [4].

influence of this wrapping on the load temperature, the steam sterilizer was loaded with eight wrapped cylinders on two trays (see Figure 3.4(a)). Figure 3.4(b) presents a picture of the wrapped cylinders. The cylinders and the trays were of the same dimensions as described in Section 3.2.1. The cylinders used in this section were made of stainless steel, aluminium and brass; because most wrapped (pouched) loads are metal, no plastic cylinders were considered for these measurements. Rather, instead of a plastic cylinder, a second steel cylinder was added to the measurement set-up (see Figure 3.4(a)). The pouch in which the loads were wrapped represents the standard wrapping material [70] used to ensure the sterilization of medical equipment. The positions of the thermocouples used to measure the load temperature at the cylinders' centre of gravity ("T Steel", "T Aluminium" and "T Brass") can be seen in Figure 3.4(a). These type J thermocouples have a maximum error of ± 0.75 % of the measured value. This error represents an uncertainty of approximately ± 1 K of the measured value.

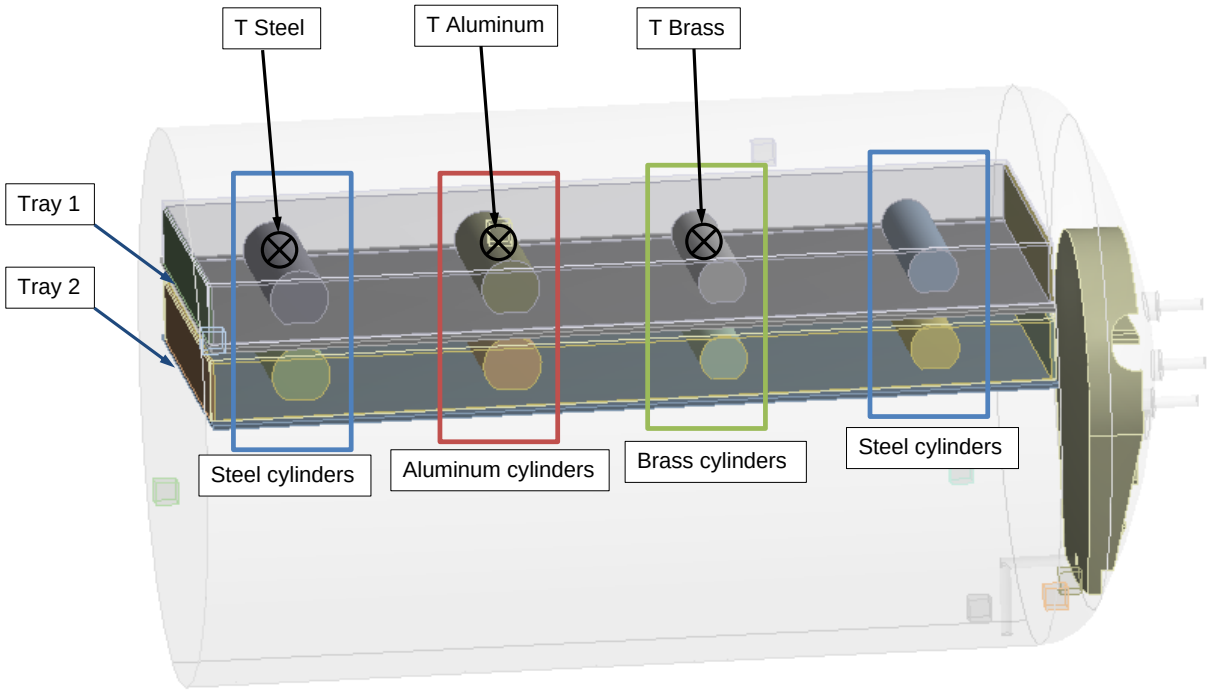

(a) Geometry of the vacuum steam sterilizer with the wrapped load and the locations of the thermocouples ("T Steel - T Brass") to measure the load temperature at the centre of gravity.

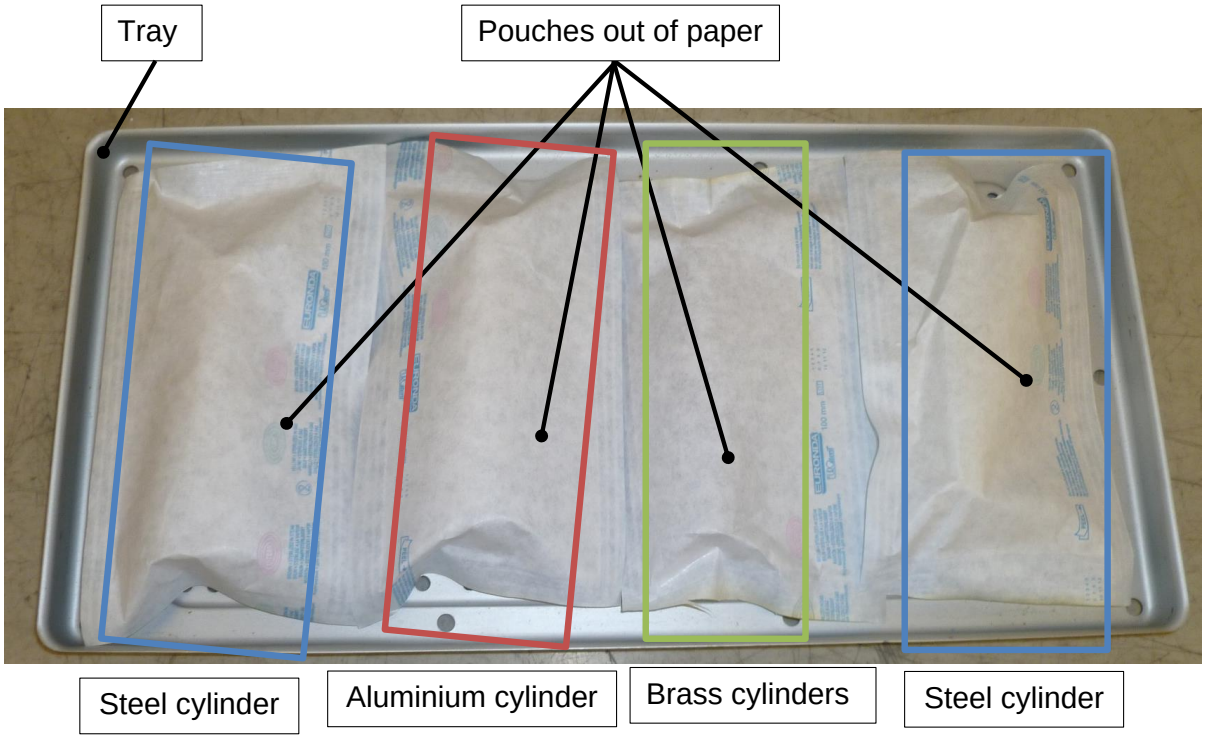

(b) Tray with the real wrapped (pouched) load.

Figure 3.4: (a) Geometry of the vacuum steam sterilizer with the wrapped load and (b) a real tray with the load wrapped in paper [1].

3.3 Experimental set-up to measure the mass flow rate of the steam generator

To simulate the steam sterilization process, the mass flow rate of the steam generator is of huge importance. As a result, the mass flow rate of the steam generator was measured during a steam sterilization cycle. The experimental set-up for these measurements is shown in Figure 3.5. The steam generator was positioned on a scale, where the total mass of the steam generator (steam sterilizer and water) was measured. During the phases when the steam generator was in operation, no water is refilled from the fresh water tank and some of the water evaporates. As a result, the total mass of the steam generator decreases. This mass decrease was measured over time, and the resulting data makes it possible to calculate the mass flow rate of the steam generator.

These measurements were performed for both the vacuum steam sterilizer (see Figure 2.1) and the non-vacuum steam sterilizer (see Figure 2.3). Due to the fact that both steam sterilizers use a 2100 W steam generator, the same mass flow rate was measured for the vacuum steam sterilizer and the non-vacuum steam sterilizer (approximately 0.92 g/s).

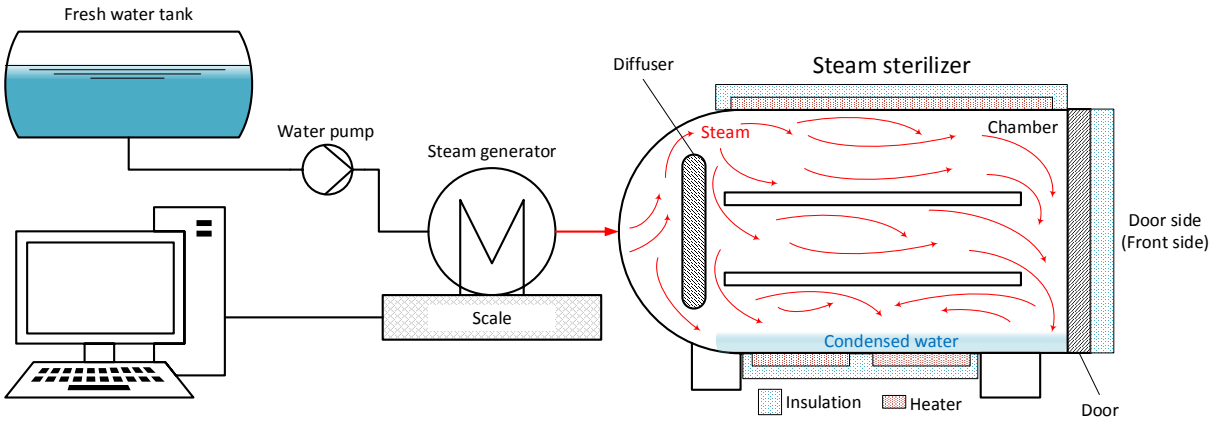

Figure 3.5: Experimental set-up to measure the mass flow rate of the steam generator.

3.4 Experimental set-up to measure the permeability of the paper [3]

To understand the full sterilization process, the properties of the paper used to wrap the load [70] are also of high interest to this research project [11, 76]. During the steam sterilization process, the paper represents a flow resistance to the outgoing air, the entering steam, and the condensing water. To simulate the influence of the paper on the sterilization process of the medical equipment (load), the permeability of the paper is of huge interest. Therefore, a test rig was developed to measure the permeability of the paper for air and steam. A functional sketch of the (permeability) test rig that was developed for these measurements is shown in Figure 3.6. A pressure reducer was used to reduce the pressure of the incoming pressurized air (approximately 5 bar) to pressures more similar to those present inside real steam sterilizers (approximately 0.3 bar to 3 bar). A flow meter was used to measure the volume flow rate of the air after the pressure reducer. The heater, which was mounted on the outside of the test rig, was used to heat the air through the whole temperature range that occurs in a real steam sterilizer (approximately 20 °C to 140 °C). The pressure adjuster at the end of the test rig was used to vary the flow rates of the air. Test rigs with similar principles can be found in literature [77]. With this test rig (see Figure 3.6), it was possible to measure the pressure drop of the air through the paper for different velocities, temperatures, and pressures.

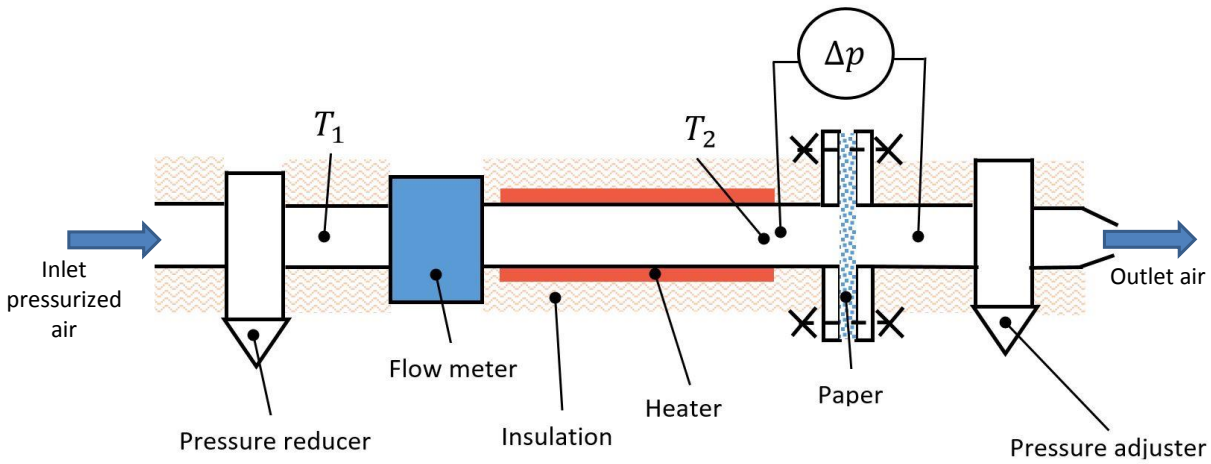

Figure 3.6: Functional sketch of the test rig to determine the permeability of the paper for air.

The test rig that was developed to measure the permeability of the paper for air (see Figure 3.6) was further developed to measure the permeability of the paper for steam

[3] Segments of this section have already been published in [1, 5].

(see Figure 3.7). The same steam generator which is integrated into the steam sterilizer feeds steam into the test rig. Afterwards, the velocity of the steam is measured. A heater was used to achieve the desired temperature and to prevent condensation. At the end of the test rig, a pressure adjuster was mounted to set the pressure in the test rig according to measured pressure in the steam sterilizer. Heat losses due to convection and radiation on the surface of the test rig were minimized with by a layer of outer insulation. The pressure drop (see $p_1 - p_2$ in 3.7) induced by the paper was measured for a temperature range between 70 °C and 140 °C and a pressure range between 300 $mbar_a$ and 3200 $mbar_a$. This temperature and pressure range represents the real range of pressures and temperatures that occur inside the sterilization chamber. 70 °C and 300 $mbar_a$ represent the point in the steam sterilization cycle at which the pressure and the temperature are reduced by the vacuum pump. 140 °C and 3200 $mbar_a$ represent the beginning of the sterilization plateau during the steam sterilization cycle (see Figure 3.1).

The measurements performed in this section were the basis of the development of a time-efficient porous media model that can be used to simulate the flow of both steam and air through the paper in which the load is wrapped (see Section 4.5).

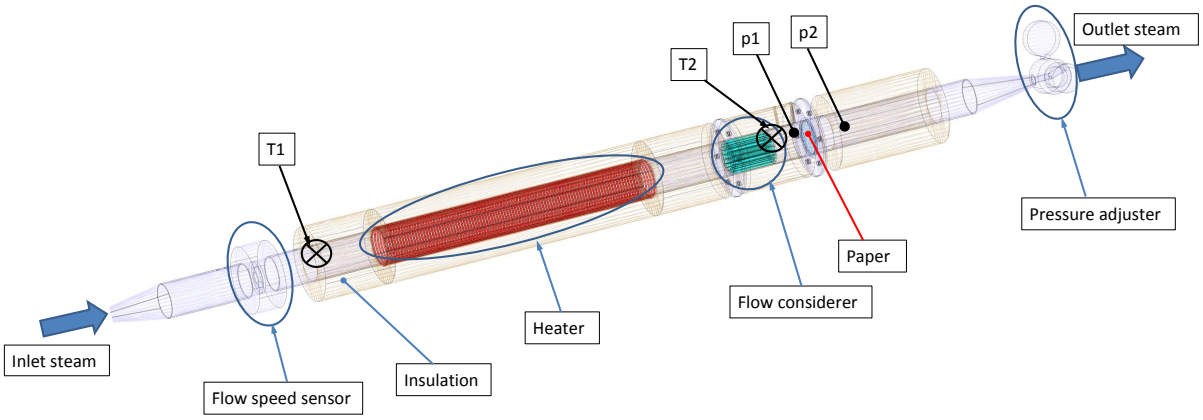

Figure 3.7: Functional sketch of the test rig to determine the permeability of the paper for steam [1].

3.5 Experimental set-up to measure NCGs inside the steam sterilizer [4]

Steam sterilization processes are based on high heat transfer rates from the steam to the load, which occur as a result of condensation. The steam condenses partially

[4]Segments of this section have already been published in [2, 3].

on the chamber walls, partially on the trays, and, of course, on the load (medical equipment) itself. Before the sterilization cycle begins, the whole steam sterilizer is filled with NCGs. During the sterilization cycle, the NCGs are partially mixed with the instreaming steam, partially not mixed with the instreaming steam, and, finally, removed from the steam sterilizer. Previous studies have shown that the heat transfer rate decreases in the presence of NCGs [27, 64]. As a result of these studies, it is known that the volume fraction of NCGs must be reduced before the sterilization of the medical equipment takes place. Eq. (3.1) shows the definition of the NCGs ratio according to the norm (ϕ_{Norm}) [8].

$$\phi_{Norm} = \frac{V_b}{V_c} \tag{3.1}$$

In this equation, V_b is the volume of the collected NCGs and V_c is the volume of the collected condensate at the considered cycle time (see Figure 3.8(b)). The NCGs ratio must be below 3.5 % according to the norm [8]. According to the norm, the measurement of the NCGs takes place during the holding time of the sterilization phase (see Figure 3.9(a) and Figure 3.9(b)). The holding time denotes the phase of the sterilization cycle during which the pressure and temperature remain at a constant, pre-defined level (here, approximately 3 bar and 134 °C, respectively) for a specified amount of time. The ratios of NCGs were measured for both steam sterilizers investigated (vacuum and non-vacuum), as well as for pre-sterilization phases of different lengths. The experimental set-up used to measure the NCGs ratios (ϕ_{Norm}), which can be seen in Figure 3.8. Figure 3.8(a) depicts the set-up before the measurements were carried out, while Figure 3.8(b) shows the measurement set-up after the measurements. Before the measurements begin, all NCGs are removed from the measurement system. At the beginning of the measurements (see the blue circles in Figure 3.9(a) and Figure 3.9(b)), the outlets of the steam sterilizer open, and all of the fluid inside the steam sterilizer flows towards the measurement system. The measurements cease when the pressure in the steam sterilizer reaches ambient conditions.

At the measurement points (see the blue circles in Figure 3.9(a) and Figure 3.9(b)), the steam sterilizer is filled with steam, water, and NCGs at a pressure of approximately 3 bar and a temperature of 134 °C, respectively. After exiting the condenser, the water (condensed steam and condensed water out of the steam sterilizer) and the NCGs (both water and NCGs with a pressure of approximately 1 bar and temperature of approximately 15 °C) flow from the condenser to a measuring cylinder, which is filled with a pre-defined volume (mass) of water. The measuring cylinder is positioned in a

water-filled tank, connected by a cavity (see Figure 3.8). If the water level in the tank rises, the over-flowing water flows into a second measuring cylinder (see Figure 3.8(b)). The mixture of water and NCGs from the condenser flows into the first measuring cylinder. The difference in density between the water and the NCGs results in the rise of the NCGs in the measuring cylinder (see Figure 3.8(b)). The ascending NCGs push down the water level in the first measurement cylinder, which, in combination with the condensate, lead the tank to overflow. The spilled water is then collected in the second measurement cylinder (see Figure 3.8(b)). The measurements end after the steam sterilizer has reached ambient pressure (approximately 1 bar) and a temperature of 100 °C.

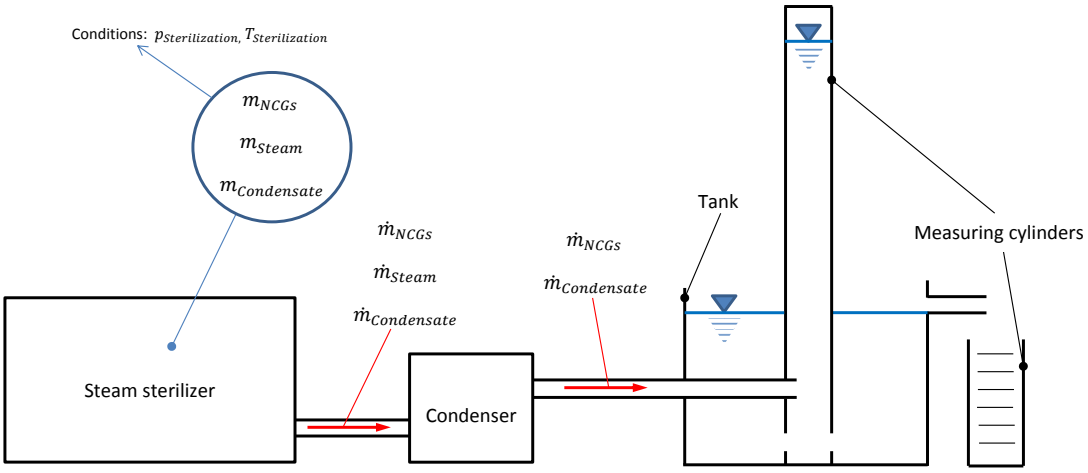

(a) Measurement set-up before the measurement of the NCGs

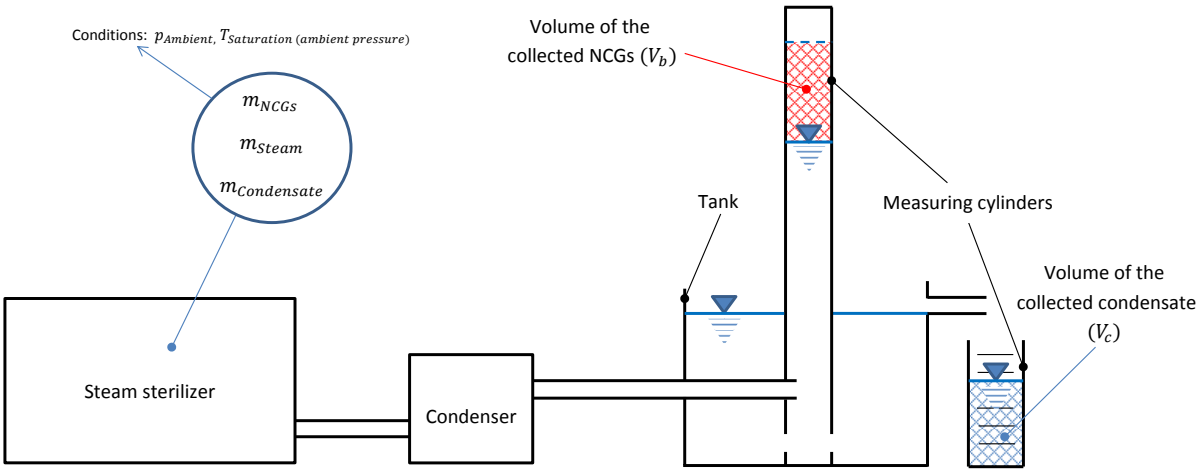

(b) Measurement set-up after the measurement of the NCGs

Figure 3.8: Measurement set-up of the NCGs (a) before and (b) after the measurements according to the norm (EN 13060 [8]) [2].

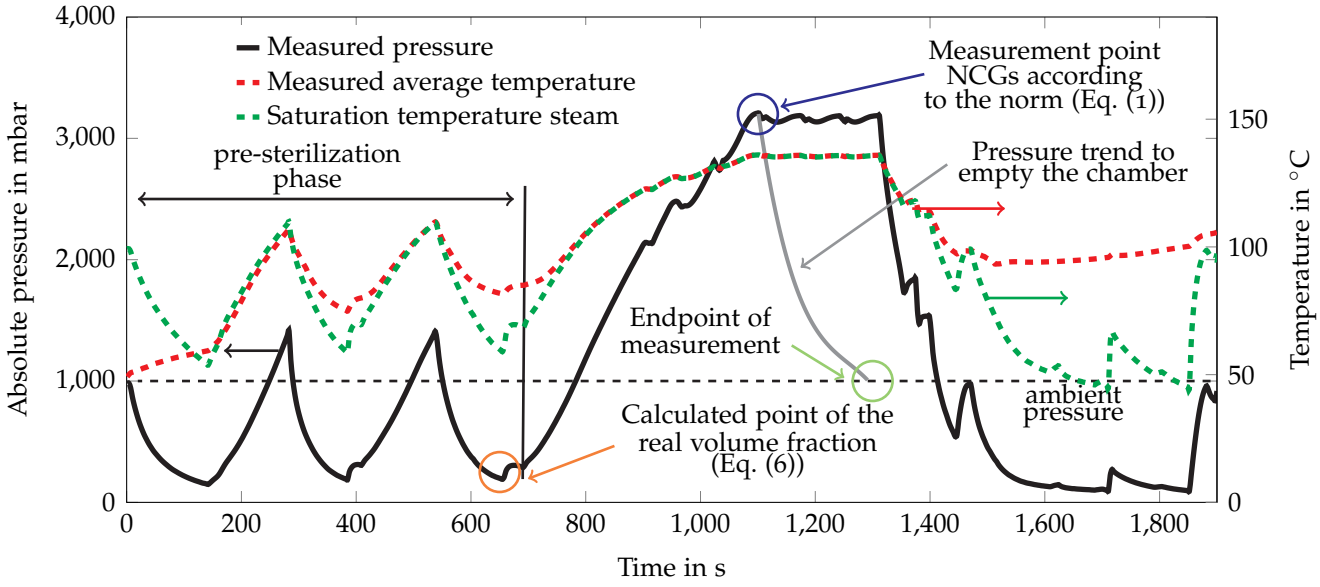

(a) Measured data of the vacuum sterilization cycle.

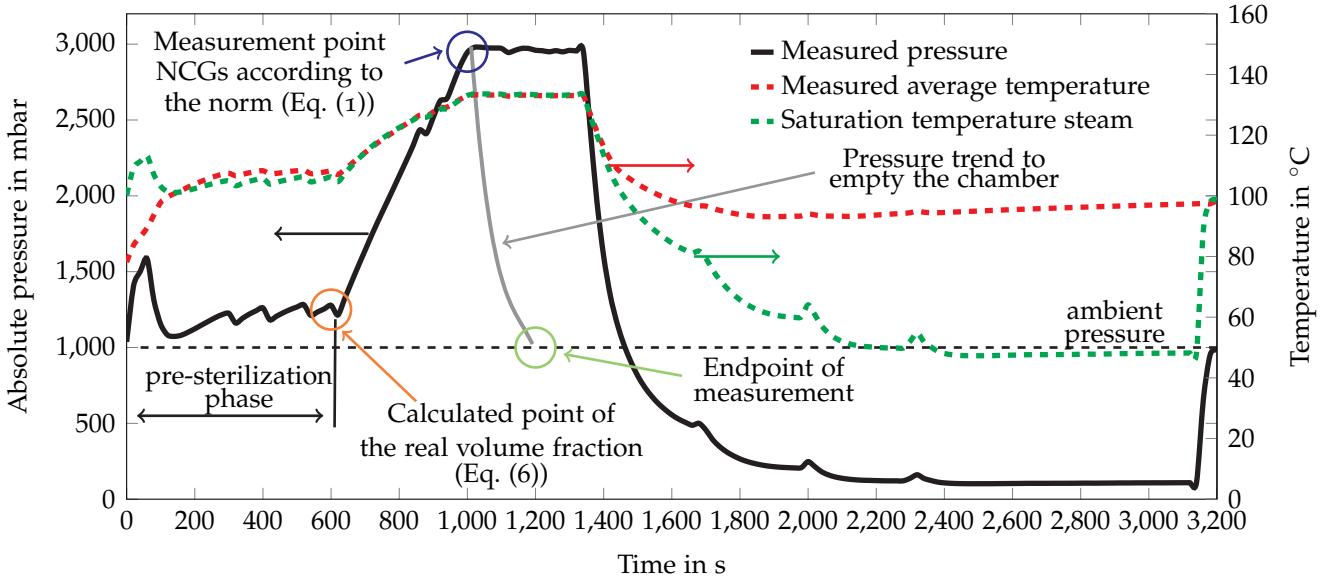

(b) Measured data of the non-vacuum sterilization cycle.

Figure 3.9: Measured pressure, average temperature, and saturation temperature of the steam for (a) the vacuum sterilization cycle and (b) the non-vacuum sterilization cycle [2].

At the end of the investigation, the volume of the collected NCGs (V_b) and the volume of the collected condensate (V_c) were measured (see Figure 3.8(b)). These measurements were performed over several cycles: for each measurement, a new sterilization cycle with a different length of the pre-sterilization was used. The NCGs ratios can be calculated with Eq. (3.1), which shows that a high volume of collected water (V_c) is beneficial to obtain low NCGs ratios according to the norm (ϕ_{Norm}).

As a result, a lot of condensation inside the steam sterilizer leads to low NCGs ratios, according to the norm. According to this definition, both a heavy chamber and cold walls are beneficial to the sterilizers' ability to surpass the norm measurements. To investigate the real ratios of NCGs inside steam sterilizers, a novel approach was developed to calculate the real volume fraction of NCGs (see Section 3.6).

3.6 Novel approach to calculate the real volume fraction of NCGs

Eq. (3.1) shows the formula for calculating the NCGs according to the European norm for small steam sterilizers [8]. It reveals that a high volume of collected water helps to ensure NCGs ratios well below the limit value of 3.5 %, as defined by the norm. Because this equation sees a volume of gas divided by a volume of water (both at ambient pressure and temperate), the norm NCGs ratio does not reflect the real ratio of NCGs in the steam sterilizer. The more water there is in the sterilizer, the easier it is to surpass the norm value since the volume of collected water (V_c) also increases. This high amount of water leads to less sterile medical devices, as a result of the poor heat transfer from the steam to the load. For this reason, a novel approach was developed to calculate the real volume fractions of the NCGs, based on the measurements of the norm test (presented in Section 3.5).

The following description of the developed approach is rather complex. Therefore, Figure 3.9 presents all of the relevant measurement points and calculation points, as well as the pressures and temperatures that were used to calculate the real volume fraction of NCGs.

First, the mass of NCGs in the measurement system (m_b) was calculated. m_b represents the mass of the volume of NCGs collected in the measurement system (see V_b in Figure 3.8(b)). The index "b" was chosen according to the norm [8]. To calculate the mass m_b, the ideal gas law was used:

$$m_b = \frac{p_m \cdot V_b}{R_{NCGs} \cdot T_m} \tag{3.2}$$

where p_m, R_{NCGs} and T_m stand for the absolute pressure in the measurement system (approximately 1 bar), the gas constant of the NCGs, and the temperature in the measurement system (approximately 15 °C), respectively. At the end of the measurement, the pressure in the steam sterilizer reaches ambient pressure (see the green circle in Figure 3.9). The mixture of water and NCGs that is collected between the sterilization pressure (approximately 3 bar, see the blue circle in Figure 3.9) and ambient pressure (see the green circle in Figure 3.9) is removed from the steam sterilizer. The mixture that is collected between the total vacuum (0 bar) and ambient pressure (approximately 1 bar) remains in the steam sterilizer. Therefore, Eq. (3.3) is used to calculate the total mass of the NCGs in the steam sterilizer (m_{NCGs}). m_{NCGs} presents the total mass of the NCGs inside the steam sterilizer before the measurement started.

$$m_{NCGs} = m_b \cdot \frac{p_{sterilization}}{p_{sterilization} - p_{ambient}} \tag{3.3}$$

Eq. (3.3) is a research achievement of this author. In this equation, both the temperature distribution inside the sterilization chamber and the distribution of the NCGs inside the steam sterilizer are neglected. Nevertheless, the results presented in Section 5.1.2 demonstrate that the Eq. (3.3) is able to accurately calculate the total mass of the NCGs in the steam sterilizer (m_{NCGs}).

During the increase in pressure after the pre-sterilization phase (pressure increase to approximately 3 bar), all of the outlets are closed (see the measured pressure between the orange and blue circles in Figure 3.9). As a result, the mass of the NCGs in the steam sterilizer remains constant. From the total mass of the NCGs (m_{NCGs}), the real volume fraction of NCGs can be determined. In this investigation, the volume of NCGs in the steam sterilizer was always calculated for the final point of the considered phase (see the orange circles in Figure 3.9(a) and Figure 3.9(b)). Due to the fact that steam is fed into the chamber to increase the pressure, the real values of the NCGs reach their maximum at this point. Eq. (3.4) shows the formula used to calculate the volume of the NCGs at the endpoint of the considered phase of the steam sterilization cycle.

$$V_{NCGs} = \frac{m_{NCGs} \cdot R_{NCGs} \cdot T_{SS}}{p_{NCGs}} \tag{3.4}$$

In Eq. (3.4), T_{SS} stands for the temperature at the final point of the considered phase of the sterilization cycle, while p_{NCGs} stands for the partial pressure of the NCGs at at which the real volume fraction of the NCGs was determined (see the orange circles in Figure 3.9). The real volume fraction of the NCGs can easily be calculated by dividing the volume of the NCGs (V_{NCGs}) by the volume of the steam sterilizer ($V_{Sterilizer}$) (see Eq. (3.5)).

$$\phi_{real} = \frac{V_{NCGs}}{V_{Sterilizer}} \tag{3.5}$$

By inserting Eq. (3.4) into Eq. (3.5), it is possible to calculate the real volume fraction of the NCGs. In this equation, the partial pressure of the NCGs (p_{NCGs}) has to be known. Using Eq. (3.6) the partial pressure of the NCGs (p_{NCGs}) can be calculated from the real volume fraction of the NCGs (ϕ_{real}) and the pressure inside the steam sterilizer (p_{SS}):

$$p_{NCGs} = \phi_{real} \cdot p_{SS} \tag{3.6}$$

Equations (3.2-3.6) were combined to a final equation (Eq. (3.7)). The negative value of the quadratic equation was ignored, due to the fact that a negative volume fraction has no physical meaning. With Eq. (3.7), it is possible to calculate the real volume fraction of the NCGs (ϕ_{real}) from the norm measurement of the NCGs (see Figure 3.8). Furthermore, using this equation, only the pressure inside the steam sterilizer (p_{SS}) and the temperature in the steam sterilizer (T_{SS}) have to be measured. The partial pressure of the NCGs (p_{NCGs}) is considered in Eq. (3.7) through thermodynamic laws.

$$\phi_{real} = \sqrt{\frac{m_{NCGs} \cdot R_{NCGs} \cdot T_{SS}}{V_{Sterilizer} \cdot p_{SS}}} \tag{3.7}$$

The major advantage of this approach is that the real volume fraction of NCGs inside the steam sterilizer at the end of the pre-sterilization phase (see the orange circles in Figure 3.9) can easily be determined based on measurable values.

As described in Section 3.5, the NCGs ratio as calculated according to the norm is not able to predict the real NCGs ratios inside the steam sterilizer due to the fact that a gas volume is divided by a water volume (see Eq. (3.1)). According to this definition, it would be beneficial if water were fed into the sterilization chamber before the normative measurement were taken. Furthermore, heavy thick walls are beneficial

to the NCGs ratio, due to the fact that more steam condenses inside the steam sterilizer. With Eq. (3.7), the "real volume fraction" of the NCGs can be calculated from the NCGs measurements, according to the norm [8]. This value is more accurate and able to predict the real conditions inside the steam sterilizer. Furthermore, with Eq. (3.7), the air-removal process inside the sterilization chamber can be investigated in more detail due to the fact that condensed water does not influence the measurement result.

3.7 Experimental set-up to measure the removal of air from hollow loads [5]

For small steam sterilizers, a PCD test (process challenge device (PCD) and indicator system) is a standard test required by EN 13060 for hollow loads (defined in the standards as a (defined in standards: length:internal diameter ratio $\leq$ 750:1, and length not exceeding 1500 mm) [8]. In this thesis, two different kinds of PCDs were used to investigate the steam penetration in hollow loads. For both tests, the tube length was 1500 mm and the inner diameter of the tube was 2 mm; the shape of the tubes was similar to a helix, and the wall thickness of both tubes was 0.5 mm. The tube used in the first test, referred to as "Process Challenge Device 1 (PCD 1)", was made of PTFE. The tube's geometry and the inlet position can be seen in Figure 3.10(a). The tube used for the second test, referred to as "Process Challenge Device 2 (PCD 2)", was made of stainless steel and surrounded by a plastic container. The container was used to make it even more difficult for the steam to enter into the tube of the PCD. Figure 3.10(b) shows the geometry and the inlet position of PCD 2. The plastic shell is a box with a rectangular base. The base is 50 mm in width and 25 mm in height, while the length of the plastic shell is approximately 143 mm. In order to experimentally investigate steam penetration through the tube, a chemical indicator was added to both of the closed ends of the helix tubes of the PCDs. The length of the indicator system was approximately 40 mm. The positions of the indicators on PCD 1 and PCD 2 can be seen in Figure 3.10. PCD 1 and PCD 2 have two different types of chemical indicators, which change colour when they come into contact with steam. To investigate the influence of the chemical indicators, two types of chemical indicators were used in both investigated helix tests. The working principle of the chemical indicators can be seen in Figure 3.11. The chemical indicator of PCD 1 changes colour from yellow to violet when the steam successful penetrates the whole helix tube of the PCD 1. If there

[5] Segments of this section have already been published in [3].

is insufficient steam penetration in the helix tube, the chemical indicator of PCD 1 remains partially or completely yellow (see Figure 3.11(a)). The chemical indicator of PCD 2 is divided into four squares. This indicator turns black when the target temperature has been reached and the steam penetration was sufficient. If the colour turns brown, the required temperature of 134 °C has been reached, but the steam penetration was insufficient (see Figure 3.11(b)). With the indicator of PCD 2, it is possible that some squares will change black (steam penetration and temperature was sufficient), whereas the other squares change to brown (temperature was achieved but the steam penetration was insufficient). Measurements with both chemical indicators were carried out on both PCD 1 and PCD 2, and repeated 20 times to ensure their repeatability. The results of these measurements can be seen in Section 5.6.4.

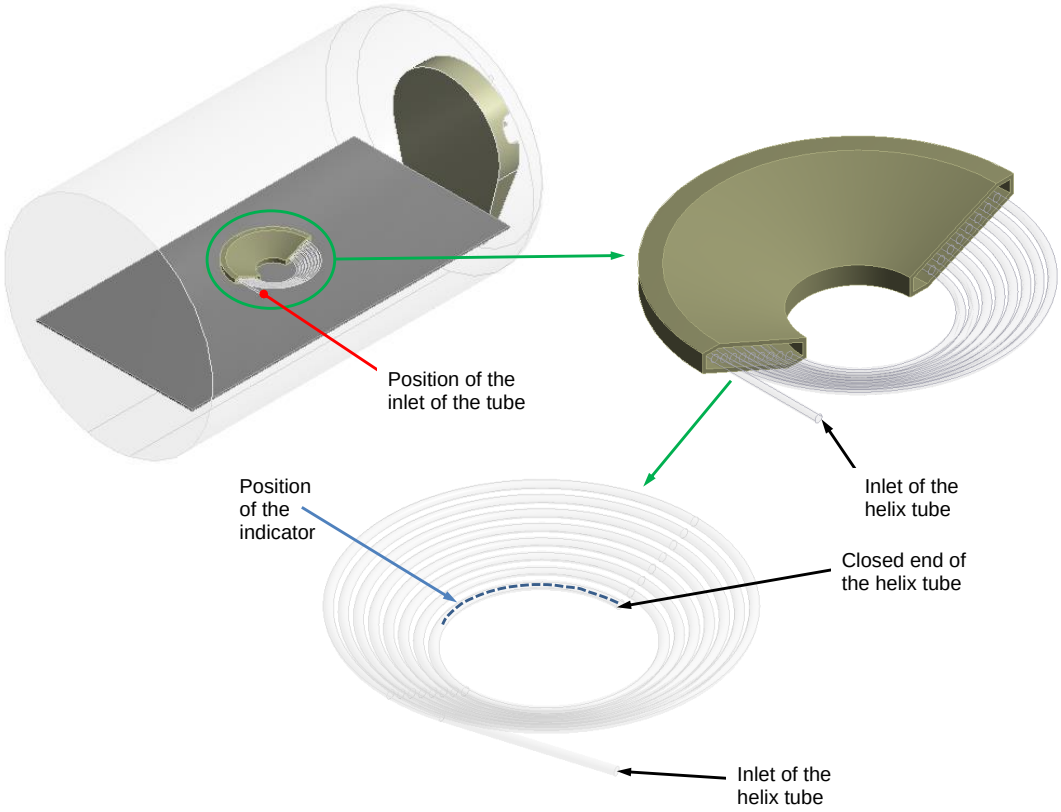

(a) Geometry of the vacuum steam sterilizer and the first helix test (PCD 1)

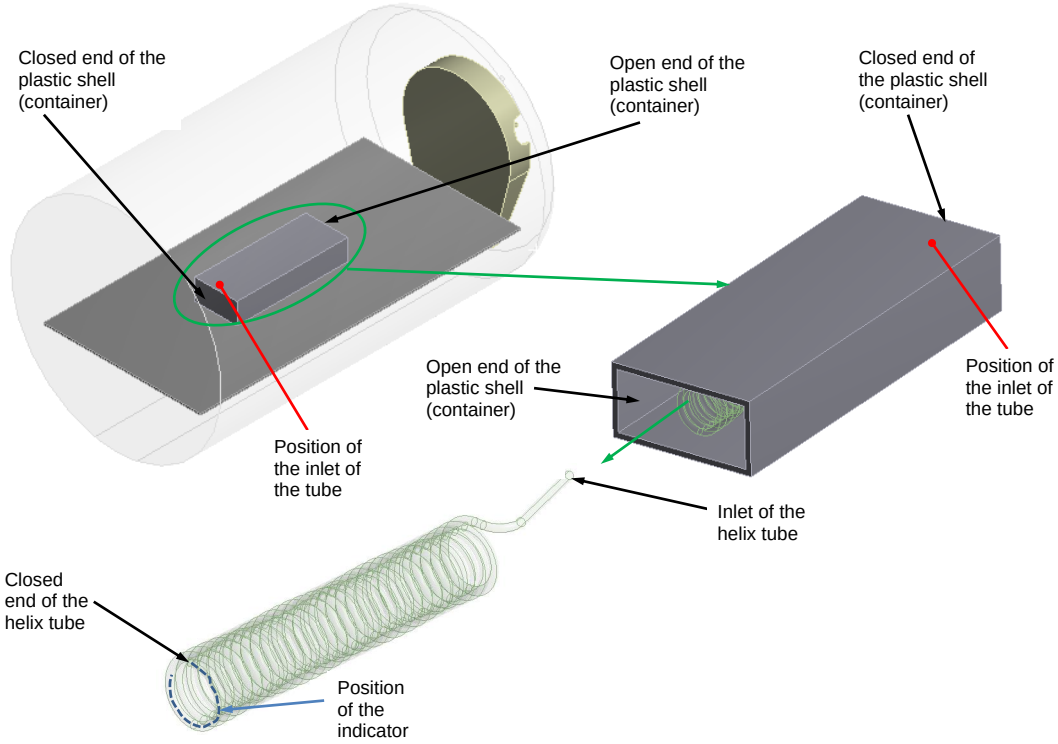

(b) Geometry of the vacuum steam sterilizer and the second helix test (PCD 2)

Figure 3.10: Geometry of the vacuum steam sterilizer with (a) the first helix test (PCD 1) and (b) the second helix test (PCD 2) [3].

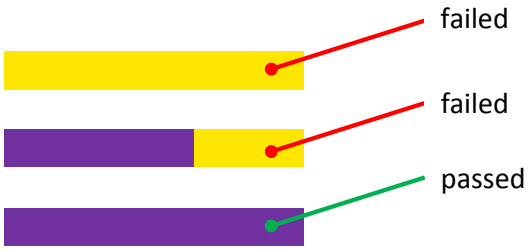

(a) Chemical indicator of PCD 1

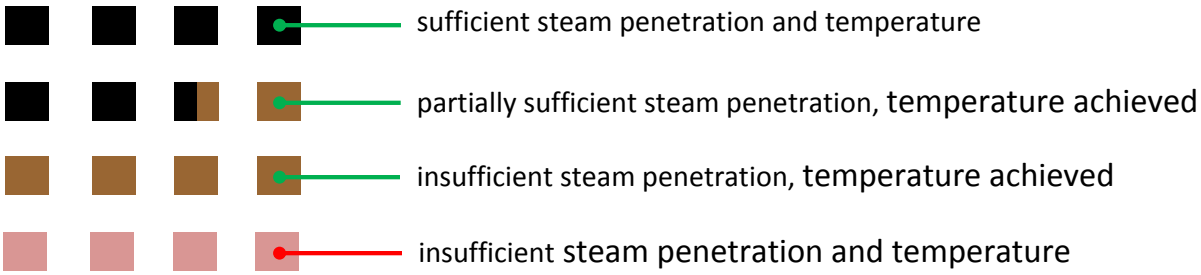

(b) Chemical indicator of PCD 2

Figure 3.11: Working principle of (a) chemical indicator of PCD 1 and (b) chemical indicator of PCD 2 [3].

4
Numerical modelling

In the course of the research carried out for this thesis, steam sterilization processes were investigated using the commercially available CFD code ANSYS Fluent [78]. The CFD method used is based on the Finite Volume Method (FVM). Using the FVM, conservation equations for mass, momentum, energy and other scalars, such as the volume fractions of the phases, can be solved for each control volume by various numerical methods. A more detailed description of the methods used in CFD can be found in literature [79, 80].

This chapter provides an overview of the various numerical models that were developed to simulate the relevant physical phenomena inside steam sterilizers. These include the flow modelling of the sterilization phase and the pre-sterilization phase, the turbulence modelling, and the modelling of the evaporation and condensation effects. Furthermore, a heat transfer model developed by the author is presented, which is capable of simulating the heat transfer that occurs from condensation effects in the presence of NCGs. A model to simulate the inactivation of bacteria is presented as well. This chapter also includes a model to simulate the permeability of the paper pouches used to store and transport medical instruments, all boundary conditions of the simulations, and the numerical grids used to simulate the investigated vacuum and non-vacuum steam sterilizers. To the best of the author's knowledge, the CFD models presented in this chapter were the first CFD models about steam sterilization processes published in the scientific literature.

4.1 Flow modelling [1]

A double precision pressure-based solver was used to achieve transient solutions of the Reynolds-Averaged-Navier-Stokes equations (RANS) for mass, momentum, and energy, as well as additional equations for turbulence, evaporation, and condensation effects. The multiphase flow inside the steam sterilizer was modelled with the Eulerian-Eulerian multiphase model.

The operating pressure was set to 0.289 bar for the simulation of the vacuum steam sterilizer and to 1.013 bar for the simulation of the non-vacuum steam sterilizer. A second-order upwind discretization scheme was chosen for the scalars mass, momentum, turbulent kinetic energy, turbulent dissipation rate, and energy. Quadratic Upstream Interpolation for Convective Kinematics (QUICK) was used for the discretization of the density and the volume fraction. The pressure velocity coupling was modelled with the Phase Coupled Semi-Implicit Method for Pressure Linked Equations (SIMPLE), while the Least Squares Cell-Based method was used to determine the gradients. The discretization scheme for the transient formulation was second-order implicit. Gravity was added to the CFD model to account for buoyancy.

The simulation was performed with a time step of 0.01 s. The maximum number of iterations per time step was set to 35. The convergence criteria for the simulation were not only low residuals (below 10^{-5}), but also monitors of pressure, temperature and volume fractions.

4.1.1 Flow modelling of the sterilization phase

The flow inside the sterilization chamber in the sterilization phase was modelled with a two-phase Eulerian-Eulerian model. The primary phase was set to steam, while the secondary phase was set to water. Because the "real volume fraction" of the NCGs (see Eq. (3.7)) was below 0.15 % at the beginning of the sterilization phase (see "sterilization phase" in Figure 2.2 and Figure 2.4), NCGs were not considered in the CFD model. As the cycle time in the sterilization phase increases, the volume fraction of NCGs further decreases due to the fact that additional steam is fed into the sterilization chamber to increase the pressure during the pressure rise of the sterilization phase (see "pressure rise" in Figure 2.2 and Figure 2.4). More information about the volume fraction of NCGs at the beginning of the sterilization phase is presented in Section 5.1.

[1] Segments of this section have already been published in [1–5].

The material properties of all phases were set to values that have been established in literature [81]. The temperature dependency of the material properties was added to the CFD code using piecewise polynomials. The density of the steam was modelled with the ideal gas law in order to reduce the numerical effort required. There are numerous studies that consider the difference between the ideal gas properties and real gas properties of steam [82, 83]. Borgnakke and Sonntag, for example, showed that the maximum deviation between the measured values and the calculated values with the ideal gas law is less than 1.5 % up to a pressure of 1 bar [84]. Klein and Nellis demonstrated that the maximum deviation for a pressure of 3.16 bar is also less than 2 % between the measured specific volumes and the calculated specific volumes with the ideal gas law [85]. Furthermore, the density of the steam was also modelled with several real gas models. As might have been expected, hardly any differences between the real gas models and the ideal gas law were detected. This is because steam sterilizers operate at much lower pressure levels compared to many other industrial applications (e.g., boilers, steam power plants, etc.) [86]. The minimum pressure in the vacuum steam sterilization cycle is approximately 0.16 bar, whereas the maximum pressure is approximately 3.16 bar. Furthermore, the steam in the steam sterilizer is saturated or wet, not overheated. At these conditions, saturated steam is very similar to an ideal gas [87].

4.1.2 Flow modelling of the pre-sterilization phase

In the pre-sterilization phase (see Figure 2.2 and Figure 3.2), steam, water, and NCGs (air) are present in the chamber of the steam sterilizer. As a result, the multiphase flow was modelled with an Eulerian-Eulerian multiphase model with three phases.

The primary phase was steam, and the material properties of the steam were set according to literature [84]. The properties of steam were added to the CFD code via piecewise polynomials. The two secondary phases were set to water and NCGs. All properties of both secondary phases were set to the values found in literature [85, 88]. The droplet diameter of the secondary water phase was set to 0.1 μm. Many studies have investigated the droplet diameter of water in steam, which is very difficult to measure. White [89] identified an average water droplet diameter of 0.07 μm. However, Ryley and Al-Azzawi [90] found that the average diameter of the water droplets is approximately 0.1 μm. In a previous study, the authors of the present work investigated simulations carried out with different droplet diameters, and found that hardly any differences in the simulation results could be identified [1]. Thus the droplet diameter

of the NCGs secondary phase was set to 0.1 μm. Droplet diameters of 0.01 μm and 1 μm were also investigated for the secondary phase of the NCGs. Again, the droplet diameter was found to have hardly any influence on the simulation results.

4.2 Turbulence modelling [2]

Turbulence is dictated by several factors, including the density, the velocity, and the characteristic length of the flow, as well as the viscosity of the fluid. All of these properties are related to the Reynolds number (Re). The Reynolds number can be calculated with Eq. (4.1) [91, 92]:

$$Re = \frac{\rho \cdot v \cdot L_c}{\eta} = \frac{v \cdot L_c}{\nu} \tag{4.1}$$

where ρ stands for the density, v for the velocity, L_c for the characteristic length, η and ν for the dynamic and the kinetic viscosity, respectively. Due to changing geometries inside the steam sterilizers (see Figure 3.1 and Figure 3.2) the Reynolds number was calculated for different regions inside the steam sterilizer. The Reynolds number near the inlet is approximately 14,500, while behind the diffuser, the Reynolds number is approximately 3,800. The average flow Reynolds number inside the sterilization chamber was approximately 1,900. Generally, pipe flows with a Reynolds number of over 2,300 are turbulent; pipe flows with lower Reynolds numbers are (usually) laminar. As the range of the Reynolds number within the sterilization chamber is between a turbulent and laminar flow, simulations were performed with and without a turbulent model. It was found that the simulations with the turbulence model exhibited better numerical robustness. Regarding the pressure and the temperature within the sterilization chamber, hardy any differences between the turbulent and the laminar simulations were identified. Due to those facts, all further simulations in this study were simulated with a turbulence model.

In the present work, the realizable k-ϵ model by Shih et al. [93] was used to deal with the turbulent flow in the steam sterilizer. The advantage of the realizable k-ϵ model is its numerical robustness. The standard wall function was used to model the near wall region of the fluid domain, because y^+ was $30 < y^+ < 200$ in > 99 % of the near wall cells of all of the numerical grids.

[2] Segments of this section have already been published in [4, 5].

Many authors have simulated industrial applications using the realizable k-ϵ turbulence model. Wurm et al., for example, used the realizable k-ϵ model to simulate the temperatures in an exhaust [94], and for the simulation of the heat transfer in continuous variable transmissions [95, 96]. Landfahrer et al. simulated the heating process of beams and steel tubes in furnaces using the realizable k-ϵ model [97, 98]. Other authors have simulated the condensation of steam [99], and the condensation of steam in the presence of NCGs [100, 101] using the realizable k-ϵ model. All of these studies demonstrate that the realizable k-ϵ model should make it possible to simulate both condensation as well as the heat transfer rate inside a steam sterilizer under turbulent flow conditions.

4.3 Condensation and evaporation modelling [3]

The condensation was modelled using a numerical technique first published by W. Lee [102]. In this approach, the mass transfer from the steam to water ($\dot{m}_{sw}$) takes place when the steam temperature (T_s) is lower than the saturation temperature (T_{sat}), and is given with:

$$\dot{m}_{sw} = r_{sw} \cdot \phi_s \cdot \rho_s \cdot \frac{T_{sat} - T_s}{T_{sat}} \tag{4.2}$$

where, ϕ_s is the volume fraction of the steam phase, ρ_s is the density of the steam and r_{sw} is a coefficient that defines "how fast" the mass transfer takes place. If the water temperature is higher than the saturation temperature, mass transfer from water to steam ($\dot{m}_{ws}$) takes place:

$$\dot{m}_{ws} = r_{ws} \cdot \phi_w \cdot \rho_w \cdot \frac{T_w - T_{sat}}{T_{sat}} \tag{4.3}$$

where, ϕ_w and ρ_w stand for the volume fraction of water and the density of water, respectively. Again, the coefficient r_{ws} defines "how fast" the mass transfer takes place.

The coefficients r_{sw} and r_{ws} are both case sensitive and difficult to detect. Overall, the optimum values for r_{sw} and r_{ws} depend on the flow rate, the size of the computational domain, the mesh size, and the size of the time step [103]. H. Lee et al. [52] measured

[3] Segments of this section have already been published in [1, 4, 5].

and simulated downflow condensation in a circular tube. In their study, simulations with $r_{sw} = 10,000\ s^{-1}$ showed the best accordance with the measurements. The same coefficient yielded good results during a simulation of upstream condensation [104]. H. L. Wu et al. [105] simulated flow boiling in serpentine tubes with $r_{ws} = 0.1\ s^{-1}$. Another work by Yang et al. [106] investigated flow boiling in a coiled tube with $r_{sw} = r_{ws} = 100\ s^{-1}$. The authors of that study investigated coefficients of $r_{sw} = 2\ s^{-1}$, $20\ s^{-1}$, $200\ s^{-1}$ and $2000\ s^{-1}$. They found that the simulations carried out with a coefficient of $200\ s^{-1}$ showed the best accordance with their experimental results. More information about selecting the coefficients r_{sw} and r_{ws} for the simulation of condensation effects can be can be found in literature [102, 103, 107, 108].

4.4 Heat transfer modelling [4]

Modelling the heat transfer induced by wall condensation is not a trivial matter for CFD simulations. Many authors have attempted to address this challenge. Yoon, Jo, and Corradini [109], for example, developed a model to predict the heat transfer due to condensation effects on a planar wall. Zschaeck et al. [110] developed a heat transfer model to simulate the heat transfer due to condensation in the presence of NCGs. J.-D. Li [60] presented a CFD model to simulate condensation on vertical cylindrical condensers, while Phan et al. [111] simulated the steam-air mixture condensation in a vertical tube. Nonetheless, all of these models require a very fine mesh near the wall in order to resolve the condensed film and the heat transfer coefficients directly on the wall, which is a disadvantage because this is such a computationally expensive process. In order to reduce the computational effort required to model heat transfer due to condensation effects, the author of this thesis took up the challenge of developing a heat transfer model of his own.

Figure 4.1 shows the schematic of heat flux in the condensation process for (a) saturated and wet steam and (b) for saturated and wet steam in the presence of NCGs. For condensation to occur, the wall temperature must be lower than the saturation temperature of the steam. For this condition, the author wanted to develop a heat transfer model that would be able to predict the heat transfer from the steam to the load as the result of condensation effects for both saturated and wet steam as well as for saturated and wet steam in the presence of NCGs. The goal of this PhD thesis was

[4] Segments of this section have already been published in [1–5].

to develop a heat transfer model that does not necessarily require the modelling of the condensation film, which can be seen in Figure 4.1.

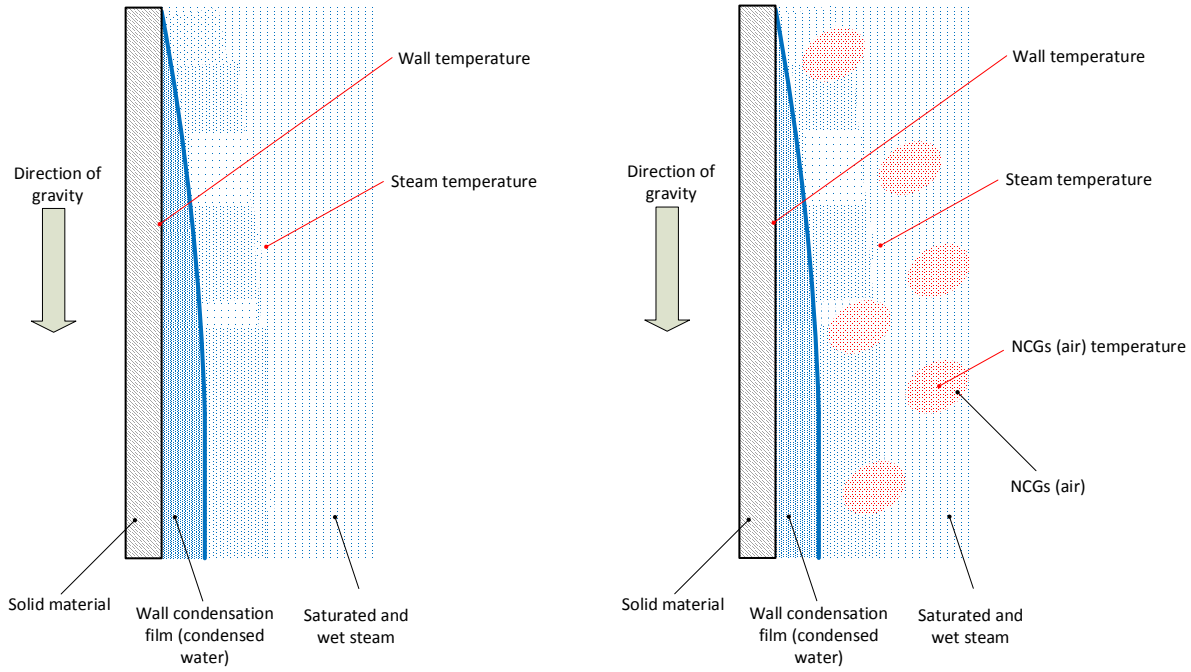

(a) Wall film condensation for saturated and wet steam.

(b) Wall film condensation for saturated and wet steam in the presence of NCGs (air).

Figure 4.1: Schematic sketch of (a) wall film condensation for saturated and wet steam and (b) wall film condensation for saturated and wet steam in the presence of NCGs (air).

The resulting heat transfer model that was developed to predict the heat transfer due to wall condensation for saturated and wet steam is presented in Section 4.4.1; the heat transfer model developed to predict the heat transfer from wall condensation for saturated and wet steam in the presence of NCGs is introduced in Section 4.4.2.

4.4.1 Heat transfer modelling in the sterilization phase

In the sterilization phase (see Figure 2.2 and Figure 2.4), hardly any NCGs are present in the steam sterilizer's chamber. This fact means that the heat transfer rate from the steam to the load that occurs due to wall condensation effects is high.

The developed heat transfer model is based on the Convective Augmentation Factor (CAF) [78], which is defined by the ratio of the "real" Nusselt number for wall condensation ($Nu_{condensation}$), divided by the Nusselt number of the ideal flow ($Nu_{ideal\ flow}$) (see Eq. (4.4)).

$$CAF = \frac{Nu_{condensation}}{Nu_{ideal\ flow}} \tag{4.4}$$

The Nusselt number of the ideal flow is the Nusselt number that results from pure (natural and forced) convection. This Nusselt number is calculated by the CFD code out of the heat flux, the thermal conductivity, the position of the cell and the temperature difference between the wall temperature and the temperature of the fluid [78].

In order to determine the real Nusselt number due to wall condensation, a User-Defined Function (UDF) was developed, which analyses two different cases in every cell near the wall of the fluid domain. The two cases are shown in Eq. (4.5).

$$Nu = \begin{cases} Nu_{ideal\ flow} & \text{for } T_{wall} \geq T_{sat} \\ Nu_{ideal\ flow} \cdot CAF & \text{for } T_{wall} < T_{sat} \end{cases} \tag{4.5}$$

In the first case, the wall temperature (T_{wall}) is higher or equal to the saturation temperature of the steam (T_{sat}) (see the left side of Figure 4.2). In this case, heat transfer only happens due to (natural and forced) convection, and, thus, the Nusselt number was set to the originally calculated Nusselt number by the CFD code due to convection. In the second case, the saturation temperature of the steam is higher than the wall temperature, which results in wall condensation (see right side of Figure 4.2). Therefore, the Nusselt number was set to the Nusselt number calculated in Fluent, multiplied by the convective augmentation factor. The value of the CAF was obtained by calculating the Nusselt number on a vertical flat plate for natural convection and for wall condensation with an analytical formula. Eq. (4.6) shows the analytical formula that was used to calculate the Nusselt number for natural convection.

$$Nu_{ideal\ flow} = (0.825 + 0.387 \cdot Ra^{\frac{1}{6}} \cdot (1 + 0.671 \cdot Pr^{-\frac{9}{16}})^{-\frac{8}{27}})^2 \tag{4.6}$$

In Eq. (4.6), Ra stands for the Rayleigh number and Pr stands for the Prandtl number. The Nusselt number for wall condensation was calculated with Eq. (4.7):

$$Nu_{condensation} = 0.943 \cdot \left[\frac{g \cdot r \cdot (\rho_w - \rho_s) \cdot L_c^3}{\lambda_w \cdot \nu_w * (T_{sat} - T_{wall})} \right]^{\frac{1}{4}} \tag{4.7}$$

where L_c stands for the characteristic length of the vertical plate, g for the gravity, r for the enthalpy of evaporation, ρ_w is the density of the water and ρ_s is the density of

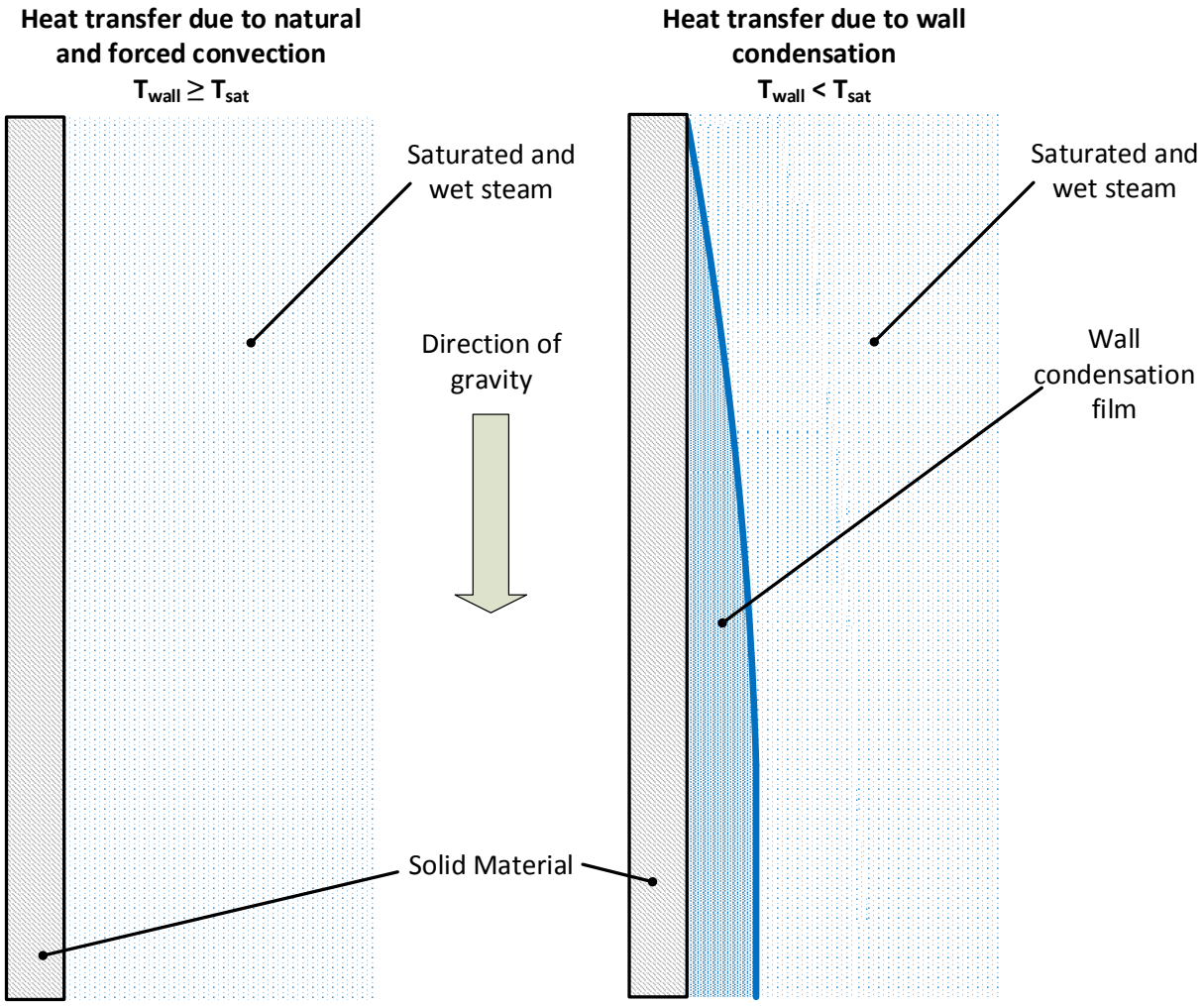

Figure 4.2: Schematic sketch of the heat transfer due to natural and forced convection (left) and due to wall condensation (right).

the steam. λ_w stands for the thermal conductivity of the water, ν_w for the kinematic viscosity of the water, and T_{sat} and T_{wall} stand for the saturation temperature and the wall temperature, respectively. Analytical calculations showed that the CAF has a value of approximately 3200 over the whole sterilization phase. Simulations were also performed with CAFs of 500, 2000, 5000 and 100,000. Simulations of the temperature of the load show hardly any difference between these convective augmentation factors. The main advantage of this approach is the efficiency with which the numerical calculation of the heat transfer can be accomplished, due to the fact that it is not necessary to simulate the wall film on the surface of the load. Therefore, a much coarser mesh can be used near the wall. This approach is able to calculate the heat transfer to unwrapped cylinders (see Section 5.3.3), wrapped cylinders (see Section 5.4.2), and both wrapped and unwrapped dental handpieces (see Section 5.5) with high accuracy.

4.4.2 Heat transfer modelling in the pre-sterilization phase

In the pre-sterilization phase (see Figure 2.2 and Figure 2.4), not only steam and condensed water are present in the sterilization chamber, but also NCGs (mainly air). Modelling the heat transfer due to wall condensation in the presence of NCGs using CFD is a difficult task. This topic has been addressed by various researchers in the past. For example, Yoon, Jo, and Corradini [109] developed a condensation model to predict the heat transfer with NCGs on a planar wall. Other works by Zschaeck et al. [110], Mimouni et al. [112] and Qiu et al. [113] also simulated heat transfer through condensation, and their simulation results were in good accordance with their experimental measurements. However, these models are limited by the fact that they only work on planar surfaces, or that they require a very fine mesh near the walls. Thus, a very numerically efficient model to predict heat transfer through wall condensation in a steam sterilizer, while NCGs are present, was developed in this PhD thesis.

This heat transfer model to predict the heat transfer due to wall condensation in the presence of NCGs is also based on the CAF. For this model, the CAF is defined by the Nusselt number due to condensation in the presence of NCGs ($Nu_{condensation\ NCGs}$) divided by the Nusselt number of the ideal flow ($Nu_{ideal\ flow}$). The Nusselt number of the ideal flow is the Nusselt number due to natural and forced convection.

$$CAF = \frac{Nu_{condensation\ NCGs}}{Nu_{ideal\ flow}} \tag{4.8}$$

The Nusselt number of the ideal flow (due to convection) ($Nu_{ideal\ flow}$) is calculated by the CFD code as a result of the flow field (see Eq. (4.9)) [78].

$$Nu_{ideal\ flow} = \frac{\dot{q}_p X_p}{(T_{wall} - T_b)\lambda} \tag{4.9}$$

In Eq. (4.9) $\dot{q}_p$, X_p, T_b and λ stand for the heat flux density at point p, the location of point p (represents the characteristic length), the bulk temperature of the fluid at point p and the thermal conductivity of the fluid, respectively. In Section 4.4.1 the CAF was obtained by calculating the Nusselt numbers using analytical formulas, and found that the CAF factor was approximately 3000. The main limitation of the heat transfer model described in Section 4.4.1 is that it is only applicable to steam and water that are not mixed with NCGs. As a result, this section seeks to expand upon the heat transfer model presented in Section 4.4.1 in order to be able to predict the heat transfer through wall condensation when NCGs are present. Therefore, the heat transfer model developed in this section separates three different cases (see Eq. (4.10)).

$$Nu = \begin{cases} Nu_{ideal\ flow} & \text{for } T_{wall} \geq T_{sat} \text{ or } 0 \leq \phi_{steam} \leq 0.02 \\ Nu_{ideal\ flow} \cdot \frac{CAF}{2} & \text{for } T_{wall} < T_{sat} \text{ and } 0.02 < \phi_{steam} \leq 0.9 \\ Nu_{ideal\ flow} \cdot CAF & \text{for } T_{wall} < T_{sat} \text{ and } 0.9 < \phi_{steam} \leq 1 \end{cases} \tag{4.10}$$

For wall temperatures (T_{wall}) higher than or equal to the saturation temperature of steam (T_{sat}), or for volume fractions of the steam ϕ_{steam} lower than 0.02, the heat transfer occurs only due to convection (see I in Figure 4.3). In this case, the Nusselt numbers were set to the Nusselt numbers of the ideal flow. The range of the volume fraction of the steam ϕ_{steam} was selected based on the fact that studies have shown that there is hardly any difference between heat transfer due to convection and heat transfer due to condensation at such low volume fractions of steam [114, 115]. In the second case, the wall temperature is lower than the saturation temperature, and the volume fraction of the steam is higher than 0.02 and lower than 0.9 (see II in Figure 4.3). In that case, the Nusselt number is set to the Nusselt number under ideal flow conditions times half of the CAF. The range of the volume fraction and the calculation of the Nusselt number was chosen by the author on the basis of studies that have investigated the heat transfer due to condensation in the presence of NCGs [116, 117]. In the third case

(see III in Figure 4.3), the wall temperature is lower than the saturation temperature, but the volume fraction of the steam at the wall is higher than 0.9. Therefore, the Nusselt number is set to the Nusselt number of the ideal flow times the CAF. This calculation of the Nusselt number was obtained from the measurement data of R. Chen et al. [118]. Their work shows that very high heat transfer rates occur at such high volume fractions of the steam.

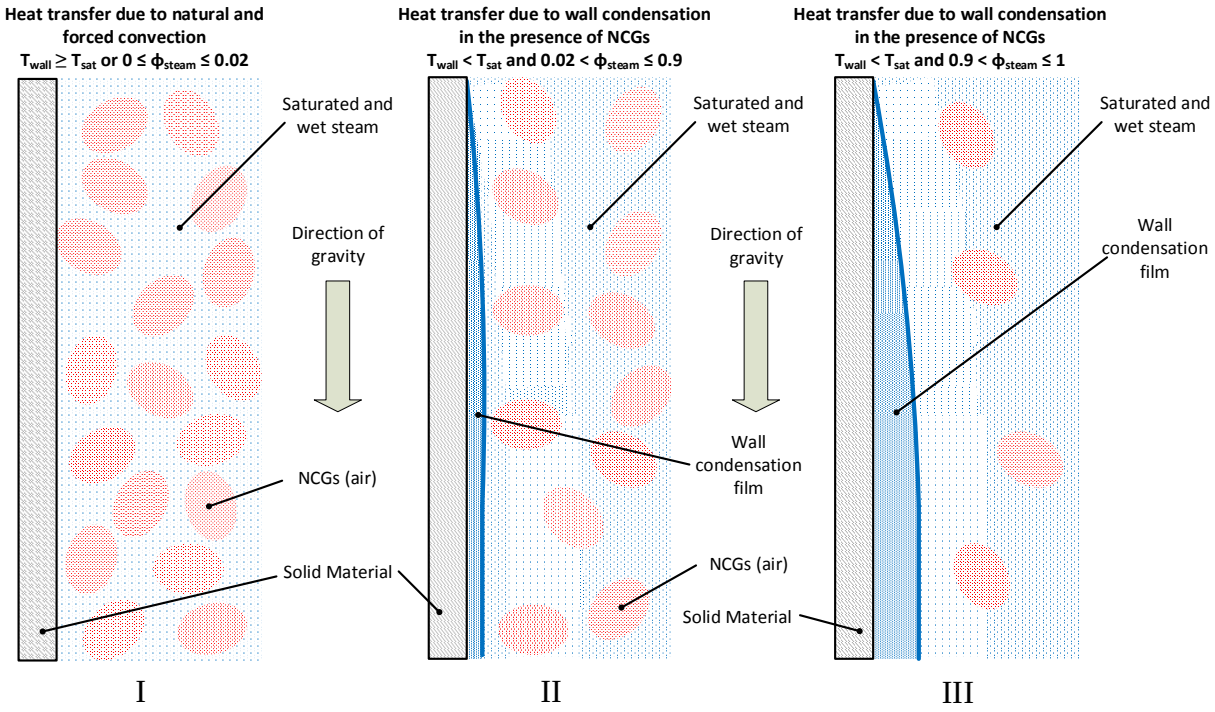

Figure 4.3: Schematic sketch of the heat transfer due to natural and forced convection (left), due to wall condensation with a high volume fraction of NCGs (middle), and due to wall condensation with a low volume fraction of NCGs (right).

The heat transfer model described in this section was used to simulate the removal of NCGs (air) inside both a vacuum and a non-vacuum steam sterilizer, and inside two different kinds of helix tests. The results presented in Section 5.1 and Section 5.6 demonstrate that the Nusselt number as calculated in the manner presented above (see Eq. 4.10) is able to predict the pressure, the temperature and the distribution of the NCGs inside the steam sterilizers as well as inside hollow loads (cavities).

4.4.3 Heat transfer between the phases

The heat transfer between the phases was modelled with an approach first published by Ranz and Marshall [119, 120]. The Nusselt number of the p^{th} phase (Nu_p) is shown in Eq. (4.11):

$$Nu_p = 2.0 + 0.6 \cdot Re_p^{\frac{1}{2}} \cdot Pr^{\frac{1}{3}} \tag{4.11}$$

where Re_p stands for the Reynolds number of the p^{th} phase and Pr for the Prandtl number of the p^{th} phase [78].

In the sterilization phase (see Figure 2.2 and Figure 2.4), only steam and condensed water are present inside the sterilization chamber. In this phase, the Ranz and Marshall model was used to calculate the heat transfer between these phases.

During the pre-sterilization phase (see Figure 2.2 and Figure 2.4) steam, condensed water, and NCGs are present inside the steam sterilizer. In this phase, the Ranz and Marshall model was used to calculate the heat transfer between the steam and the NCGs, between the steam and the condensed water, and between the NCGs and the condensed water.

4.5 Modelling the paper [5]

To investigate flow phenomena in the vicinity of the surface of the load, it is necessary to model the paper in which the load is wrapped. Therefore, a porous media model was developed to simulate the permeability of the paper. Porous media are modelled by adding a momentum source term to the standard fluid flow equation. The source term that was used in the CFD model can be seen in Eq. (4.12) [78]:

$$S_i = (\frac{\eta}{\alpha} v_i + \frac{1}{2} C_2 |\vec{v}_i| v_i) \tag{4.12}$$

where S_i is the source term, and η, v_i, $|\vec{v}_i|$ stand for the dynamic viscosity, the velocity of the i^{th} component, and the velocity magnitude, respectively. α is the permeability and C_2 is the inertial resistance factor. The pressure drop over the porous media is defined as:

$$\Delta p = -S_i \Delta n \tag{4.13}$$

where Δn stands for the thickness of the porous media. Measurements of the permeability of the paper were performed for both air and for steam. The experimental data

[5] Segments of this section have already been published in [1, 5].

are available in the form of pressure drop against velocity which was determined by an in-house test rig that was presented in Section 3.4. From this measured data, two porous media models to simulate the permeability of the paper for air and for steam were obtained. These new porous media models make it possible to simulate the fluids passing through the paper. Therefore, wrapped loads can be simulated. A validation of the new porous media models can be found in Section 5.2.

4.6 Modelling the bacteria

The inactivation of the bacteria was modelled following a first-order reaction kinetic approach (see in Eq. (2.1) and Eq. (2.2)). A source term was then used to simulate its inactivation rate. The temperature dependency of the inactivation rate was modelled with the Arrhenius equation (2.3). This source term was added to the CFD code using a UDF. More information about the approach used to model the inactivation of the bacteria can be found in literature [34, 121–123].

The active bacteria were added to every cell of the CFD code using a User-Defined Scalar (UDS). As the inactivation is dependent on the local cell temperature, the inactivation was resolved in time and space, in every cell. This novel approach to modelling the bacteria's inactivation makes it possible to simulate that inactivation both inside the steam sterilizer as well as on the surface of the load, over the whole sterilization cycle.

The reaction kinetics of the different bacteria types investigated are described in the Chapter: Results (see Section 5.3.4, Section 5.4.4 and Section 5.5.5).

4.7 Numerical grids [6]

In this section, all of the numerical grids that were used for the simulations in this thesis are presented. The geometry of the CFD models was generated in the ANSYS Design Modeller. The geometry of the CFD models was obtained from Computer-Aided Design (CAD) models of the sterilization chamber, diffusers, trays and medical equipment. Based on these geometries, all of the numerical grids were generated with the ANSYS Meshing Tool or ANSYS ICEM CFD.

[6] Segments of this section have already been published in [1–5].

4.7.1 Numerical grid for unwrapped loads

The steam sterilizer with the trays, the diffuser, and the unwrapped cylinders was analysed with approximately 550,000 polyhedral and hexahedral cells, including both the fluid and solid geometries of the steam sterilizer. The geometry of the CFD model can be seen in Figure 3.3. To get a better overview, the numerical grid is shown in Figure 4.4. As can be seen, both the fluid and the solids inside the steam sterilizer were finely resolved. The maximum skewness of the mesh was 0.799 while the maximum aspect ratio was 21.17. To verify the mesh independence, a finer grid was used. The fine numerical grid consisted of 1,445,982 (polyhedron and hexahedron) cells. The maximum aspect ratio was 35.21. The skewness of the fine mesh was 0.884. The differences in the simulated temperatures between the grid with approximately 550,000 cells and the grid with 1,445,982 cells were below the uncertainties of the thermocouples used (approximately ± 1 K).

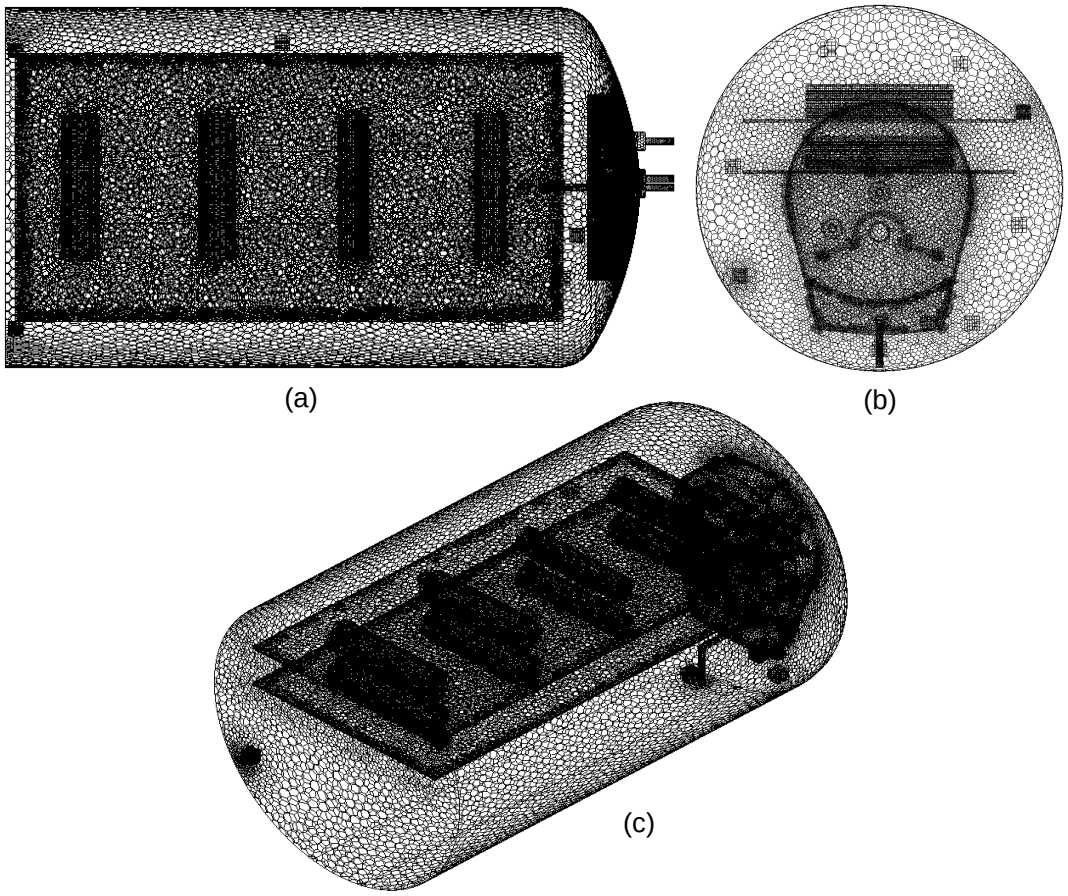

Figure 4.4: (a) Top view of the numerical grid with the unwrapped load, (b) back view of the numerical grid with the unwrapped load, and (d) a 3D-view of the numerical grid with the unwrapped load [4].

4.7.2 Numerical grid for wrapped load

As introduced in Section 3.2.2, this thesis investigated wrapped loads by simulating a sterilization cycle with eight cylinders on two trays. All eight cylinders were wrapped in paper. The whole set-up of the investigated load and a picture of the wrapped cylinders were shown in Figure 3.4. The paper in which the load is wrapped was modelled with a porous media approach, as described in Section 4.5.

To model the steam sterilizer filled with the wrapped load, in the first step, a numerical grid with 1,931,120 elements (tetrahedrons and hexahedrons) was created. As a result of the high computational costs and convergence characteristics, the tetrahedrons were converted into polyhedrons. This results in a final numerical grid with 684,478 polyhedral and hexahedral cells, including the whole fluid volume of the steam sterilizer, the porous media for the paper and the solids for the wrapped load, the trays, and the diffuser. The maximum skewness of the grid was 0.859, while the maximum aspect ratio was 20.24. The 684,478-polyhedron grid including all solids (load, trays, and diffuser) can be seen in Figure 4.5.

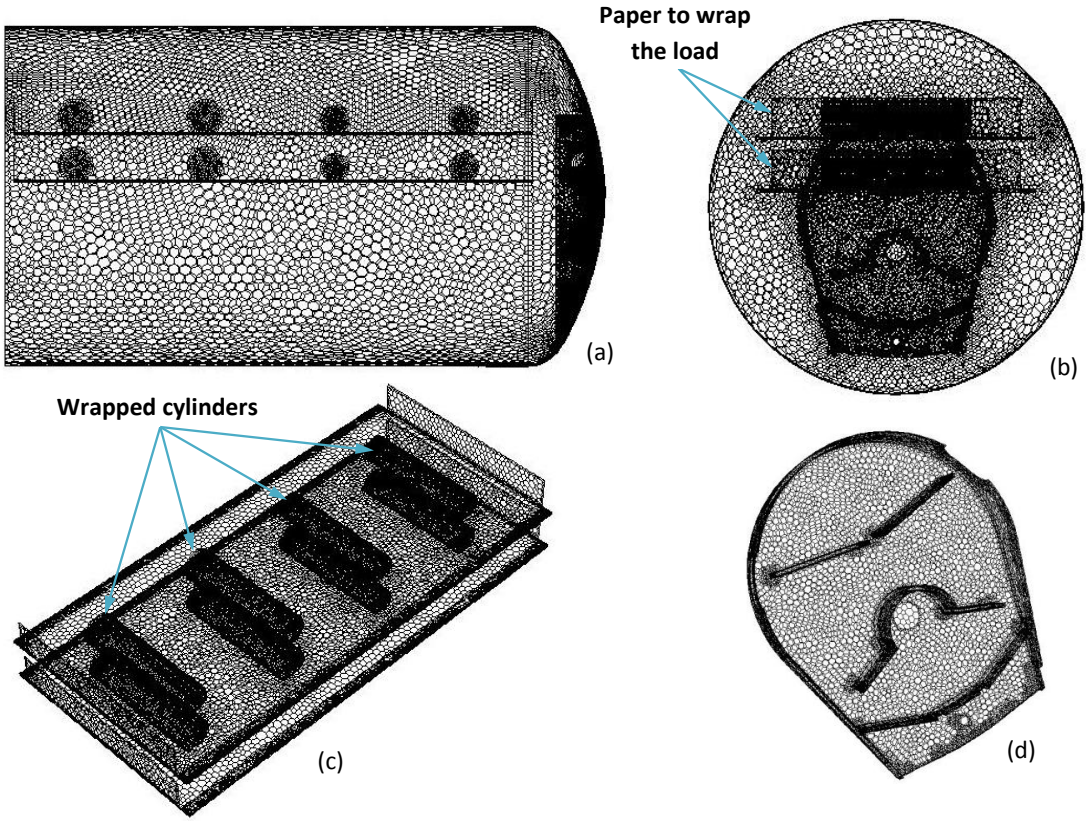

Figure 4.5: Computational grid with the wrapped load (a) view from the side, (b) view from the front, and the computational grid of the components (c) trays and load and (d) diffuser.

Several calculations with different grid sizes were performed to verify the grid independency. The number of cells was increased up to 1,841,194 cells in the whole steam

sterilizer. The influence of even more cells on the temperature and other flow variables, such as velocity and heat transfer, was also examined and the temperature of the load between the two meshes was monitored and compared. The deviation of the load temperature between these two grids was below 0.2 K, which is within the uncertainty range of the thermocouples (approximately ± 1 K).

4.7.3 Numerical grid for the dental handpieces

The simulations of dental handpieces were carried out with four Type 1 dental handpieces [124] and four Type 2 dental handpieces [125]. More information about the types of handpieces investigated can be found in Section 5.5. Two dental handpieces of each type were distributed on two trays. The four handpieces on the first tray were wrapped in paper, whereas the four dental handpieces on the second tray were unwrapped (see Figure 4.6). The paper containing the dental handpieces on the first tray was modelled using the porous media approach described in Section 4.5. Further information about the load set-up of the dental handpieces can be found in Section 5.5.

The whole steam sterilizer, including the entire fluid domain, the two trays, the diffuser, the chamber with its insulation, and the eight dental handpieces were meshed with 1,140,783 tetrahedral and hexahedral cells. Afterwards, this numerical grid was converted into a polyhedral and hexahedral mesh with 647,909 cells. The maximum skewness and aspect ratio of the numerical grid were 0.89 and 33.41, respectively. Figure 4.6 shows the numerical grid of the sterilization chamber, filled with the wrapped dental handpieces (first tray) and unwrapped dental handpieces (second tray). Furthermore, the mesh of the paper containing the dental handpieces is shown. A numerical grid with 202,985 cells was investigated as well. This numerical grid slightly over-predicted the heat fluxes due to condensation. Furthermore, two numerical grids with a higher number of cells were considered. These grids were 1,567,467 and 8,364,196 in size, respectively. Hardly any differences in any of the transported scalars were detected between the grids with 647,909 and 8,364,196 cells.

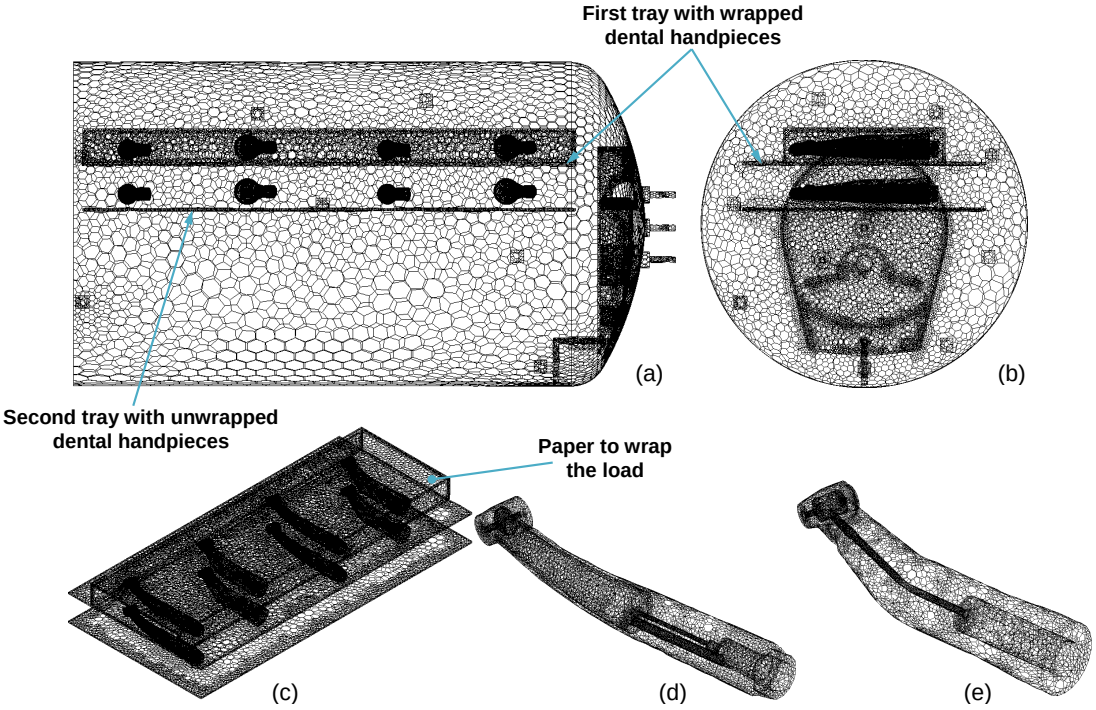

Figure 4.6: Numerical grid with the dental handpieces (647,909 cells) (a) from the side, (b) from the front, (c) view of the trays, (d) view of the dental handpiece – Type 1 and (e) view of the dental handpiece – Type 2.

4.7.4 Numerical grids to simulate the removal of the NCGs

In this thesis, the removal of the NCGs was investigated for a vacuum (see geometry in Figure 3.1) and for a non-vacuum steam sterilizer (see geometry in Figure 3.2).

The vacuum steam sterilizer was meshed with 620,776 polyhedral and hexahedral cells, including the fluid, the diffuser, the tray and the helix test. The maximum skewness and maximum aspect ratio of the mesh were 0.8963 and 30.04, respectively. A side view and a front view of the mesh used can be seen in Figure 4.7(a). The mesh of the non-vacuum steam sterilizer consists of 574,343 polyhedral and hexahedral cells. The maximum skewness of the mesh was 0.8963, and the maximum aspect ratio was 33.74. The mesh of the non-vacuum steam sterilizer is shown in Figure 4.7(b). Mesh independency studies were performed with two meshes for each steam sterilizer, with approximately 2.4 and 8 million cells, respectively. Hardly any differences were found between the solutions provided by the different meshes.

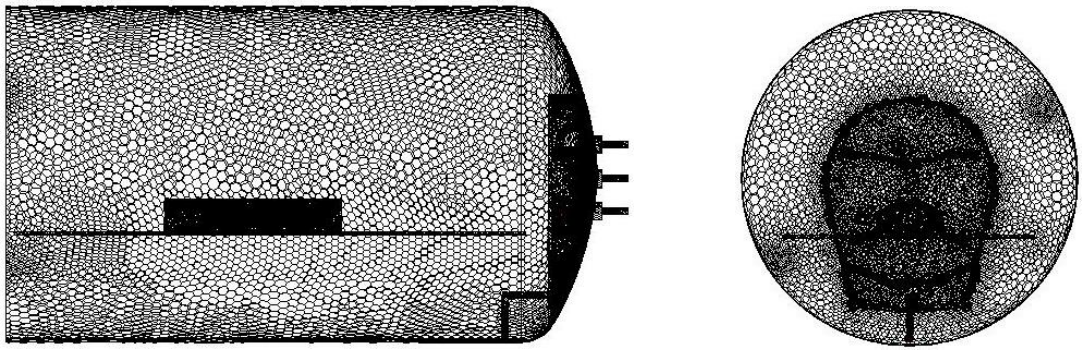

(a) Front and side view of the mesh of the vacuum steam sterilizer

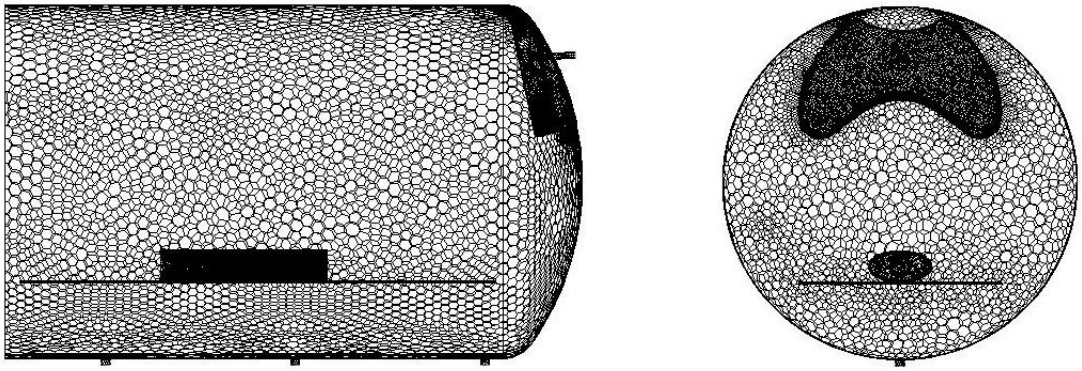

(b) Front and side view of the mesh of the non-vacuum steam sterilizer

Figure 4.7: Mesh of the (a) vacuum steam sterilizer and (b) of the non-vacuum steam sterilizer [2].

4.7.5 Numerical grids to simulate hollow loads (cavities)

The removal of the NCGs and the steam penetration into hollow loads was investigated using two different PCDs (helix tests) (see Figure 3.10).

The steam sterilizer containing PCD 1 was meshed with 695,232 polyhedral and hexahedral cells (see Figure 4.8(a)). The minimum orthogonal quality of the mesh was 0.0783, maximal aspect ratio was 26.69. The steam sterilizer containing the PCD 2 was meshed with 624,699 cells (see Figure 4.8(b)). The minimal orthogonal quality and aspect ratio were 0.1007 and 32.85, respectively. Mesh independence studies were performed with meshes of approximately 1,200,000 cells and 11,000,000 cells. Hardly any differences were found between the meshes in terms of the pressure, the temperature or the volume fractions.

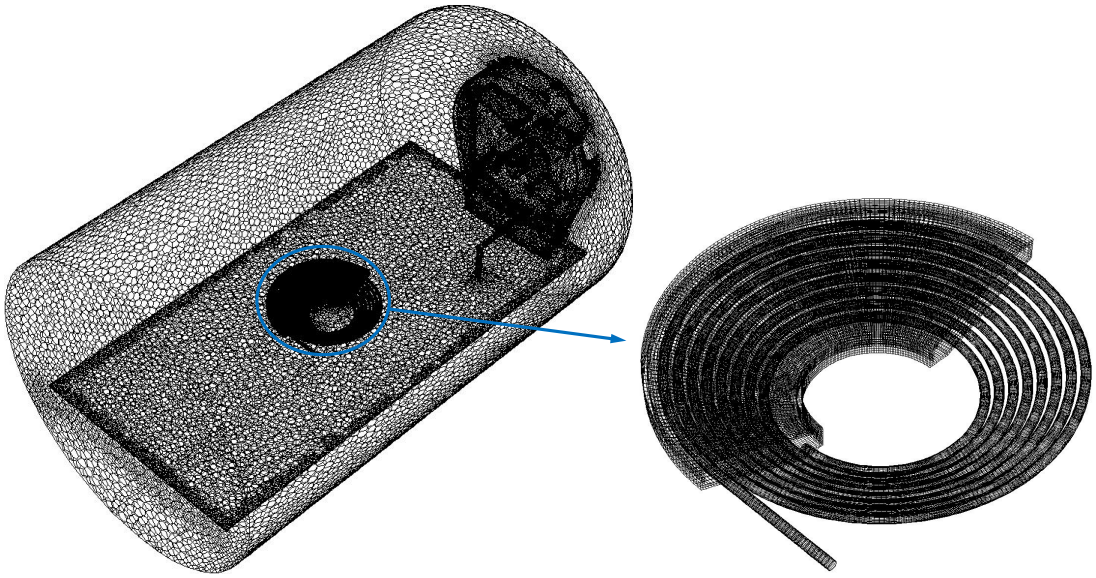

(a) Numerical grid of the vacuum steam sterilizer with the first helix test (PCD 1).

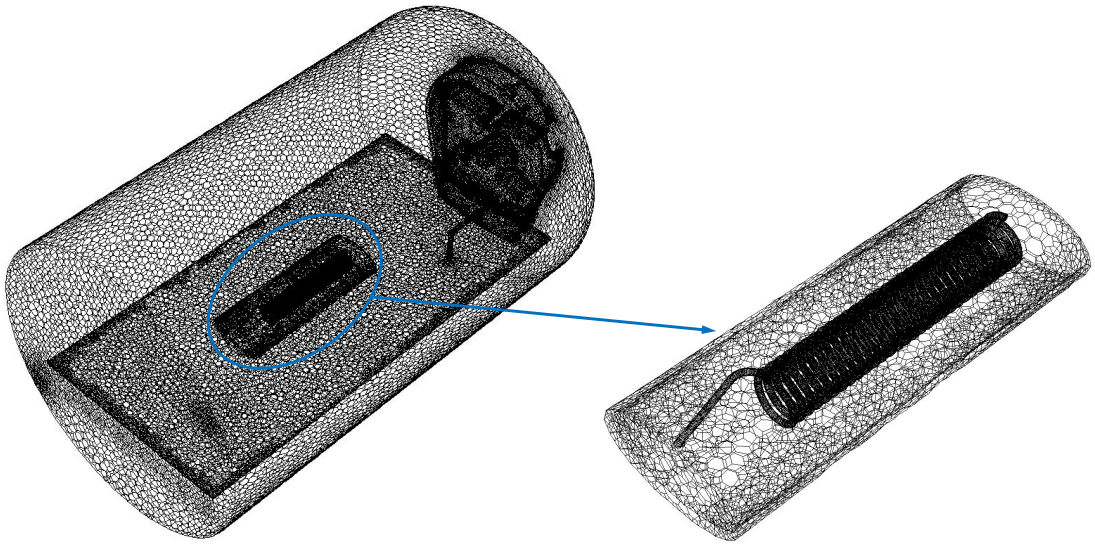

(b) Numerical grid of the vacuum steam sterilizer with the second helix test (PCD 2).

Figure 4.8: Numerical grid of the vacuum steam sterilizer with (a) the first helix test (PCD 1) and (b) the second helix test (PCD 2).

4.8 Boundary conditions [7]

This section provides a general overview of all the boundary conditions used to simulate the steam sterilization process in this thesis. Nearly all of the boundary conditions were time-dependent. These time-dependent boundary conditions were added to the CFD model using UDFs.

4.8.1 Boundary condition to simulate the sterilization phase

The 2100 W steam generator that increases the pressure inside the steam sterilizer to the sterilization plateau (see Figure 2.2 and Figure 2.4) was modelled with a pressure inlet. The steam's pressure and temperature were set to values based on measurements. According to these measurements, the steam at the inlet is saturated. Turbulence was modelled with a hydraulic diameter of 0.005 m and a turbulence intensity of 5 %. In the sterilization phase, the outlet of the steam sterilizer is always closed. Therefore, the outlet was modelled as an adiabatic wall. The outer walls of the real steam sterilizer are insulated; therefore, a convective boundary condition with a heat transfer coefficient of 5 $\frac{W}{m^2K}$ and a free stream temperature of 293.15 K was used to simulate the heat transfer from the insulation and the outer walls to the ambient air. All of the wall temperatures inside the steam sterilizer were calculated with the heat transfer model that was developed in-house and described in Section 4.4.1 (see Eq. (4.5)).

In this thesis, the sterilization phase was simulated with both unwrapped and wrapped loads, consisting of different cylinders, as well as with dental headpieces. The material properties used to simulate the fluids of the sterilization phase can be seen in Table 4.1. Table 4.2 shows the material properties of all of the solids that were used in the simulations, either as materials for the steam sterilizer or for the loads.

The pressure at the beginning of the sterilization phase was initialised with the corresponding measured pressure. The temperature inside the steam sterilizer was initialised with the average measured temperature value of the eight thermocouples. The load temperatures, the temperatures of the trays, and the temperature diffuser were also initialised according to measured values.

[7] Segments of this section have already been published in [1–5].

Table 4.1: Fluid material properties for the CFD simulation of the sterilization phase.

Steam (gas phase)	
Density (kg/m^3)	ideal gas (see section 4.1.1)
Specific heat (J/kgK)	piecewise polynomial
Thermal conductivity (W/mK)	0.0242
Viscosity (kg/ms)	$1.7894 \cdot 10^{-5}$

Water (liquid phase)	
Density (kg/m^3)	piecewise polynomial
Specific heat (J/kgK)	4246.7
Thermal conductivity (W/mK)	0.6
Viscosity (kg/ms)	0.001003

Table 4.2: Solid material properties for the CFD simulation of the sterilization phase.

Steel (stainless)	
Density (kg/m^3))	7900
Specific heat (J/kgK)	500
Thermal conductivity (W/mK)	20

Aluminium	
Density (kg/m^3)	2700
Specific heat (J/kgK)	897
Thermal conductivity (W/mK)	236

Brass	
Density (kg/m^3)	8500
Specific heat (J/kgK)	377
Thermal conductivity (W/mK)	120

Plastic (PPS)	
Density (kg/m^3)	1550
Specific heat (J/kgK)	1660
Thermal conductivity (W/mK)	0.2

Paper	
Density (kg/m^3)	800
Specific heat (J/kgK)	200
Thermal conductivity (W/mK)	0.5

4.8.2 Boundary conditions used to simulate the pre-sterilization phase

In this thesis, the removal of the NCGs during the pre-sterilization phase in both a vacuum steam sterilizer (see Figure 2.2) and a non-vacuum steam sterilizer (see Figure 2.4) was simulated. Therefore, this section describing the boundary conditions that were used to simulate the pre-sterilization phase was divided into two parts.

Boundary conditions for the pre-sterilization phase of the vacuum steam sterilizer

The pre-sterilization phase of a vacuum steam sterilization cycle was simulated so as to investigate the process of air removal from inside the steam sterilizer, as well as inside hollow loads (cavities). The measured pressure profile and the average temperature in the sterilization chamber of the investigated vacuum steam sterilization cycle are presented in Figure 4.9. Table 4.3 describes in detail the various stages that take place in the course of the investigated pre-sterilization phase, depicted graphically in Figure 4.9. Table 4.3 also provides a detailed description of the times at which the outlets were either open or closed, and of the minimum and maximum pressures that were reached at the end of the respective phases. The durations of each phase, which are presented in Table 4.3, may vary based on the chamber's load or according to the initial conditions inside the steam sterilizer.

Generally, during any period where the pressure increases, a 2100 W steam generator fed steam into the chamber of the vacuum steam sterilizer.This steam generator was modelled using a mass flow inlet. The mass flow rate, temperature, and quality of the steam were set according to the measurements. Turbulence boundary conditions were modelled with a hydraulic diameter of 0.005 m and a turbulent intensity of 5 %. When the inlet was closed (during the pressure decreases), the inlet was modelled as an adiabatic wall, due to the fact that the surface of the inlet is negligibly small compared to the other surfaces of the steam sterilization chamber. A pressure outlet represents the vacuum pump, which is mounted on the steam sterilizer to reduce pressure inside the sterilization chamber. The pressure at the outlet was set according to the measurements. All wall temperatures of both the dry and wet surfaces were calculated based on the heat transfer model described in Section 4.4.1. On the outside of the steam sterilizer, a heater (see Figure 2.1(a)) is used to heat up the chamber walls. A detailed description of the function of this heater is provided in Section 2.1.1. The outer wall temperatures were set according to the measured values.

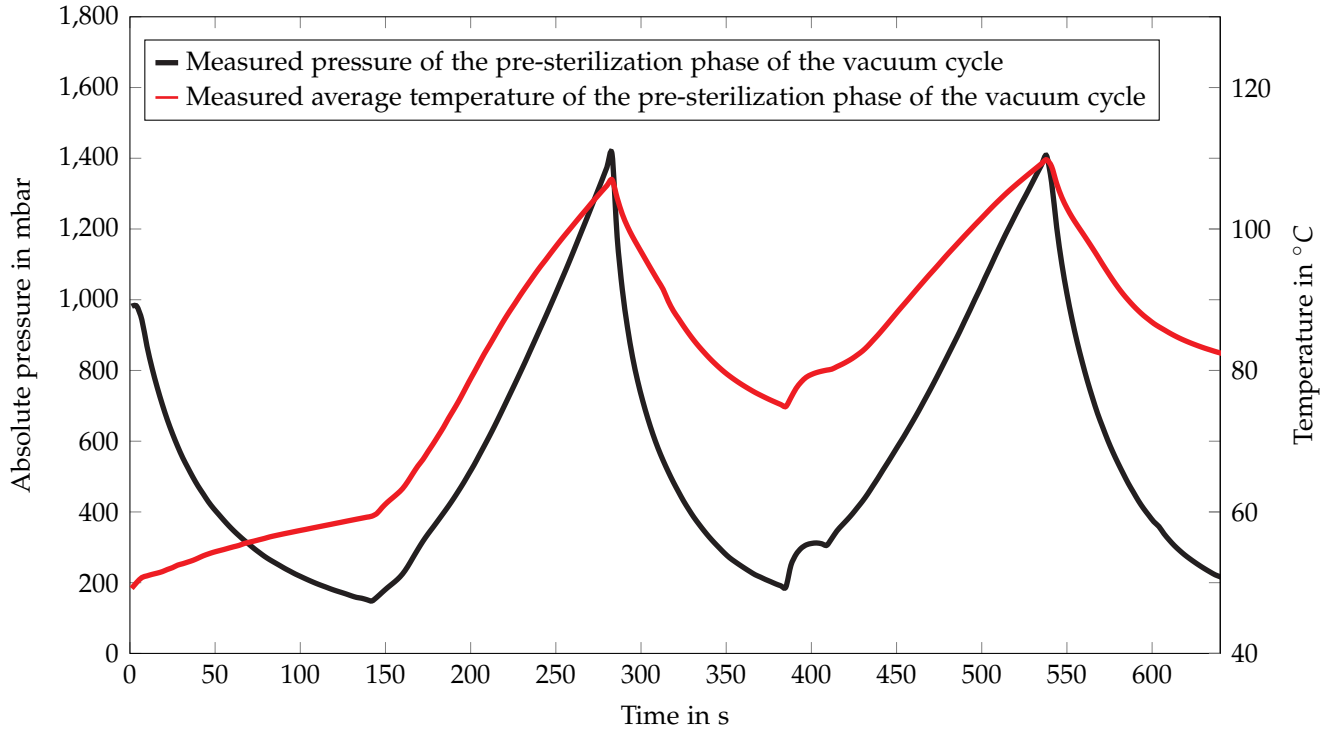

Figure 4.9: Measured pressure and measured average temperature in the pre-sterilization phase of the investigated vacuum steam sterilizer.

Table 4.3: Description of pre-sterilization phase of the vacuum steam sterilizer including the times at which the inlet and outlets were open or closed closed.

Cycle time	Inlet	Outlets	Description
0-143	closed	open	the steam sterilizer is filled with air; a vacuum pump reduces the pressure from the ambient pressure to approximately 142 mbar
143-298	open	closed	all outlets are closed; steam generator works at full power and increases the pressure to approximately 1.4 bar
298-393	closed	open	the steam generator is switched off; the vacuum pump reduces the pressure to approximately 140 mbar for a second time
393-548	open	closed	the steam generator increases the pressure to a value of approximately 1.4 bar; all outlets are closed
548-648	closed	open	the inlets are closed; the vacuum pump reduces the pressure to approximately 140 mbar a final time

Boundary conditions for the pre-sterilization phase of the non-vacuum steam sterilizer

The measured pressure and the measured average pressure during the pre-sterilization phase of the non-vacuum steam sterilizer are presented in Figure 4.10. During the pre-sterilization phase, a 2100 W steam generator fed steam into the non-vacuum sterilizer, thereby flushing NCGs out of the chamber, and, subsequently, increasing the pressure inside the chamber when the outlets were closed. The incoming steam was modelled using a mass flow inlet. The mass flow rate was set according to measurements. Turbulence was modelled with a hydraulic diameter of 0.005 m and a turbulence intensity of 5 %.

A description of the investigated pre-sterilization phase (depicted graphically in Figure 4.10) can be found in Table 4.4. Table 4.4 also presents the times at which the outlets were closed or opened. In the pre-sterilization phase, the outlets are closed for the first 59 s of the cycle. During this time, the outlets are modelled as adiabatic walls due to the small size of their surfaces compared to the other walls of the steam sterilizer. Outlets were modelled as pressure outlets during the times when the outlets were open (between 59 s and 640 s of the investigated pre-sterilization phase, see Figure 4.10). The pressure at the outlet was set according to the measured pressure profile.

An electrical heater was placed outside the chamber to heat up the chamber's walls. The outside wall temperature was set according to measurements. The position of the heater can be seen in Figure 2.3. A description of the heater's functionality is provided in Section 2.1.2.

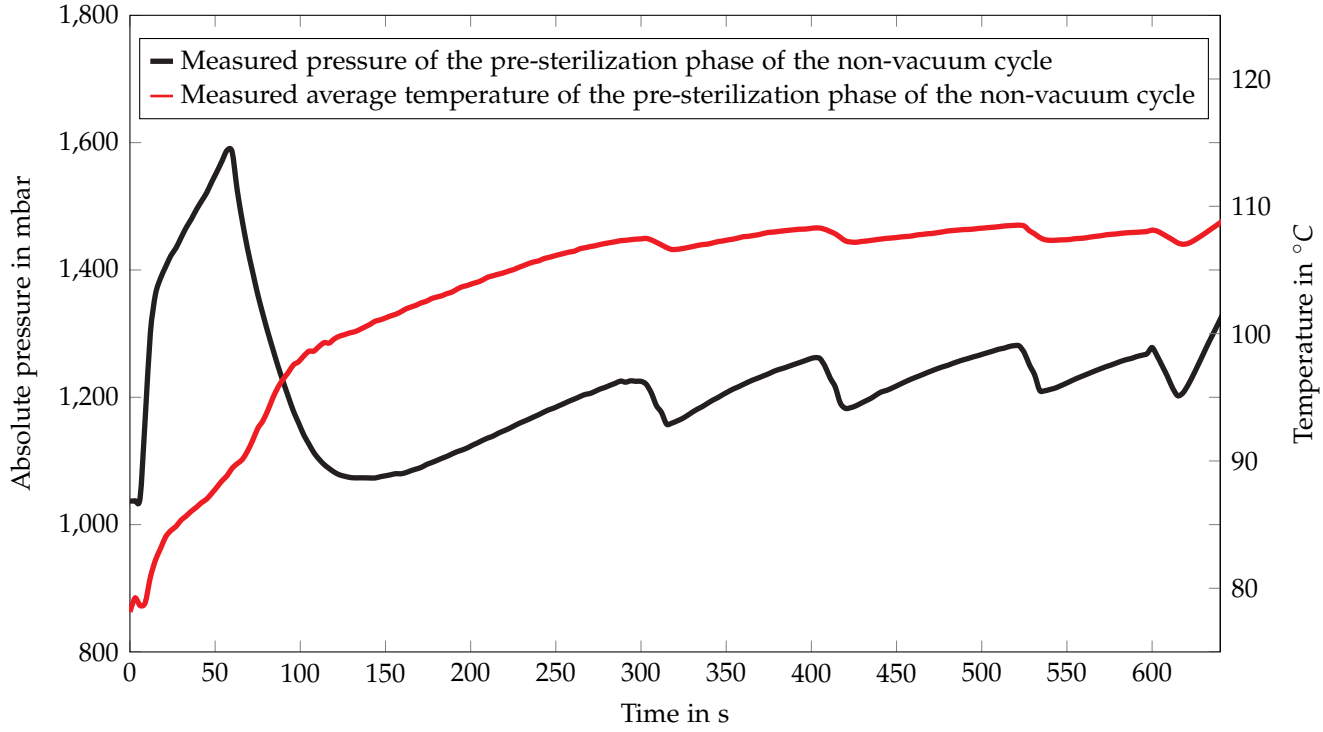

Figure 4.10: Measured pressure and measured average temperature in the pre-sterilization phase of the investigated non-vacuum steam sterilizer.

Table 4.4: Description of pre-sterilization phase of the non-vacuum steam sterilizer including the times at which the inlet and outlets were open or closed.

Cycle time	Inlet	Outlets	Description
0-59	open	closed	the steam sterilizer is filled with air; all outlets are closed; generator works at full power and increases the pressure to approximately 1.6 bar;
59-140	open	open	steam generator works at full power and feeds steam into the sterilization chamber; all outlets are open; air, wet steam and condensed water are exiting in the sterilization chamber;
140-640	open	open	steam generator works at full power and feeds steam into the sterilization chamber; all outlets are open; the pressure fluctuation are due to the control circuit of the control unit of the steam sterilizer;

5 Results

This chapter will present all of the results that were obtained in the course of this PhD thesis. First, the removal of the NCGs (air) from the vacuum and non-vacuum steam sterilizers was investigated. Second, the model that was developed to simulate the paper in which the load can be wrapped was validated. Third, simulations of the load temperature and the inactivation of different bacteria types were carried on both unwrapped and wrapped cylinders, as well as unwrapped and wrapped dental handpieces. Finally, the processes of air-removal and the steam penetration inside hollow loads and cavities were simulated.

5.1 Investigations of the removal of NCGs in the pre-sterilization phase [1]

This section presents both the simulated and the measured results of the removal of the NCGs (namely air) inside the chamber of the steam sterilizers. The removal of the NCGs was investigated in the pre-sterilization phase of both a vacuum (see "pre-sterilization phase" in Figure 5.1(a)) and a non-vacuum steam sterilizer (see "pre-sterilization phase" in Figure 5.1(b)). For this purpose, the pre-sterilization phases were simulated using CFD. The simulation results were then validated using measurement data of the pressure, the fluid temperature, and the ratio of the NCGs.

Figure 5.1 shows the measured pressures and the measured temperatures within the sterilization chamber for the vacuum sterilization cycle (see Figure 5.1(a)) and for the non-vacuum sterilization cycle (see Figure 5.1(b)). As mentioned above, in this section, only the pre-sterilization phases of the two sterilization cycles were investigated. More

[1] Segments of this section have already been published in [2].

detailed information about the entire steam sterilization cycle of each sterilizer can be found in Section 2.1.1 and Section 2.1.2. Detailed accounts of the pre-sterilization phases of the investigated steam sterilization cycles can be found in Section 4.8.2.

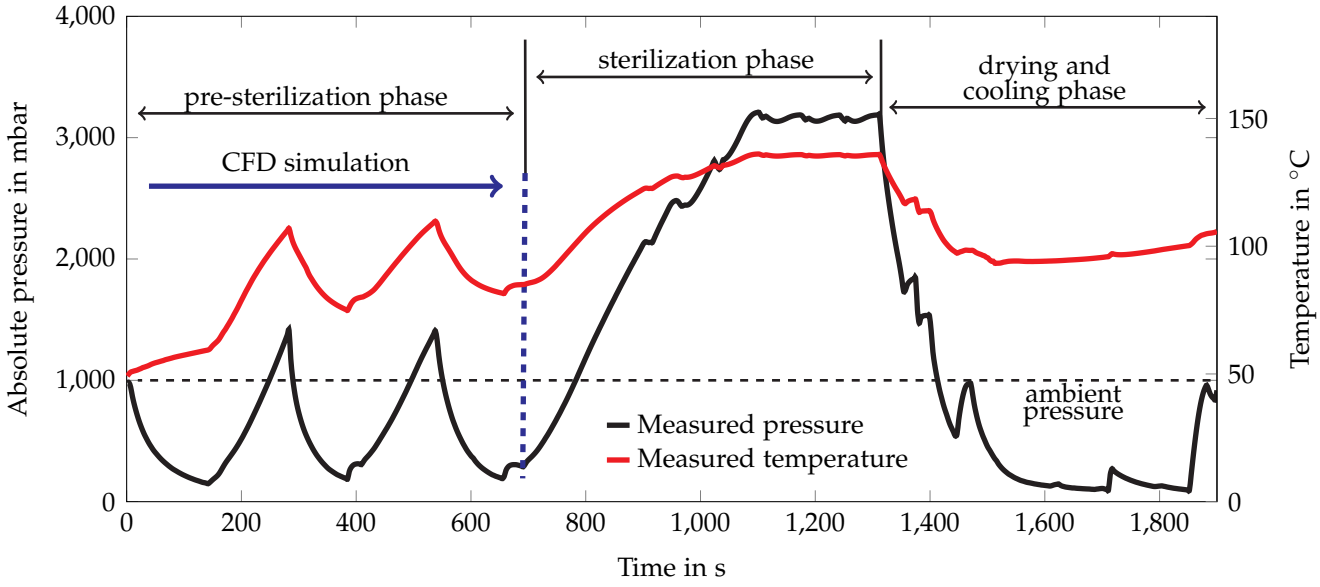

(a) Measured pressure and temperature to investigate the removal of NCGs from the vacuum steam sterilizer.

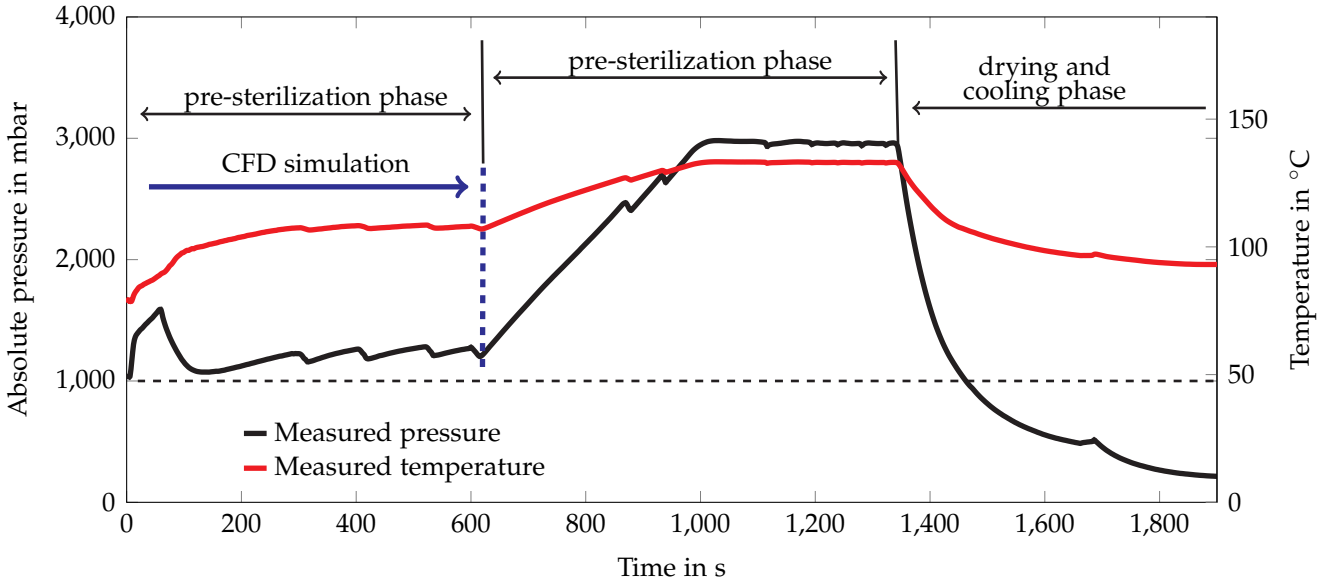

(b) Measured pressure and temperature to investigate the removal of NCGs from the non-vacuum steam sterilizer.

Figure 5.1: Measured pressure and temperature of the sterilization cycles to investigate the NCGs-removal in the (a) vacuum steam sterilizer and (b) non-vacuum steam sterilizer.

5.1.1 Pressure and temperature during the pre-sterilization phase

The results of the simulated flow inside the steam sterilizer were validated using the measurements of a pressure sensor and several thermocouples. The positions

of the pressure sensor and the thermocouples in the vacuum steam sterilizer are shown in Figure 3.1, while Figure 3.2 shows the positions of the pressure sensor and the thermocouples in the non-vacuum steam sterilizer. Small volumes of 10 mm $\times$ 10 mm $\times$ 10 mm were defined in the numerical grid of the CFD model in order to compare the measured values with the simulated ones. Using these volumes, volume average monitors of temperature or the pressure were defined for comparison with the measurements.

The temperature was measured with type J thermocouples. The diameter of the thermocouples was 1 mm and the maximum margin of error was $\pm$ 1 K. The maximum margin of error of the pressure sensor was $\pm$ 0.75 %. The measured pressure and the average temperatures of the eight thermocouples of both investigated cycles can be seen in Figure 5.1. The simulation starts at the beginning of the steam sterilization cycle and ends before the pressure starts to increase to the sterilization plateau (approximately 3 bar and 134°C) (see "pre-sterilization phase" in Figure 5.1). Figure 5.2(a) shows the simulated and measured pressures for the relevant phase of the vacuum steam sterilization cycle. This figure indicates the excellent accordance between the simulated and measured pressures. Both the simulated and measured pressures for the non-vacuum steam sterilizer can be seen Figure 5.2(b). The simulated and the measured pressures are in very good accordance for the non-vacuum steam sterilization cycle, as well. The validation of the CFD model of the non-vacuum steam sterilizer was performed in a similar manner as described above. The results indicate that the simulated temperature is in good accordance with the measured temperature (see Figure 5.3(a) and Figure 5.3(b)). The differences between the measured and the simulated temperatures are within the measuring inaccuracy of the thermocouples for 99% of the simulated time. Furthermore, a comparison between the measured and simulated temperatures at specific locations in the sterilization chamber showed that not only the average temperature, but also the measured and simulated temperature at specific locations were in very good accordance.

The differences between the measured and the simulated pressures were approximately 0.7 % throughout the entire simulated pre-sterilization phase of both the vacuum and non-vacuum steam sterilizers. Due to the fact that the pressure sensor had an uncertainty of $\pm$ 0.75 %, the measured and the simulated pressures were in excellent accordance. The average error between the simulated and measured temperatures was approximately 1.3 K in the simulated pre-sterilization phases. This difference is slightly higher compared with the uncertainties of the thermocouples, which was $\pm$ 1 K. Nevertheless, an average difference of 1.3 K is still a very good result. These

detailed validations demonstrate that the developed CFD model is able to correctly predict the fluid flow, the heat transfer due to condensation, and the temperature inside steam sterilizers. To obtain these results, the heat transfer model that was developed by the author to calculate the heat transfer due to wall condensation (see Section 4.4.2) is of high importance. Without this model, the condensation would not be simulated correctly, and, therefore, it would not be possible to predict either the pressure or the temperature with this high degree of accuracy (see Figure 5.2 and Figure 5.3). Having validated the CFD model with these accurate calculations of pressure and temperature, the model will subsequently be used to calculate the NCGs ratio inside the steam sterilizers.

5.1.2 Ratio of NCGs during the sterilization cycle

According to the EN 13060, the volume of NCGs within a steam sterilizer must be below 3.5 % of the volume of condensed steam [8]. The norm only requires one measurement at the beginning of the sterilization plateau (indicated by the blue circles in Figure 3.9). The goal of this section was to investigate the trend of NCGs inside the steam sterilizers; therefore, the NCGs ratio was measured at different cycle times. Furthermore, the difference between the NCGs ratio according to the norm (see Eq. (3.1)) and the real volume fraction of NCGs (see Eq. (3.5)) was investigated. The measurement set-up used to determine the volume of NCGs inside the steam sterilizer was shown and described in Section 3.5. A CFD model was developed to simulate the volume fraction of NCGs inside the two steam sterilization cycles that were investigated. The definition of the volume fraction in the CFD models (ϕ_{CFD}) is shown in Eq. (5.1).

$$\phi_{CFD} = \frac{\sum_{i=1}^{k} V_{Cell,i} \cdot \phi_{NCGs,i}}{V_{Sterilizer}} \tag{5.1}$$

where $V_{Cell,i}$ represents the cell volume and $\phi_{NCGs,i}$ denotes the volume fraction of NCGs in the individual cells of the numerical grid. $V_{Sterilizer}$ represents the total volume of the sterilizer and k represents the total number of the fluid cells of the numerical grid. In summary, Eq. (5.1) is equivalent to the real volume of the NCGs ϕ_{real} (see Eq. (3.5)). Figure 5.4(a) shows the time curve of the simulated volume fraction of the NCGs (see Eq. (5.1)), the NCGs according to the norm (see Eq. (3.1)), the calculated real volume fraction of the NCGs (see Eq. (3.7)) and the measured pressure for the pre-sterilization phase of the vacuum sterilization cycle (see "pre-sterilization phase" in Figure 5.1). In the first 142 seconds of the cycle, a vacuum pump reduces the pressure

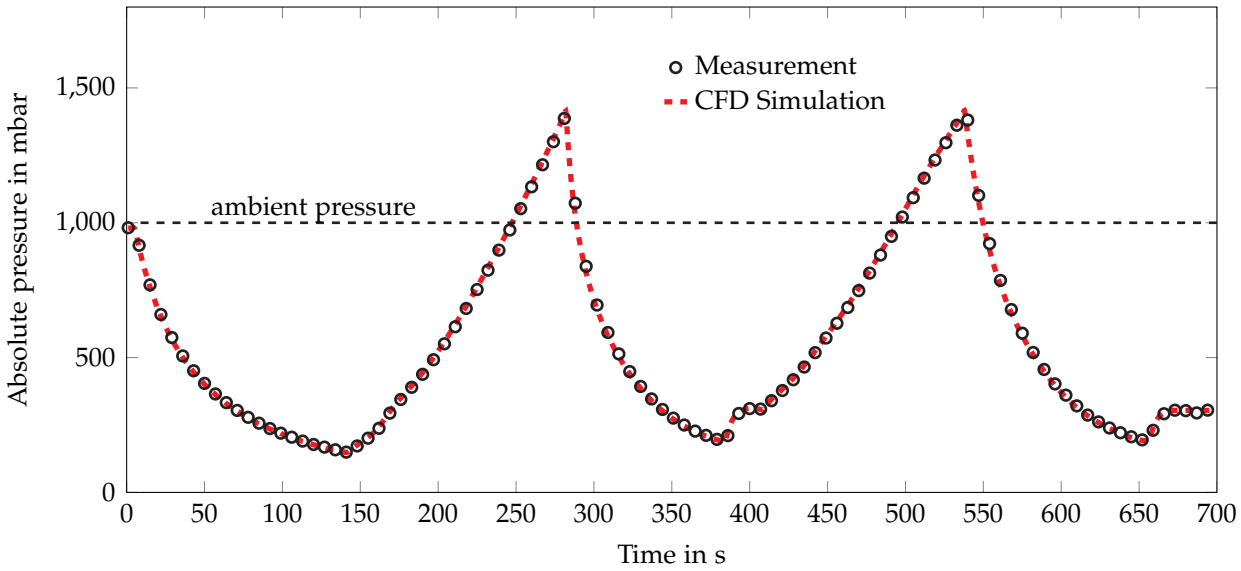

(a) Measured and simulated pressures for the vacuum steam sterilizer.

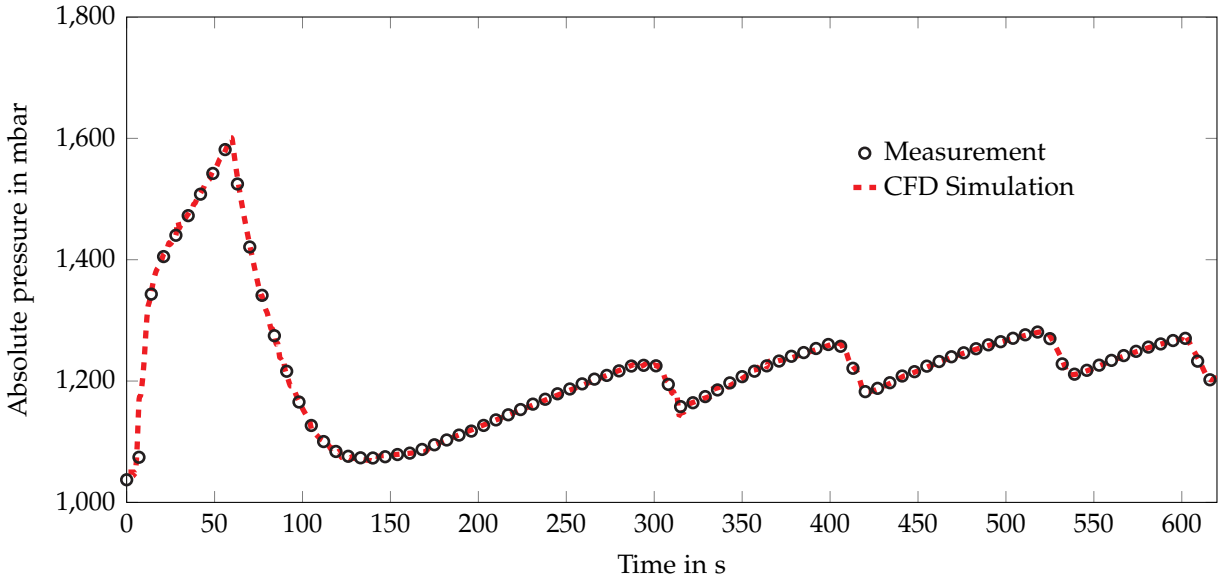

(b) Measured and simulated pressures for the non-vacuum steam sterilizer.

Figure 5.2: Measured and simulated pressures in the (a) vacuum steam sterilizer and (b) in the non-vacuum steam sterilizer [2].

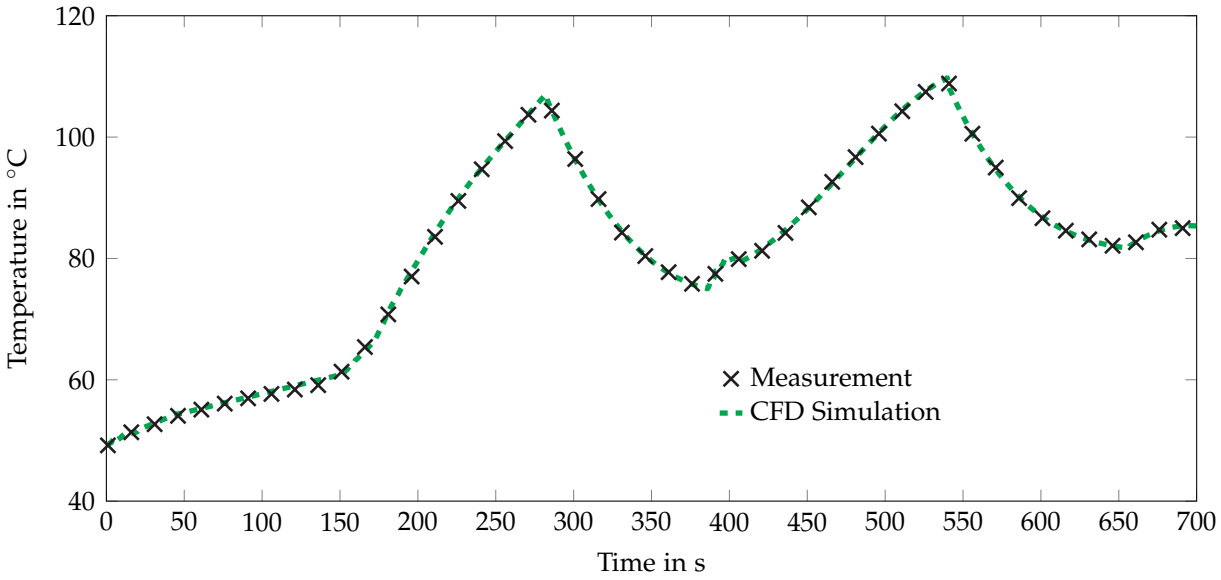

(a) Measured and simulated average temperatures in the vacuum steam sterilizer.

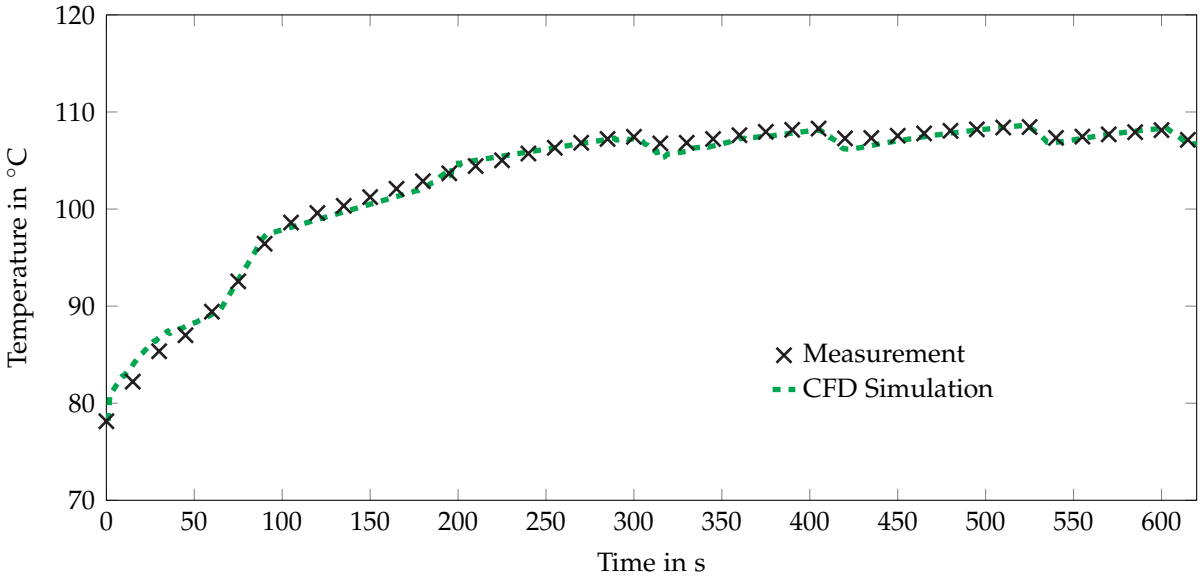

(b) Measured and simulated average temperatures in the non-vacuum steam sterilizer.

Figure 5.3: Measured and simulated average temperatures of eight thermocouples in the (a) vacuum steam sterilizer and (b) in the non-vacuum steam sterilizer [2].

and no steam enters the chamber. Therefore, the volume fraction of NCGs remains constant. Afterwards, the outlets are closed and the steam generator feeds steam to the sterilizer. This increases the pressure inside the vacuum steam sterilizer from approximately 0.142 bar to approximately 1.4 bar at 290 s of cycle time. As a result, the volume fraction of the NCGs falls to a value of approximately 0.16. Next, the steam generator stops, and the vacuum pump again reduces the pressure to a value of approximately 0.142 bar. At this point, the first measurement of the NCGs ratio was carried out, according to the norm. From this measurement, the real volume fraction of NCGs was calculated using Eq. (3.7), as well as according to the standard (Eq. (3.1)). The duration of the pre-sterilization phase was varied between the measurements in order to experimentally determine the NCGs ratio according to the norm. At the end of the pre-sterilization phase of the sterilization cycle, the second measurement was performed. The data gathered from these measurements were used to validate the CFD model. The measurements indicate that the CFD model of the vacuum steam sterilizer is able to simulate the temporal development of the real volume fraction of NCGs (see Eq. (3.7)) inside the steam sterilizer. Both the measured and simulated real volume fractions of NCGs were in very good accordance. The results indicate that calculating the NCGs ratio according to the norm (see Eq. (3.1)) does not reflect the real ratios of NCGs inside the steam sterilizer (see Section 3.5). This is because the measurements according to the norm [8] compare the gas volume of the NCGs to the liquid volume of the condensed steam and the condensed water (see see Eq. (3.1)). According to this definition, it would be beneficial to pass the norm measurement, if water were added inside the steam sterilizer before the measurement was taken. Furthermore, the use of a heavy sterilization chamber would be beneficial for the norm measurements as it would result in more condensed water inside the sterilization chamber. More information and a critical discussion of the calculation of NCGs content according to the norm can be found in Section 3.5.

The results of the simulation of the non-vacuum steam sterilizer are shown in Figure 5.4(b). In the pre-sterilization phase of this cycle (see ”pre-sterilization phase” in Figure 5.1(b)), the outlets are closed at the beginning, and the steam generator increases the pressure inside the steam sterilizer to a value of approximately 1.6 bar. As a result, the simulated volume fraction of the NCGs decreases to a value of approximately 0.68. Afterwards, the outlets were opened; the steam generator works at full power and feeds steam to the steam sterilizer for approximately 530 seconds. During this time, the NCGs ratio was measured seven times, according to the norm. With these measurements, it is possible to see the ratios of the NCGs during this phase of the sterilization cycle. To the best knowledge of the author, these are the first investigations

to simulate and measure the NCGs inside two different steam sterilizers as a function of time. The real values of the volume fraction of the NCGs were calculated from the norm measurement with Eq. (3.7). The error rate of the NCGs ratio according to the norm was determined to be $\pm$ 5 %. The results show that the CFD simulated volume fraction is in very good accordance with the real volume fraction, which was calculated with Eq. (3.7). The values of the NCGs ratio according to the norm (Eq. (3.1)) are significantly different compared to the real volume fraction of NCGs in the steam sterilizer.

From Figure 5.4, it is possible to see that a non-vacuum steam sterilizer reduces the NCGs much faster than a vacuum steam sterilizer with the same power. Furthermore, the results show that the NCGs ratio determined according to the norm is significantly higher compared to the real volume of the NCGs. For example, the NCGs ratio according to the norm is 12.78 % after 477 s of cycle time in the non-vacuum steam sterilizer (see Figure 5.4(b)), while the real volume fraction is 0.18 % at this point. Measurements in literature show that such a small volume fraction of NCGs has no influence on the heat transfer that occurs due to wall condensation [63, 126]. Similar results were obtained for the vacuum steam sterilizer (see Figure 5.4(a)). As a result, cycle time and energy can be saved thanks to a better understanding of the NCGs ratios in international norms and standards.

5.1.3 Distribution of the NCGs in the steam sterilizers

The distribution of the NCGs inside the steam sterilizer is of major interest to researchers seeking to remove the NCGs efficiently from the sterilization chamber. Figure 5.5 shows the distribution of NCGs in the vacuum and the non-vacuum steam sterilizers after 50 s, 150 s, 250 s, 350 s and 450 s of cycle time. The investigated cycle times are represented by vertical dotted green lines in Figure 5.4. Figure 5.5 shows the distribution of NCGs in the vacuum and the non-vacuum steam sterilizers after 50 s, 150 s, 250 s, 350 s and 450 s of cycle time. The investigated cycle times are represented with vertical dotted green lines in Figure 5.4. Due to density differences between the steam and the NCGs, the latter are located in the bottom regions of the steam sterilizers (see Figure 5.5). Furthermore, the condensed steam (water) is also located in the bottom regions of the steam sterilizers. To guarantee the displacement of NCGs in the steam sterilizer, steam should enter the chamber from the top. The flow of the steam should be homogenized, with a flow direction from the top to the bottom in order to minimize the mixing of NCGs and steam. The results show that the CFD model developed is

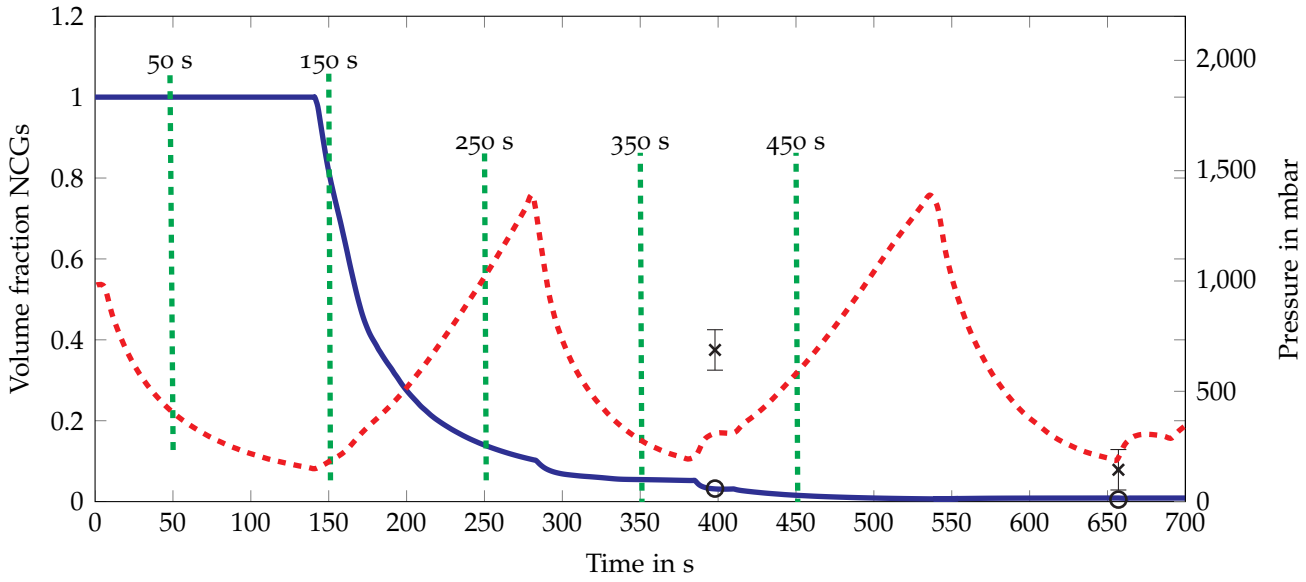

Simulated volume fraction of the NCGs inside the steam sterilizer Eq. (5.1)
Measured NCGs content according to the norm Eq. (3.1)
Calculated real volume fraction NCGs based on the norm measurement Eq. (3.6)
Measured pressure during the pre-sterilization phase of the vacuum cycle

(a) Measured and simulated volume fraction of NCGs in the vacuum steam sterilizer.

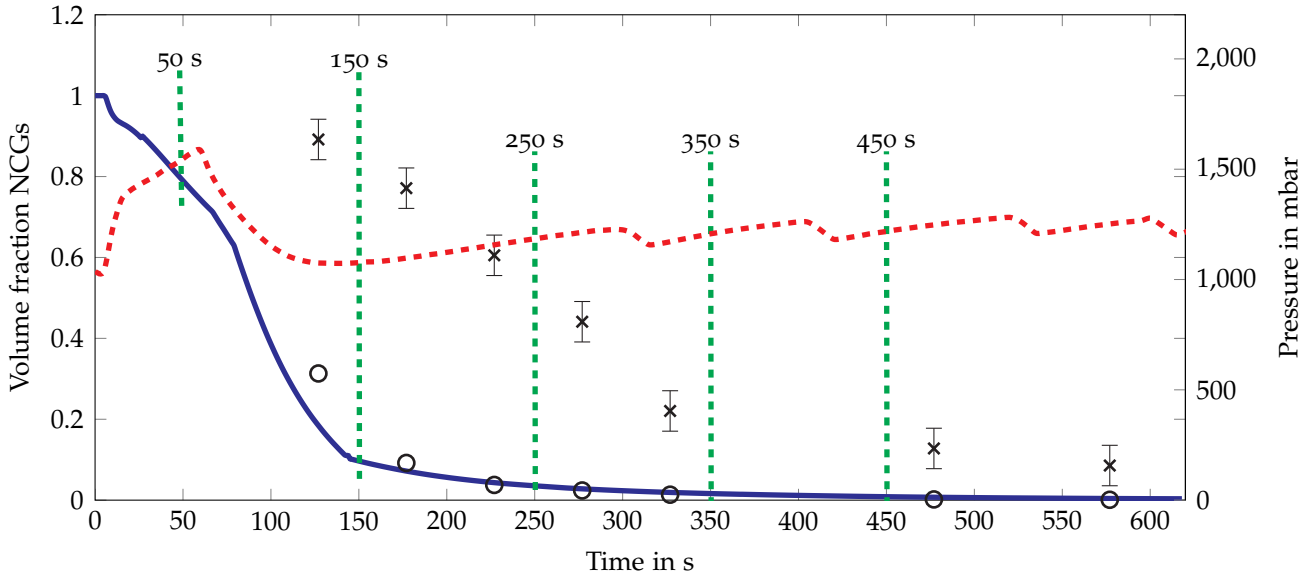

Simulated volume fraction of the NCGs inside the steam sterilizer Eq. (5.1)
Measured NCGs content according to the norm Eq. (3.1)
Calculated real volume fraction NCGs based on the norm measurement Eq. (3.6)
Measured pressure during the pre-sterilization phase of the non-vacuum cycle

(b) Measured and simulated volume fraction of NCGs in the non-vacuum steam sterilizer.

Figure 5.4: Volume fraction of NCGs in the chamber of the (a) vacuum sterilizer and (b) the non-vacuum steam sterilizer.

able to calculate the volume fraction of NCGs, the fluid flow, and the temperature, as well as the heat transfer within the steam sterilizers separated in both time and space. Thus, the CFD model developed in this work will support optimizations to both sterilization cycles as well as the geometries of steam sterilizers in the future.

With the results presented in this section, the first part of research question iv) "Which approach works best so simulate the air removal and the steam penetration inside the steam sterilizer as well as inside hollow loads (cavities)?" can be answered. The results have demonstrated that the developed CFD model is able to simulate the removal of NCGs inside the sterilization chamber. Figure 5.4(a) shows the simulated volume fraction, the NCGs content according to the norm, and the calculated real volume fraction of the NCGs of the pre-sterilization phase of the vacuum sterilization cycle. The simulated volume fraction of the NCGs and the real volume fraction of the NCGs were in very good accordance. The same results were obtained for the non-vacuum steam sterilizer (see Figure 5.4(b)). Furthermore, the distribution of the NCGs inside the steam sterilizers was also investigated (see Figure 5.5). All of these results have proven that that the developed CFD model is able to simulate the air-removal and the steam penetration inside the steam sterilizers. Section 5.6 will investigate the air-removal and steam penetration inside hollow loads.

The simulations presented in this section were performed on a cluster with 16 Intel Core i7 processors and 32 GB RAM. The total simulation time was approximately eight weeks for the vacuum steam sterilizer and approximately nine and a half week for the non-vacuum steam sterilizer.

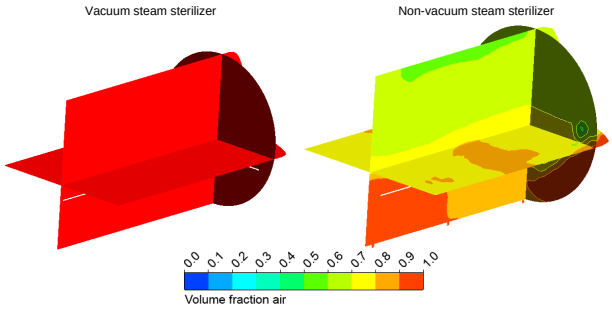

(a) NCGs in the steam sterilizers after 50 s

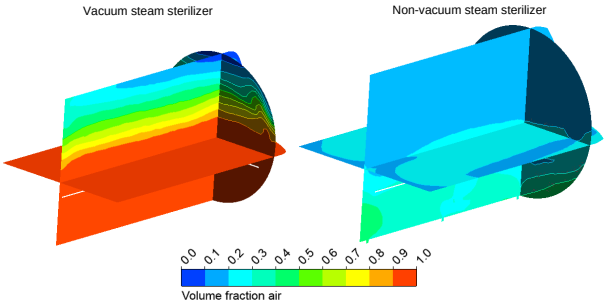

(b) NCGs in the steam sterilizers after 150 s

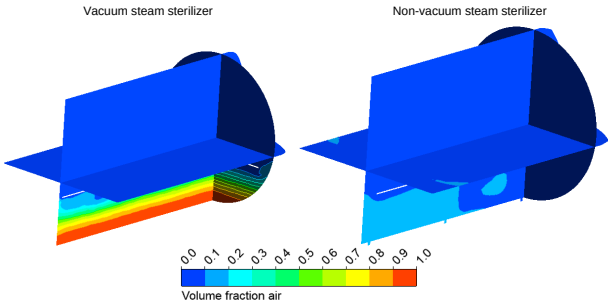

(c) NCGs in the steam sterilizers after 250 s

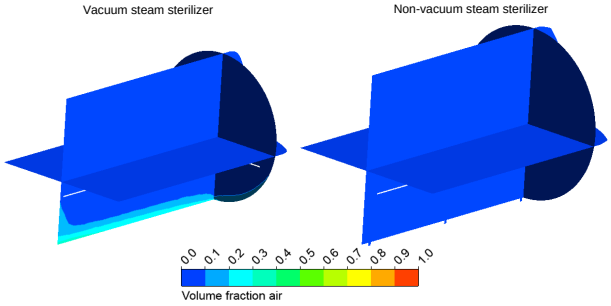

(d) NCGs in the steam sterilizers after 350 s

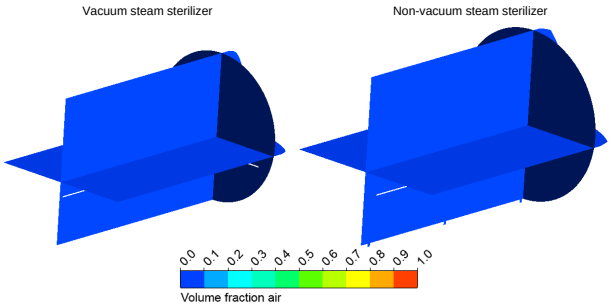

(e) NCGs in the steam sterilizers after 450 s

Figure 5.5: NCGs in the steam sterilizers after (a) 50 s, (b) 150 s, (c) 250 s, (d) 350 s and (e) 450 s [2].

5.2 Validation of the paper model [2]

As discussed in Section 2.5.2 and Section 3.4, medical equipment is often wrapped in paper for transport and storage [69, 70]. During the steam sterilization process, this paper represents a flow resistance for the NCGs (air) to leave the sterilization chamber, as well as for the steam to enter the space near the load. To simulate the paper packaging's influence on the sterilization process in a numerically efficient manner, a porous media model was developed.

The measurements that were necessary to develop this paper model were described in Section 3.4. More information about the theoretical approach to the porous media that was used is provided in Section 4.5. The following sections will present the derivation of the model parameters out of the measurement data and a validation of the developed porous media model for both steam and air.

5.2.1 Validation of the paper model for air

The experimental set-up (see Figure 3.6) made it possible to identify the correlation between the pressure drop and air velocity through the paper. The pressure drop induced by the paper for air was measured for a temperature range between 70 °C and 140 °C and a pressure range between 300 $mbar_a$ and 3200 $mbar_a$. The quadratic trend lines of the measured data of the air are shown in Eq. (5.2):

$$\Delta p_{air} = 23502 \cdot v^2 + 40052 \cdot v \tag{5.2}$$

where Δp_{air} is the pressure drop of the air (in Pa) over the paper and v is the area-weighted flow velocity (in m/s) perpendicular to the paper. This polynomial function represents a fitted function of the measurement data. In the CFD code, a porous media approach was used to simulate the permeability of the paper. Using this technique, porous media are modelled by adding a source term (S_i) to the momentum equation (see Eq. (4.12) in Section 4.5). The pressure drop over the paper is calculated by CFD code using Eq. (4.13). By comparing the coefficients of Eq. (4.13) from Section 4.5 and Eq. (5.2) with material properties from Table 4.1, the permeability α and the inertial resistance factor C_2 can be computed. Thus, the investigated paper was found [70]

[2] Segments of this section have already been published in [1, 5].

to have a permeability of $\alpha = 8.935384 \cdot 10^{-13}\ m^2$ and an inertial resistance factor of $C_2 = 19185306\ \frac{1}{m}$.

A CFD model of the test rig, which can be seen in Figure 3.6, was generated to validate the paper model based on the experimental data. The length of the model was 60 cm, which represents approximately 30 cm in front of the paper and approximately 30 cm behind the paper in the test rig. The numerical grid of this CFD model consists of 130,389 hexahedral cells of high quality. A velocity inlet was set to reach the same velocities as the real test rig. A pressure outlet represents the pressure adjuster. As a consequence of the insulation on the test rig, the walls in the CFD model were set as adiabatic. In the middle of the CFD model a small fluid domain was defined as a porous media model in order to represent the paper. The pressure drop over the paper was simulated for different velocities, temperatures, and pressures. Figure 5.6 shows the measured and simulated values of the pressure drop over the paper for air at different pressures and temperatures.

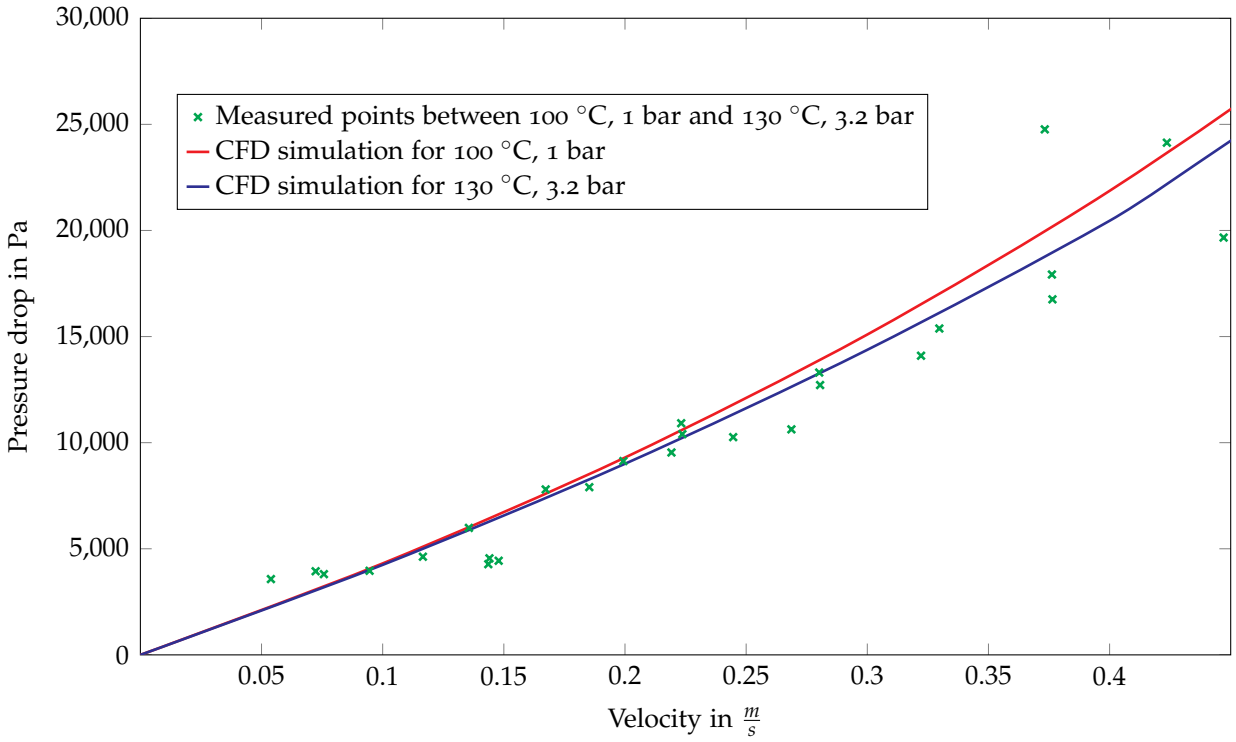

Figure 5.6: Simulated and measured pressure drops over the paper for air.

From the measured results, the pressure drop over the paper for air was found to depend mainly on the velocity. Small deviations in the measurements were detected because both wet and dry paper were measured. However, the measured and simulated results demonstrate that the pressure drop over the paper is a relatively linear function of the velocity for the investigated velocity range. Furthermore, the results demonstrate

that the developed porous media model is able to predict the pressure drop over the paper for a pressure of 1 bar and a temperature of 100 °C as well as for a pressure of 3.2 bar and a temperature of 130 °C. These results thus prove that the developed model is able to simulate the permeability of the paper for air.

5.2.2 Validation of the paper model for steam

The process used to validate the porous media model for simulations of the permeability of paper for steam was similar to the process described above validation for air (see Section 5.2.1). To measure the polynomial function of the pressure drop over the paper, the test rig shown in Figure 3.7 was used. The average pressure drop (see "p2 - p1" in Figure 3.7) induced by the paper for steam was measured for a temperature range between 70 °C and 140 °C and a pressure range between 300 $mbar_a$ and 3200 $mbar_a$. The average measured polynomial function of the velocity was thus determined to be:

$$\Delta p_{steam} = 1163950 \cdot v^2 + 2254 \cdot v \tag{5.3}$$

As described in Section 5.2.1, comparing Eq. (4.13) from Section 4.5 and Eq. (5.3) with the material properties from Table 4.1, the permeability α and the inertial resistance factor C_2 were calculated. The permeability was thus found to be $\alpha = 1.18894 \cdot 10^{-11}\ m^2$, while the inertial resistance factor was $C_2 = 2100234018\ \frac{1}{m}$.

Figure 5.7 shows the measured and simulated pressure drops over the paper over the velocity. The CFD simulations were performed with the same CFD model as described in Section 5.2.1. The deviations in the measurement points were larger compared to the measurements of the pressure drop for air (see Figure 5.6). This is because both wet and dry papers were investigated. Due to the fact that it is not known if the paper is wet or dry in the real steam sterilization process, the average of the wet and dry measurement data was used. As for the measurements of the pressure drop for air, it was found that the pressure drop over the paper for steam depends mainly on velocity as well. Simulations were performed with steam at a temperature of 100 °C, which represents a pressure of 1 bar, and steam at 130 °C, which represents a pressure of approximately 2.7 bar. The simulated pressure drop over the paper for steam was found to correspond to the average values of the measured pressure drop values. These results again prove that the developed porous media model is able to predict the permeability of the paper for steam.

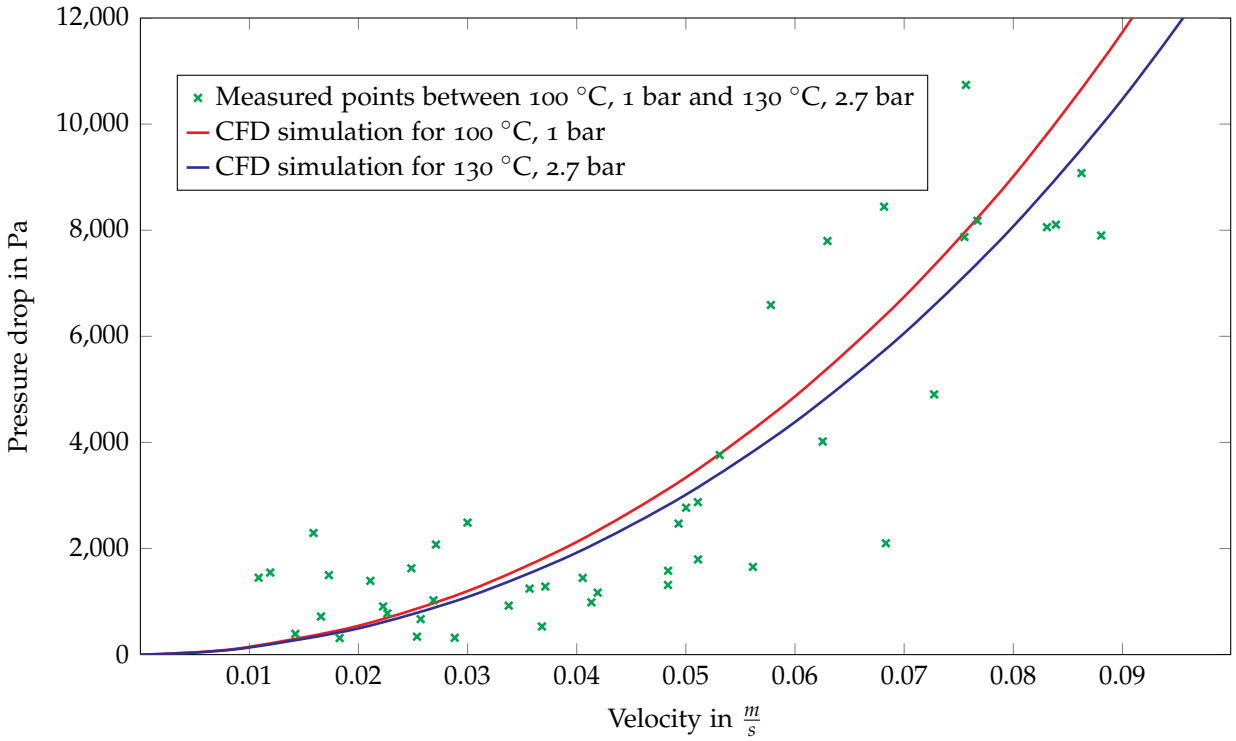

Figure 5.7: Simulated and measured pressure drops over the paper for steam [1].

5.3 Simulation of the sterilization phase with an unwrapped load [3]

The aim of this section is to simulate both the temperature and the inactivation of bacteria on the surface of an unwrapped load. To this end, the steam sterilizer was filled with eight unwrapped cylinders on two trays. The geometry of the CFD model with the unwrapped load can be seen in Figure 3.3.

This investigation of the sterilization phase (see "sterilization phase" in Figure 2.2) of the vacuum steam sterilization cycle begins, logically, at the beginning of the sterilization phase (286 mbar, 81.6 °C) and ends at the end of the sterilization phase (approximately, 3150 mbar and 136.4 °C, see "second phase" in Figure 5.8). To provide a better overview of the sterilization phase in question, Figure 5.8 shows the measured pressure and the measured average fluid temperature inside the steam sterilizer loaded with the unwrapped load. The dotted vertical lines represent the times at which the simulation results were presented.

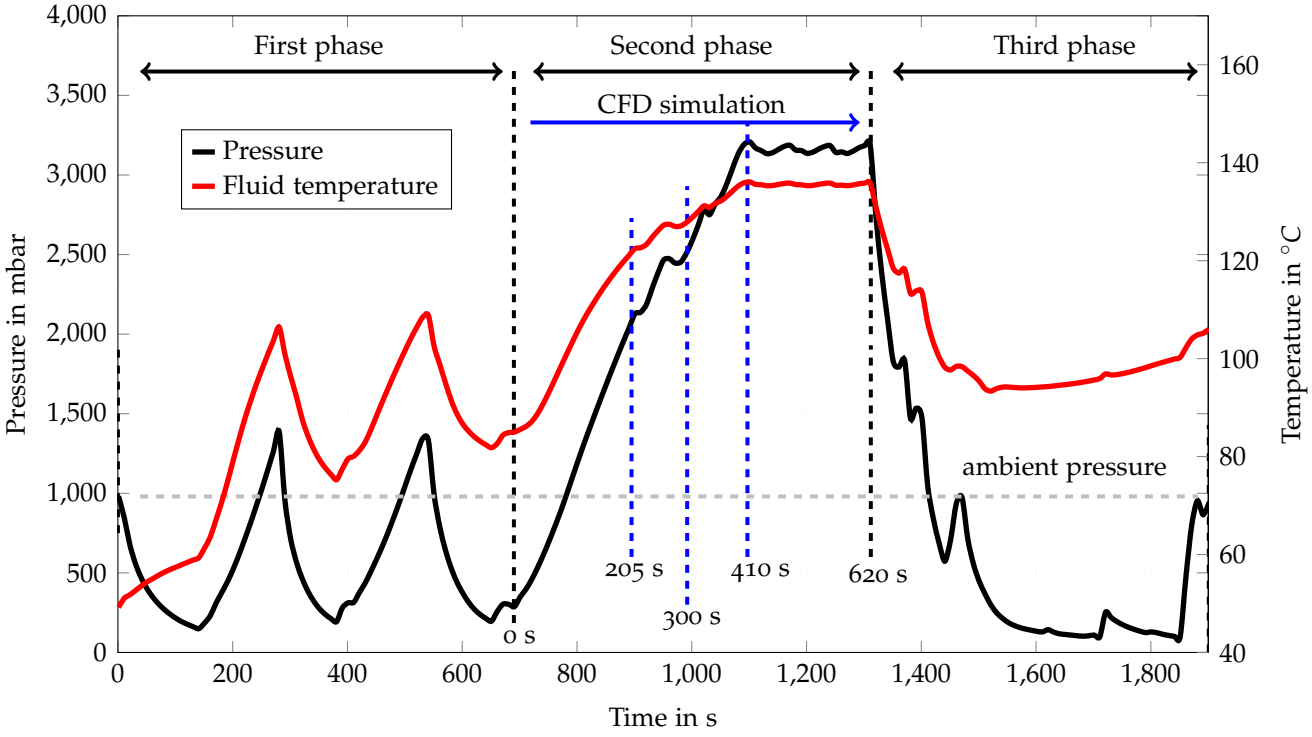

Figure 5.8: Measured pressure and fluid temperature in the steam sterilizer loaded with the unwrapped load during a sterilization cycle. First phase: Removal of the air; Second phase: Sterilization; Third phase: Drying and cooling [4].

[3] Segments of this section have already been published in [4].

5.3.1 Simulated pressure and fluid temperatures for an unwrapped load

The flow field of the CFD model was validated by the measurements of one pressure sensor and eight thermocouples in the steam sterilizer (see Figure 3.1). The pressure sensor and the thermocouples were represented in the CFD model using small volumes.

Figure 5.9 shows the measured and simulated pressures inside the steam sterilizer during the simulated sterilization phase. It is possible to see that the measured and the simulated pressures were in very good accordance.

The maximum error between the measured and the simulated pressures was below 2 %. In Figure 5.10, the temperatures calculated and measured by four thermocouples during the simulated part of the sterilization cycle can be seen. In this thesis, the temperatures of thermocouples T1, T4, T5 and T7 were compared with the simulated temperatures. The locations of the thermocouples are shown in Figure 3.1. Furthermore, the measured and simulated fluid temperatures were compared for the other four thermocouples (T2, T3, T6 and T8) as well, with similar results. The results indicate that the measured fluid temperatures were in very good accordance with the simulated fluid temperatures. In order to demonstrate the accuracy of the CFD model, the error between the measured and simulated temperatures was calculated for different cycle times (see Eq. (5.4)).

$$Error = \left(1 - \frac{T_{Simulation}}{T_{Measurement}}\right) \cdot 100\ \% \tag{5.4}$$

In this equation $T_{Measurement}$ is the measured temperature and $T_{Simulation}$ is the simulated temperature in Kelvin. The absolute errors of all eight thermocouples for 205 s, 300 s, 410 s and 620 s of simulation time are shown in Table 5.1. The times at which the errors were calculated are indicated by the blue vertical dotted lines in Figure 5.9. The largest error, with a value of 0.55 %, was detected after 205 s at the location of T2. Nevertheless, this error is still very small. The average error was below 0.2 %. These results indicate that the CFD model developed in this thesis is able to predict the fluid temperature inside the steam sterilizer.

After the validation of the simulated fluid temperature, the temperature distribution inside the steam sterilizer was investigated using CFD. Volume renderings of the fluid temperature inside the steam sterilizer are shown in Figure 5.11. Figure 5.11(a) shows

the fluid temperature after 205 s. The maximum temperature differences detected at this time were 2 K. As is to be expected, the temperature difference decreases as the cycle goes on. After 410 s of simulation time, the temperature stratification inside the steam sterilizer is below 0.6 K (see Figure 5.11(c)). These results indicate that the investigated benchtop steam sterilizer [31] works very well as the temperature inside the steam sterilizer is very homogeneously distributed. After 450 s of simulation time, the temperature difference inside the steam sterilizer is under 0.5 K (see Figure 5.11(c)). The coldest spots were detected in the middle of the steam sterilizer under the second tray for all investigated cycle times. Thus, these results prove that, using CFD, it is possible to predict the fluid temperature and the pressure within a steam sterilizer containing an unwrapped load. Furthermore, the results demonstrate that CFD is a very useful tool to predict the "cold spots" inside the steam sterilizer. In contrast, using measurements, it is only possible to detect the temperature at pre-defined locations and with a limited number of thermocouples.

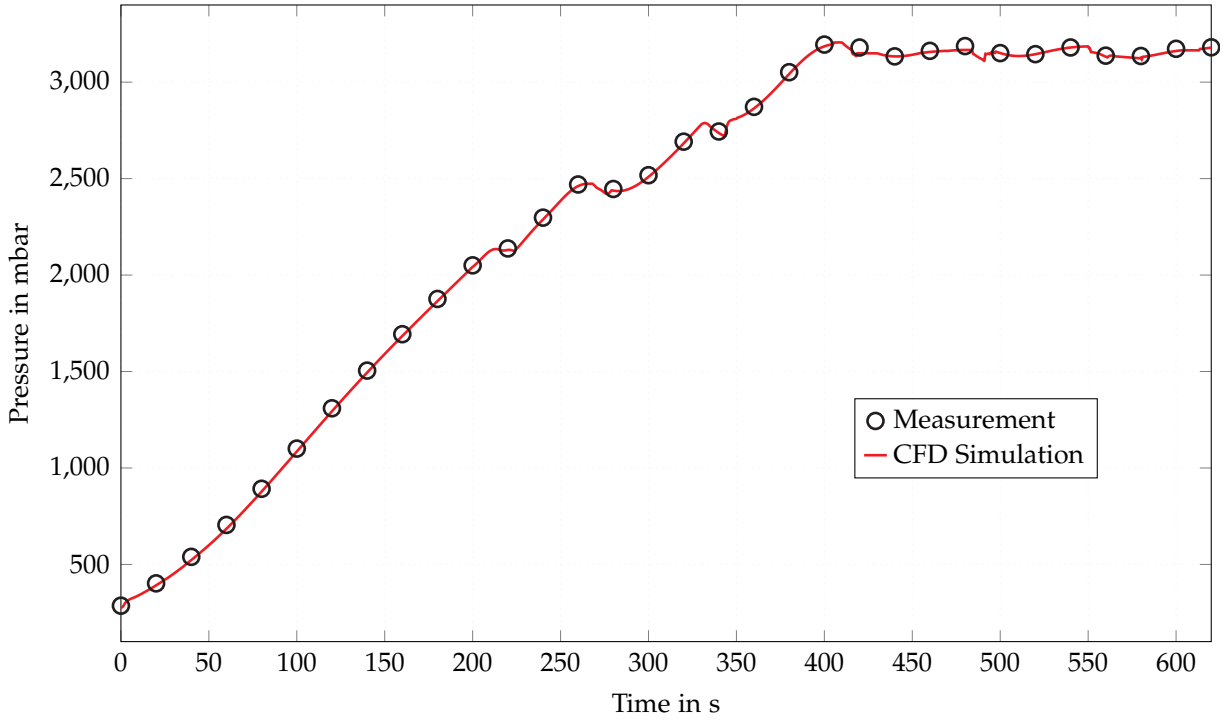

Figure 5.9: Measured and simulated pressures inside the steam sterilizer [4].

5.3.2 Simulated steam quality for an unwrapped load

The steam quality in the steam sterilizer is of interest to researchers due to the fact that low steam quality decreases the heat transfer due to wall condensation [113]. Considering that it is quite difficult to measure steam quality in a steam sterilizer,

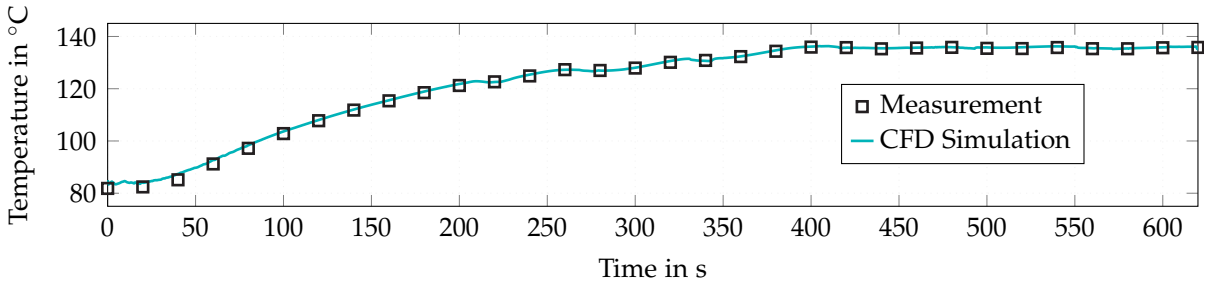

(a) Measured and simulated fluid temperatures at the location of T1.

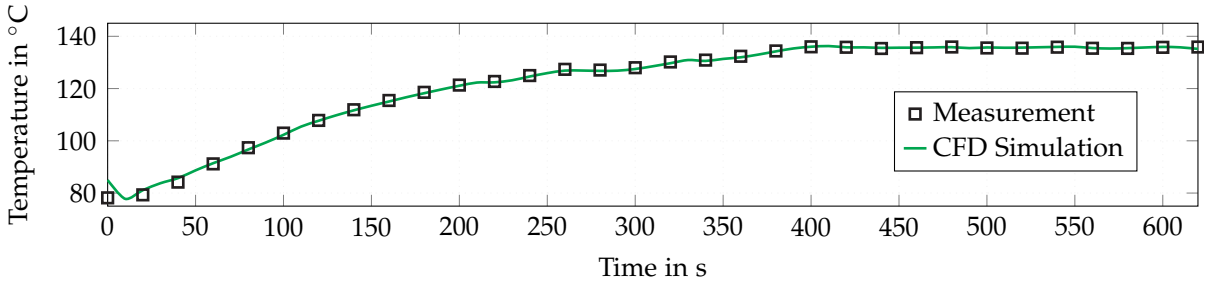

(b) Measured and simulated fluid temperatures at the location of T4.

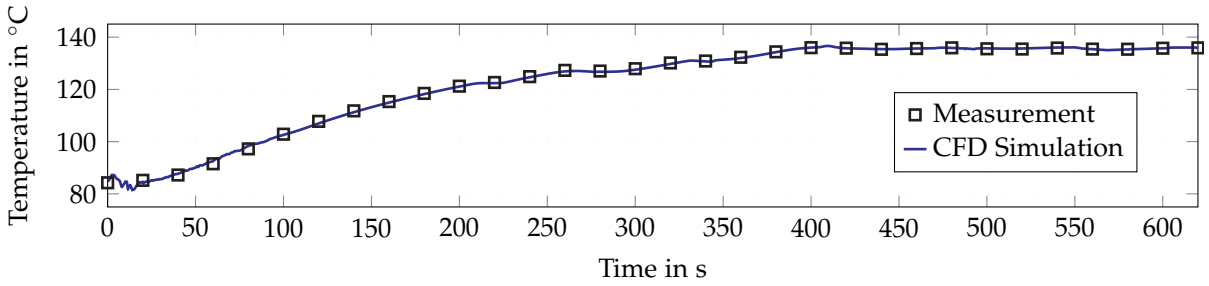

(c) Measured and simulated fluid temperatures at the location of T5.

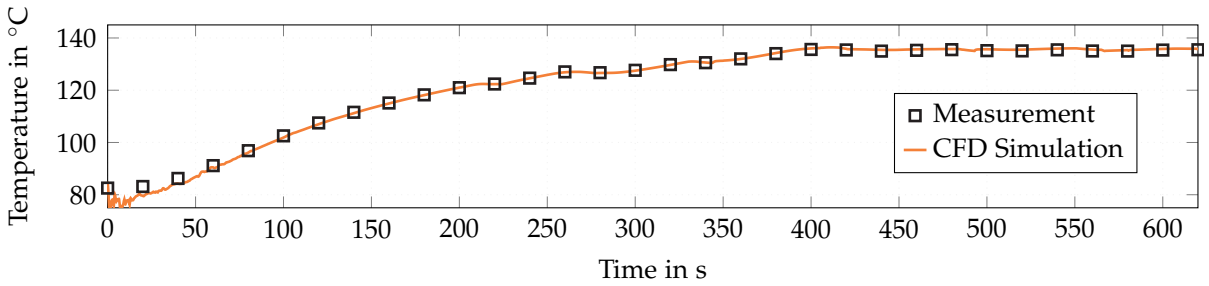

(d) Measured and simulated fluid temperatures at the location of T7.

Figure 5.10: Measured and simulated fluid temperatures at the locations (a) T1, (b) T4, (c) T5 and (d) T7 [4].

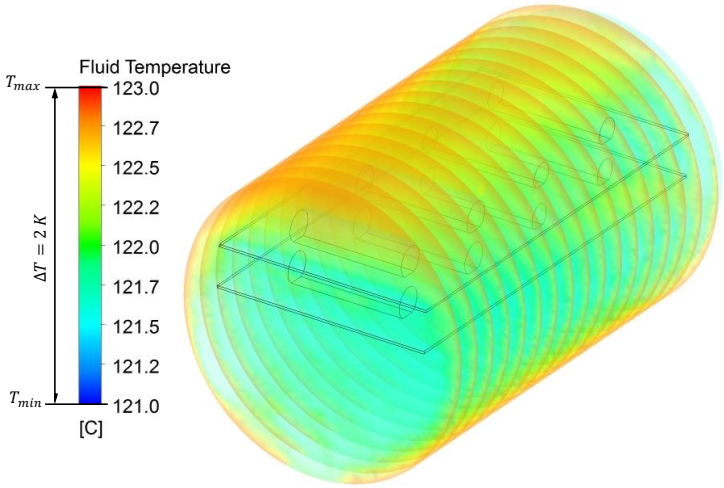

(a) Fluid temperature in the steam sterilizer after 205 s of simulation time.

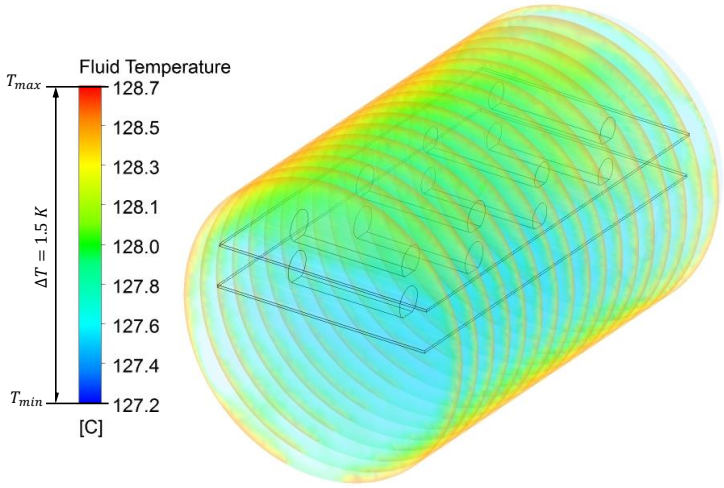

(b) Fluid temperature in the steam sterilizer after 300 s of simulation time.

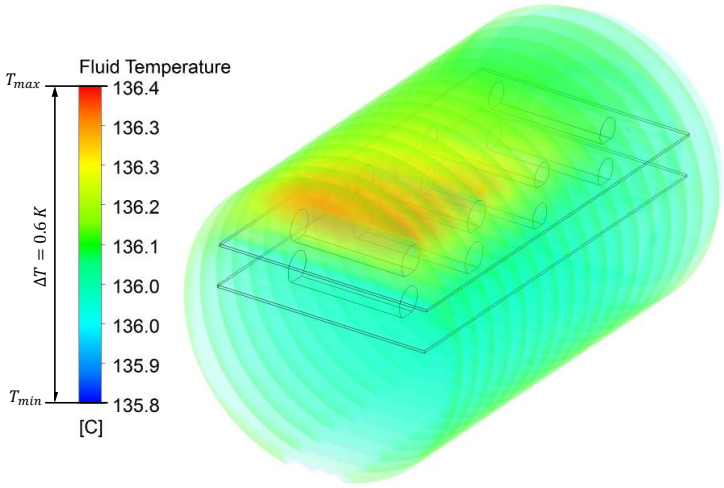

(c) Fluid temperature in the steam sterilizer after 410 s of simulation time.

Figure 5.11: Volume rendering of the fluid temperature in the steam sterilizer loaded with unwrapped load after (a) 205 s, (b) 300 s and (c) 410 s of simulation time [4].

Table 5.1: Absolute errors of the simulated fluid temperatures at eight locations.

	After 205 s	After 300 s	After 410 s	After 620 s
Error T1	-0.15 %	-0.02 %	0.10 %	-0.04 %
Error T2	0.54 %	-0.24 %	-0.16 %	-0.2 %
Error T3	-0.22 %	-0.25 %	-0.28 %	-0.20 %
Error T4	-0.16 %	-0.06 %	-0.19 %	-0.11 %
Error T5	-0.05 %	-0.09 %	-0.04 %	-0.05 %
Error T6	0.36 %	-0.05 %	-0.05 %	-0.06 %
Error T7	0.07 %	-0.18 %	-0.12 %	-0.37 %
Error T8	-0.14 %	0.19 %	0.25 %	-0.02 %

CFD calculations were used to investigate this issue. In this section, the steam quality was investigated for an unwrapped load. The simulated steam quality is shown on four planes in the steam sterilizer. Those planes are the vertical middle surface, the horizontal middle surface, and two radial planes. The latter two can be found halfway through and near the back of the steam sterilizer. Upon closer examination of additional radial planes, no further differences were found. The lowest quality steam was found in the bottom region of the steam sterilizer (see Figure 5.12) due to the fact that the density of the condensed water is much higher compared to the density of the steam. Furthermore, the results show that the steam quality decreases as the cycle time increases (see Figure 5.12). This thesis also investigates the steam quality within a steam sterilizer containing a wrapped load (see Section 5.4.3). The results of that section reveal that the average steam quality in the steam sterilizer improves when the load is wrapped, whereas the average steam quality near the load improves when the load is unwrapped. Nevertheless, hardly any differences were identified between the wrapped load and unwrapped loads in terms of the surface temperature of the load. This indicates that both the wrapping of the load and the steam quality have a negligible impact on its surface temperature, given that high heat transfer rates to the load occur regardless of either of these variables.

Without the heat transfer model developed in this thesis (described in Section 4.4.1), it would not be possible to calculate the heat transfer to the load and the chamber of the steam sterilizer in a reasonable amount of simulation time. As a result, the condensation could not be correctly predicted, and, therefore, it would not be possible to predict the steam quality inside the steam sterilizer.

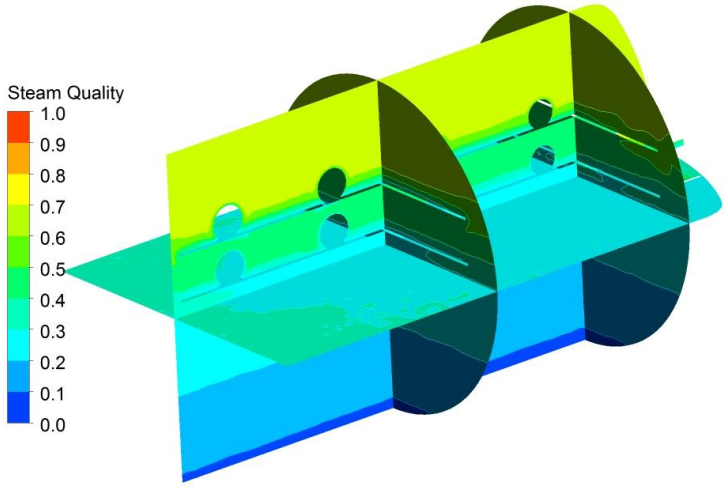

(a) Steam quality in the steam sterilizer after 205 s of simulation time.

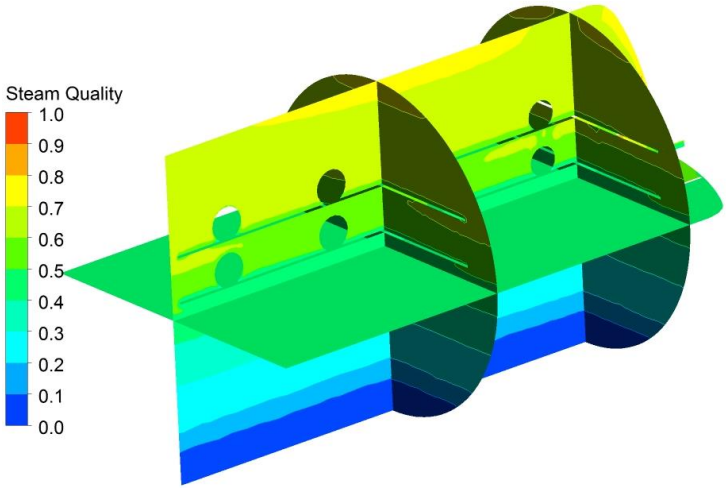

(b) Steam quality in the steam sterilizer after 410 s of simulation time.

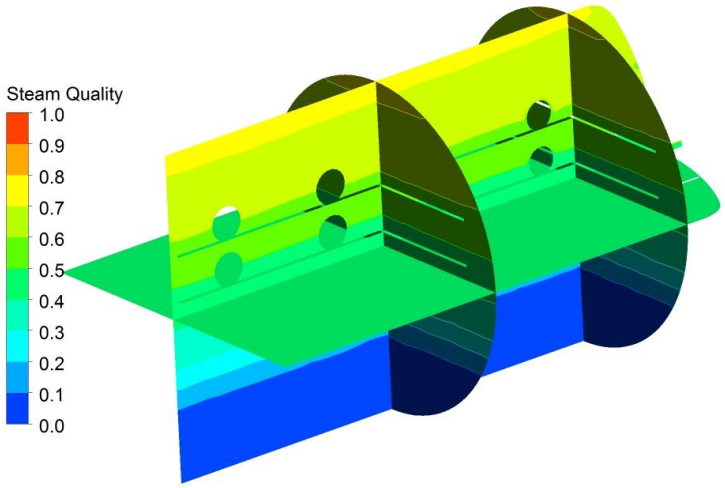

(c) Steam quality in the steam sterilizer after 620 s of simulation time.

Figure 5.12: Steam quality in the steam sterilizer loaded with unwrapped load after (a) 205 s, (b) 410 s and (c) 620 s of simulation time [4].

5.3.3 Simulated temperature of an unwrapped load

In order to understand the full sterilization process, it is essential to have thorough knowledge of the load temperature and of what constitutes sufficient process time. To reach sterility, high wall temperatures are required. To validate the predicted heat transfer of the CFD model to the load and vice versa, simulated load temperatures were compared with measured load temperatures. The temperature was recorded at the centre of all eight cylinders. Both the position and materials of the load cylinders can be seen in Figure 3.3. As shown in Figure 5.13, the simulated load temperatures are in very good accordance with the measured load temperatures throughout the investigated phase. The calculated temperatures for the materials (a) steel, (b) aluminium, (c) brass and (d) plastic were in good accordance with the measured values.

To predict the inactivation of bacteria, the surface temperature of the load is of much interest. Figure 5.14 shows the surface load temperature after (a) 205 s, (b) 410 s and (c) 620 s of simulation time. The times in the sterilization cycle at which the load temperature was investigated are shown in Figure 5.8. After 200 s of simulation time, the lowest surface temperatures were identified on the steel cylinders (see Figure 5.14(a)). This can be explained by their higher mass, compared to the other cylinders. After 620 s of cycle time, the temperature difference on the surface of the load decreased to under 0.3 K. The highest temperatures were detected on the edges of the cylinders (see Figure 5.14(c)). These small temperature differences can have a big influence on the inactivation of the bacteria due to the fact that the inactivation rate of the bacteria k_d is an exponential factor of the temperature (see Eq. (2.2)).

These results prove that the heat transfer model developed in this thesis (see Section 4.4.1) is able to accurately predict the heat transfer to the unwrapped load. With these results, the research question i) "Is it possible to simulate the heating process of the load?" can be answered with "yes" due to the fact that the measured and the simulated temperatures in the centre of gravity for four different cylinders were in very good accordance (see Figure 5.13). These results were obtained for steel, aluminium, brass, and plastic cylinders. Thus, the results of this simulation prove that the process of heating the load can be simulated accurately.

5.3.4 Simulation of active bacteria on the unwrapped load

The main goal of a sterilization cycle is to inactivate the bacteria on all surfaces of the medical equipment. To investigate this topic, a first-order reaction kinetic approach

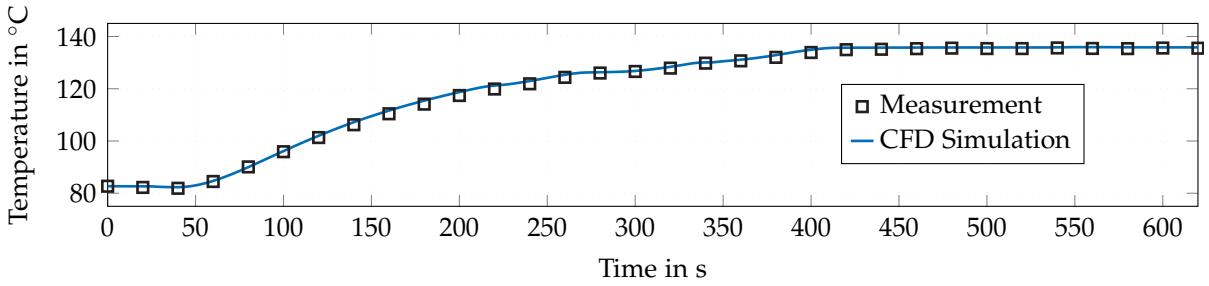

(a) Measured and simulated temperatures in the centre of the unwrapped steel cylinder.

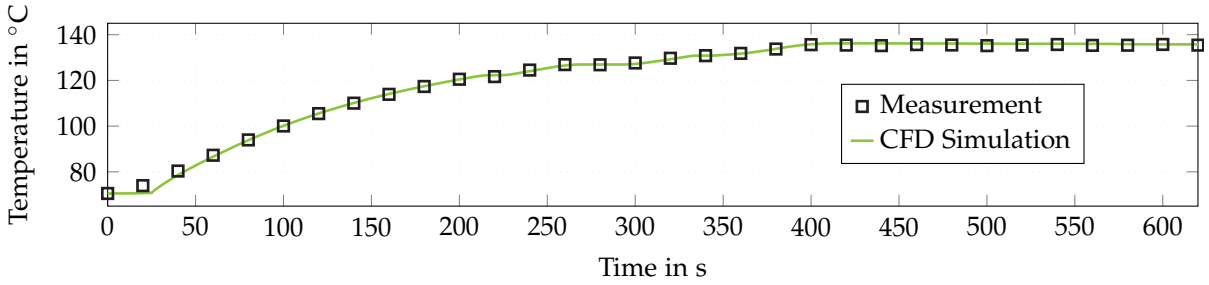

(b) Measured and simulated temperature in the centre of the unwrapped aluminium cylinder.

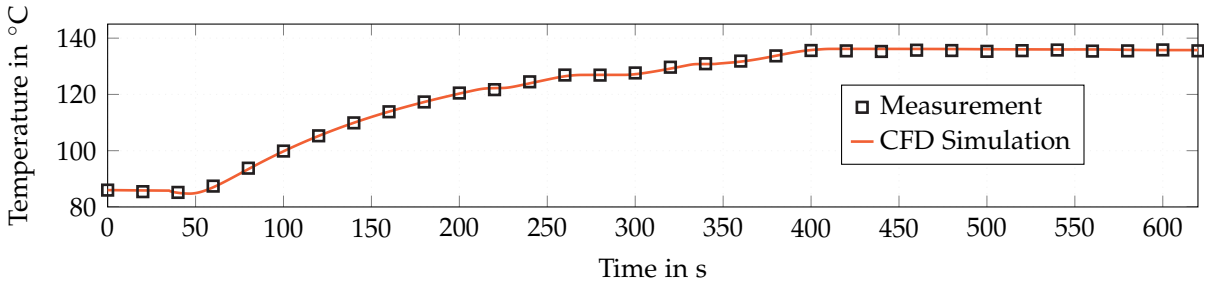

(c) Measured and simulated temperature in the centre of the unwrapped brass cylinder.

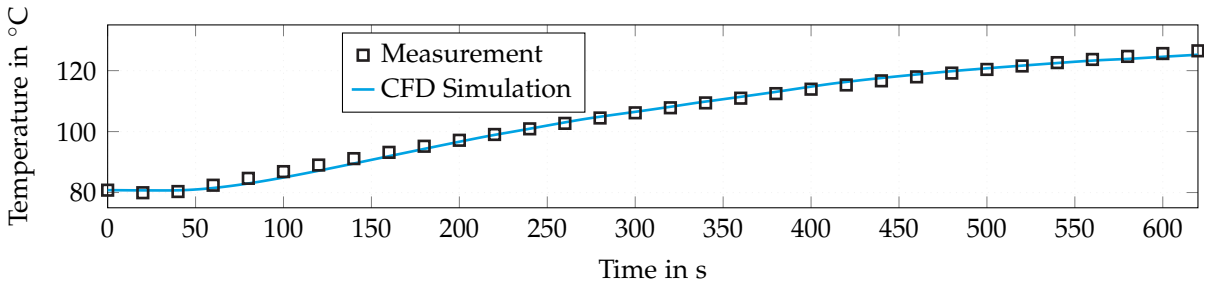

(d) (d) Measured and simulated temperature in the centre of the unwrapped plastic cylinder.

Figure 5.13: Measured and simulated temperature in the centres of the unwrapped (a) steel cylinder, (b) aluminium cylinder, (c) brass cylinder and (d) plastic cylinder [4].

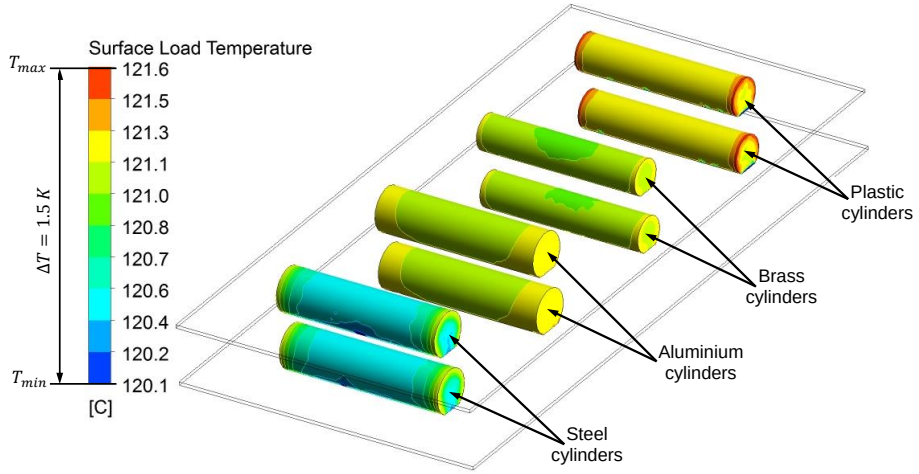

(a) Simulated surface temperatures of the unwrapped load after 205 s of simulation time

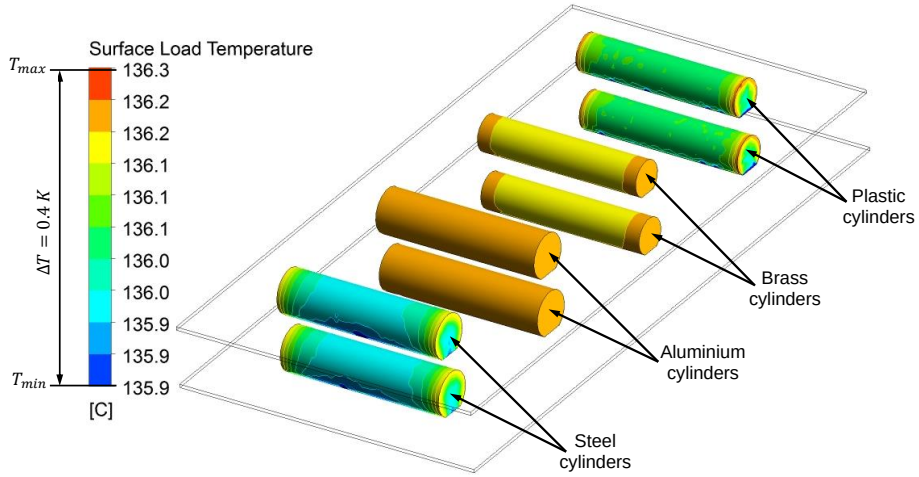

(b) Simulated surface temperatures of the unwrapped load after 410 s of simulation time

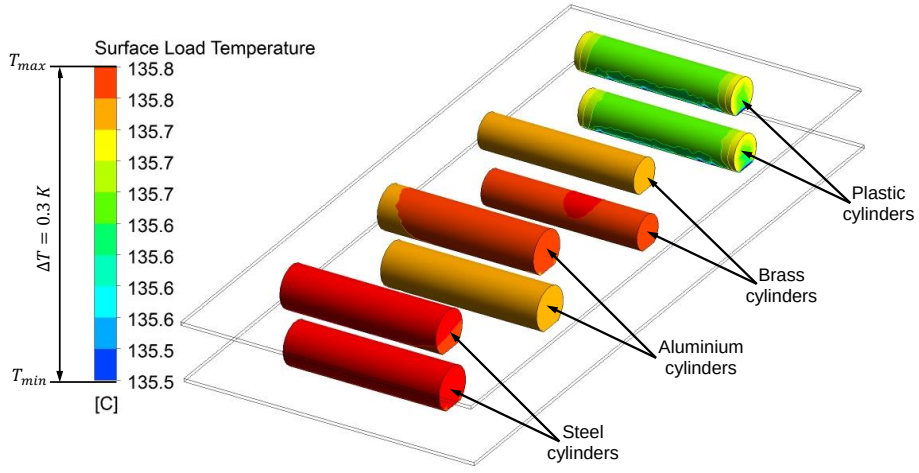

(c) Simulated surface temperatures of the unwrapped load after 620 s of simulation time

Figure 5.14: Simulated surface temperatures of the unwrapped load after (a) 205 s, (b) 410 s and (c) 620 s of cycle time [4].

was added to the CFD code, which is able to predict the active bacteria at every point of the steam sterilizer, resolved in time and space. More about the modelling of the inactivation and the inactivation rates k_d of the investigated bacteria types can be found in Section 2.2.

Two different types of bacteria were investigated (Bacteria Type 1 and Bacteria Type 2). The reaction kinetics for the first bacteria type were taken from the work of Wallhäußer [37]. The reaction kinetics for the second bacteria type were taken from the work of De Santis and Rudo [127]. Figure 5.15 shows the inactivation rate k_d of the two investigated bacteria types as a function of temperature. Furthermore, Table 5.2 shows the D-values of Bacteria Type 1 and Bacteria Type 2. As can be seen in Figure 5.15 and Table 5.2, Bacteria Type 1 represents a bacterium which is easy to inactivate, whereas Bacteria Type 2 represents a bacterium which is much more difficult to inactivate.

Table 5.2: D-values of the two investigated bacteria types [4].

	Bacteria Type 1	Bacteria Type 2
D-value for 111 °C	2.2	2.25
D-value for 121 °C	0.55	0.61

At the beginning of the simulation, both types of bacteria were initialized with a number of $N_0 = 10^{12}$ in every cell of the numerical grid. Additional information about the modelling and the inactivation of bacteria can be found in scientific literature [34, 128–131].

The active bacteria of Type 1 and Type 2 for the simulation times 205 s, 410 s and 620 s can be seen in Figure 5.16. The inactivation rate of Bacteria Type 1 is significantly higher for every temperature compared to the inactivation rate of Bacteria Type 2 (see Figure 5.15). For example, at 136 °C the inactivation rate of Bacteria Type 1 is 2.3 s^{-1}, whereas the inactivation rate of Bacteria Type 2 is 0.2 s^{-1}. As a result, the inactivation of Bacteria of Type 1 takes considerably less time. At the end of the pressure rise in the sterilization phase (410 s), hardly any active Type 1 bacteria remain (see Figure 5.16(c)). At the same time, approximately a third of the Type 2 bacteria is still active. It is also possible to see that the regions with the lowest surface temperatures are the same regions where the most bacteria are still active (see, e.g., surface of the steel cylinder in Figure 5.14 and Figure 5.16).

To gain a better understanding of the inactivation of the bacteria, the log survival ratio is often used. The log survival ratio is defined as the log of the division of active number of bacteria (N) by the initial number of bacteria (N_0). The formula of the log survival ratio is given by Eq. (2.7) in Section 2.2.5.

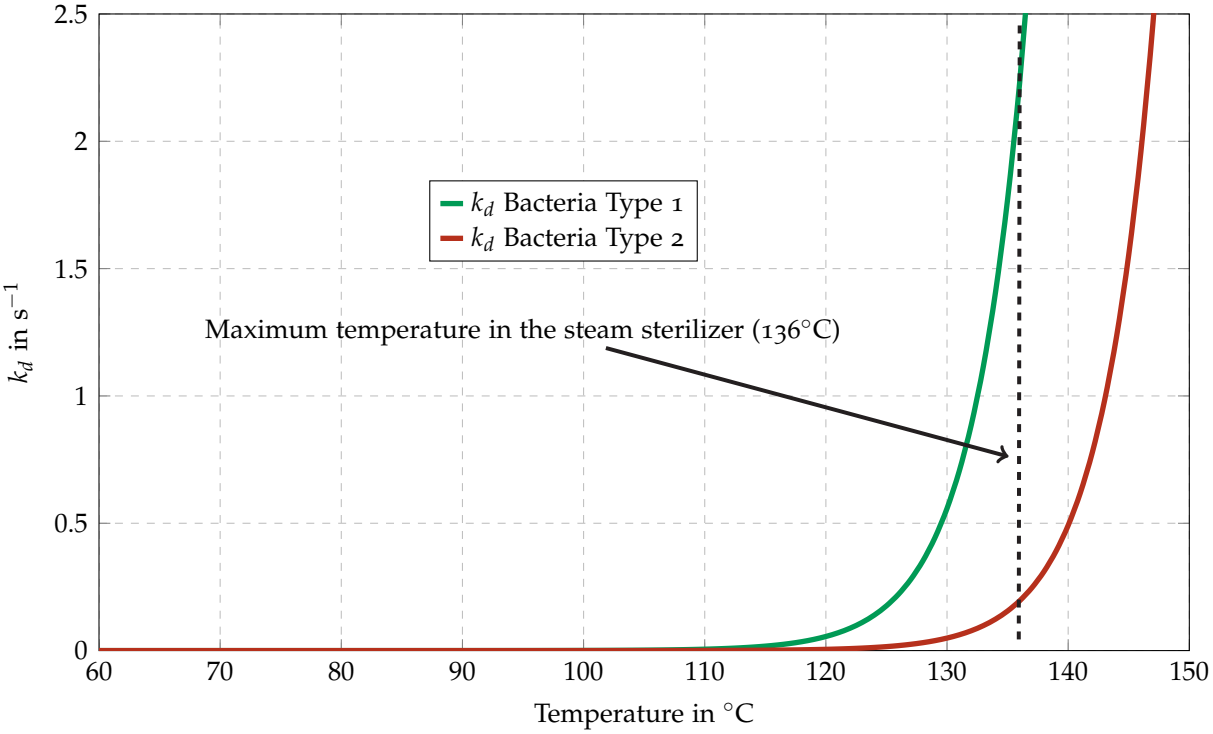

Figure 5.15: k_d values for Bacteria Type 1 and Bacteria Type 2 over temperature [4].

Table 5.3 shows the surface average logarithmic survival ratio of the steel cylinders for 205 s, 410 s, and 620 s of simulation time. As might have been expected, the log reduction ratio of Bacteria Type 1 is significantly higher compared to that of Bacteria Type 2. After 410 s, approximately 33 log ratios were inactivated for Bacteria Type 1, whereas approximately 6.45 log ratios were inactivated for Bacteria Type 2. Nevertheless, at the end of the simulated phase of the steam sterilization cycle (620 s) hardly any bacteria of Type 1 or Type 2 were active (see Figure 5.16(c)). At the end of the sterilization phase (620 s), the log reduction of Type 1 bacteria is approximately 51, while that of Bacteria Type 2 is approximately 22 (see Table 5.3). In this thesis, similar results were obtained for Bacteria Type 2 on a wrapped load (see Section 5.4.4).

These results indicate that it is possible to predict the inactivation of different types of bacteria on the surface of an unwrapped load using CFD. Once again, the heat transfer model developed in this thesis and described in Section 4.4.1 is key to the ability to perform a CFD simulation of the inactivation of bacteria. This is because the surface temperature of the load must be calculated very accurate accurately since the inactivation rate k_d is strongly dependent on the temperature (see Eq. (2.3)).

A cluster with 16 Intel i7 processors and 32 GB RAM was used to simulate the sterilization of an unwrapped load. The simulation time was approximately five weeks. Without the heat transfer model presented in Section 4.4.1, the simulation time would

Table 5.3: Surface average log survival ratio for Bacteria Type 1 and Bacteria Type 2 for different simulation times on the surface of the steel cylinder [4].

	log survival ratio of Bacteria Type 1	log survival ratio of Bacteria Type 2
After 205 s	-1.89	-1.12
After 410 s	-33.95	-6.45
After 620 s	-50.96	-22.21

have been twice as long, due to the fact that the wall condensation film would have had to be resolved.

Validating the CFD simulation of the bacteria is difficult, due to the fact that spore strips are only able to measure a log survival ratio of minus six or higher. In the present PhD thesis, the full-length sterilization phase was always simulated. As can be seen in the results, during the full sterilization phase, a log survival ratio of lower than -22 was reached for Bacteria Type 2. A log survival ratio of approximately -51 was reached for Bacteria Type 1 (see Table 5.3). Measurements with spore strips can only confirm that the steam sterilizer under investigation is able to achieve a log survival ratio of minus six or higher. Nevertheless, to fully validate the simulated inactivation of bacteria, shorter cycles would have to be investigated, in which a log survival ratio over minus six is reached. Only for such short cycles can a full validation of the simulated inactivation of the bacteria be performed. More information about this topic can be found in Chapter 6. In Section 5.5, measurements with spore strips were performed to validate the CFD results for the inactivation of bacteria type *Geobacillus stearothermophilus*.

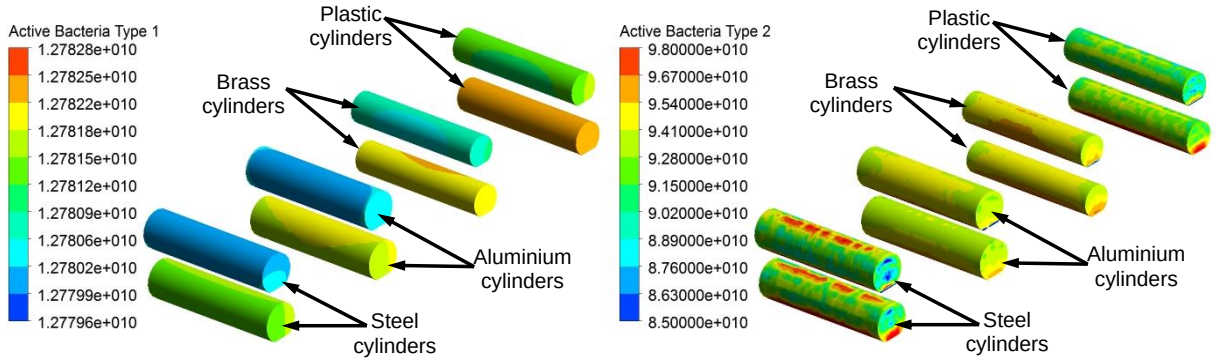

(a) Active bacteria of Type 1 (left) and Type 2 (right) after 205 s of simulation time

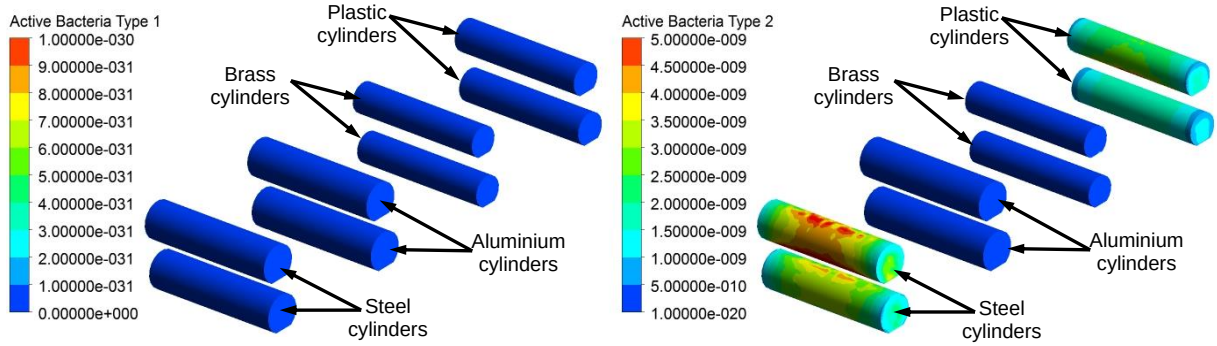

(b) Active bacteria of Type 1 (left) and Type 2 (right) after 410 s of simulation time

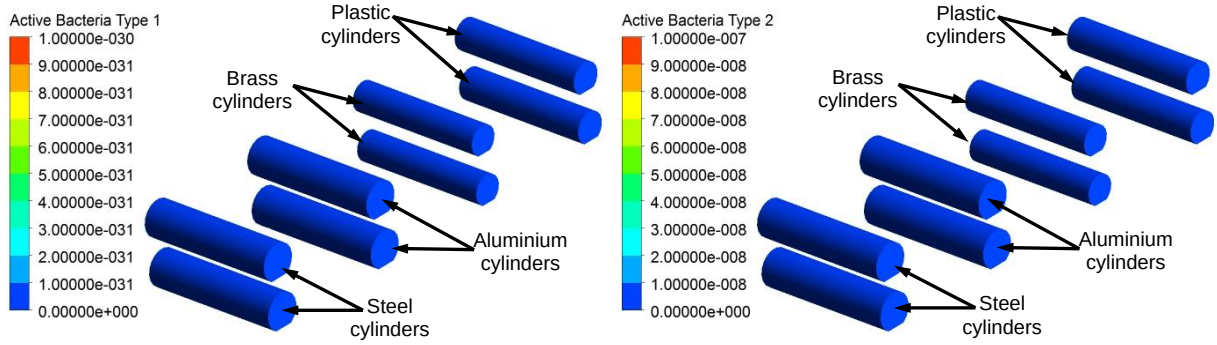

(c) Active bacteria of Type 1 (left) and Type 2 (right) after 620 s of simulation time

Figure 5.16: Active bacteria of the two investigated types on the surface of the unwrapped load after (a) 205 s, (b) 410 s and (c) 620 s of simulation time.

5.4 Simulation of the sterilization phase with a wrapped load [4]

The aim of this section was to simulate both the temperature and the inactivation of bacteria on the surface of a wrapped load. To this end, the steam sterilizer was filled with eight wrapped cylinders on two trays. The geometry of the CFD model with the wrapped load as well as the experimental set-up can be seen in Figure 3.4.

The pressure profile of the sterilization cycle for wrapped load investigated in this section can be seen in Figure 5.17 (see green arrow in Figure 5.17). The investigated sterilization phase starts at 0.29 bar and 82°C and ends at 3.16 bar and 136°C (see "sterilization phase" in Figure 5.17). The vertical blue lines represent the times at which the simulation results were analysed.

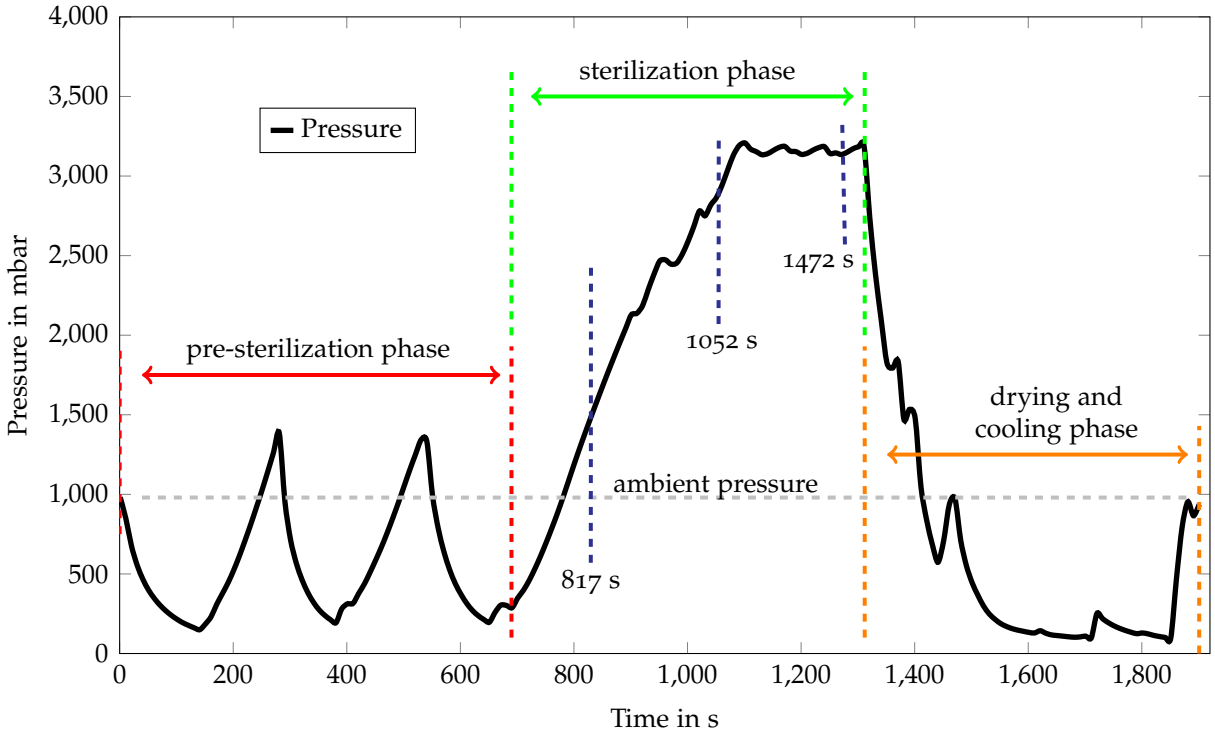

Figure 5.17: Pressure profile of the investigated sterilization cycle for the steam sterilizer loaded with wrapped load.

5.4.1 Simulated fluid temperature for a wrapped load

The results of the simulation of both flow and temperature distribution within the steam sterilizer were validated by the measurements of eight thermocouples. The

[4] Segments of this section have already been published in [1].

positions of these eight thermocouples can be seen in Figure 3.1. In the CFD model, the thermocouples were modelled as eight small volumes with dimensions of 10 mm × 10 mm × 10 mm. The positions of these eight volumes were the same as the positions of the thermocouples in the measurement set-up. The type J thermocouples with a diameter of 1 mm were used to measure the temperature within the steam sterilizer during the sterilization phase. To compare the simulated and measured temperatures, monitors of the volume average temperature were used in small volumes to investigate the temperature trend. The simulated and measured average fluid temperatures of all eight thermocouples can be seen in Figure 5.18(a). The simulated fluid temperature was in very good accordance with the measured fluid temperature. Figure 5.18(b) shows the average error between the simulated fluid temperatures and the measured ones for all eight thermocouples. The two black dashed horizontal lines in Figure 5.18(b) represent the relative average error of the thermocouples. The definition of the Error is given with Eq. (5.4) in Section 5.3.1.

As can be seen in Figure 5.18(b), the most significant error occurred in the first 150 seconds of the sterilization phase. This deviation between the measured and simulated fluid temperatures can be explained by the constant temperature initialization of the CFD simulation. In the real steam sterilization process, an inhomogeneous temperature distribution exists at the beginning of the sterilization phase. Due to the fact that the main inactivation of bacteria happens mainly at higher temperatures, these small deviations at low temperatures can be neglected. Thus, it is possible to conclude that the developed CFD model is able to predict the fluid temperature in the steam sterilizer over the whole sterilization phase.

5.4.2 Simulated load temperature of a wrapped load

The surface temperature of the load must be predicted with high accuracy in order to determine the inactivation rates of the bacteria on the load's surface, due to the exponential temperature dependency of the inactivation of the bacteria (see Eq. (2.3)). The simulated temperatures were compared with measured load temperatures in order to validate this topic. The positions of the load cylinders and the thermocouples used to measure the temperature of the load cylinders are shown in Figure 3.4(a). As can be seen in Figure 5.19, the simulated load temperatures match the measured load temperatures very well. The selected approach to calculate the heat transfer to the load and vice versa was validated by the measured data (see Figure 5.19). As described in Section 3.2.2, the investigated cylinders were wrapped in paper. The flow resistance to

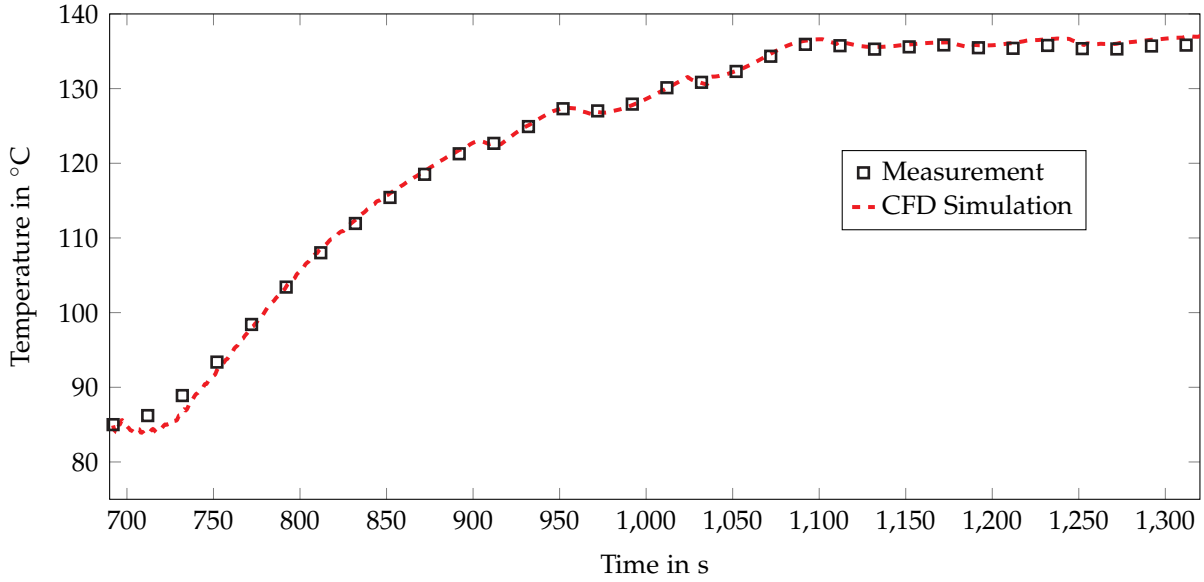

(a) Average simulated and measured fluid temperature of all eight thermocouples for wrapped load.

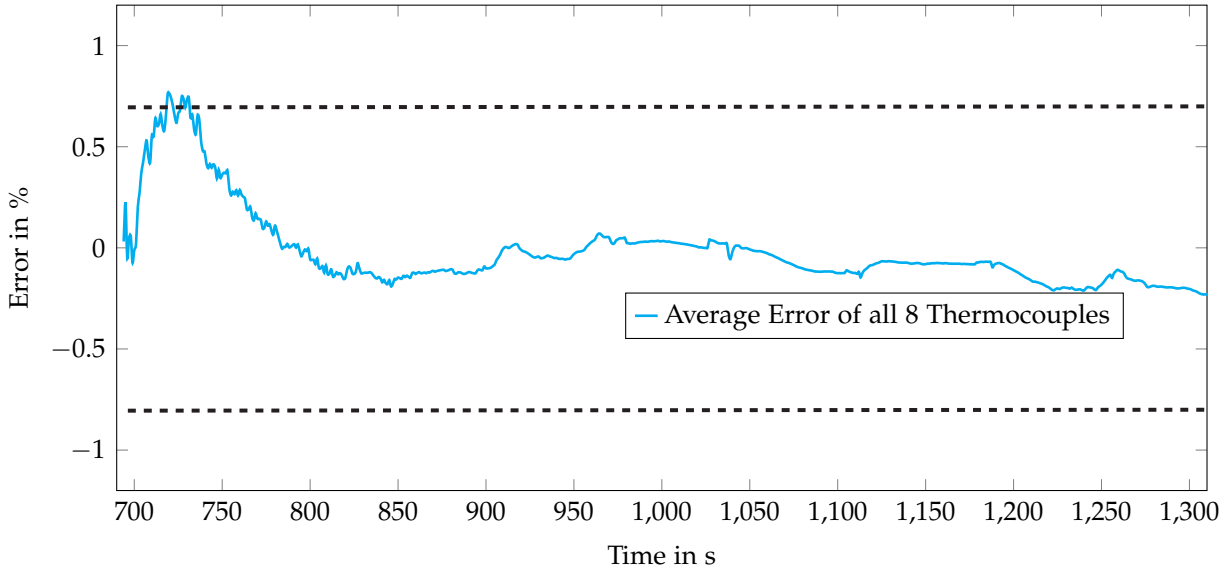

(b) Error between the CFD simulation and the measurements for wrapped load.

Figure 5.18: (a) Measured and simulated average fluid temperatures for wrapped load, (b) Average errors between the CFD simulation and the measurements of all eight thermocouples for wrapped load [1].

the steam that is introduced due to the paper was modelled with the porous media model developed in this thesis, which is explained and validated in Section 5.2.2.

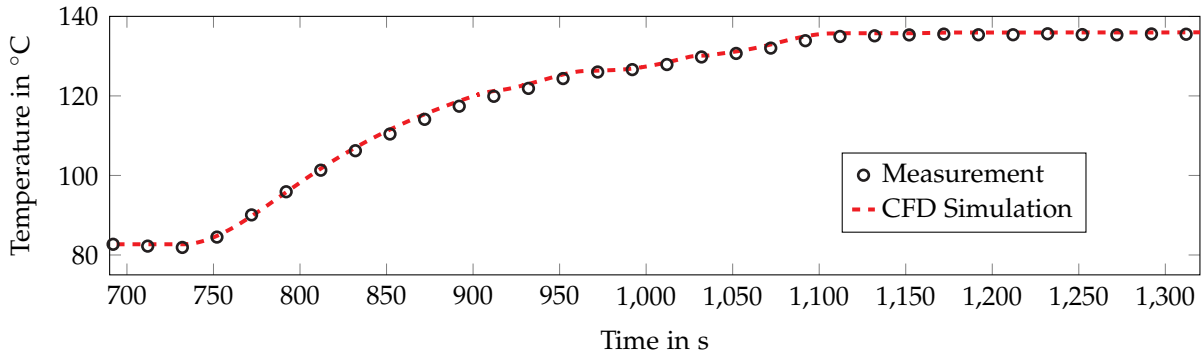

(a) Measured and simulated load temperatures of the wrapped steel cylinder.

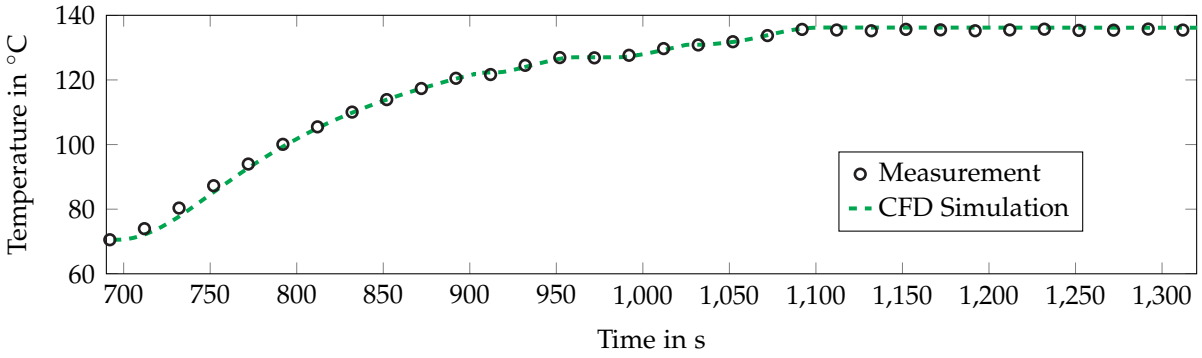

(b) Measured and simulated load temperatures of the wrapped aluminium cylinder.

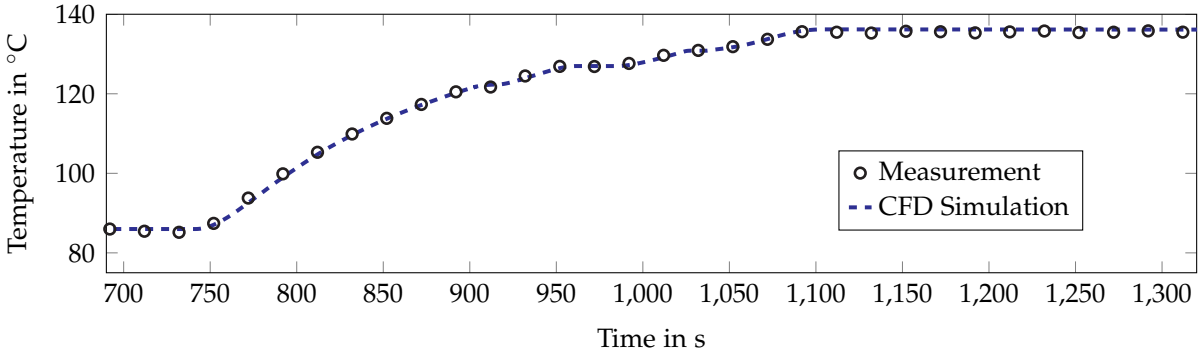

(c) Measured and simulated load temperatures of the wrapped brass cylinder.

Figure 5.19: Measured and simulated load temperatures for a wrapped (a) steel cylinder, (b) aluminium cylinder and (c) brass cylinder [1].

The simulated load temperature is in very good accordance with the measured load temperature. The maximum deviation between the measured and simulated load temperatures was under 0.2 K at the sterilization plateau (see between approximately 1100 s and approximately 1320 s in Figure 5.18(a)). The results indicate that the approach developed in this thesis to model the heat transfer due to wall condensation (described in Section 4.4.1) works quite well. The second advantage of this approach is

that computational costs can be saved. Figure 5.20 shows the simulated surface load temperature after (a) 817 s, (b) 1052 s and (c) 1272 s of cycle time. These times are indicated by the vertical dotted lines in Figure 5.17.

As it might have been expected, the heating process of the cylinders on tray 1 and tray 2 were very similar. Small temperature differences, below 0.2 K, were detected after 1272 s of cycle time between the cylinders on tray 1 and tray 2. Furthermore, the results show that the difference between the highest and lowest surface load temperature of the different materials decreases as the cycle time increases. These results also confirm that the investigated steam sterilizer [31] works very well. The generation of such a homogeneous surface load temperature is the result of the significant effort that went into its development.

A comparison of the simulated results presented in Figure 5.14 and Figure 5.20 confirms that the influence of the wrapping on the surface temperature is negligible. A more detailed comparison of the unwrapped and wrapped loads is presented in Section 5.5. Without the heat transfer model developed in this thesis (presented in Section 4.4.1) and the novel model used to simulate the paper in which the load was wrapped (presented in Section 3.4 and Section 4.5), it would not have been possible to obtain these results.

5.4.3 Simulated steam quality for a wrapped load

High wall temperatures are beneficial during the sterilization process. To achieve high wall temperatures, high heat transfer coefficients due to wall condensation are desired. In order to analyse heat transfer within a steam sterilizer, a good understand of the distribution of the steam quality inside the steam sterilizer is crucial. The results of the steam quality were depicted in the symmetry plane of the steam sterilizer as well as on two radial surfaces (see Figure 5.12). The selected cycle times represent a time at the beginning, in the middle, and at the end of the sterilization phase. The cycle times at which the steam quality was evaluated are shown in Figure 5.17. Figure 5.21 shows the steam quality in the steam sterilizer after 817 s, 1052 s and 1272 s.

The lowest values of steam quality were detected within the pouches on tray 2. However, as the cycle time increases, the steam quality in the pouches also increases. The highest steam quality outside the pouches was found on the top of the steam sterilizer, where the highest temperatures were obtained. The steam quality outside the pouches decreases as the cycle time increases. As the simulation time goes on, the quality could

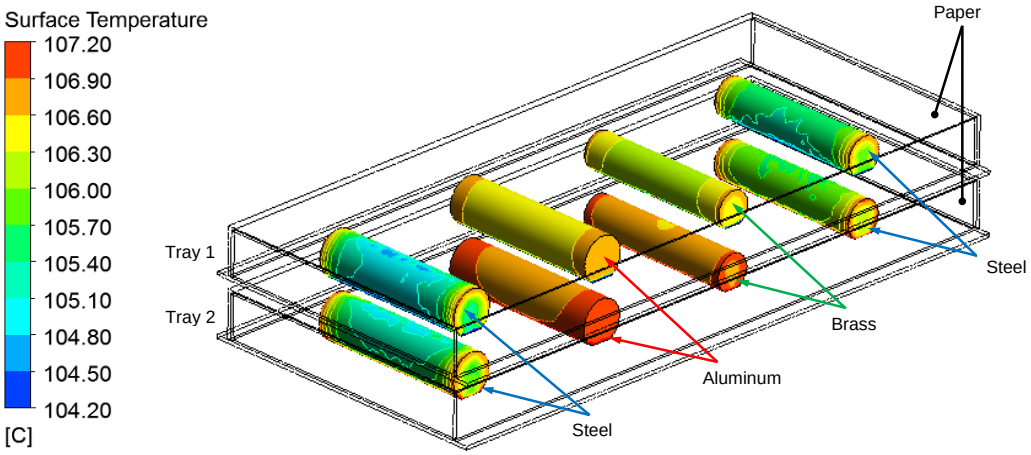

(a) Surface temperatures on the surface of the wrapped load after 817 s.

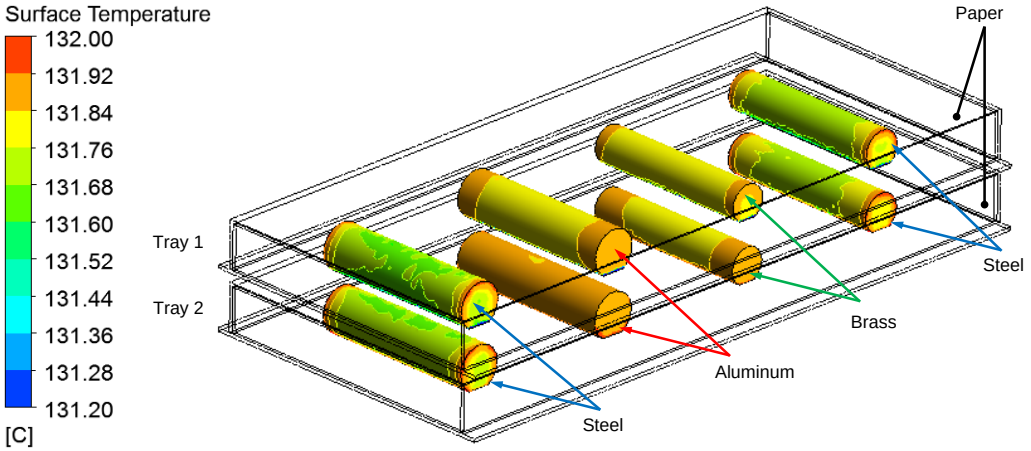

(b) Surface temperatures on the surface of the wrapped load after 1052 s.

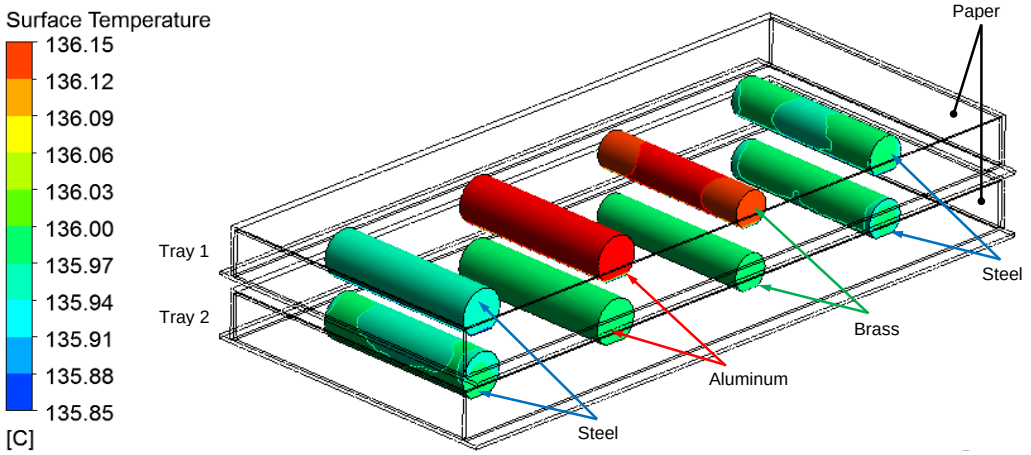

(c) Surface temperatures on the surface of the wrapped load after 1272 s.

Figure 5.20: Surface temperatures on the surface of the wrapped load after (a) 817 s, (b) 1052 s and (c) 1272 s of cycle time [1].

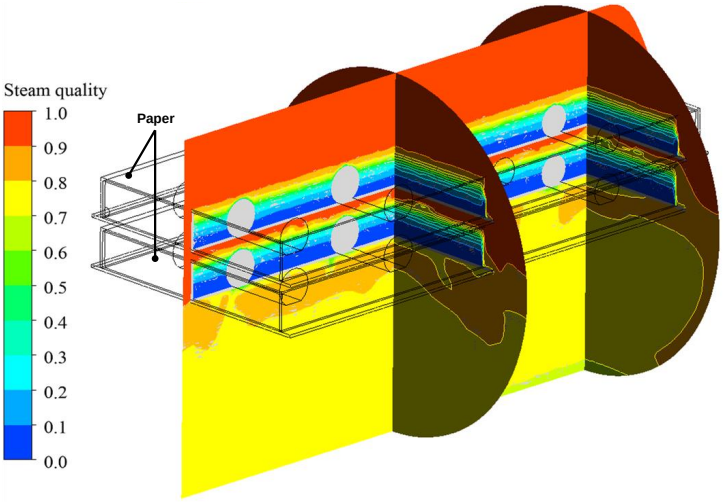

(a) Steam quality for wrapped load after 817 s of cycle time.

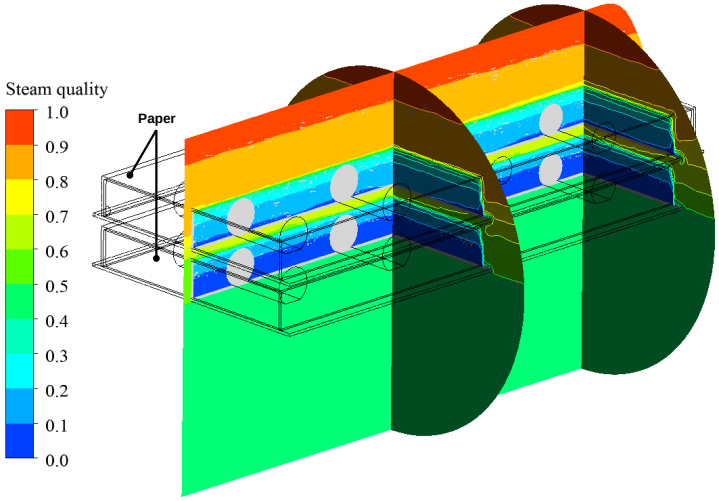

(b) Steam quality for wrapped load after 1052 s of cycle time.

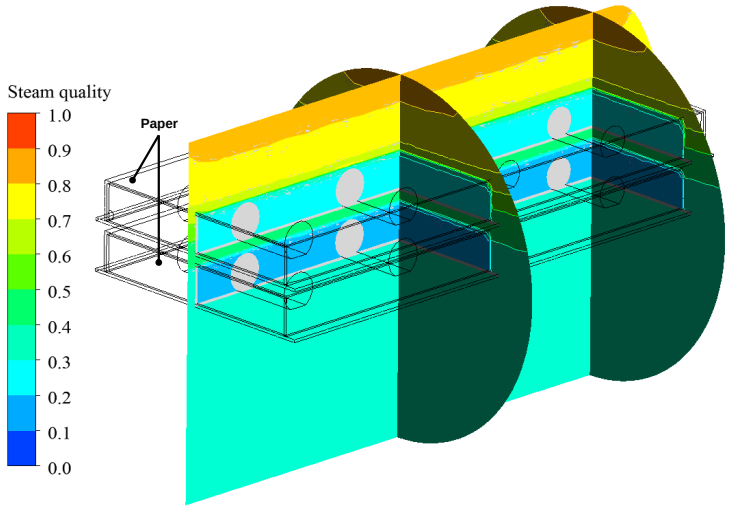

(c) Steam quality for wrapped load after 1272 s of cycle time.

Figure 5.21: Steam quality in the steam sterilizer loaded with wrapped load after (a) 817 s, (b) 1052 s and (c) 1272 s of cycle time [1]. The materials of the investigated cylinders can be seen in Figure 5.20.

reaches approximately 0.4 in the lower part of the steam sterilizer. At this quality, the assumption of a constant droplet diameter might fail. However, as the load is only present in the upper part of the chamber, water droplets in the lower part of the steam sterilizer may not affect the surface temperature of the load.

Measurements of steam quality are very difficult to obtain. As a result, it is difficult to validate the simulation results of the steam quality. In this thesis, an indirect validation of the steam quality was performed. This validation was based on a comparison between the mass of the condensate simulated with CFD and the calculated mass of the condensate out of a mass and energy balance. The resulting difference of this comparison was always below 11 %. Thus, these results prove that the CFD model developed in this thesis is able to accurately predict the steam quality. In order to carry out a more detailed validation, it would be necessary to obtain detailed measurements of the condensate. Though beyond the scope of this thesis, this is a field for further research.

With the paper model developed in this thesis, it is possible to simulate the steam quality both outside as well as inside the paper pouches containing the cylindrical load; knowing this value makes it possible accurately predict the inactivation of bacteria on the surface of the load. This novel the time-efficient porous media model also makes it possible to simulate the distribution of the steam quality within the steam sterilizer as well as the distribution of the fluid temperature inside the steam sterilizer. The difference between the measured and simulated fluid temperatures was below the accuracy of the thermocouples (see Figure 5.18(b)). Furthermore, this paper model made it possible to simulate the load temperature in a very accurate manner (see Figure 5.19). All of these results show that research question ii) "What model can be used to simulate the wrapping of the load?" can be answered as follows: The porous media model developed in this thesis is able to simulate the wrapping of the load in a very accurate manner.

5.4.4 Simulated active bacteria on the wrapped load

In order to understand the full sterilization process, it is essential to have knowledge of the inactivation log ratio within the steam sterilizer as well on the surface of the load. A definition of the inactivation log ratio is given in Eq. (2.6) in Section 2.2.

Values from the work of De Santis and Rudo [127] were used to simulate the inactivation of bacteria. The first-order reaction reaction kinetic approach is shown in Section 2.2.

The pre-exponential factor of the investigated bacteria was ($k_{d0} = 2.38053 \cdot 10^{-42}\ 1/s$) and the activation energy was ($E_d = 1.914477928\ J/mol$).

According to norms and standards, a sterilization process for medical devices should reach an inactivation log ratio of six or higher [132]. The big advantage of the developed CFD model is that this model can predict the inactivation log ratios resolved in time at every point in the steam sterilizer. Figure 5.22 presents the simulated volume average inactivated log ratio of the fluid as well as the area-weighted average of the steel cylinders on the upper tray during the sterilization phase. The pressure profile of the sterilization cycle is shown in Figure 5.17).

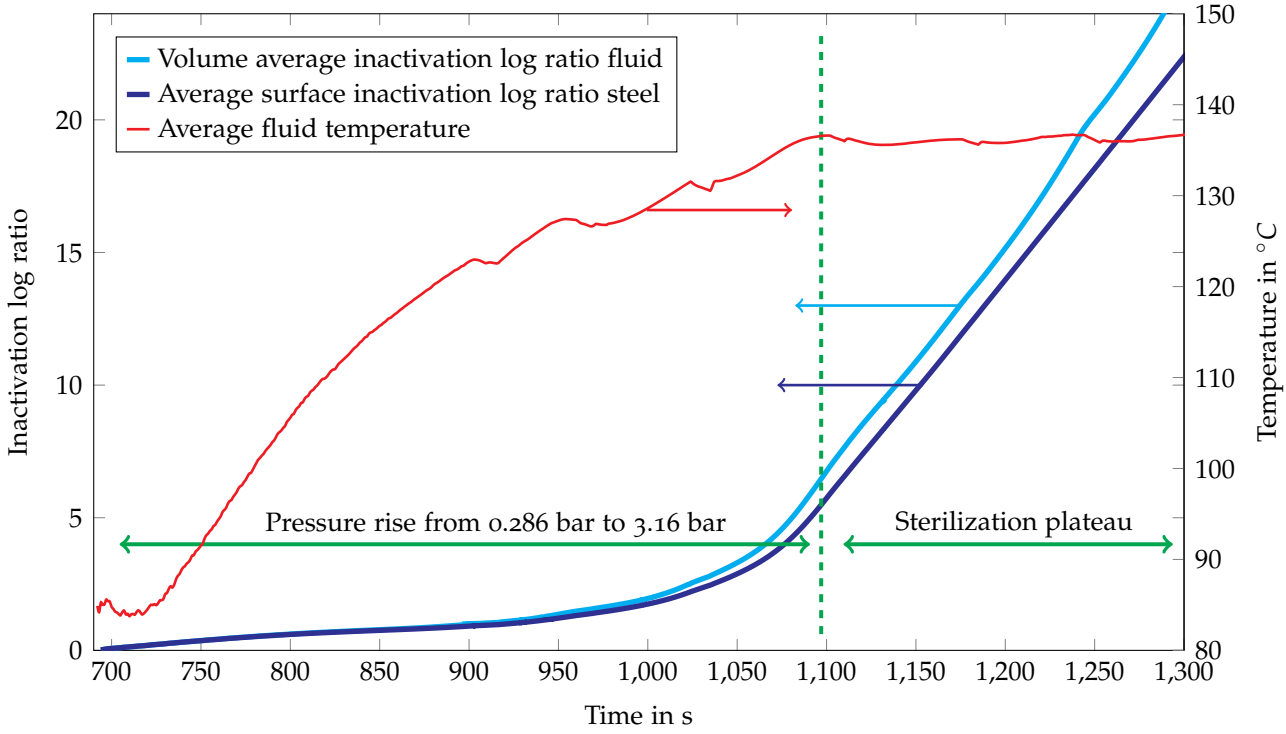

Figure 5.22: Time-resolved simulated inactivation log ratio in the fluid of the steam sterilizer and on the surface of the wrapped steel cylinder [1].

As might have been expected, hardly any inactivation of the bacteria takes place at temperatures below 120 °C (see the first 900 s in Figure 5.22). In the first part of the sterilization phase, when the pressure rises from 0.29 bar to the sterilization plateau (3.16 bar), the volume average in the fluid of the inactivation log ratio has already reached a level of approximately six. The area-weighted average of the steel cylinders is slightly lower compared to the inactivation log ratio value of the fluid. This is the result of a temperature difference between load and fluid. At the sterilization plateau, where the pressure and the temperature are constant at 3.16 bar and 135 °C, the inactivation log ratio rises from approximately six to values of 22 and higher. These results demonstrate that the investigated steam sterilizer [31] is extremely effective and

able to inactivate all bacteria on the surface of the load. These results can be attributed to the homogeneously high temperatures that the investigated steam sterilizer is able to generate on the surface of the load (see Figure 5.20).

Figure 5.23 shows the active bacteria (microorganisms) after 817 s, 1052 s and 1272 s of cycle time. As might have been expected, hardly any differences in terms of the quantities of active bacteria are visible at the beginning of the sterilization phase (see Figure 5.23(a)). As the cycle time increases, the active number of bacteria decreases. At the end of the sterilization phase, hardly any active bacteria are present on the surface of the cylinder. Furthermore, the results show that there were hardly any differences between tray 1 and tray 2 (see Figure 5.23(c)). Again, these results can be attributed to the homogeneously high temperatures that the investigated steam sterilizer is able to generate on the surface of the load (see Figure 5.20). Without this excellent temperature distribution inside the steam sterilizer, it would not be possible to inactivate all of the bacteria.

The results presented in Section 5.4 show that the CFD model developed in this thesis is able to calculate the inactivated log ratio in the fluid as well as on the surface of the load. Additionally, the number and distribution of active bacteria (microorganisms) on the load surface can be determined.

For the simulations of the sterilization phase with a wrapped load, a cluster with 16 Intel i7 processors and 32 GB RAM was used. The simulations took approximately five and a half weeks.

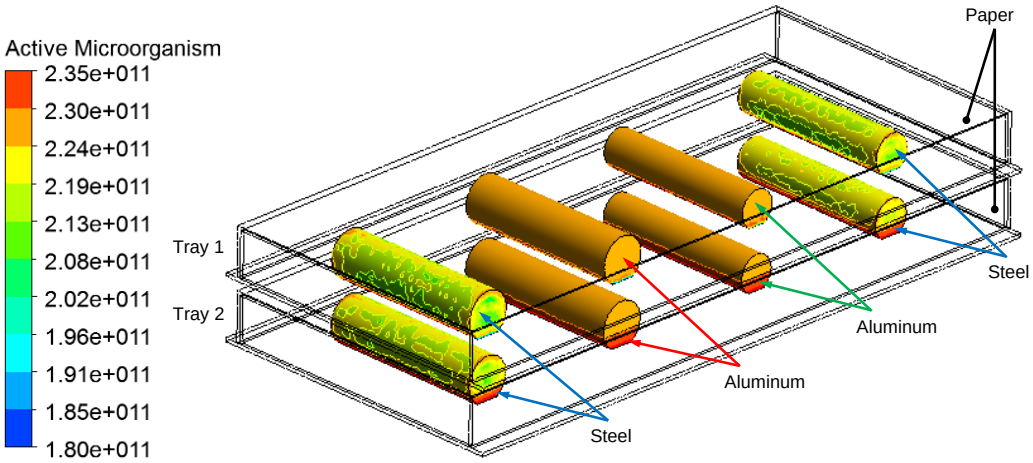

(a) Active bacteria on the surface of the wrapped load after 817 s.

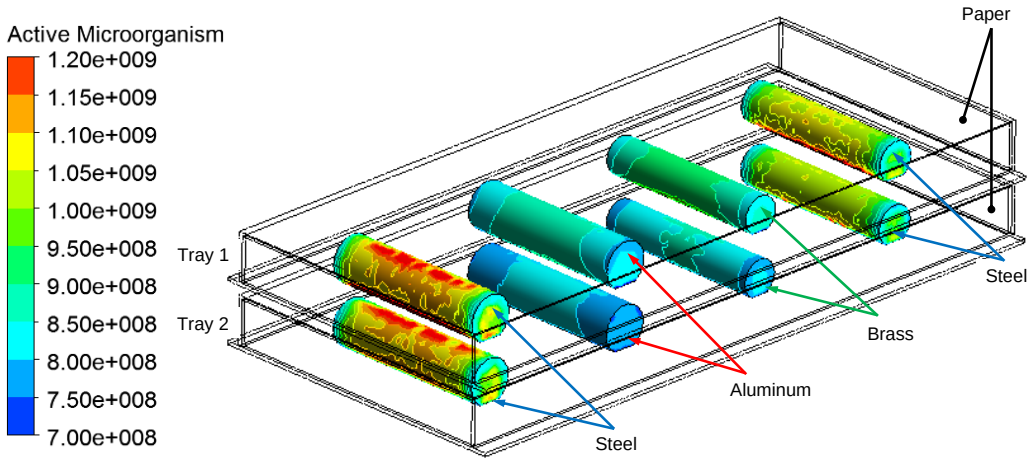

(b) Active bacteria on the surface of the wrapped load after 1052 s.

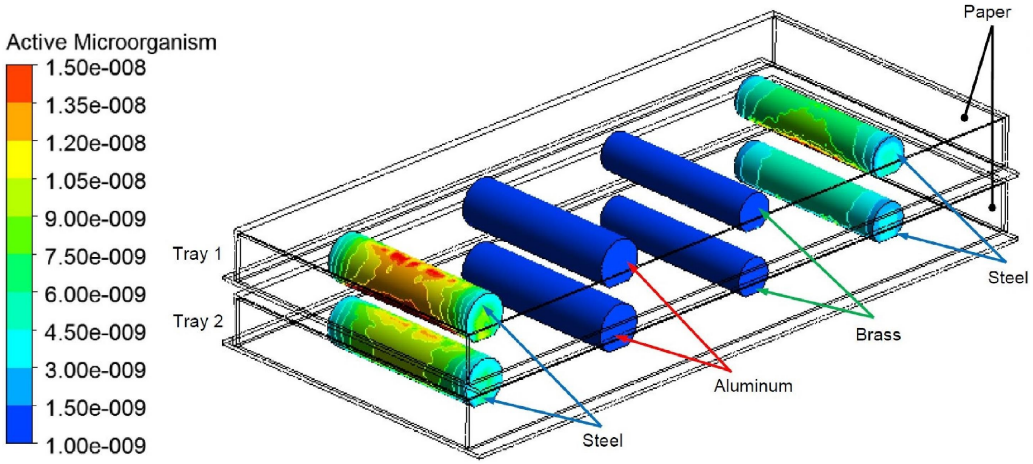

(c) Active bacteria on the surface of the wrapped load after 1272 s.

Figure 5.23: Active bacteria on the surface of the wrapped load after (a) 817 s, (b) 1052 s and (c) 1272 s of cycle time [1].

5.5 Simulation of the sterilization phase with dental handpieces [5]

In the previous sections (Section 5.3 and Section 5.4), the load temperature and the inactivation of bacteria were simulated on unwrapped and wrapped cylinders. In this section, the CFD model is further developed to simulate both the load temperature and the inactivation of the bacteria type *Geobacillus stearothermophilus* on dental handpieces. For this purpose, the steam sterilizer was loaded with four Type 1 dental handpieces and four Type 2 handpieces. The two types of dental handpieces are not only different in terms of their masses and shapes, but also in their working principles.

All of the models that were employed and validated in Section 5.3 and Section 5.4 were used for the simulation in this section. In this section, only the reaction kinetics were changed in order to simulate the inactivation of *Geobacillus stearothermophilus*. The same heat transfer model that has already been validated for unwrapped and wrapped loads was used to simulate the heating process of the two types of dental handpieces as well as both wrapped and unwrapped dental handpieces. As a result, this section presents a further use of the CFD models presented in Section 5.3 and Section 5.4 so as to demonstrate that dental handpieces can also be simulated in a time-efficient manner using the developed CFD models.

The eight handpieces were distributed on two trays, each of which held two Type 1 handpieces and two Type 2 handpieces. The geometries and shapes of the two types of dental handpieces used in this thesis are shown in Figure 5.24(b). A picture of the unwrapped dental handpieces that were investigated can be seen in Figure 2.6, and a picture of the wrapped dental handpieces can be found in Figure 2.7. All of the dental handpieces were made of stainless steel, while the trays they were placed on were made of aluminium. In practice, dental handpieces such as these are sometimes wrapped, in case they need to be stored or transported after the sterilization process [69]. In order to investigate the influence of wrapping on the load, the four handpieces on the first tray were wrapped in paper [70], while the four handpieces on the second tray were left unwrapped (see Figure 5.24(a)).

As in the two previous sections (Section 5.3 and Section 5.4), this section investigates the sterilization phase of the steam sterilization cycle (see "sterilization phase" in Figure 5.8 and Figure 5.17). The measured pressure and fluid temperatures of the

[5] Segments of this section have already been published in [5].

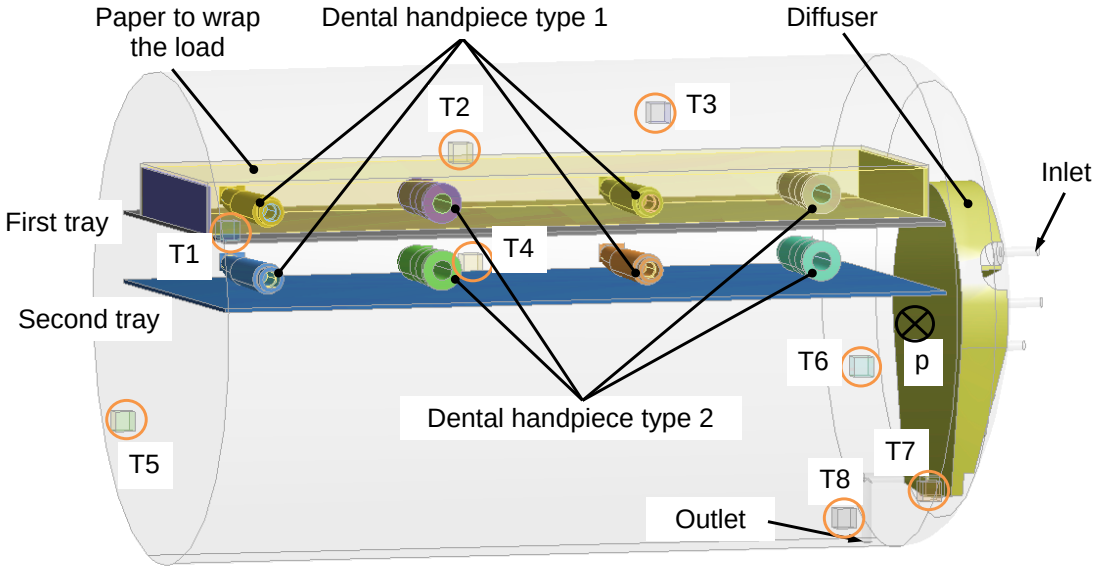

(a) Geometry of the CFD model with the positions of the thermocouples T1 - T8 and the pressure sensor p.

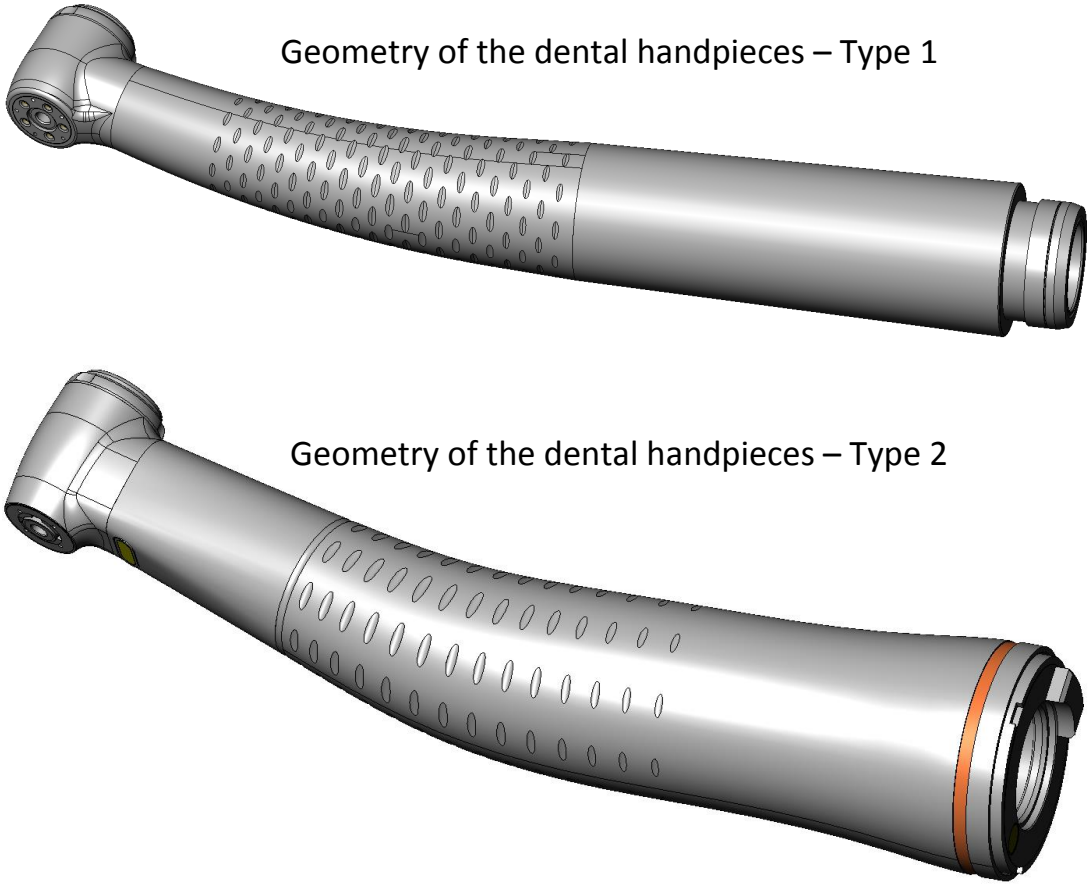

(b) Geometry of the dental handpiece Type 1 and Type 2.

Figure 5.24: Geometry of (a) CFD model of the steam sterilizer with the experimental set-up, (b) the dental handpieces, Types 1 and 2 [5].

sterilization phase are shown in Figure 5.25. The green vertical lines represent the times within the sterilization phase at which the simulation results are presented.

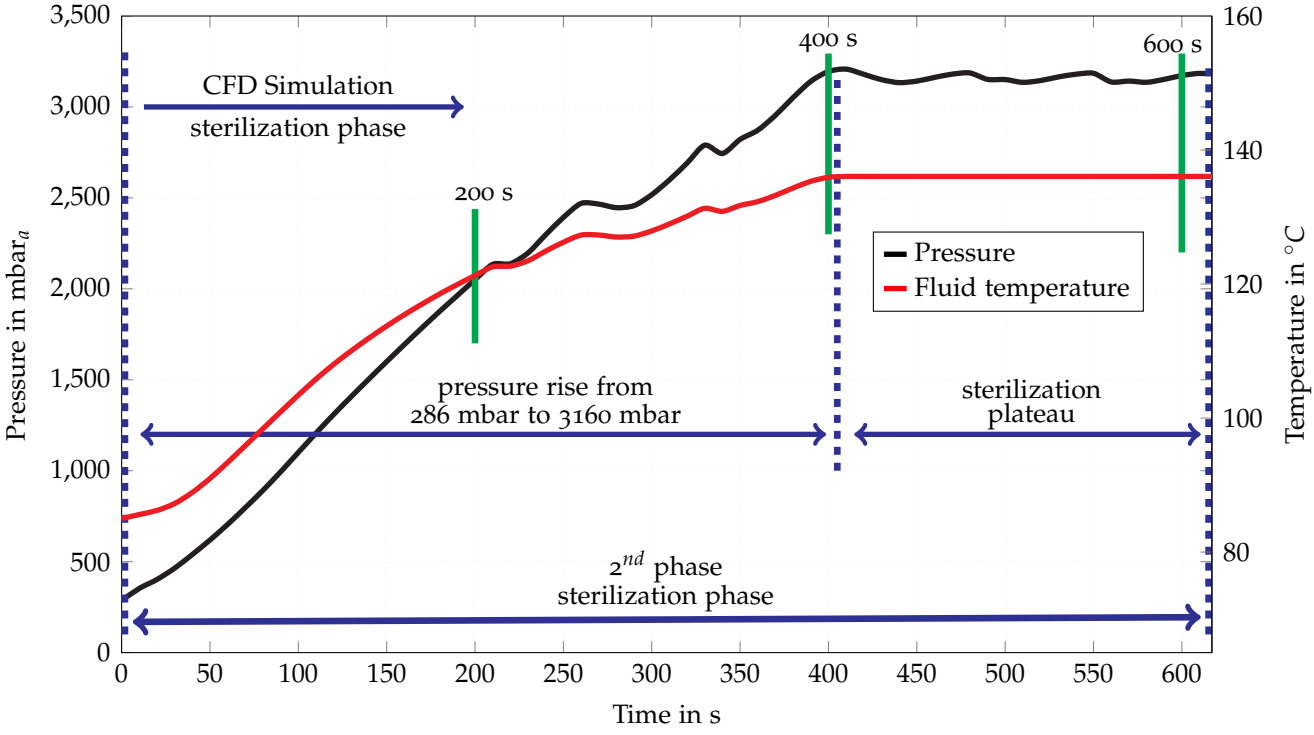

Figure 5.25: Measured pressure and fluid temperatures during the sterilization phase while the steam sterilizer was filled with dental handpieces [5].

5.5.1 Validation of the CFD model for dental handpieces

In order to simulate the inactivation of bacteria, it is crucial to accurately predict the temperatures on the surface of the load (see Eq. (2.3) and Eq. (2.5)). The saturation temperature of the steam is a function of the pressure in the steam sterilizers' chamber [8]. Thus, in order to validate the CFD model, the measured pressure and the simulated pressure as well as the measured and simulated fluid temperatures inside the steam sterilizer were compared. Figure 5.26(a) shows the measured and simulated pressures during the sterilization phase of the steam sterilization cycle. It is possible to see that the simulated pressure is in very good accordance with the measured one. Furthermore, it is possible to see that between 250 s and 300 s, a small pressure decrease occurs due to the fact that, at this point, the steam generator is refilled with water. Therefore, the mass flow rate of the steam generator decreases slightly, and, consequently, the pressure inside the steam sterilizer decreases due to the condensation effects that occur. The novel CFD model presented in this thesis was also able to predict these phenomena.

To investigate the difference between the measured and the simulated pressures in more detail, the error between the measured and simulated pressures ($x_{pressure}$) was calculated using Eq. (5.5) in order to demonstrate the accuracy of the CFD model.

$$x_{Pressure} = 1 - \frac{p_{CFD}}{p_{Measurement}} \tag{5.5}$$

where, $p_{Measurement}$ stands for the measured pressure and p_{CFD} stands for the pressure calculated by the CFD model. Figure 5.26(b) presents the error of the simulated values of the pressure during the sterilization phase of the steam sterilization cycle. Small deviations between the measured and the simulated values can be seen within the first 100 s of simulation time. This can be explained by the constant initialization of the temperature at the beginning of the simulation. After 100 s, the difference between the measured and the simulated pressures is within the uncertainty of the pressure sensor, which was $\pm$ 1 %.

Next, the average fluid temperatures measured by means of eight thermocouples were compared with the simulated temperature values (see Figure 5.27(a)). Here, too, the temporally resolved error between the measured and the simulated temperatures ($x_{Temperature}$) was investigated using Eq. (5.4).

The calculated error for each thermocouple can be seen in Figure 5.27(b), which shows that the error between the measured and the simulated temperatures was below the measurement uncertainties of the thermocouples for the entirety of the sterilization phase. Small deviations between the measured and the simulated temperatures are seen only within the first 50 s of the simulation (see Figure 5.27(b)). On the one hand, these deviations occur because of radiation effects from the chamber walls to the thermocouples because of high temperature differences. As the cycle time goes on, the temperature difference between the chamber walls and the fluid decreases; thus, the error between the measured and simulated temperatures decreases as well. On the other hand, the initial deviations can also be attributed to the non-uniform temperature stratification (at $t = 0\ s$) inside the real steam sterilizer. This temperature stratification is difficult to measure and therefore very difficult to initialize. Due to the fact that the inactivation of bacteria occurs at higher temperatures, and the F_0 value was only calculated for temperatures above 100 °C (see Eq. (2.5)), these small deviations can be neglected.

Overall, the results show that the CFD model developed in the course of this thesis is able to predict both the pressure and the temperature within a steam sterilizer over

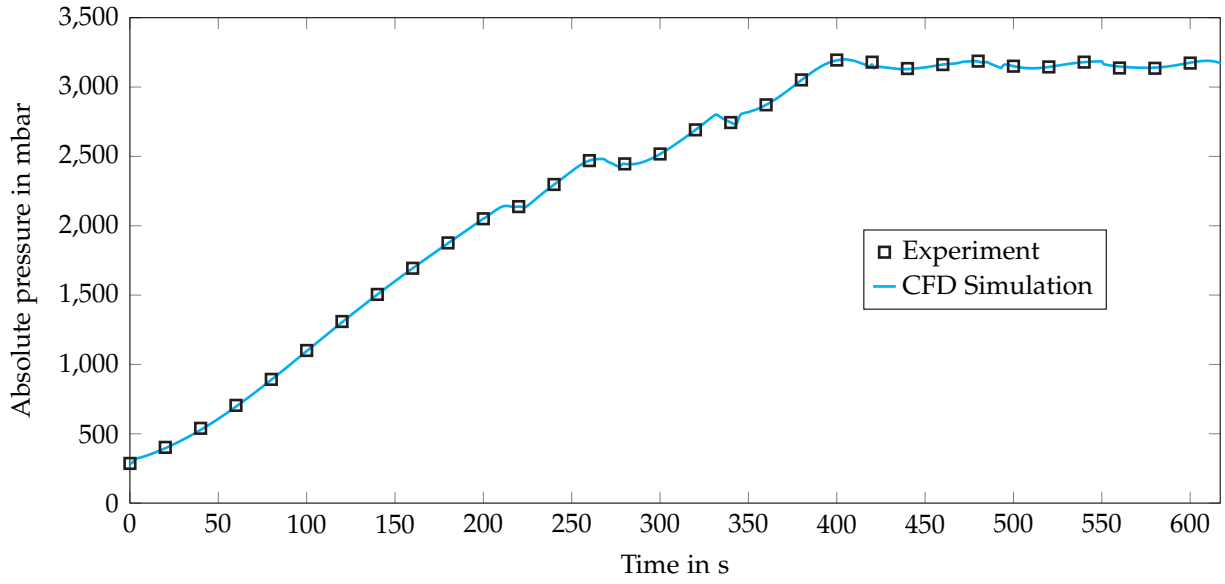

(a) Measured and simulated absolute pressures in the steam sterilizer.

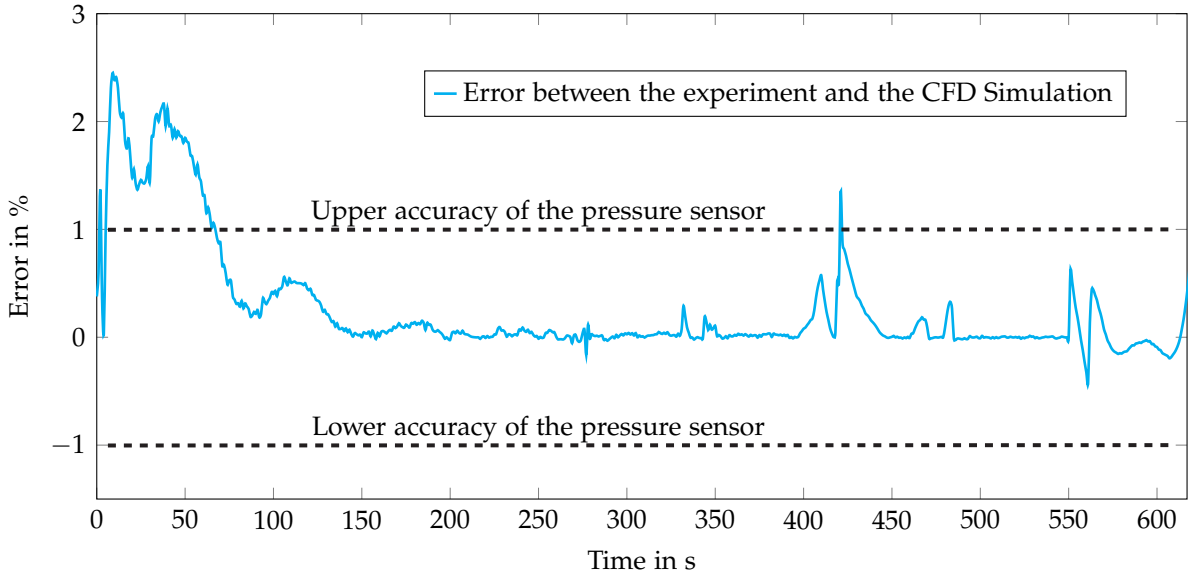

(b) Error between the measured and the simulated absolute pressures.

Figure 5.26: (a) Measured and simulated absolute pressures in the steam sterilizer and (b) error between the measured and the simulated pressures over the simulated phase of the sterilization cycle [5].

the entire sterilization phase with very high accuracy. Furthermore, the results confirm that the heat transfer model developed in this thesis (see section 4.4.1) and the selected condensation model (see Section 4.3) were able to accurately predict both the heat transfer and the condensation inside the steam sterilizer.

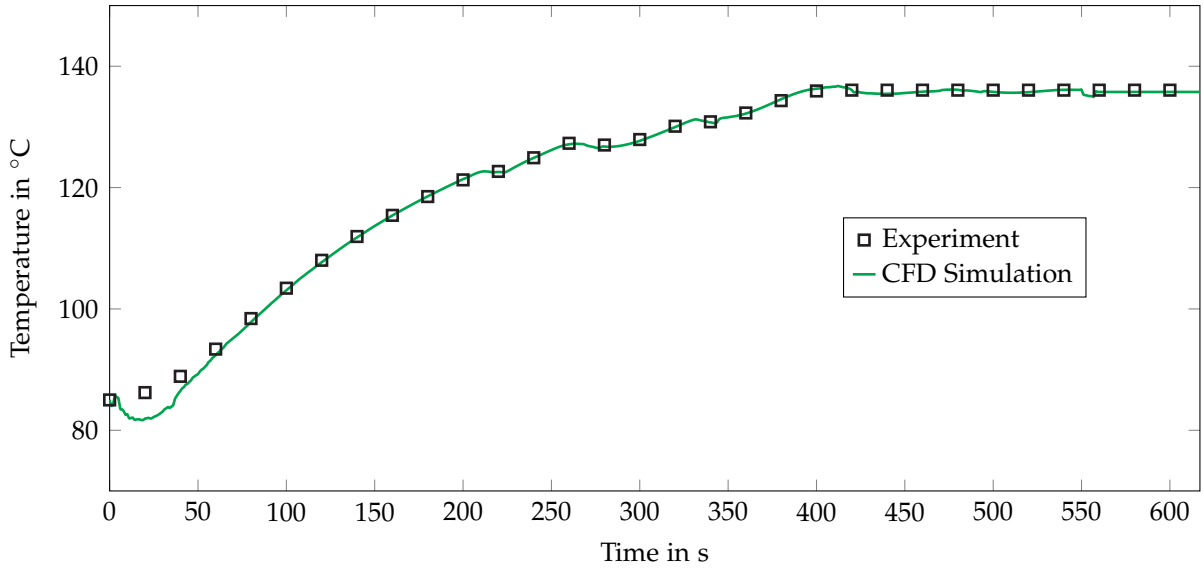

(a) Measured and simulated average fluid temperatures of eight thermocouples.

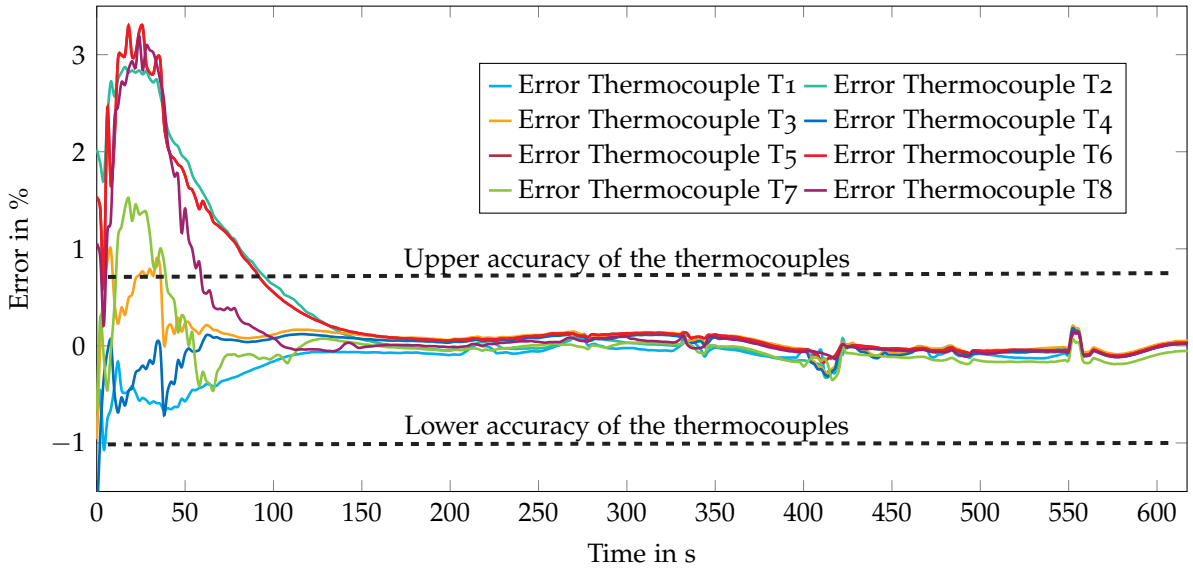

(b) Error between the measured and the simulated fluid temperatures for each thermocouple.

Figure 5.27: (a) Measured and simulated average fluid temperatures of eight thermocouples and (b) error between the measured and the simulated fluid temperatures for each thermocouple [5].

5.5.2 Fluid temperatures inside the steam sterilizer with dental handpieces

Using thermocouples, it is only possible to measure the fluid temperatures at certain pre-defined locations. In contrast, the fluid temperature of the entire steam sterilizer can be modelled by means of CFD. To guarantee that the fluid is uniformly heated and that no cold spots are present within the steam sterilizer, Figure 5.28 presents volume renderings of the fluid temperatures at different times of the sterilization phase (see the vertical green lines in Figure 5.25). After 200 s and 400 s of the sterilization phase, the maximum temperature difference inside the steam sterilizer was calculated to be 2 K. At these times, the lowest temperatures were identified to be in the middle of the steam sterilizer, near the trays. These lower temperatures are caused by the thermal inertia of the dental handpieces and the trays. As the sterilization phase continues, the temperature difference between the walls and the fluid decreases to a value of only 0.3 K (see Figure 5.28(c)). After 600 s, the location of the lowest temperature moved from the middle of the steam sterilizer to the wall regions of the steam sterilizer's chamber. To illustrate the fluid temperature distribution in the sterilization plateau in more detail, Figure 5.29 shows the fluid temperature on two radial planes after 600 s of simulation time. The highest temperatures can be found near the load, due to the stored heat of the dental handpieces and the trays. The coldest regions were found near the walls of the steam sterilizer due to free convection on the outside of the steam sterilizer (see Section 4.8.1). Nevertheless, the difference between the highest and the lowest fluid temperature was only approximately 0.3 K. Furthermore, no differences between the fluid temperatures near the wrapped dental handpieces (first tray) and the unwrapped dental handpieces (second tray) were identified.

These low temperature differences confirm the fact that the temperature distribution inside the steam sterilizer investigated in this work is excellent and the most homogeneous ever investigated by the author of this thesis. Furthermore, without the CFD model presented in this section, we would have no way to gain insight into the temporally resolved fluid temperatures of all locations within the steam sterilizer.

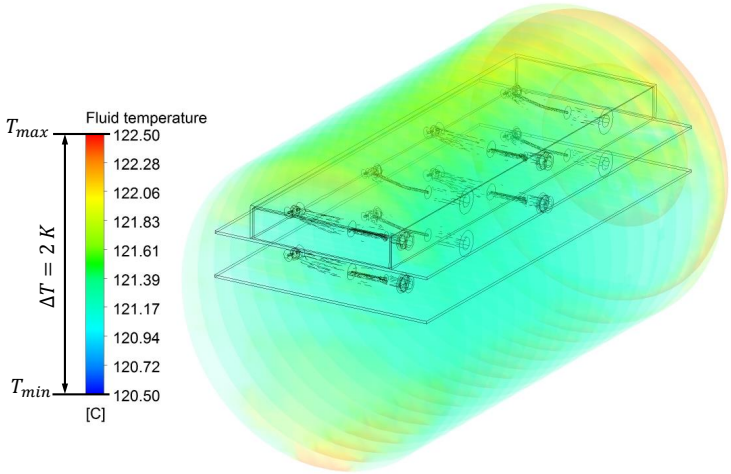

(a) Fluid temperatures in the steam sterilizer after 200 s of simulation time.

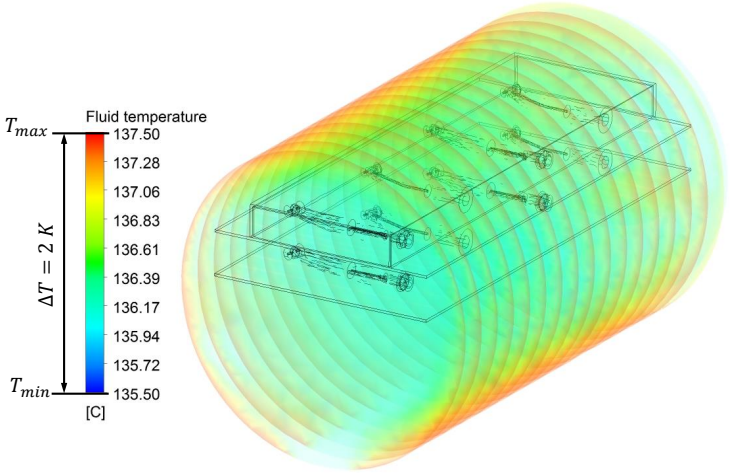

(b) Fluid temperatures in the steam sterilizer after 400 s of simulation time.

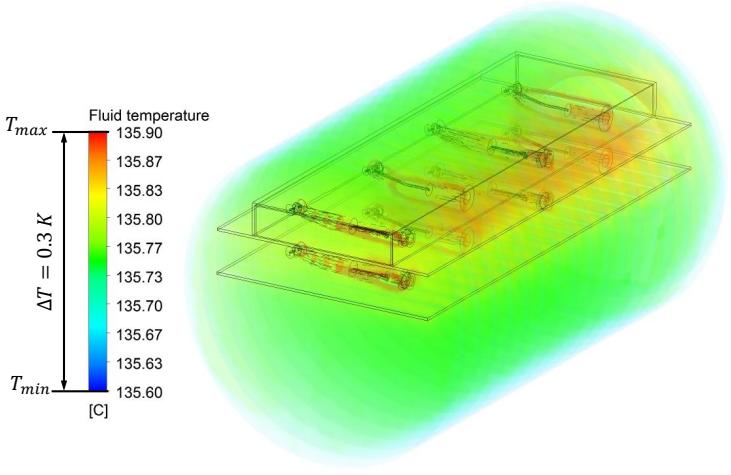

(c) Fluid temperatures in the steam sterilizer after 600 s of simulation time.

Figure 5.28: Volume rendering of the fluid temperatures in the steam sterilizer after (a) 200 s, (b) 400 s and (c) 600 s of simulation time [5].

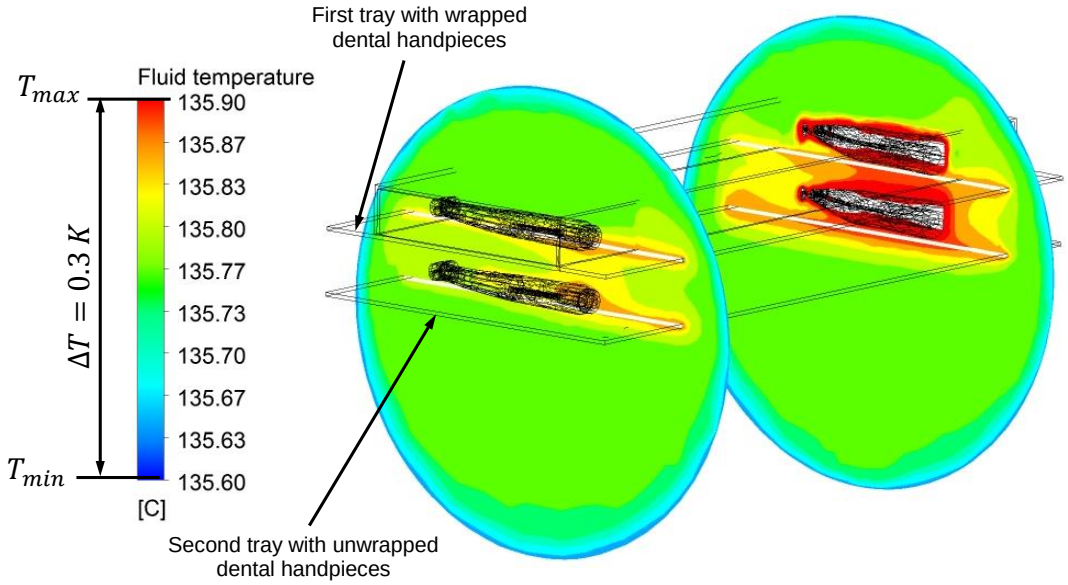

Figure 5.29: Fluid temperatures on a radial plane at the front and at the back of the steam sterilizer after 600 s of simulation time [5].

5.5.3 Simulated steam quality on dental handpieces

Bacteria can be inactivated on the surface of dental handpieces by means of high surface temperatures. Within steam sterilizers, these high surface temperatures occur thanks to the high heat transfer rates that result from condensation effects (see Eq. (2.3) and Eq. (2.5)). Thus, the distribution of the steam quality is of great interest to a study of the heat transfer rates. In this PhD thesis, the steam quality (x) inside the steam sterilizer was investigated at the vertical middle surface, the horizontal middle surface, and on two radial planes. The definition of steam quality is shown in Eq. (2.8).

Figure 5.30 shows the calculated steam quality after 200 s, 400 s and 600 s of simulation time. Due to density differences, the highest steam quality could be seen in the top region of the steam sterilizer throughout the entire simulation. As might have been expected, the steam quality decreases as it nears the bottom of the steam sterilizer (see Figure 5.30(c)).

In the present thesis, the dental handpieces on the first tray were wrapped in paper, whereas the dental handpieces on the second tray were unwrapped (see Figure 5.24(a)). The results show that the wrapping of the handpieces has a significant influence on the steam quality. The steam quality near the wrapped handpieces is clearly lower compared to the steam quality near the unwrapped handpieces. Nevertheless, many authors have shown that almost all steam qualities still have high heat transfer rates [51–53]. As a result, the influence of the steam quality on the surface temperatures of

the dental handpieces is very low.A more detailed discussion of the influence of the steam quality can be found in Section 5.5.4.

The results presented in this section show that the CFD model developed in this thesis is able to predict the steam quality inside a steam sterilizer, as resolved in both time and space. Furthermore, this CFD model makes it possible to investigate the influence of the wrapping on the steam quality. Prior to this thesis, it was nearly impossible to investigate the steam quality as resolved in time and space. Without the time-efficient heat transfer model presented in Section 4.4.1 and the adapted Lee model, which simulates condensation (see Section 4.3), it would be impossible to obtain these results. A validation of the models used in this section can be found in Section 5.3 and Section 5.4.

5.5.4 Simulated temperatures and F0-values on the dental handpieces

In order to fully understand the steam sterilization process, it is important to consider not only the fluid temperatures inside the steam sterilizer, but also the surface temperature of the load. Both the bacteria's inactivation rate and the F_0 values are extremely temperature-sensitive (see Eq. (2.3) and Eq. (2.5)). Therefore, the temperature distribution on the surface of the dental handpieces was also investigated by means of a CFD simulation. Figure 5.31 shows the simulated surface temperature of the eight dental handpieces after 200 s, 400 s and 600 s. The times at which the surface temperatures were simulated are indicated by the vertical green lines in Figure 5.25.

As might have been expected, the temperature differences on the surfaces of the handpieces are very small. After 200 s of simulation time (approximately 2 bar and 120 °C), the highest temperature difference was 0.25 K. During the sterilization phase, the temperature difference decreased further. Hardly any differences between the wrapped handpieces (first tray) and the unwrapped handpieces (second tray) were identified (see also "fluid temperature" Figure 5.28 and Figure 5.29). At the beginning of the sterilisation plateau (after 400 s, see Figure 5.25), the temperature difference on the surface of the wrapped dental handpieces (first tray) and the unwrapped dental handpieces (second tray) was below 0.05 K. At this time, the steam sterilizer has already reached sterilization conditions (approximately 3.15 bar and 134 °C). At the end of the sterilization phase (after approximately 600 s), the maximum temperature difference on the surface of the dental handpieces was 0.08 K. These results once again prove that

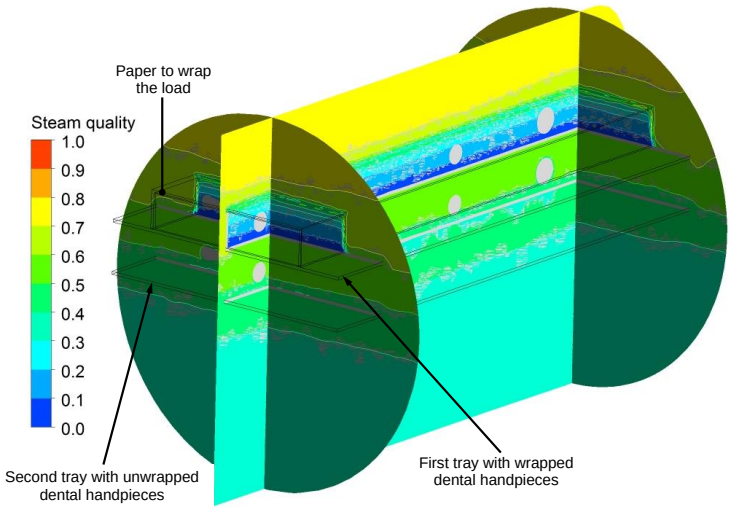

(a) Steam quality in the steam sterilizer after 200 s of simulation time.

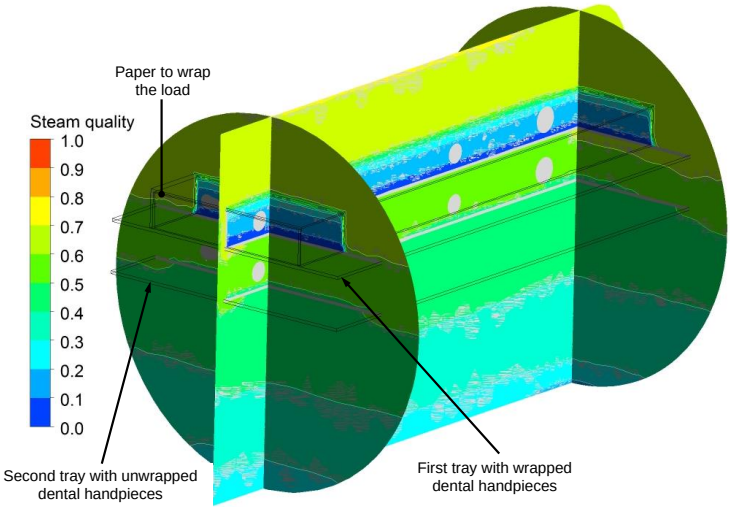

(b) Steam quality in the steam sterilizer after 400 s of simulation time.

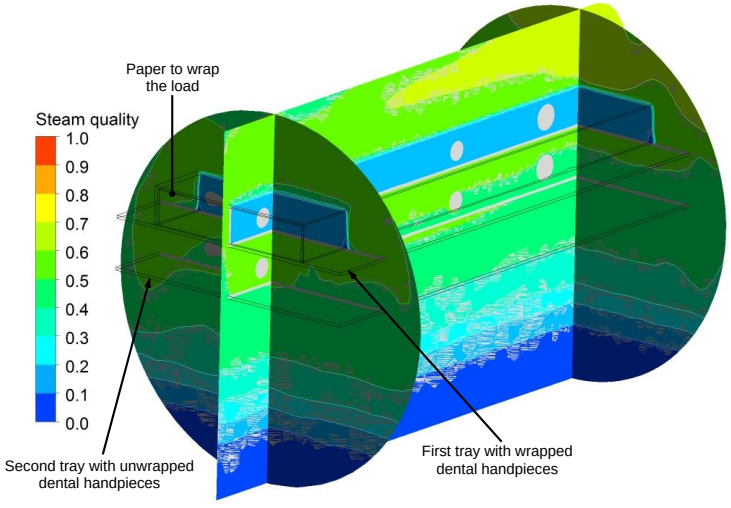

(c) Steam quality in the steam sterilizer after 600 s of simulation time.

Figure 5.30: Steam quality in the steam sterilizer after (a) 200 s, (b) 400 s and (c) 600 s of simulation time.

there are hardly any differences to be found between the wrapped and the unwrapped dental handpieces.

As can be seen in Figure 5.30 and as discussed in Section 5.5.3, the steam quality is lower near the wrapped load (first tray) compared to near the unwrapped load (second tray). Furthermore, Figure 5.31 shows that the surface temperature difference between the wrapped and unwrapped handpieces is negligibly small. These results demonstrate that the steam quality near the dental handpieces (see Figure 5.30) has a negligible influence on the surface temperature of the load. This fact, along with the excellent temperature distribution (seen in Figure 5.28), indicate that the steam sterilizer investigated in this PhD thesis performs extremely well due to the fact that it is able to ensure homogeneous conditions inside the entire volume of the steam sterilizer. The same results were achieved during another cycle with a cylindrical load (see Section 5.4.2).

The F_0-value of *Geobacillus stearothermophilus* was calculated based on the surface temperature of the handpieces. Figure 5.32 shows the simulated F_0-values and simulated average surface temperatures of the dental handpieces during the investigated sterilization phase (see Figure 5.25). The definition of the F0 value was introduced in Section 2.2. The accumulation of the F_0-values starts at temperatures equal to or above 100 °C (see Figure 5.32). Nevertheless, at temperatures below 120 °C, hardly any F_0-value were generated. During the pressure rise phase (between 0 s and 405 s), an F_0-value of approximately 25 min was generated. In the plateau phase, the F_0-value rises (from approximately 25 min) to approximately 155 min. Such high F_0-values are very beneficial to inactivate all types of bacteria, especially *Geobacillus stearothermophilus*, which was the subject of this investigation.

The results of this line of inquiry demonstrate that the CFD model developed in this thesis is able to predict the surface temperatures of dental handpieces, in addition to the F_0-values inside the steam sterilizer and on the surface of the dental handpieces, resolved in both time and space.

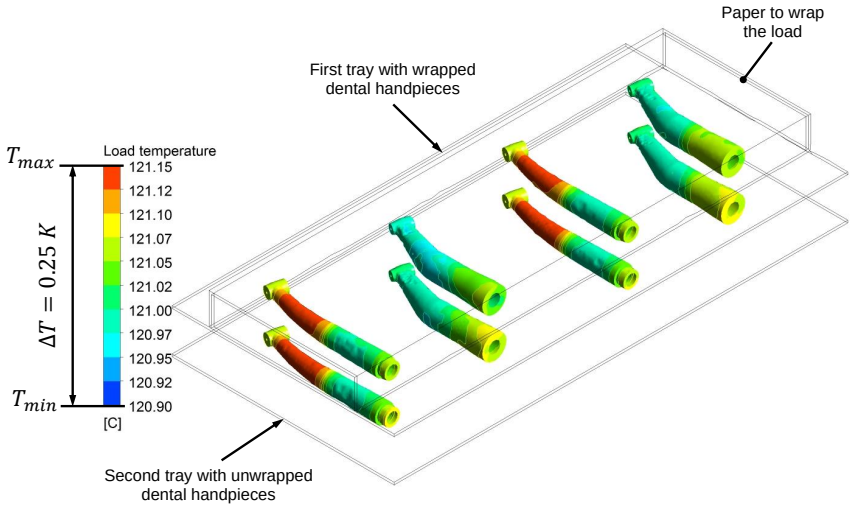

(a) Surface temperatures of the dental handpieces after 200 s of simulation time.

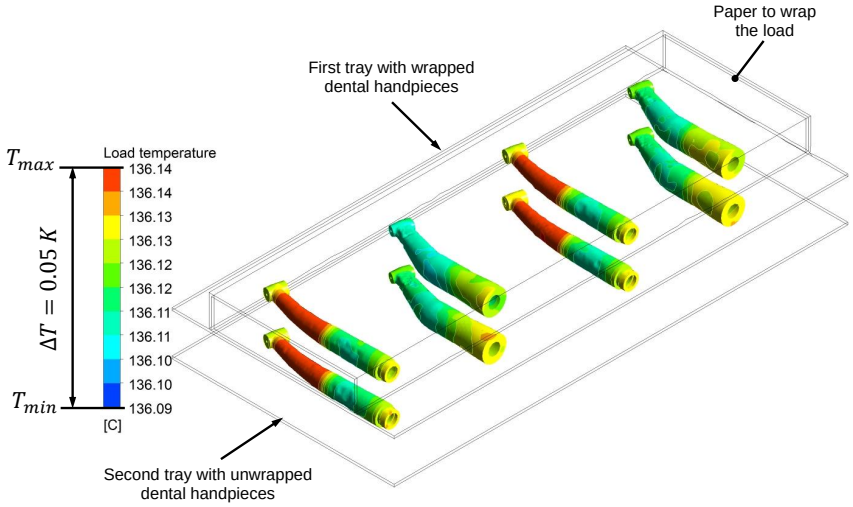

(b) Surface temperatures of the dental handpieces after 400 s of simulation time.

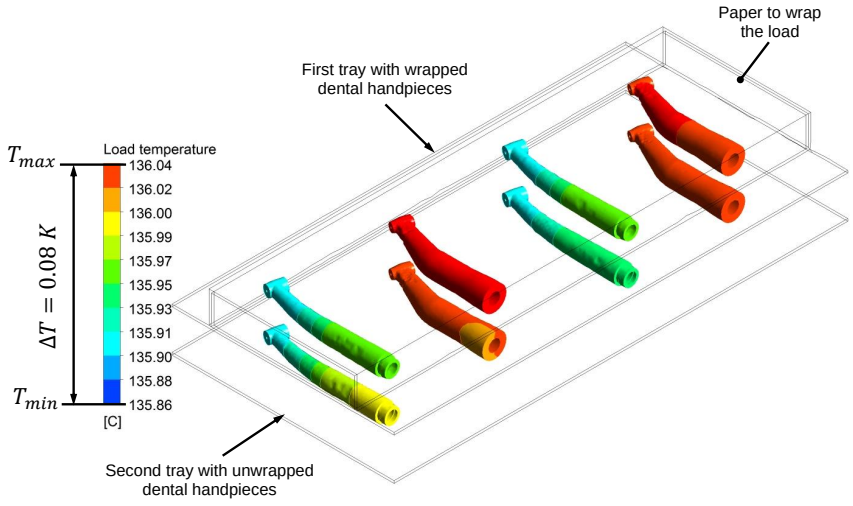

(c) Surface temperatures of the dental handpieces after 600 s of simulation time.

Figure 5.31: Surface temperatures of the dental handpieces after (a) 200 s, (b) 400 s and (c) 600 s of simulation time.

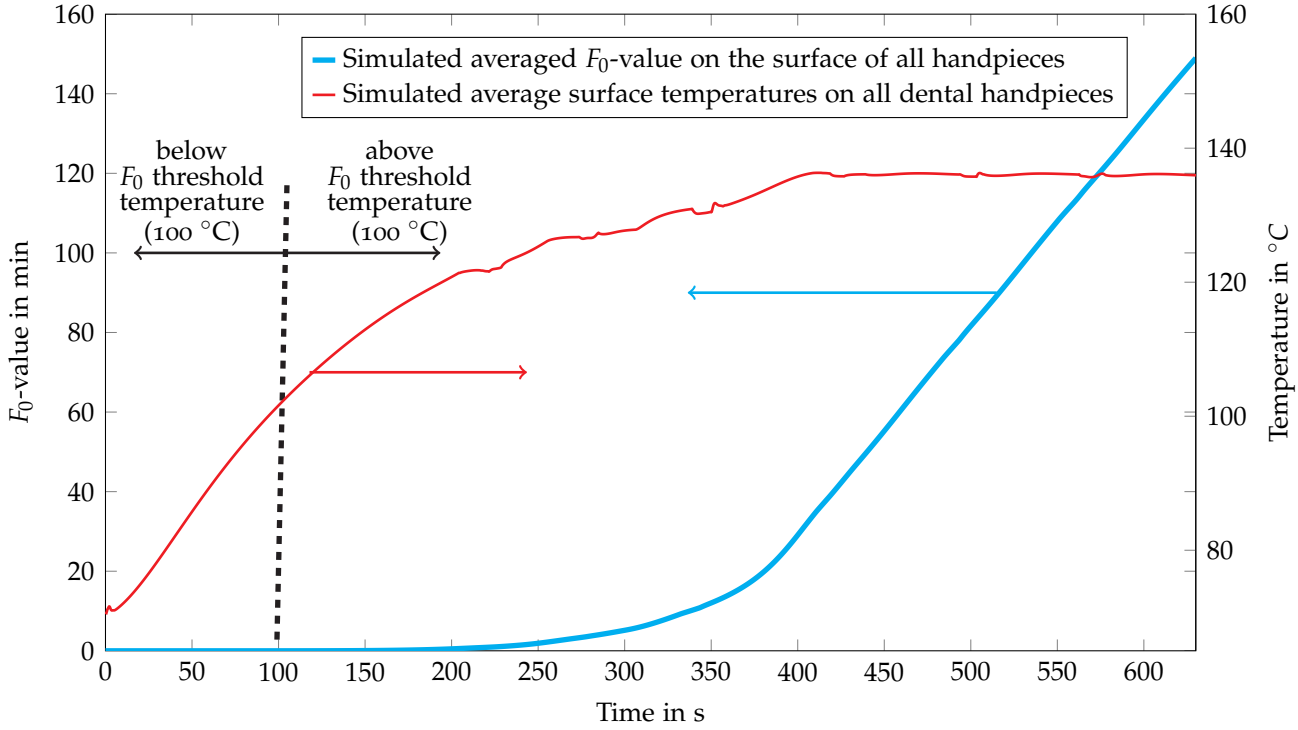

Figure 5.32: Simulated F_0-value and simulated surface average temperatures of all dental handpieces during the sterilization phase [5].

5.5.5 Simulated active bacteria on dental handpieces

To guarantee the safe re-usability of medical equipment, its SAL is taken into account. According to international norms and standards, the SAL must be 10^{-6} or lower [7, 8]. To achieve a SAL of 10^{-6} or lower, the inactivation log ratio must exceed 12. Therefore, the inactivation log ratio was investigated on the surface of the dental handpieces. More information about the SAL and the inactivation log ratio, as well as their definitions can be found in Section 2.2.5.

In this section, the inactivation of the bacteria type *Geobacillus stearothermophilus* was simulated using CFD. The reaction kinetic of the bacteria was calculated from its D value and its z value. The D value and the z value for the bacteria type *Geobacillus stearothermophilus* are presented in Table 5.4. These values were taken from literature [37], and represent the highest possible values to inactivate this bacteria type.

Table 5.4: D value and z value of *Geobacillus stearothermophilus*.

	D value for 121 °C	z value
Geobacillus stearothermophilus	4.0 min	10 °C

The simulated average inactivation log ratio for all the dental handpieces is presented in Figure 5.33. The results show that the steam sterilizer investigated in this thesis is able

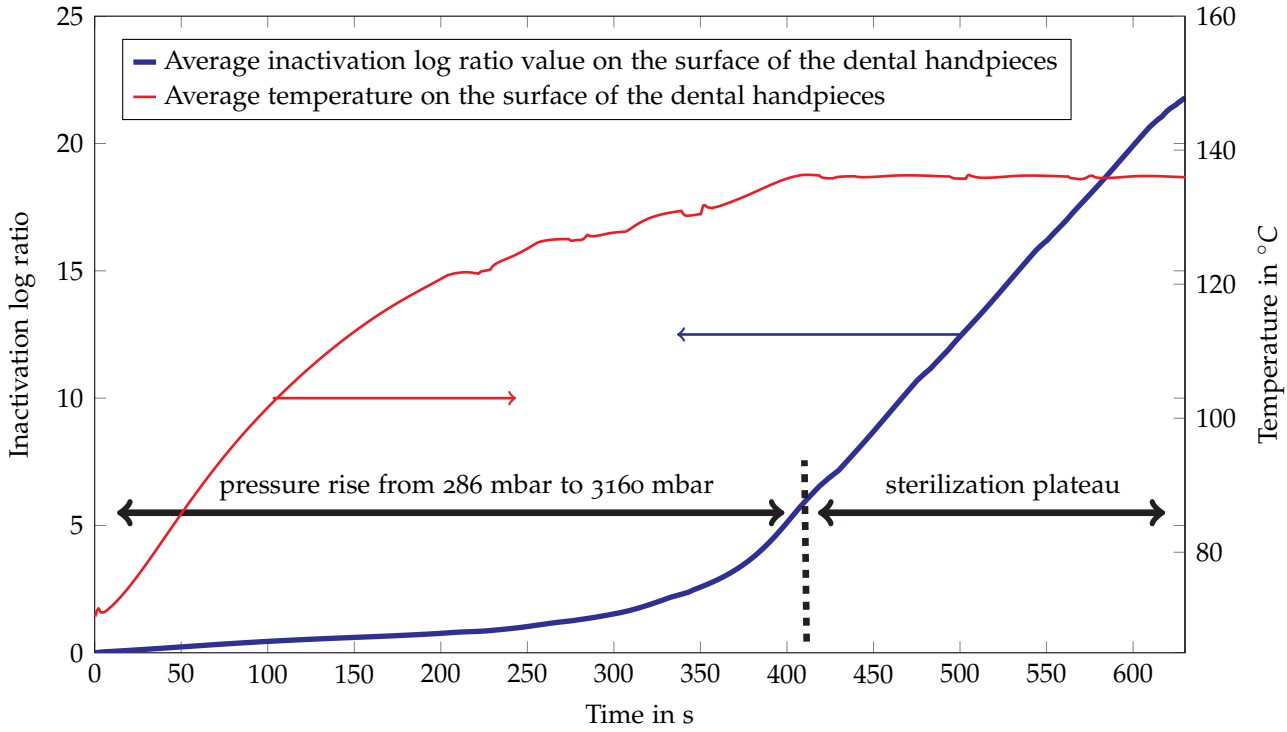

Figure 5.33: Simulated average inactivated log ratio on the surface of all dental handpieces and simulated average surface temperature of all dental handpieces [5].

to reach a inactivation log ratio of six as early as the pressure rise of the investigated sterilization phase (see "pressure rise" in Figure 5.25). During the sterilization plateau, the inactivation log ratio rises from approximately six to a level of approximately 22. In order to validate the simulations, measurements with spore strips were taken inside the steam sterilizer as well. Using spore strips, it is only possible to determine whether or not the steam sterilizer is able to reach the minimum inactivation log ratio of six.

Figure 5.34 presents the simulated inactivation log ratio on the surface of the dental handpieces after (a) 200 s, (b) 400 s and (c) 600 s of simulation time (times can be seen in Figure 5.25). The results show that the difference between the maximum inactivation log ratio and the minimum inactivation log ratio increases as the simulation time increases. Nevertheless, the largest difference between the maximum and the minimum inactivation log ratio was detected after 600 s, with $2.17 \cdot 10^{-4}$. Such small differences in the inactivation log ratio values are negligible and impossible to measure. This low difference in the inactivation log ratio between the wrapped and the unwrapped dental handpieces confirms that the wrapping has hardly any influence on the inactivation of the bacteria.

Measurements of *Geobacillus stearothermophilus* were also performed with spore strips in order to validate the simulated inactivation log ratio. As described in Section 5.3.4,

using spore strips, it is not possible to measure an inactivation log ratio higher than six. Despite this, all of the measurements performed showed that the steam sterilizer investigated in this work is able to reach an inactivation log ratio of over six. Thus, these results prove that the CFD model developed in this thesis is able to predict the inactivation log ratio of *Geobacillus stearothermophilus*. However, this cannot be considered a full validation of the reaction kinetic approach that was used (presented in Section 2.2); to fully validate this reaction kinetic approach, shorter cycles must be investigated. This is a topic for further research (see Chapter 6).

All of the results presented in this section confirm that the steam sterilizer investigated in this work [31] performs extremely well. This high performance can be attributed to the fact that the temperature distribution inside is very homogeneous. It was able to reach the required inactivation log ratio of six as early as the pressure rise in the steam sterilization phase (see Figure 5.34), which is an excellent result for a benchtop steam sterilizer. To obtain these results, the heat transfer model described in Section 4.4.1 and the first-order reaction kinetic approach that was used to simulate the inactivation of bacteria (see Section 4.6) are crucial. Furthermore, these results have confirmed that the developed CFD model is able to predict the inactivation of *Geobacillus stearothermophilus* on the surface of dental handpieces. The simulation time for these results was approximately five weeks on a cluster with 16 Intel Core i7 processors and 32 GB RAM.

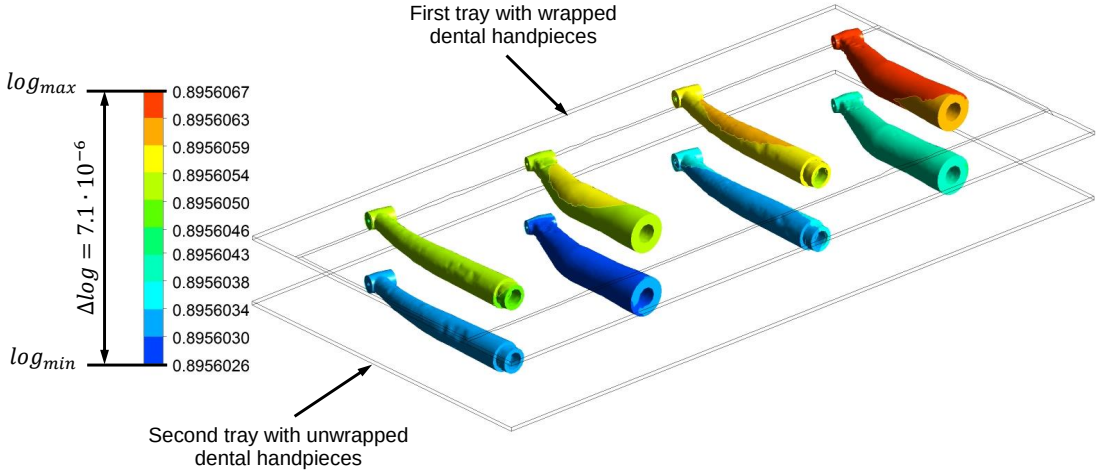

(a) Inactivated log ratio of the dental handpieces after 200 s of simulation time.

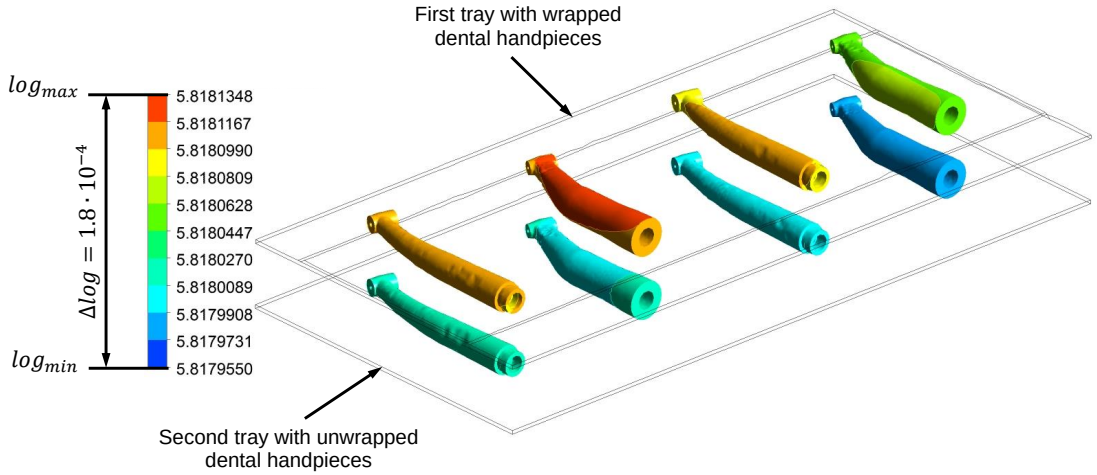

(b) Inactivated log ratio of the dental handpieces after 400 s of simulation time.

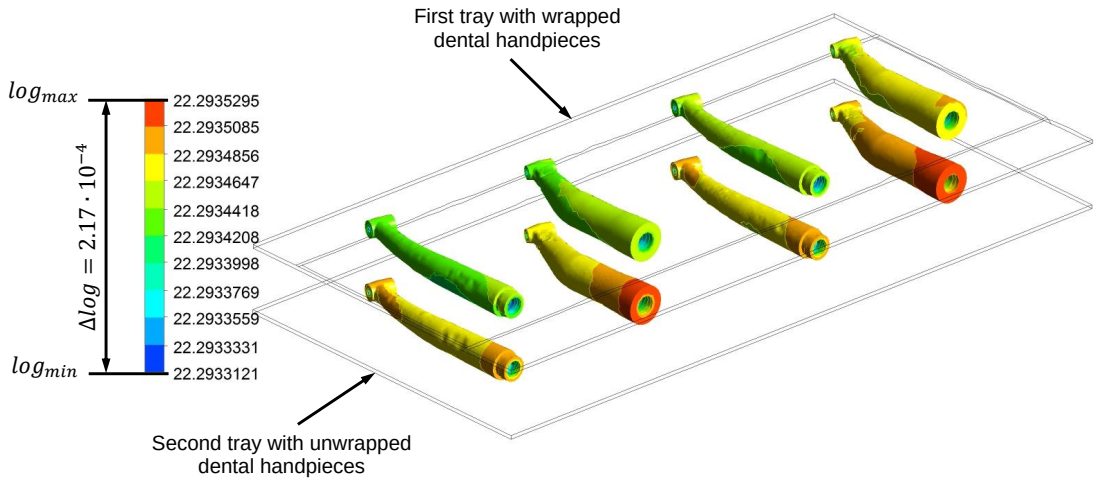

(c) Inactivated log ratio of the dental handpieces after 600 s of simulation time.

Figure 5.34: Inactivated log ratio of the dental handpieces after (a) 200 s, (b) 400 s and (c) 600 s of simulation time.

5.6 Simulation of the air-removal and the steam penetration in hollow loads (cavities) [6]

In this section, not only the air-removal in the steam sterilizer, but also the air-removal inside hollow loads (cavities) were investigated. Due to the fact that hollow load tests are only required for vacuum steam sterilizers, the following numerical and experimental investigation was only performed on the vacuum steam sterilization cycle. Different types of helix tests were investigated in order to take the geometry of the helix tests into account. The simulation results were validated with the measurements of two different chemical indicators. These chemical indicators change colour when they come into contact with steam or when a certain temperature is reached. The chemical indicators were put near the closed ends of the helix tests to measure whether or not steam reaches the closed ends. More information about the measurements with these chemical indicators can be found in Section 3.7.

The goal of the vacuum steam sterilization cycle is to remove as much air from the sterilization chamber and hollow loads as possible in order to ensure the high heat transfer rates that occur thanks to the condensation of hot steam on the cooler surface of the load. The measured pressures and temperatures of the investigated vacuum steam sterilization cycle can be seen in Figure 5.35. To investigate whether the air-removal and the steam penetration inside hollow loads is successful, both the pre-sterilization phase and the sterilization phase must be considered. Therefore, both phases were simulated using CFD. The simulation started at the beginning of the pre-sterilization phase (ambient conditions, approximately 1 bar and 45 °C) when the steam sterilizer is completely filled with air, and ends at the end sterilization phase (approximately 3.16 bar and 134.5 °C). The simulated part of the vacuum sterilization cycle is presented with ”CFD simulation” in Figure 5.35.

[6] Segments of this section have already been published in [3].

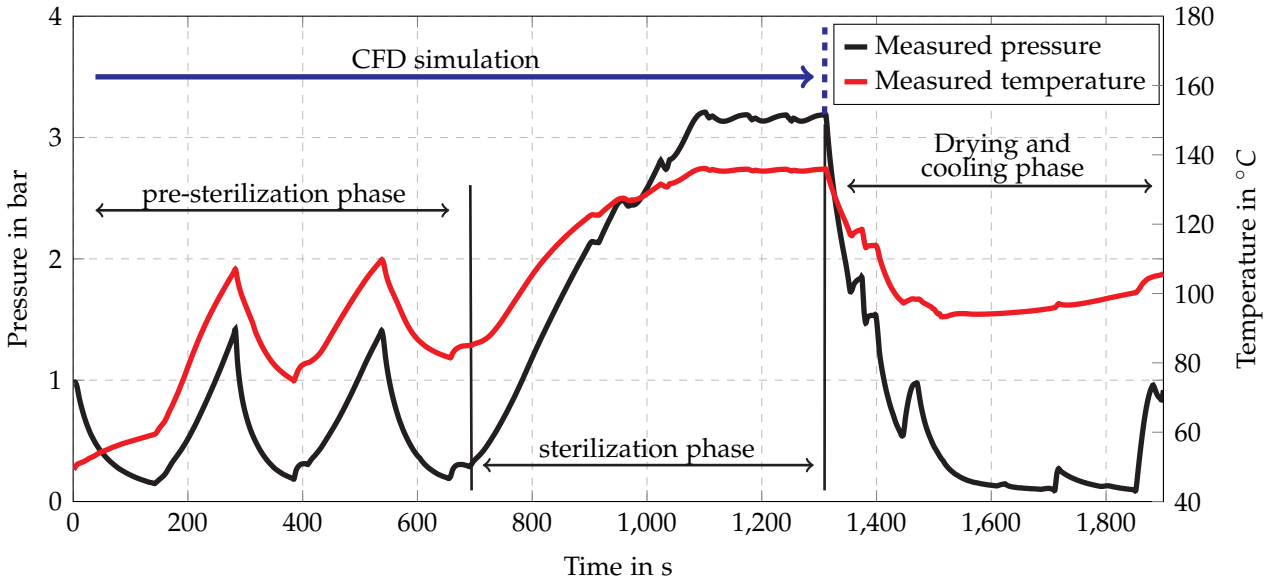

Figure 5.35: Measured pressure and measured temperature in the steam sterilizer loaded with hollow loads.

5.6.1 Pressures and temperatures in the steam sterilizer

The average simulated and measured temperatures taken by the eight thermocouples, and the simulated and measured pressures were compared in order to validate the CFD model. Volume-average monitors at the positions of the measured points were defined in the CFD model in order to compare the simulation results with the measurements. To demonstrate the accuracy of the CFD model, the average errors between the measured and the simulated values ($\overline{Error}$) were calculated (see Eq. (5.6)).

$$\overline{Error} = \frac{\sum_{t=1}^{t_{Cycle}} 1 - \frac{f_{CFD}}{f_{Measurement}}}{t_{Cycle}} \tag{5.6}$$

In Eq. (5.6) $f_{Measurement}$ stands for the measured physical values and f_{CFD} stands for the simulated physical values (pressure and temperature). The cycle duration in seconds is given by t_{Cycle}.

Figure 5.36 shows the simulated and the measured pressures inside the steam sterilizer. As can be seen, the simulated pressure is in excellent accordance with the measured pressure. The average error between the measured and simulated pressure was -0.16 %, which is lower than the uncertainty of the pressure sensor. The average simulated and measured temperatures taken by the eight thermocouples can be seen in Figure 5.37, and are also in very good accordance. Small deviations can be seen between 200 s and 400 s of cycle time; however, these deviations can be explained by to the heat transfer

rate to the thermocouples. After 400 s, the second purging phase starts, and the steam sterilizer is re-filled with steam (see Table 4.3). As a result, the heat transfer rate to the thermocouples increases due to the steam's higher heat transfer rate in comparison to the heat transfer rate of the steam-air mixture. This decreases the difference between the simulated and the measured temperatures. The differences between the simulated and the measured temperatures before 200 s and after 400 s of cycle time were always lower than the uncertainty of the thermocouples. The average error between the simulated and measured temperatures over 1308 s was -0.53 %. Furthermore, comparing the simulated and the measured temperatures reveals good accordance at the locations of the eight thermocouples. Thus, the CFD model implemented with the heat transfer model – both developed in this thesis – was able to predict the temperature and the pressure in the steam sterilizer, separated in time and space. This validation was used as the basis for the calculations of steam penetration inside the hollow loads and cavities.

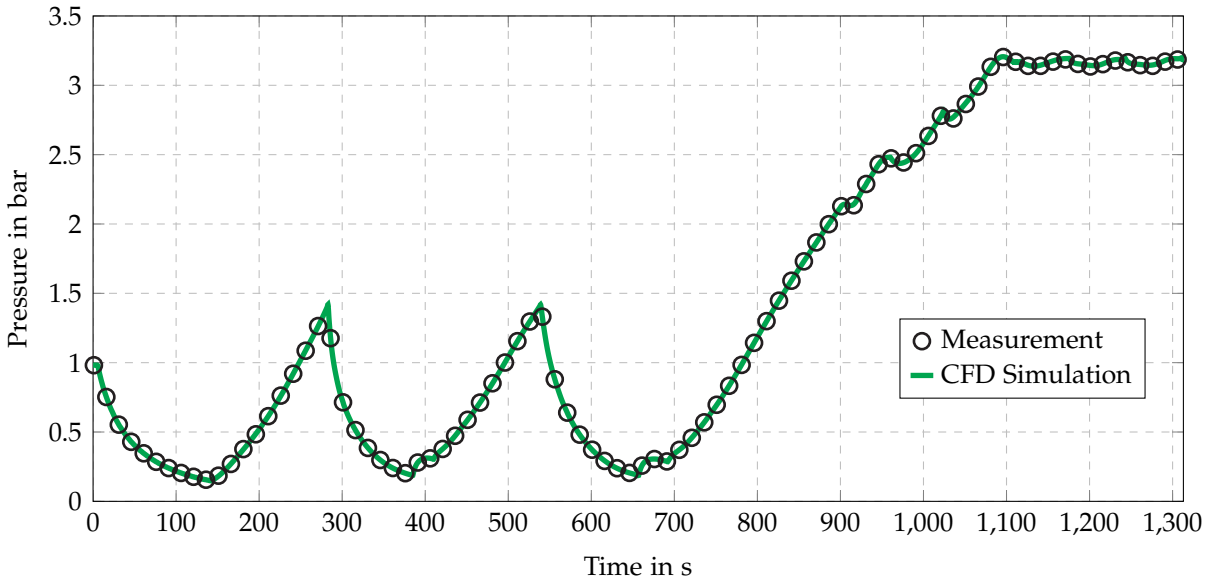

Figure 5.36: Measured and simulated pressures in the vacuum steam sterilizer (pre-sterilization and sterilization phase) [3].

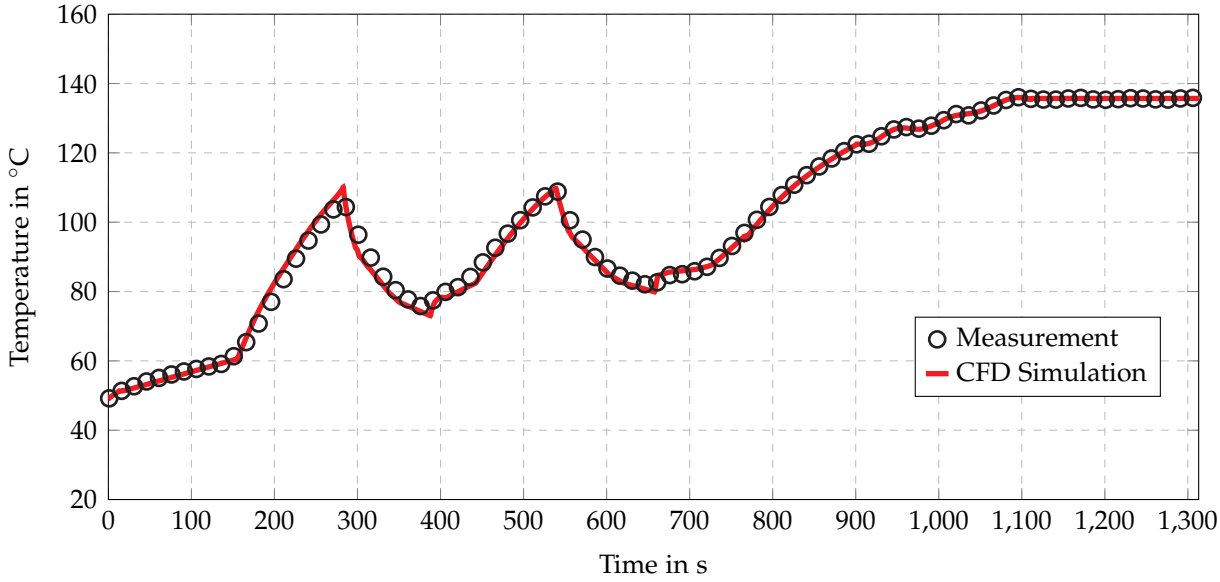

Figure 5.37: Measured and simulated average temperatures of eight thermocouples in the vacuum steam sterilizer (pre-sterilization and sterilization phase) [3].

5.6.2 NCGs inside the steam sterilizer

The goal of the pre-sterilization phase of a steam sterilization cycle is to remove all NCGs from the steam sterilizer. High amounts of NCGs lead to poor heat transfer through wall condensation [133]. A study by Hoyt et al. [134] demonstrated that a high amount of NCGs has a negative impact on the sterilization process. As has been mentioned above, the volume of the collected NCGs must be below 3.5 % of the volume of the collected water [8]. In this PhD thesis, the NCGs were measured after 398 s and after 648 s of cycle time. These measurements of the volume fraction of the NCGs were the basis for the validation of the CFD-simulated volume fractions inside the sterilization chamber.

Figure 5.38 shows the simulated volume average content of NCGs in the chamber over the course of one cycle. The dotted vertical lines in Figure 5.38 represent the times at which the distribution of NCGs inside the steam sterilizer was analysed. In the first 143 seconds, only NCGs are present in the steam sterilizer, as a vacuum pump is reducing the pressure, but no steam is being fed into the sterilizer. The real volume fraction of the NCGs was measured at that time with a value of 1.0 (see between 0 s and 143 s in Figure 5.38); this value was used for the initialization of the CFD model. From 143 s to 260 s (see Figure 5.38), the outlets are closed, and the steam generator injects steam into the chamber. Therefore, the volume average of NCGs drops sharply. After the vacuum pump had reduced the pressure for the second time (at 393 s, see Figure 5.38), the real volume fraction of NCGs was measured, with a result of 3.2 %.

After 398 s, the volume fraction of NCGs simulated by the CFD model was 2.8 %. The third measurement was taken after the vacuum pump had reduced the pressure for a third time (at 648 s, see Figure 5.38). At this point, the measured real volume fraction was 0.5 %, while the simulated value was 0.59 %. Thus, all of the simulated values were in excellent accordance with the measurements. At the sterilization plateau (between 1098 s and 1308 s in Figure 5.38), the simulated volume fraction of NCGs dropped to a value of 0.15 %. Past studies have shown that these low amounts (< 3 %) of NCGs have hardly any influence on the heat transfer rate due to wall condensation [59].

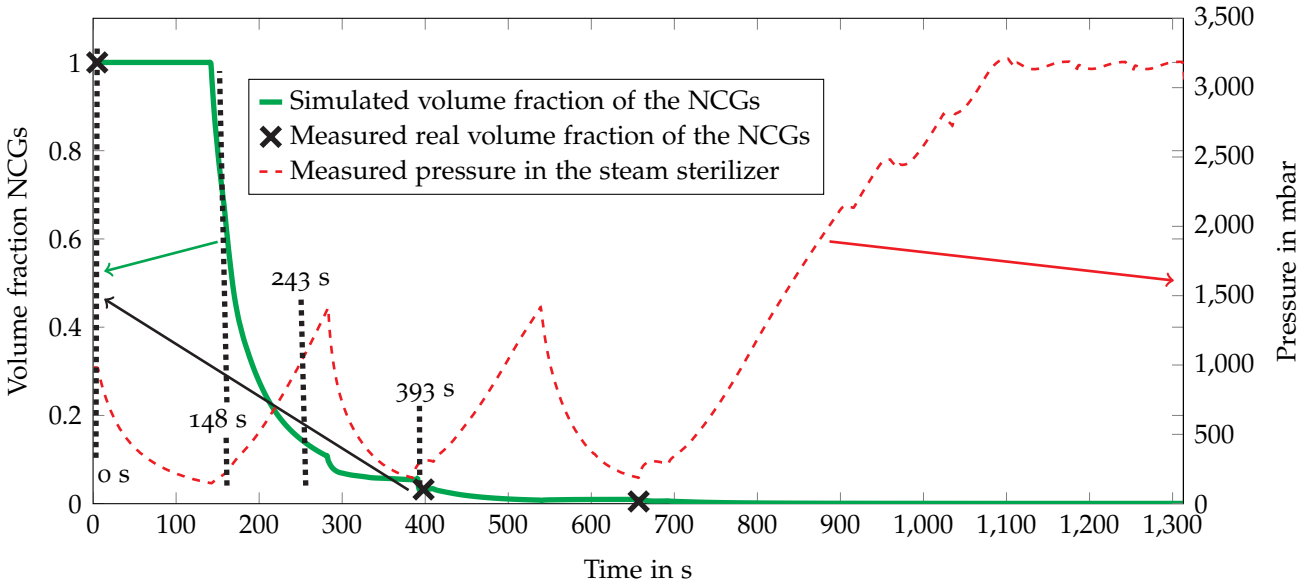

Figure 5.38: Volume average of the simulated and measured NCGs in the steam sterilizer [3].

Figure 5.39 shows contour plots of volume fractions of NCGs in different planes in the steam sterilizer: the vertical middle plane, a plane below the helix test device (PCD 1), and two planes through the steam sterilizer (containing PCD 1). All of the times at which the CFD results were analysed are indicated by the vertical black dashed lines in Figure 5.38. At the beginning of the sterilization cycle, the steam sterilizer is filled with air (see Figure 5.39(a)). After 143 s of cycle time, the steam generator begins to inject steam into the steam sterilizer. Therefore, steam is found near the inlet and at the top of the steam sterilizer after 148 seconds of cycle time (see Figure 5.39(b)). This is caused by the lower density of the steam in comparison to the NCGs. After 243 seconds of cycle time, the top of the steam sterilizer is completely filled with steam, and NCGs are only present in its bottom region (see Figure 5.39(c)). After 393 seconds of cycle time, hardly any NCGs are present in the steam sterilizer (see Figure 5.39(d)). These results demonstrate that the CFD model developed for this thesis is able to generate spatially and temporally resolved predictions of the volume fraction of NCGs in the steam sterilizer. Furthermore, the results indicate that the heat transfer model (see

Section 4.4.2) is able to simulate condensation on all wet surfaces. Without this heat transfer model, it would not be possible to calculate the NCGs content inside the steam sterilizer, due to the fact that condensation on the walls would be under-predicted or even neglected. With other wall condensation models, computational costs would increase dramatically due to the fact that the wall condensation film must be resolved, which requires a very fine mesh near the wall. The heat transfer model that was developed and presented in this PhD thesis is able to predict the heat transfer that occurs due to condensation in a numerically efficient manner.

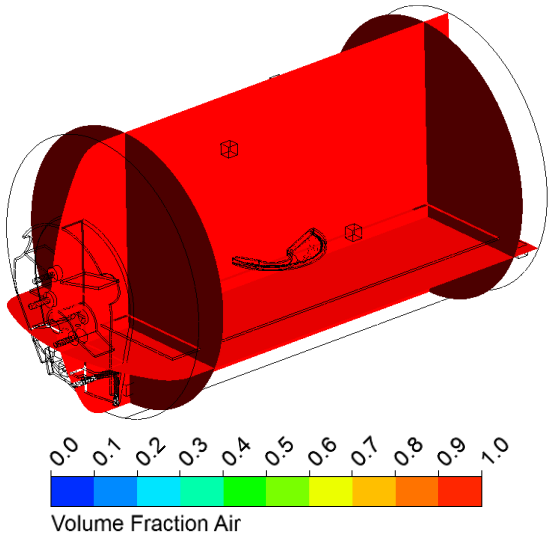

(a) Volume fraction of the NCGs after 0 s of cycle time.

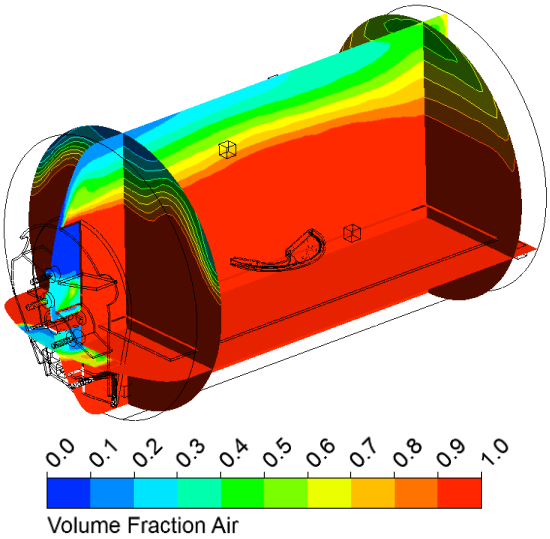

(b) Volume fraction of the NCGs after 148 s of cycle time.

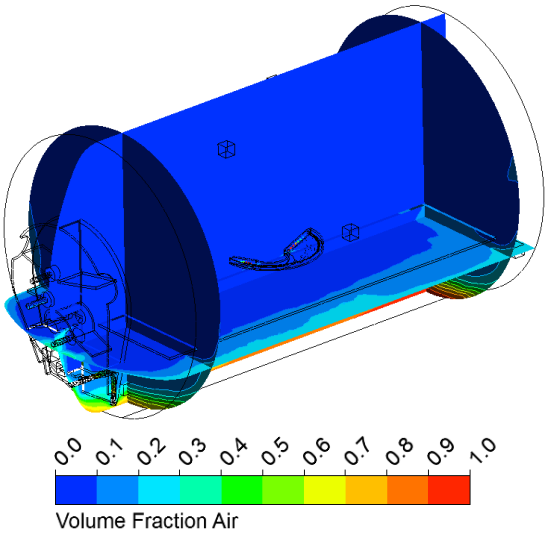

(c) Volume fraction of the NCGs after 243 s of cycle time.

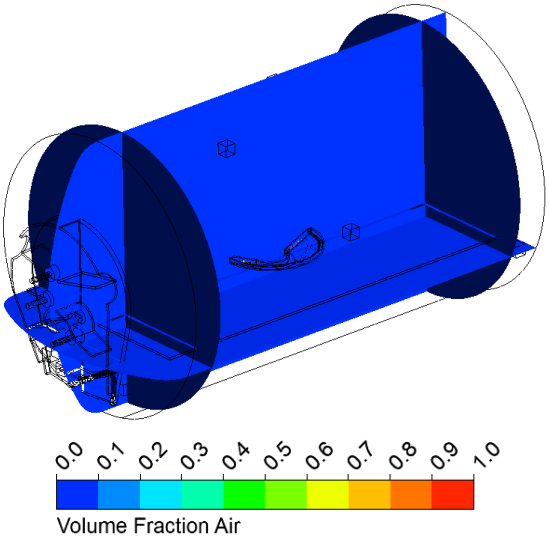

(d) Volume fraction of the NCGs after 393 s of cycle time.

Figure 5.39: Volume fractions of NCGs in the steam sterilizer after (a) 0 s, (b) 148 s, (c) 243 s and (d) 393 s of cycle time [3].

5.6.3 NCGs in the hollow loads during the sterilization cycle

Two different types of PCDs (hollow loads) were investigated in this thesis, and their geometry and inlet positions can be seen in Figure 3.10. The aim of the PCD investigations was to identify the effects of the geometry and the inlet positions of the helix tubes on the NCGs contained in the PCD. Furthermore, these investigations allowed the heat transfer model developed in this PhD thesis (see Section 4.4.2) to be validated for hollow loads as well. For this purpose, two CFD simulations were carried out.

Figure 5.40 shows the volume averages of the volume fractions of NCGs in the helix tubes. The shapes of the helix tubes can be seen in Figure 3.10. Because the steam sterilizer is filled with NCGs at the beginning of the sterilization process, and no steam is fed into the steam sterilizer in the first 143 s of the cycle, the volume average of the volume fraction of NCGs remains constant at a level of 1 (see between 0 s and 143 s in Figure 5.40). The subsequent pressure decrease (as steam is fed into the steam sterilizer) leads to a reduction in NCGs in both PCDs (between 143 s and 273 s, see Figure 5.40). However, in this phase of the sterilization cycle, small differences can be seen between the two PCDs. Between 143 s and 273 s, PCD 2 showed higher values of NCGs since the tube inlet is located inside a plastic container (see Figure 3.10). This means that the steam must replace the NCGs in the container before it can penetrate into the helix tube of PCD 2. With the next drop in pressure (between 273 s and 393 s, see Figure 5.40), the volume fraction of NCGs in both PCDs increases to a value of approximately 1. After this point, the steam generator begins to increase the pressure in the steam sterilizer again (between 393 s and 548 s, see Figure 5.40). Therefore, the volume fraction of NCGs in the PCDs decreases once again. In the last pressure decrease of the pre-sterilization phase, the volume fraction of NCGs rises to a value of approximately 0.9 (at 648 s, see Figure 5.40). Following this, the sterilization phase begins, in which the pressure is increased from 0.15 bar to 3.16 bar. In this phase of the process, the volume average volume fraction of NCGs in the helix tube of the PCDs falls to a value of approximately 0.07 (at 1098 s, see Figure 5.40). At the sterilization plateau (3.16 bar, 134 °C, starts at 1098 s in Figure 5.40), there is only a negligible change to the volume fraction of NCGs in the PCDs (between 1098 s and 1313 s, see Figure 5.40). This is because the pressure remains constant, and, as a result, no steam flows into the helix tube. Small changes in volume fraction can only be attributed to condensation in the tube. Van Doornmalen et al. [135] discovered that the level of NCGs inside the PCDs never reaches zero, unless a perfect vacuum can be achieved within the steam sterilizer.

To validate the CFD simulation, 20 measurements were carried out with PCD 1's chemical indicator and 20 measurements were taken with PCD 2's chemical indicator. Figure 3.11 shows the two different indicators that were used in this thesis. The chemical indicators were mounted near the closed ends of the PCDs' helix tubes (see Figure 5.41). Therefore, the chemical indicators were able to measure the steam penetration at the closed ends of the PCDs' helix tubes. Both devices passed all of the measurement tests performed using the chemical indicator that is included with PCD 1 (see Table 5.5). The indicator that is included with PCD 2 was only able to achieve sufficient steam penetration in all of its squares in one of the measurement tests with PCD 1, although it also achieved sufficient steam penetration in all of its squares in two of the measurement tests carried out with PCD 2 (see Table 5.5). In all of the other measurement tests using the PCD 2-indicator, partially sufficient steam penetration was measured, which means that some squares turned black, while the others turned brown (see Figure 3.11(b)). However, the temperature level achieved (square of the chemical indicator turns brown, see Figure 3.11(b)) was satisfactory in all of the measurement tests performed (see Table 5.5). The measured results confirm that the simulated values of NCGs in the PCDs are correct, given that investigations of both PCDs led to the same results. Furthermore, it was found that the measurement results primarily depend on the type of chemical indicator, rather than the type of PCD. The next section presents a detailed validation of the simulated volume fraction of the NCGs inside the two investigated PCDs.

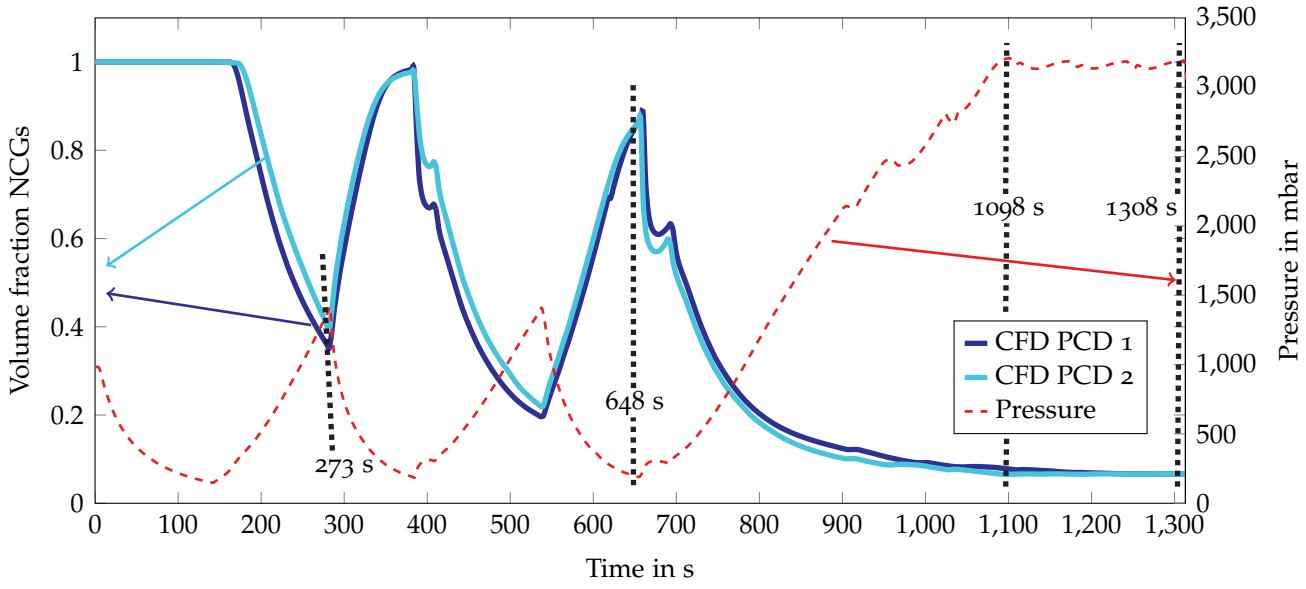

Figure 5.40: Volume averages of the simulated volume fractions of NCGs in both of the PCD helix tubes [3].

Table 5.5: Measurement results of both helix tests with both chemical indicators

		PCD 1	PCD 2
Indicator PCD 1	passed	20	20
	failed	0	0
	total number of measurements	20	20

		PCD 1	PCD 2
Indicator PCD 2	sufficient steam penetration and temperature	1	2
	partially sufficient steam penetration, temperature achieved	19	18
	insufficient steam penetration, temperature achieved	0	0
	total number of measurements	20	20

5.6.4 Distribution of the non-condensable gases in the hollow loads

Steam penetration inside PCDs is a topic of major interest in the field of steam sterilizers. Therefore, a CFD model was developed to numerically analyse the NCGs content and steam penetration inside hollow loads (PCDs). Figure 5.41 shows the volume fraction of the NCGs (air) for both investigated PCDs at 273 s, 648 s, 1098 s, and 1308 s of cycle time. The times at which the volume fractions of NCGs were analysed are indicated by the vertical black dotted lines in Figure 5.40. The first investigation of NCGs content in the PCDs was performed after 273 s of cycle time (see Figure 5.41(a)). Before that point, the vacuum pump reduces the pressure to approximately 0.15 bar. During that pressure reduction, no steam enters the chamber of the steam sterilizer. Afterwards, the steam generator increases the pressure to approximately 1.4 bar (see Figure 5.40). As a result, the half of the PCD's helix tube that is near the inlet is filled with steam. Because it is more difficult for the steam to reach the tube inlet of PCD 2 (see Figure 3.10), more steam is visible inside PCD 1 (see Figure 5.41(a)). Figure 5.41(b) shows the volume fraction of NCGs inside both PCDs after 648 s. Because these simulation results come directly after the pressure is reduced to 0.15 bar, the NCGs content inside the PCDs is high. However, the previous phase results in a lot of steam in front of the tube inlet and in the PCD near the inlet (see Figure 5.41(b)). Between 648 s and 1098 s, the steam generator increases the pressure from approximately 0.15 bar to the pre-defined sterilization pressure (here, approximately 3.16 bar). The PCDs are then filled with steam, except the part near the closed end of the tube, which still contains NCGs (see Figure 5.41(c)). Between 1098 s and 1308 s, the pressure remains constant. As a result, the mass of NCGs in the PCDs also remains constant. During that time, steam condenses inside the tube, and natural convection between the steam and the NCGs takes place. This phenomenon, in combination with diffusion effects, leads to the

mixture of the steam and the NCGs (see Figure 5.41(d)). These results show that the CFD model developed in this thesis is able to predict steam penetration in PCDs (as well as in the steam sterilizer). In the sterilization phase (between 1098 s and 1308 s of cycle time), hardly any differences were detected between the two investigated PCDs. The same results were obtained using two different chemical indicators (see Table 5.5). To the best knowledge of this author, this is the first thesis that has investigated steam penetration inside hollow loads using CFD simulations.

The results depicted in Figure 5.41 show that the steam is easily able to reach volume fractions of over 95 % in 1450 mm of the 1500 mm-long helix tube. However, since the chemical indicators were mounted on the closed ends of the helix tubes, the steam penetration near the closed ends of the tubes is of huge interest. Therefore, the volume fraction of NCGs near the closed ends of the tubes was analysed at the beginning and at the end of the sterilization plateau (see the vertical dotted black lines at 1098 s and 1308 s in Figure 5.40). The position at which the chemical indicator was mounted is shown with dotted lines in Figure 3.10, Figure 5.41 and in Figure 5.42. Figure 5.42(a) shows the volume fraction of NCGs (air) near the closed end of the tube within PCD 1. It can be seen that steam is present at every point in the PCD's helix tube. The total volume fraction of steam near the closed end was below 10 %. As a result, it is possible to conclude that it is not possible to achieve complete air-removal in the helix tube PCD.

Similar results were reported in a previous study by van Doormalen et al. [135]. Nevertheless, the 10 % of steam near the closed end of the tube is beneficial for the sterilization process, due to the fact that the enthalpy of the steam-NCGs mixture at 3.15 bar and 135 °C is 0.21 J and, therefore, higher than that the enthalpy of pure saturated steam at a level of 1 bar which is 0.19 J. The enthalpy values were calculated for the volume near closed end of the helix tube. The simulation result show that a low steam concentration is able to change the colour of the chemical indicator, due to the pressure level of 3.15 bar and temperature of 135 °C, resulting in a higher enthalpy of the steam-NCGs mixture (see Figure 5.42). Furthermore, past investigations have shown that the heat transfer coefficient increases with increasing air humidity [136–138]. This also leads to better sterilization inside hollow loads and cavities. In the sterilization plateau, where the pressure remains constant (see between 1098 s and 1308 s in Figure 5.40), some steam condenses and some natural convection takes place near the closed end of the tube. Therefore, the steam mixes with the NCGs (see Figure 5.42). As a result, the sterilization plateau is of high importance for the steam penetration in hollow loads. Similar results were found for PCD 2 (see Figure 5.42(b)).

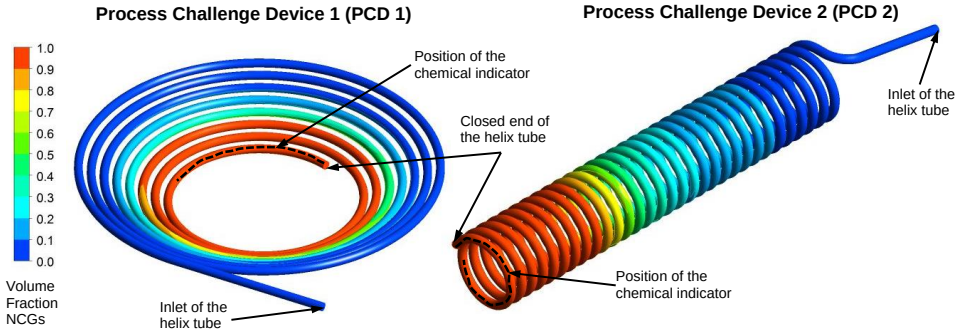

(a) Volume fractions of NCGs in the PCDs after 273 s.

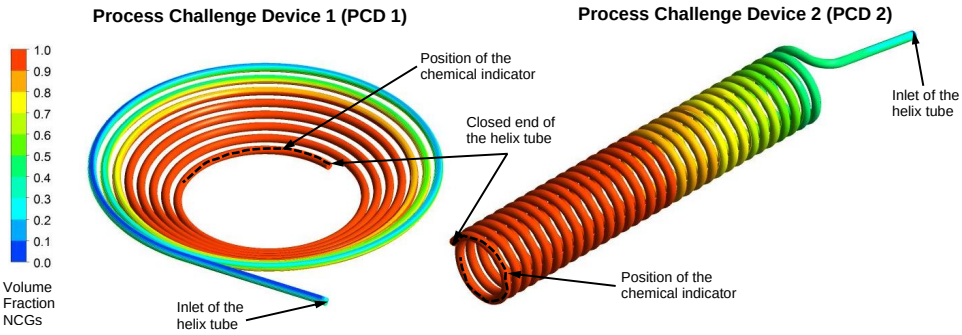

(b) Volume fractions of NCGs in the PCDs after 648 s.

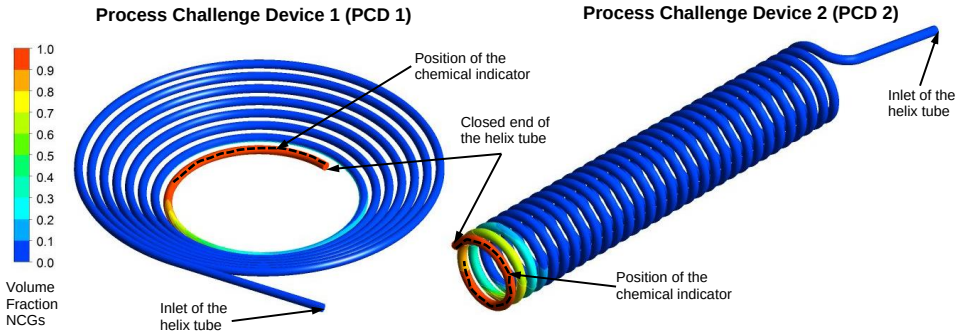

(c) Volume fractions of NCGs in the PCDs after 1098 s.

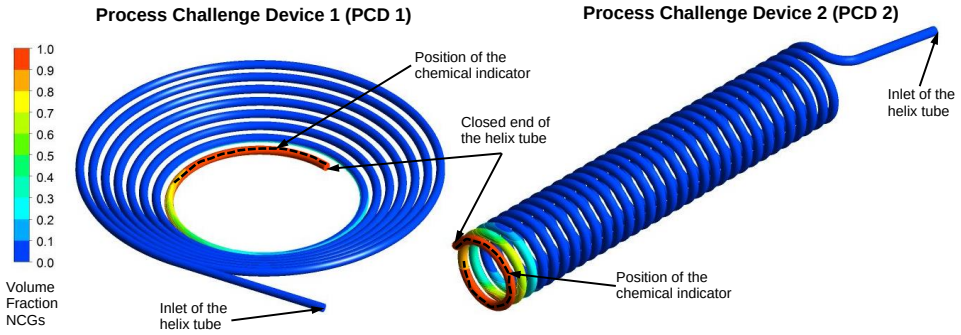

(d) Volume fractions of NCGs in the PCDs after 1308 s.

Figure 5.41: Volume fractions of NCGs in PCD 1 and PCD 2 after (a) 273 s, (b) 648 s, (c) 1098 s and (d) 1308 s of cycle time [3].

This underlines the fact that the differences between the two PCDs are minimal.

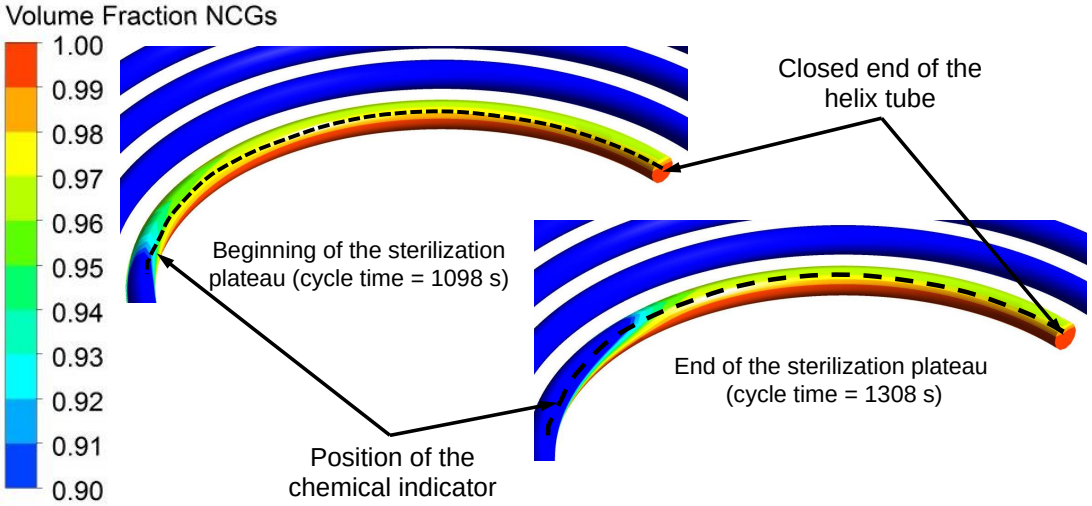

(a) Volume fractions of the NCGs near the closed end of PCD 1.

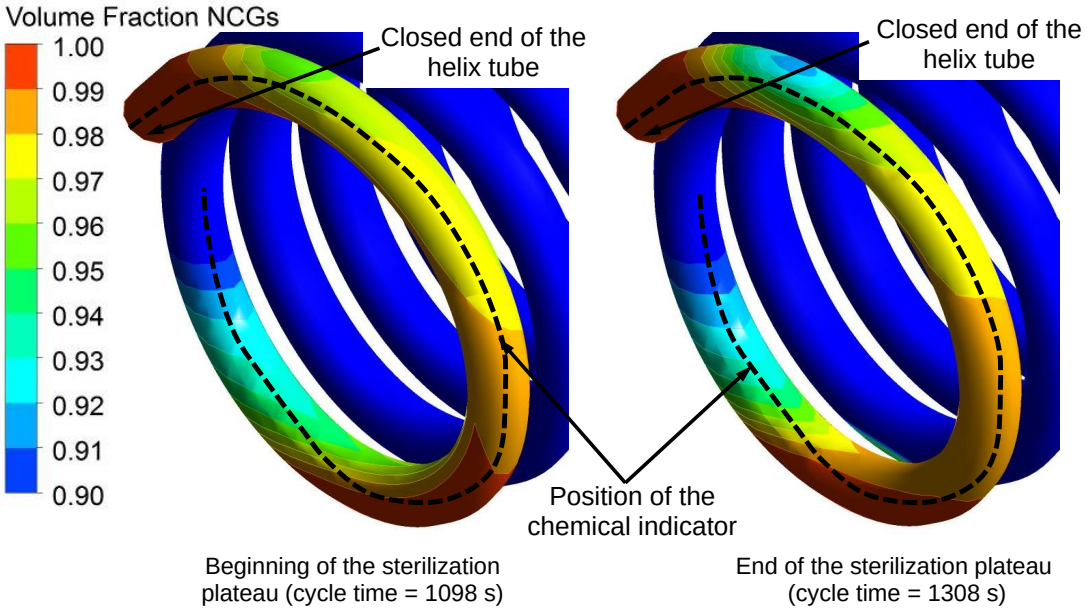

(b) Volume fractions of the NCGs near the closed end of PCD 2.

Figure 5.42: Volume fractions of the NCGs near the closed end of the helix tube of (a) PCD 1 and (b) PCD 2 at the beginning of the sterilization plateau (t = 1098 s) and at the end of the sterilization plateau (t = 1308 s) [3].

Table 5.6 summarizes the simulated and the measured results near the closed ends of the helix tubes of both PCDs. Both the simulated and measured results of the steam concentration and temperature investigations were compared in order to validate the CFD model. The average steam concentration along the chemical indicator was predicted by the CFD model to be approximately 5 % for PCD 1 and PCD 2. In both PCDs, sufficient steam concentration was determined using the chemical indicator of PCD 1. Partially sufficient steam penetration was also determined in both PCDs with PCD 2's indicator. Furthermore, the CFD simulation predicted a temperature

Table 5.6: Comparison between the CFD simulation and the measurements with two chemical indicators regarding the steam concentration and the temperature near the closed end of both helix tubes of the PCDs.

	Steam concentration/temperature		
	CFD Simulation	Indicator PCD 1	Indicator PCD 2
PCD 1	predicted (approximately 5 %) \ 135.85 °C	determined	determined \ indicated over 134 °C
PCD 2	predicted (approximately 5 %) \ 135.74 °C	determined	determined \ indicated over 134 °C

of approximately 135 °C near the closed end of the tube. Since PCD 2's chemical indicator only changes colour if the temperature reaches 134 °C (see Figure 3.11(b)), this simulation results can be confirmed. A volume fraction of approximately 5 % and a temperature of over 134 °C must be achieved in order to change the colour of the chemical indicators. With this knowledge, it is possible to confirm that the results measured by the chemical indicators indicate that the simulated volume fraction of the NCGs and the simulated temperature near the closed end of the tube were accurate. Thus, the CFD model developed in this PhD thesis was able to predict the fluid flow and temperature in addition to the condensation and evaporation effects in hollow loads. The heat transfer model developed in this thesis is able to predict the heat transfer through wall condensation in the presence of NCGs, both within a steam sterilizer, as well as inside hollow loads and small cavities.

The simulation time for the results presented in this section was approximately ten weeks on a cluster with 16 Intel Core i7 processors and 32 GB RAM.

With the results presented in this section, the fourth research question: "Which approach works best to simulate the air-removal and the steam penetration inside the steam sterilizer as well as inside hollow loads (cavities)?" can be answered with an indirect validation. The simulation results showed that the average volume fraction of the NCGs near the indicator was approximately 5 % (see Figure 5.42). All of the measurements with the chemical indicator indicated that steam must be present near the chemical indicator. Thus, these results indirectly validate that the CFD model developed in this work is able to accurately predict the volume fraction inside hollow loads (cavities). To achieve a full validation, very difficult, time-consuming and expensive measurements would have to be performed. This is a potential field for further research. However, the results presented in Section 5.1.2 and Section 5.6.2 have already demonstrated that the CFD model in question is able to predict the volume fraction of the NCGs inside the sterilization chamber in a very accurate manner.

6

Conclusion and outlook

In the present thesis, the steam sterilization processes that are often used to sterilize re-usable pieces of medical equipment were investigated using CFD simulation. Hardly any publications regarding CFD simulations of steam sterilization cycles have been published in recent years. Most publications regarding investigations of steam sterilization processes are based on experiments. In order to overcome the limitations of experimental investigations, the author of this work developed several CFD submodels in order to numerically investigate all relevant phenomena that take place inside both vacuum and non-vacuum steam sterilizers. In the course of this thesis, all of the CFD models developed by this author were validated by comparing the simulated values with measured ones. These CFD models were able to answer the following four research questions:
i) Is it possible to simulate the heating process of the load?
ii) Which approach can be used to simulate the influence of the wrapping of the load?
iii) Is it possible to simulate the inactivation of different bacteria types on the surface of the load?
iv) Which approach works best to simulate the air removal and the steam penetration inside the steam sterilizer as well as inside hollow loads (cavities)?

The answers to these questions, based on the investigations carried out in this thesis, are presented briefly in the following paragraphs:

i) The heating process of the load was simulated. For this purpose, a very numerically efficient heat transfer model was developed in order to simulate the heat transfer that results from condensation effects. The heat transfer model developed by the author was validated with temperature measurements of both unwrapped and wrapped cylindrical loads. Four different materials were used for this validation. The measured

and simulated load temperatures were in very good accordance for all four investigated cylinder materials, as well as for both unwrapped and wrapped cylinders. This validation made it possible to predict the F_0-values at every point inside the steam sterilizer, as well as on the surfaces of the dental handpieces.

ii) A time-efficient porous media approach was used to simulate the permeability of the paper in which loads can be wrapped. To determine the permeability of this paper, a test-rig was built to measure the pressure drop over the paper for different fluids (air and steam), temperatures, and pressures. From this measurement data, the permeability of the paper could be determined. The paper model developed in this thesis was validated by a CFD simulation of the test-rig. The simulated values matched the measured values very well. This paper model also made it possible to simulate the load temperature of both wrapped and unwrapped loads. The results showed that the influence of the paper on the load temperature is negligible. Nevertheless, the wrapping of the load does have a significant influence on the steam quality within the sterilization chamber and especially near the load (pouch).

iii) A first-order reaction kinetic approach coupled with the Arrhenius equation was added to the CFD code in order to simulate the inactivation of different types of bacteria, especially the hardest bacteria type to inactivate, *Geobacillus stearothermophilus*. The results demonstrated that the CFD model developed in this thesis is able to predict the inactivation of different bacteria types inside the steam sterilizer as well as on the surface of the load, resolved in both time and space. Spore strips were used to measure the inactivation of the *Geobacillus stearothermophilus* bacteria. The simulation results showed that the steam sterilizer was able to reach an inactivation log ratio of approximately 22 for *Geobacillus stearothermophilus*. All of the measurements with the spore strips confirmed that the investigated steam sterilizer was able to reach an inactivation log ratio of over six. However, spore strips are not able to measure an inactivation log ratio higher than six; therefore, the measured inactivation log ratio is not a full validation of the simulated one.

iv) The removal of the NCGs (namely air) was simulated using a three-phase Eulerian-Eulerian multiphase model. The heat transfer model was further developed to predict the heat transfer due to condensation in the presence of NCGs. With this CFD model, the removal of NCGs both inside the steam sterilizer and inside helix tests (hollow loads) was investigated. The simulated volume fraction of the NCGs inside the steam sterilization chamber was in good accordance with measured values. The simulated values of the NCGs inside the helix tests were validated with chemical indicators. All of the chemical indicator measurements showed that steam reaches the closed end of

the helix tube. These measurements confirm that the CFD model developed in this work is able to predict the steam penetration inside hollow loads (cavities).

In the course of these investigations, the CFD model developed by this author has been validated by comparing its results to the measured results of pressure, fluid temperature, load temperature, spore strips, and chemical indicators. All of the simulated pressures and temperatures were in very good accordance with the measured ones, thus proving that the CFD models developed in this thesis are able to predict the pressure, the fluid temperature, condensation effects, and heat transfer to the load in a very accurate manner.

Furthermore, a new approach was developed to calculate the real volume fraction of NCGs inside the sterilization chamber from the measurements required by EN 13060. The results proved that the developed approach is more accurate and able to predict the real conditions inside the steam sterilizer. Using this approach, the air-removal process inside the sterilization chamber can be improved in future generations of steam sterilizers.

In further works, the first-order reaction kinetic approach used to predict the inactivation of bacteria could be fully validated. As mentioned above, using spore strips, it is not possible to measure an inactivation log ratio higher than six. In order to validate the complete simulation of the inactivation of bacteria, much shorter cycles would have to be investigated so as to reach inactivation log ratios lower than six. Furthermore, the inactivation of bacteria in a saturated steam atmosphere, in a steam-air mixture atmosphere, in an air atmosphere, and inside a liquid load could all be simulated using CFD, and validated with the measurements of spore strips.

Bibliography

[1] M. Feurhuber, A. Cattide, M. Magno, et al. Prediction of the fluid flow, heat transfer and inactivation of microorganism at medical devices in modern steam sterilizers using computational fluid dynamics. *Applied Thermal Engineering*, **127** (2017): 1391–1403.

[2] M. Feurhuber, M. Magno, M. Miranda, et al. CFD Investigation of Non-Condensable Gases in Vacuum and Non-Vacuum Steam Sterilizers. en. *Chemie Ingenieur Technik*, **91 (4)** (2019): 1–13.

[3] M. Feurhuber, M. Magno, M. Miranda, et al. CFD investigations of steam penetration, air-removal and condensation inside hollow loads and cavities. *Applied Thermal Engineering*, **147** (2019): 1070–1082.

[4] M. Feurhuber, P. Burian, M. Magno, et al. *Development of a spatially and timely resolved CFD model of a steam sterilizer to predict the load temperature and the inactivation of bacteria, under review*. 2019.

[5] M. Feurhuber, P. Burian, M. Magno, et al. CFD simulation of the inactivation of Geobacillus stearothermophilus on dental handpieces. *International Journal of Heat and Mass Transfer*, **144** (2019): Article 118649.

[6] S. J. Dancer, M. Stewart, C. Coulombe, et al. Surgical site infections linked to contaminated surgical instruments. *Journal of Hospital Infection*, **81** (4) (2012): 231–238.

[7] B. E. 285:2006+A2:2009. *BS EN 285:2006+A2:2009 - Sterilization. Steam sterilizers. Large sterilizers – BSI British Standards*. 2009.

[8] *EN 13060:2004 - Small steam sterilizers*. 2004.

[9] I. 17665-1:2006(en). *ISO 17665-1:2006(en), Sterilization of health care products — Moist heat — Part 1: Requirements for the development, validation and routine control of a sterilization process for medical devices*. 2006.

[10] J. P. C. M. van Doornmalen. "Surface steam sterilization: Steam penetration in narrow channels." English. PhD thesis. University of Technology Eindhoven, 2013.

[11] J. P. C. M. van Doornmalen Gomez Hoyos, R. A. C. van Wezel, and H. W. J. M. van Doornmalen. Case study on the orientation of phaco hand pieces during steam sterilization processes. *Journal of Hospital Infection*, **90** (1) (2015): 52–58.

[12] J. H. Bowie, J. C. Kelsey, and G. R. Thompson. THE BOWIE AND DICK AUTOCLAVE TAPE TEST. *The Lancet*. Originally published as Volume 1, Issue 7292 **281** (7292) (1963): 1215–1216.

[13] J. P. C. M. van Doornmalen and J. Dankert. A validation survey of 197 hospital steam sterilizers in The Netherlands in 2001 and 2002. *Journal of Hospital Infection*, **59** (2) (2005): 126–130.

[14] D. Esel, M. Doganay, N. Bozdemir, et al. Polymicrobial ventriculitis and evaluation of an outbreak in a surgical intensive care unit due to inadequate sterilization. *Journal of Hospital Infection*, **50** (3) (2002): 170–174.

[15] C. Vadrot and J. .-.-C. Darbord. Quantitative evaluation of prion inactivation comparing steam sterilization and chemical sterilants: proposed method for test standardization. *Journal of Hospital Infection*, **64** (2) (2006): 143–148.

[16] N. Lapanaitis, L. Frizzell, A. Downing, et al. Case study: Correlation between the duration of a steam sterilization process and the weight of the processed load. *Zentralsterilisation - Central Service*, **26** (4) (2018): 225–230.

[17] J. Grömann, U. Kaiser, and R. Menzel. Entlüftungsverhalten von unterschiedlichen Dampf-Sterilisationsprozessen gegenüber porösen und hohlen Sterilisiergütern. *Zentralsterilisation - Central Service*, **9** (3) (2001): 177–186.

[18] U. Kaiser and J. Göman. Investigations of Air Removal from Hollow Devices in Steam Sterilisation Processes. *Zentralsterilisation - Central Service*, **6** (6) (1998): 401–413.

[19] A. De Bruijn and A. Van Drongelen. Performance evaluation of hispital steam sterilizers using the european helix test. English. *Zentralsterilisation - Central Service*, **13(5)** (Volume 13) (2005): 330–336.

[20] U. Kaiser. Simple Method to Assess Efficacy of Sterilisation Processes for Hollow Instruments. *Zentralsterilisation - Central Service*, **7** (6) (1999): 393–395.

[21] U. Kaiser. Auswirkungen von nicht-kondensierbaren Gasen (NKG) in Dampfsterilisationsprozessen. *Zentralsterilisation - Central Service*, **13** (2005): 45–47.

[22] S. Winter, A. Smith, D. Lappin, et al. Failure of non-vacuum steam sterilization processes for dental handpieces. *Journal of Hospital Infection*, **97** (4) (2017): 343–347.

[23] S. Winter, A. Smith, D. Lappin, et al. Steam penetration using thermometric methods in dental handpieces with narrow internal lumens during sterilizing processes with non-vacuum or vacuum processes. *Journal of Hospital Infection* (2017).

[24] W. L. Lau, J. Reizes, V. Timchenko, et al. Numerical modelling of an industrial steam–air sterilisation process with experimental validation. *Applied Thermal Engineering*, **75** (2015): 122–134.

[25] W. L. Lau, J. Reizes, V. Timchenko, et al. Heat and mass transfer model to predict the operational performance of a steam sterilisation autoclave including products. *International Journal of Heat and Mass Transfer*, **90** (2015): 800–811.

[26] A. Villamarin, S. Roy, R. Hasballa, et al. 3D simulation of the aqueous flow in the human eye. *Medical Engineering & Physics*, **34** (10) (2012): 1462–1470.

[27] G. H. Tang, H. W. Hu, Z. N. Zhuang, et al. Film condensation heat transfer on a horizontal tube in presence of a noncondensable gas. *Applied Thermal Engineering*, **36** (2012): 414–425.

[28] A. M. Fic, D. B. Ingham, M. K. Ginalski, et al. Heat and mass transfer under an infant radiant warmer—development of a numerical model. *Medical Engineering & Physics*, **32** (5) (2010): 497–504.

[29] M. K. Ginalski, A. J. Nowak, and L. C. Wrobel. A combined study of heat and mass transfer in an infant incubator with an overhead screen. *Medical Engineering & Physics*, **29** (5) (2007): 531–541.

[30] J. Jung and A. Hassanein. Three-phase CFD analytical modeling of blood flow. *Medical Engineering & Physics*, **30** (1) (2008): 91–103.

[31] *W&H Lisa, Instruction for use, Available at: www.wh.com, accessed at 12.09.2019.*

[32] *W&H MS, Instruction for use, Available at: www.wh.com, accessed at 12.09.2019.*

[33] A. Rodriguez, J. Larkin, J. Dunn, et al. Model of the Inactivation of Bacterial Spores by Moist Heat and High Pressure. en. *Journal of Food Science*, **69** (8) (2004): E367–E373.

[34] M. S. Hossain, N. N. N. A. Rahman, V. Balakrishnan, et al. Mathematical modeling of Enterococcus faecalis, Escherichia coli, and Bacillus sphaericus inactivation in infectious clinical solid waste by using steam autoclaving and supercritical fluid carbon dioxide sterilization. *Chemical Engineering Journal*, **267** (2015): 221–234.

[35] J. P. C. M. V. Doornmalen and K. Kopinga. Temperature dependence of F-, D- and z-values used in steam sterilization processes. en. *Journal of Applied Microbiology*, **107** (3) (2009): 1054–1060.

[36] D. Haider, J. Göman, U. Junghannß, et al. Kill Kinetics Study of Bacillus subtilis Spores in Ethylene Oxide Sterilisation Processes. *Zentral Sterilisation*, **10** (3) (2002): 158–167.

[37] K. H. Wallhäußer. Praxis der Sterilisation, Desinfektion, Konservierung : Keimidentifizierung, Betriebshygiene. 4. überarbeitete und erweiterte Auflage. Thieme, 1988.

[38] D. I.-C. Wang, J. Scharer, and A. E. Humphrey. Kinetics of Death of Bacterial Spores at Elevated Temperatures. en. *APPL. MICROBIOL.* (): 4.

[39] P. G. Mazzola, T. C. V. Penna, and A. M. da S Martins. Determination of decimal reduction time (D value) of chemical agents used in hospitals for disinfection purposes. *BMC Infectious Diseases*, **3** (2003): 24.

[40] P. F. Stanbury, A. Whitaker, and S. J. Hall. "Chapter 5 - Sterilization." In: *Principles of Fermentation Technology (Third Edition)*. Oxford: Butterworth-Heinemann, 2017, 273–333.

[41] M. C. Jones. The temperature dependence of the lethal rate in sterilization calculations. en. *International Journal of Food Science & Technology*, **3** (1) (1968): 31–38.

[42] A. Mann, M. Kiefer, and H. Leuenberger. Thermal sterilization of heat-sensitive products using high-temperature short-time sterilization. *Journal of Pharmaceutical Sciences*, **90** (3) (2001): 275–287.

[43] A. Kramer, O. Assadian, M. Exner, et al., eds. Krankenhaus- und Praxishygiene (Dritte Ausgabe). Munich: Urban & Fischer, 2016.

[44] J. W. Richards. Introduction to industrial sterilization. English. *Introduction to industrial sterilization.* (1968).

[45] L. D. Boeck, R. W. Wetzel, S. C. Burt, et al. Sterilization of bioreactor media on the basis of computer calculated thermal input designated as Fo. en. *Journal of Industrial Microbiology*, **3** (5) (1988): 305–310.

[46] B. H. Junker, B. Beshty, and J. Wilson. Sterilization-in-place of concentrated nutrient solutions. en. *Biotechnology and Bioengineering*, **62** (5) (1999): 501–508.

[47] R. Kouhikamali, H. Hesami, and A. Ghavamian. Convective heat transfer in a mixture of cooling water and superheated steam. *International Journal of Thermal Sciences*, **60** (2012): 205–211.

[48] H. Liu, L. Cheng, S. Huang, et al. Heat and mass transfer characteristics of superheated fluid for hybrid solvent-steam process in perforated horizontal wellbores. *International Journal of Heat and Mass Transfer*, **122** (2018): 557–573.

[49] W. D. W. Company Eli Lilly and. Succeed at Steam Sterilization. en. *Chemical Processing* (2005).

[50] W. J. Rogers. "2 - Steam and dry heat sterilization of biomaterials and medical devices." In: *Sterilisation of Biomaterials and Medical Devices*. Ed. by S. Lerouge and A. Simmons. Woodhead Publishing Series in Biomaterials. Woodhead Publishing, 2012, 20–55.

[51] Y. Xiao, Z. Hu, S. Chen, et al. Experimental investigation and prediction of post-dryout heat transfer for steam-water flow in helical coils. *International Journal of Heat and Mass Transfer*, **127** (2018): 515–525.

[52] H. Lee, C. R. Kharangate, N. Mascarenhas, et al. Experimental and computational investigation of vertical downflow condensation. *International Journal of Heat and Mass Transfer*, **85** (2015): 865–879.

[53] C. Qi, X. Chen, W. Wang, et al. Experimental investigation on flow condensation heat transfer and pressure drop of nitrogen in horizontal tubes. *International Journal of Heat and Mass Transfer*, **132** (2019): 985–996.

[54] S. K. Park, M. H. Kim, and K. J. Yoo. Condensation of pure steam and steam-air mixture with surface waves of condensate film on a vertical wall. *International Journal of Multiphase Flow*, **22** (5) (1996): 893–908.

[55] H. M. Sabir, I. W. Eames, and K. O. Suen. The effect of non-condensable gases on the performance of film absorbers in vapour absorption systems. *Applied Thermal Engineering*, **19** (5) (1999): 531–541.

[56] K. Hijikata, S. J. Chen, and C. L. Tien. Non-condensable gas effect on condensation in a two-phase closed thermosyphon. *International Journal of Heat and Mass Transfer*, **27** (8) (1984): 1319–1325.

[57] V. D. Stevanovic, Z. V. Stosic, and U. Stoll. Three-dimensional numerical simulation of non-condensables accumulation induced by steam condensation in a non-vented pipeline. *International Journal of Heat and Mass Transfer*, **49** (15) (2006): 2420–2436.

[58] D. W. Tanner, D. Pope, C. J. Potter, et al. Heat transfer in dropwise condensation at low steam pressures in the absence and presence of non-condensable gas. *International Journal of Heat and Mass Transfer*, **11** (2) (1968): 181–190.

[59] J. Huang, J. Zhang, and L. Wang. Review of vapor condensation heat and mass transfer in the presence of non-condensable gas. *Applied Thermal Engineering*, **89** (Supplement C) (2015): 469–484.

[60] J.-D. Li. CFD simulation of water vapour condensation in the presence of non-condensable gas in vertical cylindrical condensers. *International Journal of Heat and Mass Transfer*, **57** (2) (2013): 708–721.

[61] X. Ma, J. W. Rose, D. Xu, et al. Advances in dropwise condensation heat transfer: Chinese research. *Chemical Engineering Journal*, **78** (2) (2000): 87–93.

[62] Q. Yi, M. Tian, W. Yan, et al. Visualization study of the influence of non-condensable gas on steam condensation heat transfer. *Applied Thermal Engineering*, **106** (2016): 13–21.

[63] G. Liu, J. Wang, T. Chen, et al. Experimental study on heat transfer characteristics of a condenser in the presence of air. *Applied Thermal Engineering*, **120** (Supplement C) (2017): 170–178.

[64] H. F. Gu, Q. Chen, H. J. Wang, et al. Condensation of a hydrocarbon in the presence of a non-condensable gas: Heat and mass transfer. *Applied Thermal Engineering*, **91** (Supplement C) (2015): 938–945.

[65] J. Ling and Y. Cao. Closed-form analytical solutions for radially rotating miniature high-temperature heat pipes including non-condensable gas effects. *International Journal of Heat and Mass Transfer*, **43** (19) (2000): 3661–3671.

[66] D. G. Kroger and W. M. Rohsenow. Condensation heat transfer in the presence of a non-condensable gas. *International Journal of Heat and Mass Transfer*, **11** (1) (1968): 15–26.

[67] W. J. Rogers. "7 - Sterilisation techniques for polymers." In: *Sterilisation of Biomaterials and Medical Devices*. Ed. by S. Lerouge and A. Simmons. Woodhead Publishing Series in Biomaterials. Woodhead Publishing, 2012, 151–211.

[68] B. Kirk. An evaluation of nine Bowie and Dick test products available in the United Kingdom. *Medical Device Decontamination*, **17** (1) (2012): 1–12.

[69] *EN ISO 11607-1 Packaging for terminally sterilized medical devices - Part 1: Requirements for materials, sterile barrier systems and packaging systems (ISO/DIS 11607-1:2017);* 2017.

[70] *EURONDA, Technical Data Sheet, Mod. 80, available at: www.euronda.de, accessed at 12.09.2019*.

[71] T. A. Augurt and J. A. A. M. v. Asten. *Sterilization Techniques*. en. 2000.

[72] T. Sandle. "12 - Sterilization and sterility assurance." In: *Pharmaceutical Microbiology*. Ed. by T. Sandle. Oxford: Woodhead Publishing, 2016, 147–160.

[73] R. Vaishya, A. K. Agarwal, M. Tiwari, et al. Medical textiles in orthopedics: An overview. *Journal of Clinical Orthopaedics and Trauma*, **9** (2018): S26–S33.

[74] S. Lerouge. "16 - Sterilization and cleaning of metallic biomaterials." In: *Metals for Biomedical Devices (Second Edition)*. Ed. by M. Niinomi. Woodhead Publishing Series in Biomaterials. Woodhead Publishing, 2019, 405–428.

[75] EN 867-5:2001. *Non-biological systems for use in sterilizers - Part 5: Specifications for indicator systems and process challenge devices for use in performance testing for small sterilizers Type B and Type S*.

[76] J. van Doornmalen and K. Kopinga. Review of surface steam sterilization for validation purposes. *American Journal of Infection Control*, **36** (2) (2008): 86–92.

[77] R. Prommas, P. Rattanadecho, and D. Cholaseuk. Energy and exergy analyses in drying process of porous media using hot air. *International Communications in Heat and Mass Transfer*, **37** (4) (2010): 372–378.

[78] *ANSYS Fluent Theory Guide*. 2016.

[79] J. H. Ferziger and M. Perić. Computational methods for fluid dynamics. en. 3rd, rev. ed. Berlin ; New York: Springer, 2002.

[80] F. Moukalled, L. Mangani, and M. Darwish. The Finite Volume Method in Computational Fluid Dynamics: An Advanced Introduction with OpenFOAM® and Matlab. en. Fluid Mechanics and Its Applications. Springer International Publishing, 2016.

[81] W. M. Rohsenow, J. P. Hartnett, and Y. I. Cho. Handbook of Heat Transfer, 3th Edition. Third Edition. McGraw-Hill, 1998.

[82] H. D. Baehr and S. Kabelac. Thermodynamik: Grundlagen und technische Anwendungen. de. 16th ed. Springer Vieweg, 2016.

[83] C. P. Kothandaraman. Steam Tables. en. Google-Books-ID: tIZ_ODxwVmEC. New Age International, 2007.

[84] C. Borgnakke and R. Sonntag. Fundamentals of Thermodynamics, 8th Edition SI Version. English. Eight Edition. WILEY, 2014.

[85] S. Klein and G. Nellis. Thermodynamics. 1st Edition. CAMBRIDGE UNIVERSIY PRESS, 2012.

[86] T. C. Elliott. Standard Handbook of Powerplant Engineering. Englisch. Revised. New York: McGraw-Hill Education Ltd, 1997.

[87] H.-J. Kretzschmar and W. Wagner. International Steam Tables: Properties of Water and Steam based on the Industrial Formulation IAPWS-IF97. en. 3rd ed. Springer Vieweg, 2019.

[88] VDI e.V. (Hrsg.) VDI-Wärmeatlas. Heidelberg: Springer-Verlag Berlin, 2013.

[89] A. J. White. Numerical investigation of condensing steam flow in boundary layers. *International Journal of Heat and Fluid Flow*, **21** (6) (2000): 727–734.

[90] D. J. Ryley and H. K. Al-Azzawi. Suppression of the deposition of nucleated fog droplets on steam turbine stator blades by blade heating. *International Journal of Heat and Fluid Flow*, **4** (4) (1983): 207–216.

[91] R. M. Lust. Physical Gas Laws. Ed. by S. J. Enna and D. B. Bylund. New York: Elsevier, 2007, 1–3.

[92] P. K. Kundu, I. M. Cohen, and D. R. Dowling, eds. Founders of Modern Fluid Dynamics. Boston: Academic Press, 2012, ii.

[93] T.-H. Shih, W. W. Liou, A. Shabbir, et al. A new k-ϵ eddy viscosity model for high reynolds number turbulent flows. *Computers & Fluids*, **24** (3) (1995): 227–238.

[94] J. Wurm, B. Martschini, R. Prieler, et al. Numerical and experimental investigation of post-oxidation of a four-stroke SI engine under fuel-rich conditions. *Fuel*, **225** (2018): 411–418.

[95] J. Wurm, M. Fitl, M. Gumpesberger, et al. Novel CFD approach for the thermal analysis of a continuous variable transmission (CVT). *Applied Thermal Engineering*, **103** (2016): 159–169.

[96] J. Wurm, M. Fitl, M. Gumpesberger, et al. Advanced heat transfer analysis of continuously variable transmissions (CVT). *Applied Thermal Engineering*, **114** (2017): 545–553.

[97] M. Landfahrer, C. Schluckner, R. Prieler, et al. Development and application of a numerically efficient model describing a rotary hearth furnace using CFD. *Energy*, **180** (2019): 79–89.

[98] M. Landfahrer, C. Schluckner, R. Prieler, et al. Numerical and experimental investigation of scale formation on steel tubes in a real-size reheating furnace. *International Journal of Heat and Mass Transfer*, **129** (2019): 460–467.

[99] G. Francesco, M. Federico, and M. Adriano. CFD modelling of the condensation inside a cascade of steam turbine blades: comparison with an experimental test case. *Energy Procedia*. ATI 2017 - 72nd Conference of the Italian Thermal Machines Engineering Association **126** (2017): 730–737.

[100] H. Bian, Z. Sun, X. Cheng, et al. CFD evaluations on bundle effects for steam condensation in the presence of air under natural convection conditions. *International Communications in Heat and Mass Transfer*, **98** (2018): 200–208.

[101] L. Vyskocil, J. Schmid, and J. Macek. CFD simulation of air–steam flow with condensation. *Nuclear Engineering and Design*. SI : CFD4NRS-4 **279** (2014): 147–157.

[102] W. Lee. A Pressure Iteration Scheme for Two-Phase Flow Modeling. *T.N. Veziroglu (Ed.), Multiphase Transport Fundamentals, Reactor Safety, Applications, vol. 1, Hemisphere Publishing, Washington, DC, 1980.* (1980).

[103] C. R. Kharangate and I. Mudawar. Review of computational studies on boiling and condensation. *International Journal of Heat and Mass Transfer*, **108** (2017): 1164–1196.

[104] C. R. Kharangate, H. Lee, I. Park, et al. Experimental and computational investigation of vertical upflow condensation in a circular tube. *International Journal of Heat and Mass Transfer*, **95** (2016): 249–263.

[105] H. L. Wu, X. F. Peng, P. Ye, et al. Simulation of refrigerant flow boiling in serpentine tubes. *International Journal of Heat and Mass Transfer*, **50** (5) (2007): 1186–1195.

[106] Z. Yang, X. F. Peng, and P. Ye. Numerical and experimental investigation of two phase flow during boiling in a coiled tube. *International Journal of Heat and Mass Transfer*, **51** (5) (2008): 1003–1016.

[107] E. Da Riva and D. Del Col. Numerical Simulation of Laminar Liquid Film Condensation in a Horizontal Circular Minichannel. *Journal of Heat Transfer*, **134** (5) (2012): 051019–051019.

[108] G. Qiu, W. Cai, Z. Wu, et al. Numerical simulation of forced convective condensation of propane in a spiral tube. *Journal of Heat Transfer*, **137** (4) (2015).

[109] D. S. Yoon, H. Jo, and M. L. Corradini. CFD modeling of filmwise steam condensation with noncondensable gas with modified boundary condition. *International Journal of Heat and Mass Transfer*, **125** (2018): 485–493.

[110] G. Zschaeck, T. Frank, and A. D. Burns. CFD modelling and validation of wall condensation in the presence of non-condensable gases. *Nuclear Engineering and Design*. SI : CFD4NRS-4 **279** (2014): 137–146.

[111] T.-H. Phan, S.-S. Won, and W.-G. Park. Numerical simulation of air–steam mixture condensation flows in a vertical tube. *International Journal of Heat and Mass Transfer*, **127** (2018): 568–578.

[112] S. Mimouni, A. Foissac, and J. Lavieville. CFD modelling of wall steam condensation by a two-phase flow approach. *Nuclear Engineering and Design*. 13th International Topical Meeting on Nuclear Reactor Thermal Hydraulics (NURETH-13) **241** (11) (2011): 4445–4455.

[113] G. Qiu, X. Wei, W. Cai, et al. Development and validation of numerical model of condensation heat transfer and frictional pressure drop in a circular tube. *Applied Thermal Engineering*, **143** (2018): 225–235.

[114] H. Bian, Z. Sun, N. Zhang, et al. A new modified diffusion boundary layer steam condensation model in the presence of air under natural convection conditions. *International Journal of Thermal Sciences*, **145** (2019): 105948.

[115] P. Tong, G. Fan, Z. Sun, et al. An experimental investigation of pure steam and steam–air mixtures condensation outside a vertical pin-fin tube. *Experimental Thermal and Fluid Science*, **69** (2015): 141–148.

[116] Y.-G. Lee, Y.-J. Jang, and D.-J. Choi. An experimental study of air–steam condensation on the exterior surface of a vertical tube under natural convection conditions. *International Journal of Heat and Mass Transfer*, **104** (2017): 1034–1047.

[117] J. Lu, H. Cao, and J. Li. Condensation heat and mass transfer of steam with noncondensable gases outside a horizontal tube under free convection. *International Journal of Heat and Mass Transfer*, **139** (2019): 564–576.

[118] R. Chen, P. Zhang, B. Tan, et al. Steam condensation on a downward-facing plate in presence of air. *Annals of Nuclear Energy*, **132** (2019): 451–460.

[119] W. Ranz and W. Marshall. Evaporation from Drops, Part I. *Chemical Engineering Progress*, **48** (3) (1952): 141–146.

[120] W. Ranz and W. Marshall. Evaporation from Drops, Part II. *Chemical Engineering Progress*, **48** (4) (1952): 173–180.

[121] H.-S. Kim, D. H. Lee, A. Fridman, et al. Residual effects and energy cost of gliding arc discharge treatment on the inactivation of Escherichia coli in water. *International Journal of Heat and Mass Transfer*, **77** (2014): 1075–1083.

[122] S. R. Kim, M. S. Rhee, B. C. Kim, et al. Modeling of the inactivation of Salmonella typhimurium by supercritical carbon dioxide in physiological saline and phosphate-buffered saline. *Journal of Microbiological Methods*, **70** (1) (2007): 132–141.

[123] S. R. Kim, M. S. Rhee, B. C. Kim, et al. Modeling the inactivation of Escherichia coli O157:H7 and generic Escherichia coli by supercritical carbon dioxide. *International Journal of Food Microbiology*, **118** (1) (2007): 52–61.

[124] *W&H Primea, Restoration & Prosthetics, Available at: www.wh.com, accessed at 12.09.2019*.

[125] *W&H Synea, Restoration & Prosthetics, Available at: www.wh.com, accessed at 12.09.2019*.

[126] G. Caruso, D. Vitale Di Maio, and A. Naviglio. Condensation heat transfer coefficient with noncondensable gases inside near horizontal tubes. *Desalination*, **309** (Supplement C) (2013): 247–253.

[127] P. De Santis and V. S. Rudo. "Validation of Steam Sterilization in Autoclaves", in Validation of Aseptic Pharmaceutical Processes, F. J. C a r l e t o n and J.P. Agalloco, Eds. (Marcel Dekker, New York, 2d ed., 1986), pp. 279–317. (1986).

[128] M. S. Hossain, V. Balakrishnan, N. N. N. A. Rahman, et al. Modeling the inactivation of Staphylococcus aureus and Serratia marcescens in clinical solid waste using supercritical fluid carbon dioxide. *The Journal of Supercritical Fluids*, **83** (2013): 47–56.

[129] G. Mendes-Oliveira, J. L. Jensen, K. M. Keener, et al. Modeling the inactivation of Bacillus subtilis spores during cold plasma sterilization. *Innovative Food Science & Emerging Technologies*, **52** (2019): 334–342.

[130] Evelyn and F. V. M. Silva. Heat assisted HPP for the inactivation of bacteria, moulds and yeasts spores in foods: Log reductions and mathematical models. *Trends in Food Science & Technology*, **88** (2019): 143–156.

[131] R. Simpson, H. Nuñez, and S. Almonacid. "3 - Modeling thermal processing and reactions: sterilization and pasteurization." In: *Modeling Food Processing Operations*. Ed. by S. Bakalis, K. Knoerzer, and P. J. Fryer. Woodhead Publishing Series in Food Science, Technology and Nutrition. Woodhead Publishing, 2015, 67–93.

[132] EC (European Commission). *EC Guidelines of Good Manuf acturing Practice for Medical Products. Pharm Ind. 1990;52:853-74.*

[133] X. Wu, F. Chu, Y. Zhu, et al. Vapor free convection film condensation heat transfer in the presence of non-condensable gases with smaller molecular weights than the vapor. *Applied Thermal Engineering* (2017).

[134] A. Hoyt, A. L. Chaney, and K. Cavell. Studies on Steam Sterilization and the Effects of Air in the Autoclave. *Journal of Bacteriology*, **36** (6) (1938): 639–652.

[135] J. P. C. M. v. Doornmalen, M. Verschueren, and K. Kopinga. Penetration of water vapour into narrow channels during steam sterilization processes. en. *Journal of Physics D: Applied Physics*, **46** (6) (2013): 065201.

[136] H. Hu, X. Weng, D. Zhuang, et al. Heat transfer and pressure drop characteristics of wet air flow in metal foam under dehumidifying conditions. *Applied Thermal Engineering*, **93** (2016): 1124–1134.

[137] H. Hu, Z. Lai, and G. Ding. Heat transfer and pressure drop characteristics of wet air flow in metal foam with hydrophobic coating under dehumidifying conditions. *Applied Thermal Engineering*, **132** (2018): 651–664.

[138] C. Chantana and S. Kumar. Experimental and theoretical investigation of air-steam condensation in a vertical tube at low inlet steam fractions. *Applied Thermal Engineering*, **54** (2) (2013): 399–412.